Donor-Acceptor Block Copolymers in Organic Electronics

Spectroscopy, Charge Transport, Morphology and Device Application

Dissertation

zur Erlangung des akademischen Grades
eines Doktors der Naturwissenschaften (Dr. rer. nat.)
im Fach Chemie der Fakultät für
Biologie, Chemie und Geowissenschaften der Universität Bayreuth

vorgelegt von
Sven Hüttner

geboren in Hof

Bayreuth 2010

Die vorliegende Arbeit wurde in der Zeit von Januar 2006 bis Januar 2010 am Lehrstuhl Angewandte Funktionspolymere / Makromolekulare Chemie I unter der Betreuung von Prof. Dr. Mukundan Thelakkat angefertigt.

Vollständiger Abdruck der von der Fakultät für Biologie, Chemie und Geowissenschaften der Universität Bayreuth genehmigten Dissertation zur Erlangung des akademischen Grades Doktor der Naturwissenschaften (Dr. rer. nat.).

Amtierender Dekan:	Prof. Dr. Stephan Clemens
Dissertation eingereicht am:	19. Januar 2010
Wissenschaftliches Kolloquium am:	5. Mai 2010

Prüfungsausschuss:

Prof. Dr. Mukundan Thelakkat	(Erstgutachter)
Prof. Dr. Peter Strohriegl	(Zweitgutachter)
Prof. Dr. Anna Köhler	
Prof. Dr. Jürgen Senker	(Vorsitzender)

Contents

Chapter 1

Summary

Organic electronic devices have attracted increasing attention over the last decade. The use of organic materials allows the creation of large area, flexible and low-cost light-emitting devices, transistors and photovoltaics. The development of new organic materials contributes to a successful commercialisation. The present work deals with the characterisation of novel donor-acceptor block copolymers and their constituent polymer blocks that are well-suited for organic photovoltaics. In conventional approaches, blends of polymers are used with limited morphological control. Block copolymers, however, phase-separate and self-assemble into nanostructured morphologies due to the covalent linkage of the two blocks. The interplay between intermolecular interactions, mesoscopic crystalline structures and the block copolymer microphase separation determine the material properties and therefore the device characteristics. Thus, these block copolymers offer a unique platform to study the electronic and photophysical properties of confined donor-acceptor systems. This work is concerned with the fundamental characterisation of these properties as well as the application in organic field effect transistors and organic solar cells.

The acceptor polymer block poly(perylene bisimide acrylate) (PPerAcr) consists of perylene bisimide (PBI) units that are linked to a polyacrylate backbone. We have investigated the homopolymer PPerAcr, a model block copolymer in conjunction with polystyrene (PS), as well as fully functionalised block copolymers with a donor block either made of poly(vinyl triphenylamine) (PvTPA) or poly(3-hexylthiophene) (P3HT). These polymers offer a set of electronically active materials with several hierarchical structures: The PBI moieties feature intermolecular $\pi - \pi$ interactions that lead to crystalline side chains of PPerAcr that form a monoclinic lattice of one-dimensional stacks of PBI. Further nanoscopic structures are induced by the combination of PPerAcr with another amorphous block or another semi-crystalline block such as P3HT due to phase separation.

Since PPerAcr is used as an electron transporting material in all subsequent block copolymers, its structural, optical and electronic properties are investigated in detail. The planar PBI moieties feature strong $\pi - \pi$ interactions, rendering PPerAcr crystalline, which is important for charge transport. As tested in organic field effect transistors, PPerAcr exhibits excellent electron transport properties for an n-type polymer with mobilities around $10^{-3}\,\frac{\mathrm{cm}^2}{\mathrm{Vs}}$. Furthermore, a cylindrical block copolymer of PS-*b*-PPerAcr shows the same charge transport properties as the homopolymer PPerAcr, indicating that the incorporation of PPerAcr into a block copolymer does not necessarily reduce its charge transport performance.

The intermolecular interactions of the PBI moieties favor not only charge transport, but also affect the optical properties, due to the electronic coupling of the transition dipole moments. Thus, optical spectroscopy such as absorption and fluorescence spectroscopy give access to information about the intermolecular packing, which is correlated with temperature dependent X-ray diffraction studies. The strong intermolecular packing of the PBI units can be overcome by solvent-vapour exposure. This is specially helpful to induce polymer chain mobility, enabling the completion of block copolymer phase separation for example. This method was studied in detail by means of in-situ spectroscopy and ellipsometry during controlled solvent-vapour exposure. Spin-coated films of PvTPA-*b*-PPerAcr exhibit an incomplete phase separation and can be transformed into an ordered lamellar morphology by solvent-vapour annealing.

In addition to PvTPA, we have characterised further poly(triarylamines) with different electron-rich substituents at the TPA units in OFETs. All these polymers are amorphous side-chain polymers. We found the charge carrier mobility to be independent of the molecular weight, though allowing an adjustment of their thermal properties for device fabrication.

This is in contrast to P3HT, which is a semi-crystalline, conjugated main chain polymer. X-ray diffraction, steady state and time-resolved spectroscopy, as well as the transistor device characterisation were employed to establish a charge transport - morphology relation for the donor-acceptor block copolymers P3HT-*b*-PPerAcr containing two crystalline blocks. Controlling the crystallisation preferences of the two blocks leads to a new processing route for OFETs with tunable p-type, ambipolar, or n-type transport through a one-time thermal annealing step.

The application of P3HT-*b*-PPerAcr in organic photovoltaic devices showed also very promising results. Maximum external quantum efficiencies of up to 31% have been measured. The performance was strongly dependent on the molecular weight. In block copolymers with the same block ratio but with only half the molecular weight, the performance decreased by almost a factor of 10. The reduced domain size caused by the lower segment length and the reduced P3HT crystallinity led to a decreased hole carrier mobility which was responsible for the large difference in performance between the two block copolymers.

Subsequently, the photophysics of P3HT-*b*-PPerAcr by means of absorption and fluorescence spectroscopy as well as time-resolved transient absorption spectroscopy were investigated. All block copolymers exhibited an ultra-fast charge-pair formation and a strongly reduced photoluminescence, suggesting domain sizes of only some nanometres. Although efficient charge separation could be accomplished, a good charge percolation was lacking due to small domain sizes. Furthermore the herein presented results emphasis the fundamental importance of morphology and interfacial properties such as crystallinity. These findings motivate the further use of block copolymers as compatibilising agents for polymer blends to improve their interface and morphology.

Chapter 2

Zusammenfassung

Organische Elektronik hat sich über das letzte Jahrzehnt zu einem viel beachteten Gebiet entwickelt. Organische Materialen ermöglichen die Entwicklung großflächiger, flexibler und preisgünstiger Anwendungen von lichtemittierenden Bauelementen, Transistoren und Solarzellen. Die stetige Entwicklung neuer organischer Materialien trägt maßgeblich zu diesem Erfolg bei. Die vorliegen Arbeit befasst sich deshalb mit der Charakterisierung von neuen Donor-Akzeptor Blockcopolymeren, die sich zur Anwendung in organischen Solarzellen eignen. Herkömmliche Polymersolarzellen bestehen aus einem Blend des Akzeptor- und Donormaterials, welches nur eine sehr eingeschränkte Kontrolle über deren Phasenseparation erlaubt. Im Gegensatz dazu phasenseparieren Blockcopolymere in selbst-organisierte Nanostrukturen, da beide Blöcke kovalent miteinander verbunden sind. Das Zusammenspiel von intermolekularen Wechselwirkungen, mesoskopisch kristallinen Strukturen und Microphasenseparation prägen die Eigenschaften dieser Materialen. Somit eignen sich diese funktionalisierten Blockcopolymere als ein Modelsystem, grundlegende elektrische und photophysikalische Eigenschaften strukturierter Donor-Akzeptor-Systeme zu untersuchen. Diese Arbeit befasst sind sowohl mit der Charakterisierung dieser Eigenschaften als auch der Anwendung in Organischen Feldeffekttransistoren (OFETs) und Organischen Solarzellen.

Der Akzeptorblock Poly(Perylene Bisimide Acrylate (PPerAcr) besteht aus Perylene Bisimide (PBI) Einheiten, die an ein Polyacrylat gebunden sind. Neben dem Homopolymer PPerAcr werden Model-Blockcopolymere mit Polystyrol (PS), sowie vollfunktionalisierte Blockcopolymere mit verschiedenen Donorblöcken untersucht. Diese bestehen entweder aus amorphen Poly(Triphenylamin) (PvTPA) oder semikristallinen Poly(3-Hexylthiophen) (P3HT). Diese Systeme bilden somit ein Sortiment an elektronisch aktiven Materialien welche verschieden komplexe hierarchische Strukturen formen: Die PBI-Einheiten besitzen intermolekulare $\pi - \pi$ Wechselwirkungen, die letzten Endes zur Seitenkettenkristallinität von PPerAcr führt, deren Struktur monoklin geordneter eindimensionaler Kolumnen aus PBI gleicht. Durch die Kombination mit einem weiteren amorphen oder einem weiteren semi-kristallinen Block und deren Phasenseparation findet eine Strukturbildung auch auf nanoskopischer Ebene statt. Zunächst wurden die Eigenschaften von PPerAcr untersucht. Die $\pi - \pi$ Wechselwirkungen der PBI Einheiten sind für einen guten Ladungsträgertransport in diesen Materialen ausschlaggebend. PPerAcr wurde in OFETs untersucht, wobei Elektronmobilitäten um $10^{-3}\,\frac{\mathrm{cm}^2}{\mathrm{Vs}}$ erzielt wurden. Auch in Blockcopolymeren mit einem inerten Polystyrolblock (PS-*b*-PPerAcr) und einer zylindrischen Morphologie konnten diese Mobilitäten gemessen werden, so dass die Inkorporation von PPerAcr in Blockcopolymeren sich nicht unbedingt negativ auf die Ladungsträgermobilität auswirkt.

Die Intermolekularen Wechselwirkungen der PBI-Einheiten beeinflussen auch deren optische Eigenschaften. Somit eignet sich Absorptions- und Fluoreszenzspektroskopie, die intermolekularen Wechselwirkungen aufzuzeichnen, und es lassen sich diese mit Röntgenstrukturdaten aus temperaturabhängigen Messungen zu korrelieren. Durch die gezielte Aussetzung im Lösemitteldampf erreichen, diese π-Wechselwirkungen zu stören. Diese Methode ist vor allem dann von Bedeutung, wenn es darum geht den Polymerketten auseichende Kettenmobilität zur Verfügung zu stellen, um zum Beispiel Phasenseparationsprozesse zu aktivieren. Diese Methode wurde mittels in-situ Ellipsometrie und Spektroskopie untersucht. So kann die zunächst unvollständige Phasenseparation, wie sie nach dem Prozessieren von PvTPA-*b*-PPerAcr Filmen vorliegt, in eine geordnete, lamellare Struktur überführt werden. Entsprechend wurden verschiedene amorph-kristallinen PPerAcr Homo- und Blockcopolymere hinsichtlich optischer und elektronischer Eigenschaften untersucht, um eine Relation zu den intermolekularen Wechselwirkungen und mesoskopischen Strukturbildung zu schaffen.

Neben PvTPA als Donor wurden weitere polymerisierte Triarylamine, welche durch unterschiedliche elektronenreiche Gruppen modifiziert wurden, mittels OFETs untersucht. Die Ladungsträgermobilität ist unabhängig vom Molekulargewicht, die Änderung dessen erlaubt aber eine Anpassung gewünschter thermischer Eigenschaften, was wichtig bei der Prozessierung sein kann. Dies ist anders im Vergleich zu P3HT, welches ein semi-kristallines Hauptkettenpolymer ist. Methoden wie Röntgenstreuung, statische und zeitaufgelöste Spektroskopie sowie Transistormessungen wurden verwendet, um eine Ladungsträgertranport-Morpholgie-Relation aufzuzeigen. Durch die Kontrolle über die präferenzielle Kristallisation beider Blöcke, lassen sich neue Bauelementeigenschaften von organischen Transistoren verwirklichen. Durch einen einmaligen thermischen Konditionierungsschritt kann der Transistor von ursprünglich p-leitend in einen ambipolaren oder n-leitenden Transistor – je nach Blocklängenverhältnis – überführt werden.

Die Anwendung von P3HT-*b*-PPerAcr in Solarzellen liefert vielversprechende Ergebnisse. Maximale externe Quanteneffizienzen von bis zu 31% konnten gemessen werden. Allerdings ist dies stark molekulargewichtsabhängig – bei halbem Moleklargewicht um mehr als 10-fach reduziert. Dies liegt an der reduzierten Domänengröße aufgrund kürzerer Kettenlängen, was wiederum eine Reduktion der Kristallinität und Ladungsträgermobilität zur Folge hat.

Im Weiteren wurden die photophysikalischen Eigenschaften von P3HT-*b*-PPerAcr mittels Absorptions-, Fluoreszenz- und zeitaufgelöster transienter Absorptionsspektroskopie untersucht. Unter Anderem lässt sich bei allen Blockcopolymeren eine ultraschnelle Ladungsträgerpaargeneration ermitteln, was zusammen mit einer stark reduzierten Photolumineszenz auf äußerst kleine Domänengrößen im Bereich weniger Nanometer schließen lässt. Allerdings haben die kleinen Domänen der Donor-Akzeptor Morphologie zur Folge, dass die Ladungsträgerperkolation stark eingeschränkt ist. Ferner verdeutlichen die hier gewonnen Ergebnisse die Bedeutung fundamentaler Grenzflächeneigenschaften wie die der Kristallinität von P3HT. Dies ist wichtig für die weitere Entwicklung organischer Solarzellen und motiviert die weitere Anwendung von vollfunktionalisierten Blockcopolymeren zur Kompatibilisierung von Polymerblends.

Chapter 3

Introduction

3.1 Motivation

The earliest report of optoelectronic properties in conjugated organic molecules was made in 1906 by Pochettino on photoconductivity of anthracene.[1] The most significant developments in organic electronics, however, have been made in the last 30 years, starting from the demonstration of electrical conductivity in conjugated polymers by Heeger, Diarmid and Shirakawa in the late 70s (Nobel prize in chemistry in 2000). First organic light-emitting and photovoltaic devices have been demonstrated by Tang in 1986.[2] Polymer-based devices followed shortly from several groups: organic light-emitting devices (OLEDs),[3] organic field effect transistors (OFETs)[4,5] and organic photovoltaics (OPVs).[6]

Electronics based on organic molecules open up new applications in consumer electronics such as displays, flexible circuits and large area applications such as solar cells. The potential of organic electronics is manifold and includes low-cost applications, printability of electronic circuitry and tunability of their optoelectronic properties through tailored synthetic modification. The field has matured considerably over the last years and products - especially for the application in active displays and light emitting devices (OLEDs) are commercially available.

The industrial realisation of the inverse process – converting light into electric power – is still in development. Today's most efficient organic solar cells show efficiencies of around 5-6.8%.[7,8] In terms of pure light conversion performance inorganic solar cells may be superior to organic, however, the targeted application for organic solar cells is complementary – aiming for flexible or low-cost devices.[9] Furthermore, the research in organic photovoltaics[10] is motivated by the world's energy needs – the search for cost-efficient, renewable energy sources – as well as the virtually limitless amount of solar energy – approximately one hour of solar irradiation onto our planet corresponds the world's annual energy consumption.[11]

Organic based field effect transistors offer a complete range of new applications. The performance of the best organic materials reaches that of amorphous silicon and can therefore potentially be used in active matrix displays or RFID-tags.[12] Furthermore, low temperature processing and printability enables electronic circuitry on flexible substrates with extreme low production costs targeting a complete new market.

Organic electronics are mainly based on conjugated polymers and small molecules. The interactions between these π-conjugated systems have decisive effects on the in-

trinsic structural and electronic properties on an intermolecular scale (i.e. π-π stacking, polycrstallinity).[13] Furthermore, devices such as organic photovoltaics[14] or certain ambipolar transistors[15] rely on binary systems, composed of two materials, an acceptor and a donor or a n-type and a p-type material, respectively. The interplay between donor and acceptor on a mesoscopic level has consequences on the device function as it influences the charge generation or charge transport properties for example.[16–19] These composites are usually achieved by blending both materials, the acceptor with the donor material.

This thesis is concerned with the application and optoelectronic characterisation of novel donor-acceptor block copolymers as they have been synthesised in the group of Prof. Thelakkat.[20,21] The covalent linkage between the donor and the acceptor block influences the phase separation of both components. These donor acceptor block copolymers and their constituent homopolymers are suited for organic photovoltaic devices, but they also offer a unique platform to study spectroscopic and photophysical properties of confined donor-acceptor systems. Organic field effect transistors serve as an important characterisation tool and also demonstrate new potential of block copolymers in field effect transistor applications.

3.2 Organic Photovoltaics

In organic materials, the electronic coupling of the molecules is weak, so that no band-like electronic structure forms as in crystalline inorganic materials. The energy levels of each molecule are localised to the HOMO (highest occupied molecular orbital) and LUMO (lowest unoccupied molecular orbital) levels. The photogeneration of separate charges is a multiple-step process. Unlike in inorganic semiconductors, absorbed photons do not create free charges upon absorption but bound electron-hole pairs, so-called excitons. These states lower their energy through lattice distortions as a combination of electronic excitation and associated geometric relaxations. The electron-phonon coupling leads to a strong localisation of the excitons (Frenkel type excitons, in contrast to Wannier-Mott excitons which are free excitons and existing for example in inorganic semiconductors with high dielectric constants). This evokes a strong Coulombic electron-hole binding which is also given through the low dielectric constant of organic materials. As a consequence that does not screen the electric field between the oppositely charged carriers resulting in large exciton binding energies of around 0.4 eV which in return inhibits activated charge separation. In order to overcome the exciton binding energy, a second semiconducting material with different energy levels is brought into contact with the first one. This concept was first introduced by Tang in 1986[2], creating a heterojunction interface between a donor and an acceptor material.

Figure 3.1 shows the energy levels of a heterojunction where both, the ionization potential (I_P) and the electron affinity (E_A) of the donor are higher than those of the acceptor material. I_P is equivalent to the HOMO level and E_A is equivalent to the LUMO. Depending on whether the donor or the acceptor material provides the exciton, the offset of the energy levels determines whether the exciton binding energy can be

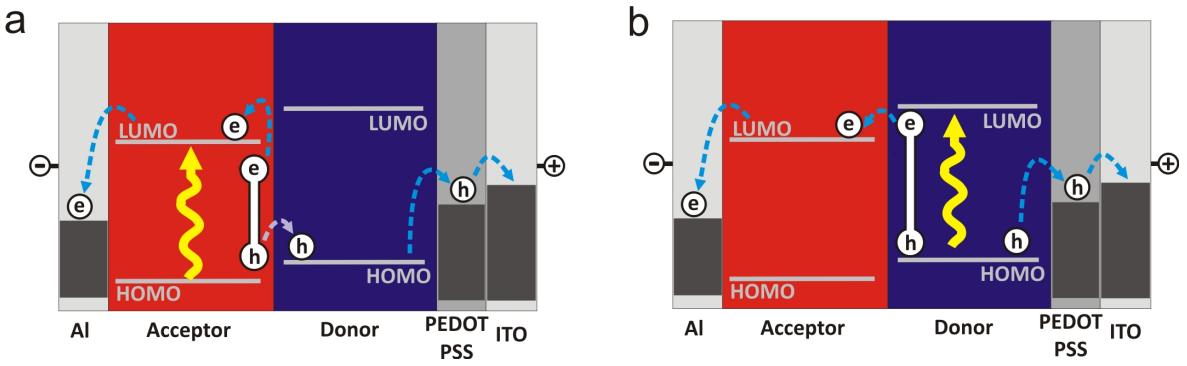

Figure 3.1: Schematic of a bilayer donor-acceptor system with its energy levels. If a photon is absorbed, an excited stated, a so-called exciton, is formed. The exciton is separated at the donor-acceptor interface. A prerequisite for charge separation is the proper alignment of the energy levels of both materials offering an energetically more favourable state. a) If the exciton is absorbed in the acceptor material, the difference between the two HOMO levels has to be larger than the exciton binding energy. b) In case the exciton is absorbed by the donor material, the offset of the LUMO levels has to be larger than the exciton binding energy, that is the HOMO-LUMO difference between donor and acceptor has to be smaller than the energy of the exciton.

overcome. For the actual energy of the exciton E_{Exciton} in relation to E_A and I_P, this means, if $E_{\text{Exciton}} > I_P(Donor) - E_A(Acceptor)$, it is energetically more favourable for the exciton to be separated into a hole and an electron. The donor-acceptor material is located between two electrodes. The work functions of the electrode materials have to be selected according to the hole or electron injection to minimise the contact resistance.

The overall efficiency is a product of the several steps that occur from light absorption to a measurable photocurrent (Fig. 3.2):
The energy gap between the ground state and the first singlet state represents the minimum energy for **absorption** of a photon by the material. This gap should well match the solar spectrum for a sufficient **creation of excitons**. In most materials, the Frank Condon principle holds and photons are absorbed into higher vibrational levels. Those excitons can decay on different ways. One is the decay from the lowest excited vibrational level into vibrational levels of the ground state upon emission of a photon which resulting in a red-shifted photoluminescence (Stokes shift).[22] As mentioned

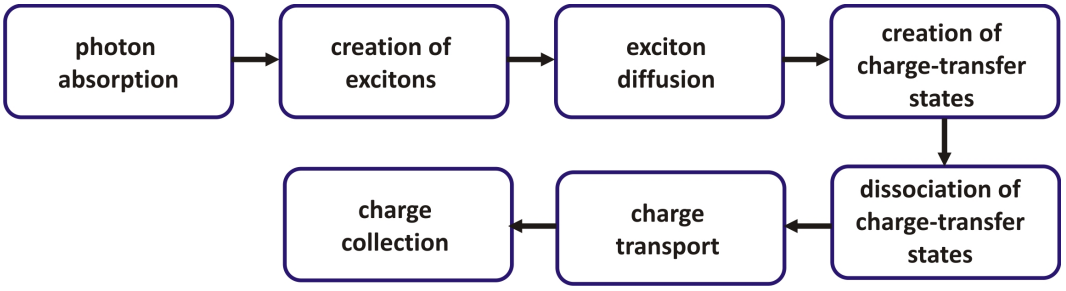

Figure 3.2: Processes occurring in organic photovoltaic devices from light absorption to photo current generation.

above, these excitons are localised on the molecules of a material. **Exciton diffusion** takes place from site to site, decribed by Förster transfer.[23] If the excitons reach the donor-acceptor interface within their exciton diffusion length (i.e. their life-time), the exciton may form a **charge-transfer state** at the interface. Recombination processes such as geminate recombination,[24] via exciplex formation[25] or triplet state formation[26] may take place at this stage, but the charge-transfer state can also simply **dissociate into free charge carriers** which are not coulombically bound to each other anymore. Different models to describe the charge separation have been developed,[24,27] whereby the Onsager-Braun model is one of the most popular ones. The separated charges have to migrate to the electrodes. Different **charge transport** models have been developed for systems with a high disorder as in polymer semiconductors. The polaron model as described by Marcus,[28] which considers "self-trapped" polarons (charges on conjugated polymer chains). These need to overcome an energy barrier associated with its reorganisation in order to move. The hopping model by Bässler[29] assumes solely hopping processes of the charge carriers between the molecule sites, where the density of states is assumed to be a Gaussian distribution. The **charge collection** is the last step for photocurrent generation. Ideally the workfunctions of the electrode materials are aligned to create ohmic contacts with the semiconductors, which is the case if the barrier of injection is less than the available thermal energy.

The above mentioned limiting factors impose certain requirements on the design of a photovoltaic device.[30] Only excitons that reach the donor-acceptor interface during their lifetime can potentially contribute to the photocurrent. Their lifetime is usually expressed as an average diffusion length which is less than 10 nm in most conjugated materials.[31] Only excitons created in the proximity of a donor-acceptor interface contribute to the charge separation process. In order to increase the interface and decrease the average distance between the donor and acceptor material, bulk heterojunction device structures were developed.[6] (Fig. 3.3) They consist of a blend of two organic materials. The aim is the formation of an interpenetrating network with a large interfacial area, but still with sufficient percolation paths to the electrodes. Various combinations of donor and acceptor materials and polymers have been reported in the literature.[6,14,19,32–35] The most ubiquitous material system is based on poly(hexylthiophene) (P3HT) and the fullerene derivative PCBM, where efficiencies up to 5-6 % have been observed.[7] Fig. 3.3 shows the photophysical process in a bulk heterojunction device. Other material combinations consisting of low molecular weight molecules and polymers have also been studied.[36]

Once the donor and acceptor materials have been chosen, the morphology becomes the crucial parameter in bulk heterojunction solar cells. The most common method of creating the thin active layers is by spin-casting films from a solution of the blend. For most commonly used solvents, film formation takes place within several seconds, freezing-in a non-equilibrium morphology of a polymer blend.[38,39] The detailed demixing process during film preparation, therefore, determines the internal structure of binary polymeric thin films. In order to influence and adjust the morphology, additional annealing steps are needed. The film is then quenched as soon as optimal morphology is achieved on the way towards the thermodynamic equilibrium of the blend. The work presented herein controls this morphology via the use of diblock

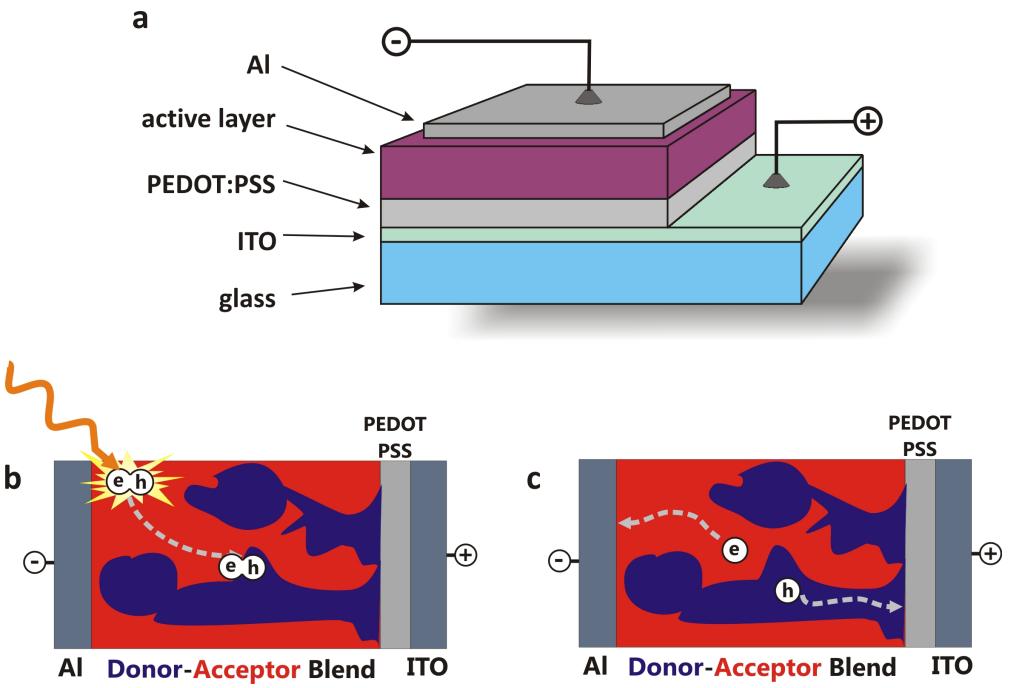

Figure 3.3: a) Schematic of an organic photovoltaic device. As a substrate indium tin oxide (ITO) coated glass is used, covered by a Poly(3,4-ethylenedioxythiophene)/poly(styrenesulfonate) (PEDOT:PSS) layer.[37] This layer serves for blocking electrons. It is spin-coated from an aqueous dispersion and therefore does not dissolve during further processing. The active layer comprises the donor-acceptor blend (thickness $\sim 60 - 200\,\mathrm{nm}$. On top of the active layer a metal electrode is evaporated (e.g. aluminum). b) Schematic of a bulk heterojunction solar cell, where the donor and acceptor materials are blended, ideally phase separating into an interpenetrating network. Exciton are created in one or both of the materials and diffuse to the interface. c) Charge separation occurs at the interface, and the charges then percolate to their respective electrodes, driven by the built-in potential created by the different work functions of the electrode materials.

copolymers, which consist of a donor and an acceptor block. The following section describes the morphologies formed by block copolymers.

Fig. 3.4 depicts the typical device characteristics of an organic photovoltaic devices. The open circuit voltage V_{OC}, the short circuit current I_{SC}, the fill factor FF and the power conversion efficiency η are determined by the $J-V$ characteristics. The fill factor is the fraction of maximum power and $J_{SC} \cdot V_{OC}$. In order to maintain internationally accepted testing procedures, the devices were measured under simulated sunlight of 100 $\frac{\mathrm{mW}}{\mathrm{cm}^2}$, comparable to solar irradiance at 1.5 airmass (1.5 AM). The simulated sunlight is calibrated with a certified silicon test cell and the spectral mismatch between the calibration cell and the tested cell has to be taken into account. The external quantum efficiency is measured under monochromatic light and spectrally resolves the incident photon conversion efficiency, i.e. by measuring the short circuit current based on the amount of photons incident onto the device at a specific wavelength.

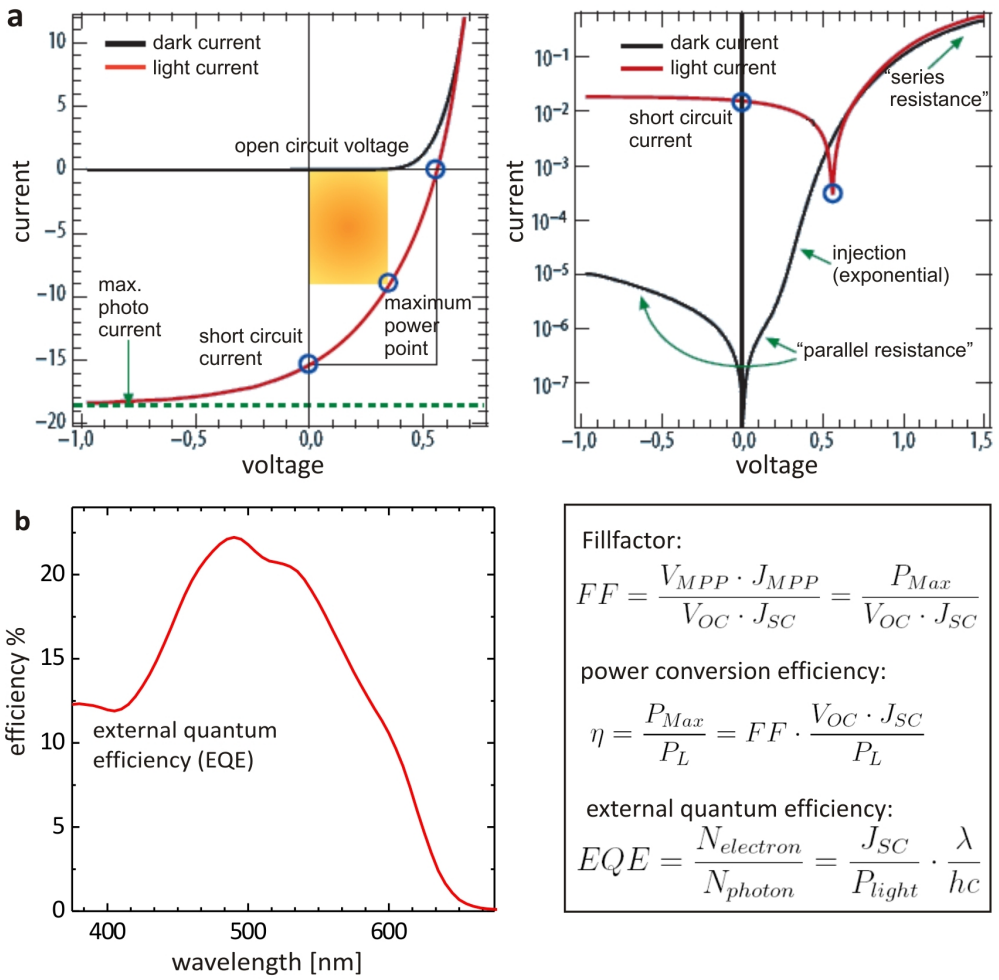

Figure 3.4: Characterization of solar cells. a) The open circuit voltage V_{OC}, the short circuit current J_{SC}, the fill factor FF and the power conversion efficiency η are determined form the $J-V$ characteristics (linear and log-plot are shown). Since the conductivity of organic materials is low, the formation of space charges leads to a voltage dependent series resistance also expressed as a space charge limited current (SCLC) *(reproduced from Deibel et al.[40])*. b) The spectral reference spectra plots the external quantum efficiency (EQE) in dependence of the wavelength λ is calculated gives the efficiency of conversion of number of photons N_{photon} to number of electrons $N_{electron}$ measured by measuring the short circuit current with a given power of illumination P_{light}.

3.3 Polymer Blends and Block Copolymers

Polymer Blends

The ability of using polymer blends in heterojunction solar cells is based on the fact that most polymers phase separate. A theoretical description of polymer phase separation is given by the mean field theory of Flory and Huggins.[41,42] In general, the entropy S in polymers is strongly reduced due to the long chain character of the molecules and the limited positional freedom of each monomer unit. The interaction between the monomer units is quantified by the Flory-Huggins interaction parameter χ, a dimensionless expression of the enthalpy of mixing H which plays a crucial role for mixing and demixing.

Suppose polymers A and B are mixed to form a blend, where $\Phi_A = \Phi$ is the monomer volume fraction of polymer A with N_A monomer units and $\Phi_B = 1 - \Phi$ is the monomer volume fraction of polymer B with N_B monomer units. The starting point for a thermodynamical treatment of miscibility is to find an expression for the free enthalpy of mixing ΔG for a mixture of polymers, which contains an enthalpic part ΔH and an entropic part ΔS,

$$\Delta G = \Delta H - T\Delta S, \tag{3.1}$$

$$\frac{\Delta G}{k_B T} = \chi \cdot \Phi(1-\Phi) + \left(\frac{\Phi}{N_A} \ln \Phi + \frac{1-\Phi}{N_B} \ln(1-\Phi) \right). \tag{3.2}$$

A phase diagram (Fig. 3.5) shows the parameter space in which a polymer blend mixes or demixes, as a function of the free energy, the volume fraction Φ and temperature T. Points with the same tangent at a certain temperature T in the free energy plot determine the volume fractions of a stable mixture. For temperatures below the critical point, this leads to the binodal locus in the phase diagram in a temperature vs. volume fraction plot, which separates the stable region from the metastable and unstable regions. The common tangent $\frac{dG}{dn_1} = \frac{dG}{dn_2}$ implies chemical potentials being equal $\mu_1 = \mu_2$, which results in a stable state.

The inflection points in the free entropy plot lead to the "spinodal" curve in the phase diagram, delimiting the unstable and metastable regions. In both regions, phase separation leads to decomposed domains of volume fraction ϕ_1 and ϕ_2 settled on the binodal. The two different demixing processes have consequences for the final morphology. Spinodal decomposition is governed by a spontaneous amplification of concentration variations, often leading to a fast coarsening of the morphology (Fig. 3.5b). In the metastable region composition fluctuation have to be nucleated, followed by domain growth, typically leading to a slower phase separation (Fig. 3.5c).
The important point is that polymer blends phase separate on a macroscopic scale. Furthermore, the phase purity (meaning Φ_1 and Φ_2) is not 100% polymer A or B, respectively.

In practice, polymer films are processed from solutions, for example, by spin-coating, blade-casting or ink-jet printing. The demixing kinetics are dominated by the evaporation of the solvent. Additional annealing procedures are applied to further

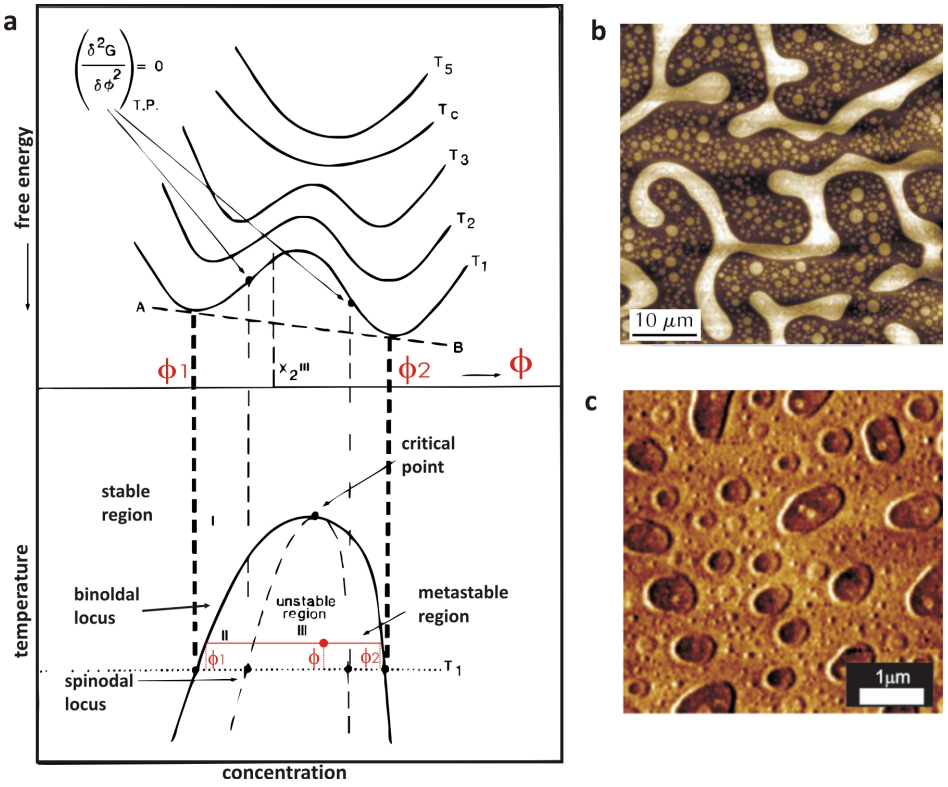

Figure 3.5: a) Free energy and temperature vs. volume fraction of a polymer of a blend. Blend demixes if it is within the parameter range of the phase diagram of the unstable or metastable region. The blend with a fraction Φ decomposes into two different domains, where one is enriched with polymer A (Φ_1) and the other with polymer B (Φ_2), as indicated in red. *(reproduced from[42])*. The decomposition process determines the morphology of the blend as shown in the AFM images: b) Coarsening of the morphology is possible as a result from decomposition from the unstable region *(reproduced from[43])* and c) nucleation and growth as a result of binodal decomposition.

adjust the frozen-in morphology, for example by thermal annealing or solvent-vapour annealing. Other strategies involve the use of different solvents or cosolvents[44] to control the evaporation rate and therefore the phase separation. The morphologies achieved are usually kinetically trapped, non-equilibrium structures. Polymer blends that are annealed for too long may exhibit domain sizes of few micrometres which are too large and not suited for bulk heterojunction solar cells.

Block Copolymers

Block copolymers are covalently linked polymers. The interconnectivity of the polymers restricts the formation of large domains, leading to a so called microphase separation. Helfand, Wassermann[45] and Leibler[46] developed theoretical descriptions of microphase separation. Matsen and Bates finally combined them in 1996.[47] The theories predict the phase morphology of an ordered block copolymer as a function of the volume fraction of the blocks A and B. Increasing the volume fraction of the minor block results in a sequence of morphologies starting from a spherical, to cylindrical, on to a gyroid

structure, and ending up with a lamellae structure for roughly equal volume fractions (Fig. 3.6). The length scale of each domain is of the order of the corresponding radius of gyration,[48] which results in structure sizes of $\sim 10 - 40\,\mathrm{nm}$.

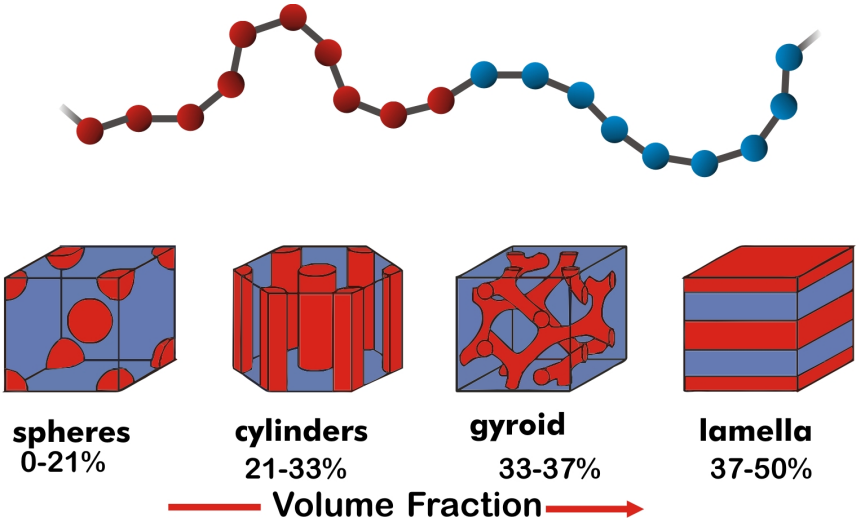

Figure 3.6: A diblock copolymer consists of two covalently linked polymers (red-blue). Block copolymers can phase separate into highly ordered nanostructures, by the so-called microphase separation. For amorphous-amorphous (coil-coil) block copolymers, morphologies range from spheres and cylinders to gyroids and lamellae, depending on the volume ratio of the blocks.

Block copolymers can be aligned in the bulk and thin films. Several concepts have been proposed to make block copolymers highly interesting for technological applications such as nanofabrication.[49] It is known that block copolymers films can be aligned by shear[50], or by exploiting surface properties such as the surface roughness,[51,52] or else by using electric fields.[53–55] This way large-area ordered nanostructures can be processed cost-efficiently, without the use of lithography[56] which can be used as nanostructured templates for example.[57]

The given phase morphologies in Fig. 3.6 is valid for fully-flexible amorphous-amorphous block copolymers. Crystallinity of one or both of the polymers blocks has a significant contribution to the enthalpy of the material system, thereby influencing the microphase separation.[58,59] The consequence is a rich phase behaviour that can be unique for each composite.[60] A more complex phase behaviour is also observed in rod-coil or rod-rod block copolymers. The term "coil" describes amorphous polymer segments, and the term "rods" is used for stiffer polymer segments. Rods often occur in conjugated polymers or in polymers containing helical secondary structures, aromatic groups and complex chain units.[61]

3.4 Fully Functionalised Block Copolymers for Organic Electronic Applications

With the domain size on the order of the exciton diffusion length and the ability to create highly ordered phases and self-assembled nanostructures, block copolymers provide an ideal platform for the realisation of bulk heterojunction solar cells. Fig. 3.7 shows an idealised structure of a bulk heterojunction solar cell: phase separation on the range of some tens of nanometers together with a mostly perpendicular orientation would provide a perfect structure. Such a morphology would

- allow sufficient light absorption, since the films could be made relatively thick,
- suit the short exciton diffusion length together with a large D-A interface, creating good charge generation,
- offer good charge percolation to the electrodes within the domains.

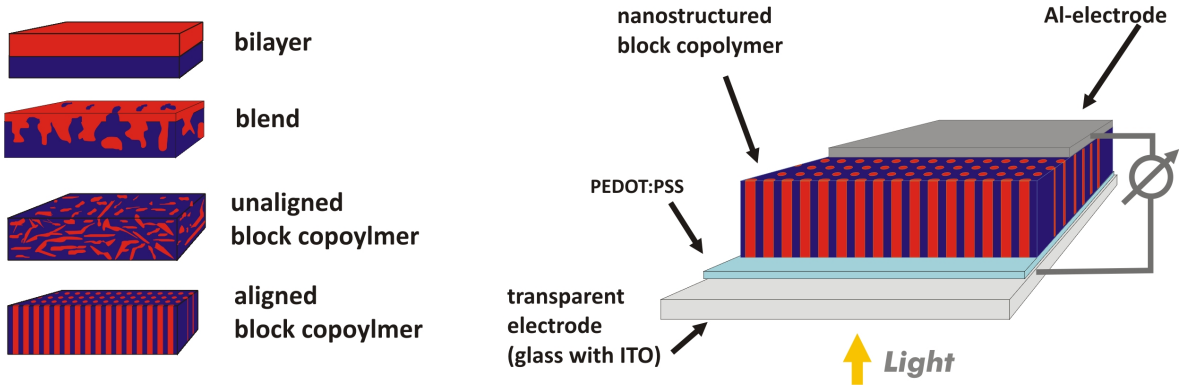

Figure 3.7: Morphologies for heterojunction concepts with increasing interface and decreasing donor acceptor separation. An aligned block copolymer as shown in the right cartoon fulfills the requirements for small, nanosized domains, high donor-acceptor interface and good charge percolation pathways to the electrodes.

The crucial point for the application of donor-acceptor block copolymers is the complex synthesis of the materials. The first synthesis on a donor-acceptor block copolymer has been reported by Hadziiannou et. al.[62] using a conjugated poly(phenylenevinylene) (PPV) and C_{60}-functionalised coil block. However, the strong interactions of the fullerenes prevent the expected microphase separation by cross-linking or aggregation.[63,64] In another study, Frechét et al. polymerised two macromonomers containing P3HT and fullerene which were used as compatibilisers in bulk heterojunction solar cells.[65] A first block copolymer-based solar cell has been reported based on a polymerised perylene bisimide derrivative and a polymerised triphenylamine.[66] This study was followed by other block copolymers using different donor blocks of additional triarylamines[67,68] and finally P3HT.[69] A detailed review summarizing various synthetic approaches can be found in Thelakkat et al.[70]

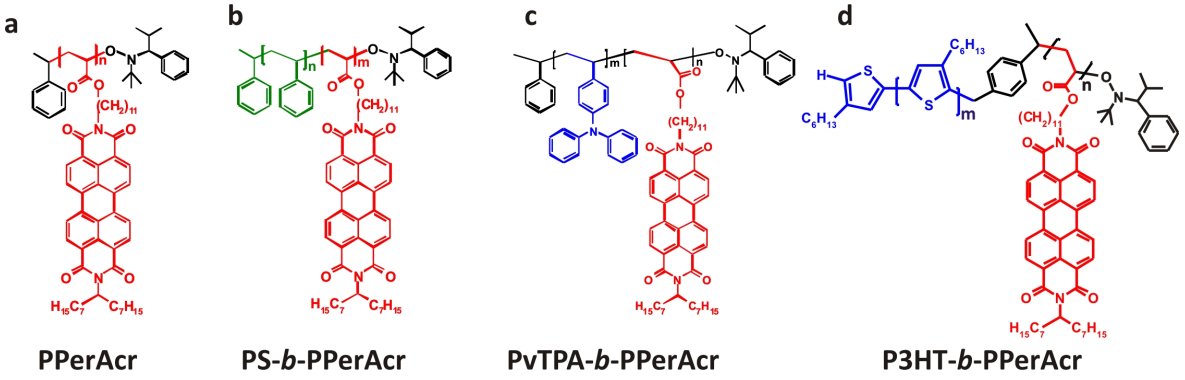

Figure 3.8: Molecular structures of perylene bisimide-based polymers and block copolymers. The perylene bisimide core is asymmetrically substituted. At one imide position the swallow's tail of alkyl chains provides the necessary solubility for the monomer. The other imide position is linked to an alkyl spacer which again is linked to a polyacrylate backbone. a) Homopolymer poly(perylene bisimide acrylate) PPerAcr, b) block copolymer of polystyrene and PPerAcr PS-*b*-PPerAcr, c) block copolymer of poly(triphenylamine) and PPerAcr PvTPA-*b*-PPerAcr, d) block copolymer of poly(hexylthiophene)(P3HT) and PPerAcr P3HT-*b*-PPerAcr.

The polymer and block copolymers that are presented here are based on the same acceptor block, poly(perylene bisimide acrylate) (PPerAcr) as shown in Fig. 3.8a. The PPerAcr block is used either as homopolymer alone, or is combined with electronically inactive polystyrene (PS), hole transporting amorphous poly(triphenylamine) (PvTPA) or semicrystalline poly(3-hexylthiophene) (P3HT). Perylene bisimides (PBIs) are well known electron acceptors. They show a broad absorbance in the visible light and they feature good n-type charge transport properties with a high air stability.[71,72] Their applications range from thin film transistors to photovoltaic devices and detectors.[36,73] PBIs have been synthetically modified in various ways from low molecular weight molecules that often exhibit liquid crystalline behaviour[74,75] to polymerised derivatives.[76–78] The electronic properties of a single PBI do not change upon substitution at the imide positions, which is due to the nodes of the wavefunctions at the imide groups.[79,80]

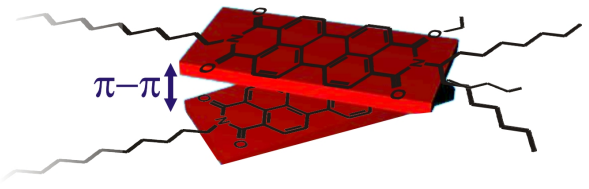

Figure 3.9: $\pi - \pi$ stacking of two perylene bisimide moieties. The strong interactions are caused by the overlap of the p-orbitals of the planar PBI cores. The interactions affect the optical and electrical properties, but also play a significant role in the formation of mesoscopic structures. The geometric alignment is influenced by the side groups attached at the nitrogen ends of the molecule.

These features make PBIs excellent candidates for n-type organic semiconductors. A major use for perylene bisimides is in the form of low molecular weight molecules. The incorporation of PBI moieties into polymers leads to new and unique material properties. A part of this thesis will focus on the characterisation and related optoelectronic properties of these materials. An important property is the strong $\pi - \pi$ interaction of the PBI moieties that lead to side chain crystallinity. Fig. 3.9 shows a scheme of the planar PBI cores. The crystallinity and the interaction of the PBI cores will dominate the ultimate structure formation. The incorporation of PPerAcr into block copolymers leads to hierarchical structures on different length scales: the intermolecular $\pi - \pi$ interactions on a length scale of $\sim$0.35 nm, the formation of crystalline stacks of PPerAcr in the range of 2-3 nm and the block copolymer microphase separation up to some tens of nanometers.

3.5 Organic Field Effect Transistors

A field effect transistor is one of the basic devices for most active electronics and circuits. Organic field effect transistors (OFETs) based on polymeric semiconductors have gathered a great deal of attention for their applications in printable electronics as well as in flexible electronics and displays.[81] From a basic science point of view, OFETs serve as very efficient tools for characterizing new organic materials in terms of their charge transport properties. After organic photovoltaic devices, they are another important organic electronic device described in this thesis. In the following, a short introduction to the working principles of field effect transistors is given. A more detailed description

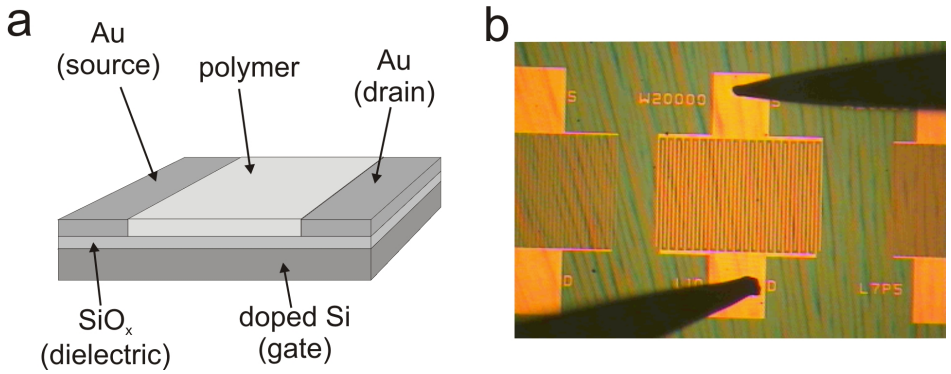

Figure 3.10: a) A Schematic of a bottom-gate, bottom-contact transistor processed on a silicon substrate. The gate is highly doped, conductive silicon. A silicon oxide layer (usually grown by wet oxidation) of around 200-250 nm serves as the gate dielectric. The source and drain contacts are lithographically patterned on top, where L is the separation of the source and drain electrode and W is the width of the electrodes. In order to increase the gate-width W, the electrodes are often patterned as interpenetrating electrodes. The polymer semiconductor is spincoated on top of the device. b) Microscopy image of the interpenetrating gold electrodes with a gate width $W = 20\,\mathrm{mm}$ and gate length $L = 10\,\mu\mathrm{m}$ covered by a spin-cast semiconductor film. The electrodes are contacted with probe tips that penetrate through the polymer film to the metal contact pads.

can be found in the literature.[15,82] Field effect transistors consist of a semiconducting material placed between a source and a drain contact. The semiconductor is separated by an insulator (often a gate oxide) from another electrode - the gate. Fig. 3.10 shows a schematic of an OFET in a bottom-gate bottom-contact configuration.

The substrates used in this work were highly-doped silicon wafers with a layer of silicon-oxide as a gate dielectric (200 nm). These are inert to solvents and stable at high temperatures and are, therefore, perfectly suited for targeting the characterisation of the active layer. Flexible substrates and polymer gate dielectric layers have also been used with the view of printable and flexible electronic circuitry applications. In addition, different configurations such as bottom gate – top contact or top contact – top gate can be used according to the application.

The basic operation regimes of a field effect transistor are shown in Fig. 3.11. A gate voltage V_G is applied across the gate dielectric controls the source-drain current. Charge carriers are induced through the source electrode and accumulate at the semiconductor-dielectric interface. Depending on the organic semiconductor material and the gate bias, either holes (negative gate potential) or electrons (positive gate potential) can be accumulated. First, deep traps have to be filled up and as soon as the gate voltage V_G exceeds the threshold voltage V_{Th}, a channel of mobile charge carriers

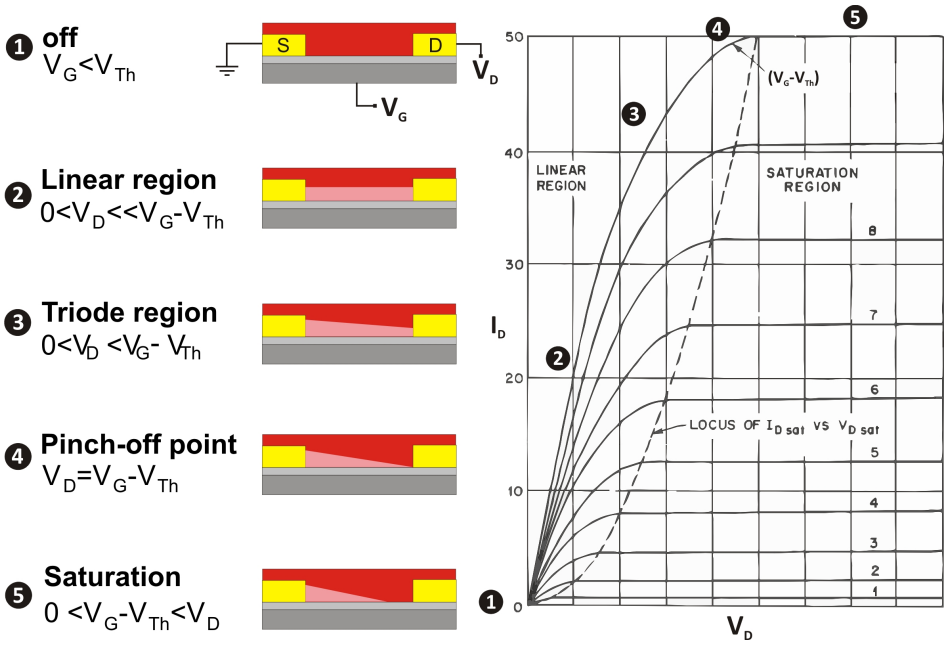

Figure 3.11: Schematic of a field effect transistor and its operation at different voltages. The graph shows the output characteristics, where the drain current I_D is plotted versus the drain-source voltage V_D for several gate voltages V_G. The gate and the drain voltage create a local potential and determine the charge carrier concentration within the channel. An accumulation of charges at semiconductor-dielectric interface is formed as soon as the gate voltage V_G exceeds the threshold voltage V_{Th} and the transistor works in the linear region, where V_D is proportional to the current I_D (2). Once V_D reaches the pinch-off point at $V_D = V_G - V_{Th}$, the current I_D ideally becomes independent of the drain voltage and is mainly controlled by the gate voltage V_G (5). The transistor is in saturation. (Reproduced from Sze[83])

accumulates. Additional voltage applied between the drain and the source V_D creates a current I_D. The magnitudes of the potentials V_G and V_D add up to a local potential, which determines the overall electric field at the channel and therefore the shape of the charge-carrier concentration in the channel. If $V_D \geq V_G - V_{Th}$, the channel is pinched off. A depletion zone may be created in the proximity of the drain electrode, if the local potential is below the threshold voltage. A space-charge limited current flows from the pinch-off point to the drain electrode. With even higher drain voltages V_D, the depletion zone becomes larger. Since the pinch-off point remains at nearly identical potential, the current I_D becomes virtually independent of the drain voltage, causing the current to saturate.

The current-voltage characteristics can be derived with the help of the gradual channel approximation. This model assumes that the electric field perpendicular to the source-drain current is much larger than the parallel field. This is correct for a sufficiently large channel length L. For channels with approximately $L < 10 \cdot d_{dielectric}$, short channel effects become increasingly important so that the gradual channel approximation no longer holds.[84]

Mobile charges Q_{mob} are induced and accumulate at the semiconductor-dielectric interface:

$$Q_{mob} = C_i(V_G - V_{Th}), \tag{3.3}$$

where C_i is the capacitance of the dielectric insulator. As soon as a source-drain bias is applied, an additional potential $V(x)$ has to be taken into account. It varies with distance x from the source electrode, so that

$$Q_{mob}(x) = C_i(V_G - V_{Th} - V(x)). \tag{3.4}$$

The source-drain current can be expressed as

$$I_D = W\mu Q_{mob} E_x, \tag{3.5}$$

where $E_x = \frac{dV}{dx}$ is the local field at the position x, W the gate width and μ the charge carrier mobility, so that we can write:

$$I_D dx = W\mu C_i(V_g - V_{Th} - V(x))dV \tag{3.6}$$

In the gradual channel approximation, an integration x from 0 to L corresponds an integration of $V(x)$ from 0 to V_D. This results in the following expression:

$$I_D = \frac{W}{L}\mu C_i[(V_G - V_{Th})V_D - \frac{1}{2}V_D^2] \tag{3.7}$$

Equation 3.7 can be simplified for the linear regime, where $V_D \ll V_G$ as

$$I_D = \frac{W}{L}\mu_{lin} C_i(V_G - V_{Th})V_D. \tag{3.8}$$

The charge carrier mobility then can be extracted form first derivative of I_d with respect to V_g, yielding the so-called transfer characteristics:

$$\mu_{lin} = \frac{\partial I_D}{\partial V_G}\frac{L}{WC_iV_D} \tag{3.9}$$

Once the pinch-off point is reached at $V_D = V_G - V_{Th}$, equation 3.7 no longer holds. The current stays constant, if we disregard the channel shortening. Thus in the saturation regime with $V_D = V_G - V_{Th}$ we can express the current as:

$$I_{Dsat} = \frac{W}{2L}\mu_{sat}C_i(V_G - V_{Th})^2. \tag{3.10}$$

The charge carrier mobility in the saturation regime can therefore be extracted with the help of the first derivative of $\sqrt{I_D}$ with respect to V_G:

$$\mu_{sat} = (\frac{\partial\sqrt{I_D}}{\partial V_G})^2 \frac{2L}{WC_i} \tag{3.11}$$

Fig. 3.11 shows the output characteristics of a FET. The current I_D is plotted versus the drain-source voltage V_D at different gate voltages. The transfer characteristics plot the current I_D as a function of the gate voltage V_G at constant V_D (Fig. 3.12a). The on-off ratio is given by the ratio of the currents when the transistor is turned on and off. A high on-off ratio with a small leakage current is desirable for the application of OFETs with clean switching properties. In order to determine the threshold voltage, a linear fit in the saturation regime of a $\sqrt{I_D}$ vs. V_G plot can be used. The intercept voltage is the threshold value V_{Th} (Fig. 3.12b).

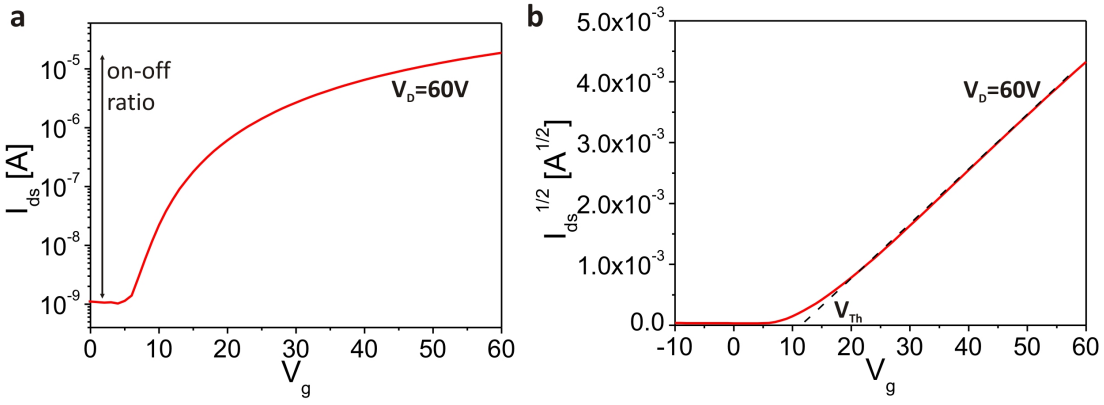

Figure 3.12: a) Logarithmic transfer plot of an n-type OFET. The transistor turns on as soon a certain voltage is exceeded, called onset voltage (V_{on}). The on-off ratio is the ratio of the drain current in the on and off states of the transistor. b) The threshold voltage V_{Th} is determined with the help of a $\sqrt{I_D}$ vs. V_G by linear extrapolation to 0. The intercept with the abscissa is the threshold voltage V_{Th}.

Bibliography

[1] A. Pochettino, Accad. Lincei Rend. **15**, 355 (1906).

[2] C.W. Tang, *Two-layer organic photovoltaic cell*, Appl. Phys. Lett. **48**, 183 (1986).

[3] J. H. Burroughes, D. D. C. Bradley, A. R. Brown, R. Marks, K. Mackey, R. H. Friend, P. L. Burns, and A. B. Holmes, *Light-emitting-diodes based on conjugated polymers*, Nature **347**, 539 (1990).

[4] C.J. Drury, C.M.J. Mutsaers, C.M. Hart, M. Matters, and D.M. de Leeuw, *Low-cost all-polymer integrated circuits*, Appl. Phys. Lett. **73**, 108 (1998).

[5] H. Sirringhaus, N. Tessler, and R. H. Friend, *Integrated optoelectronic devices based on conjugated polymers*, Science **180**, 1741 (1998).

[6] G. Yu, J. Gao, J. Hummelen, F. Wudl, and A. Heeger, *Polymer photovoltaic cells: enhanced efficiencies via a network of internal donor-acceptor heterojunctions*, Science **270**, 1789 (1995).

[7] J. Peet, J. Y. Kim, N. E. Coates, W. L. Ma, D. Moses, A. J. Heeger, and G. C. Bazan, *Efficiency enhancement in low-bandgap polymer solar cells by processing with alkane dithiols*, Nat. Mater. **6**, 497 (2007).

[8] H.-Y. Chen, J. Hou, S. Zhang, Y. Liang, G. Yang, Y. Yang, L. Yu, Y. Wu, and G. Li, *Polymer solar cells with enhanced open-circuit voltage and efficiency*, Nat. Phot. **3**, 649 (2009).

[9] C.J. Brabec, *Organic photovoltaics: technology and market*, Sol. energy Mater. Sol. Cells **83**, 273 (2004).

[10] Z. Valy Vardeny, Alan J. Heeger, and Ananth Dodabalapur, *Fundamental research needs in organic electronic materials*, Synth. Met. **148**, 1 (2005).

[11] V.S. Arunachalam and E.L. Fleischer, *The global energy landscape and materilas innovation*, MRS Bulletin **33**, 264 (2008).

[12] W. Fix, *Elektronik von der Rolle*, Physik Journal **7**, 47 (2008).

[13] S. A. Jenekhe, *Polymer semiconductors: A fast mover with a bright spark*, Nat. Mater. **7**, 354 (2004).

[14] H. Hoppe and N.S. Sariciftci, *Organic solar cells: An overview*, J. Mater. Res. **19**, 1924 (2004).

[15] J. Zaumseil and H. Sirringhaus, *Electron and ambipolar transport in organic field-effect transistors*, Chem. Rev. **107**, 1296 (2007).

[16] S. Westenhoff, I.A. Howard, and R.H. Friend, *Probing the morphology and energy landscape of blends of conjugated polymers with sub-10 nm resolution*, Phys. Rev. Lett. **101**, 016102 (2008).

[17] A. Babel and S.A. Jenekhe, *Morphology and field-effect mobility of charge carriers in binary belnds of poly(3-hexylthiophene) with poly[2-methoxy-5-(2–ethylhexoxy)-1,4-phenylenevinylene] and polystyrene*, Macromolecules **37**, 9835 (2004).

[18] Th. B. Singh, S. Günes, N. Marjanovic, N. S. Sariciftci, and R. Menon, *Correlation between morphology and ambipolar transport in organic field-effect transistors*, J. Appl. Phys. **97**, 114508 (2005).

[19] K.M. Coakley and M.D. McGehee, *Conjugated polymer photovoltaic cells*, J. Chem. Mater. **16**, 4533 (2004).

[20] Stefan Lindner, Ph.D. thesis, University of Bayreuth, 2005.

[21] Michael Sommer, Ph.D. thesis, Univeristy of Bayreuth, 2009.

[22] M. Schwoerer and H.C. Wolf, *Organische Molekulare Festkörper* (Wiley-VHC, Weinheim, 2005).

[23] Martin Pope and Charles E. Swenberg, *Electronic processes in organic crystals* (Oxford University Press, New York, 1999).

[24] V. D. Mihailetchi, L. J. A. Koster, J. C. Hummelen, and P. W. M. Blom, *Photocurrent generation in polymer-fullerene bulk heterojunctions*, Phys. Rev. Lett. **94**, 216601 (2004).

[25] A.C. Morteani, P. Sreearunothai, L.M. Herz, R.H. Friend, and C. Silva, *Exciton regeneration at polymeric semiconductor heterojunctions*, Phys. Rev. Lett. **92**, 247402 (2004).

[26] S. Westenhoff, I.A. Howard, J.M. Hodgkiss, K.R. Kirov, H.A. Bronstein, C.K. Williams, N.C. Greenham, and R.H. Friend, *Charge recombination in organic photovoltaic devices with high open-circuit voltages*, J. Am. Chem. Soc. **130**, 13653 (2008).

[27] H. Sano and M. Tachiya, *Partially diffusion-controlled recombination*, J. Am. Chem. Soc. **71**, 1276 (1979).

[28] R. A. Marcus, *Nonadiabatic processes involving quantum-like and classical-like coordinates with applications to nonadiabatic electron transfers*, J.Chem. Phys. **81**, 4494 (1984).

[29] H. Bässler, *Charge transport in organic disordered photoconductors*, Phys. Stat. Sol. (b) **175**, 15 (1993).

[30] S.R. Forrest, *The limits to organic photovoltaic cell efficiency*, MRS Bulletin **30**, 28 (2005).

[31] D. E. Markov, E. Amsterdam, P. W. M. Blom, A. B. Sieval, and J. C. Hummelen, *Accurate measurement of the exciton diffusion length in a conjugated polymer using a heterostructure with a side-chain cross-linked fullerene layer*, J. Phys. Chem. A **109**, 5266 (2005).

[32] N. S. Sariciftci, D. Braun, C. Zhang, V. I. Srdanov, A. J. Heeger, G. Stucky, and F. Wudl, *Semiconducting polymer-buckminsterfullerene heterojunctions: Diodes, photodiodes, and photovoltaic cells*, Appl. Phys. Let. **62**, 585 (1993).

[33] J.J.M. Halls, C.A. Walsh, N.C. Greenham, E. A. Marseglia, R.H. Friend, S. C. Moratti, and A.B. Holmes, *Efficient photodiodes from interpenetrating polymer networks*, Nature **376**, 498 (1995).

[34] C. J. Brabec, N. S. Saricifti, and J. C. Hummelen, *Plastic solar cells*, Adv. Func. Mater. **11**, 15 (2001).

[35] H. Spanggard and F.C. Krebs, *A brief history of the development of organic and polymeric photovoltaics*, Sol. energy Mater. Sol. Cells **83**, 125 (2004).

[36] L. Schmidt-Mende, A. Fechtenkötter, K. Müllen, E. Moons, R.H. Friend, and J.D. MacKenzie, *Self-organized discotic liquid crystals for high-efficiency organic photovoltaics*, Science **293**, 1119 (2001).

[37] B. Friedel, P.E. Keivanidis, T.J.K. Brenner, A. Abrusci, C.R. McNeill, R.H. Friend, and N.C Greenham, *Effects of layer thickness and annealing of PEDOT:PSS layers in organic photodetectors*, Macromol. **42**, 6741 (2009).

[38] S. Y. Heriot and R. A. L. Jones, *An interfacial instability in a transient wetting layer leads to lateral phase separation in thin spin-cast polymer-blend films*, Nat. Mater. **4**, 782 (2005).

[39] P. Peumans, S. Uchida, and S.R. Forrest, *Efficient bulk heterojunction photovoltaic cells using small-molecular-weight organic thin films*, Nature **425**, 158 (2003).

[40] C. Deibel and V. Dyakonov, *Sonnenstrom aus Plastik*, Physik Journal **7**, 51 (2008).

[41] G.R. Strobl, *The physics of polymers* (Springer Verlag, Berlin, 1996).

[42] J. M. G. Cowie, *Polymers - chemistry and physics of modern materials* (Blackie Acad. & Professional, London, 1994).

[43] G. Malliaras and R. Friend, Physics Today **58**, 53 (2005).

[44] A.R. Campbell, J.M. Hodgkiss, S. Westenhoff, I.A. Howard, R.A. Marsh, C.R. McNeill, R.H. Friend, and N.C. Greenham, *Low-temperature control of nanoscale morphology for high performance polymer photovoltaics*, Nanolett. **8**, 3942 (2008).

[45] E. Helfand and Z.R. Wassermann, *Block copolymer theory. 4. Narrow interphase approximation*, Macromolecules **9**, 879 (1976).

[46] L. Leibler, *Theory of microphase separation in block copolymers*, Macromolecules **13**, 1602 (1980).

[47] M.W. Matsen and F.S. Bates, *Unifying weak- and strong-segregation block copolymer theories*, Macromolecules **12**, 1091 (1996).

[48] I.W. Hamley, *The physics of block copolymers* (Oxford University Press, Oxford, 1998).

[49] C. Park, J. Yoon, and E.L. Thomas, *Enabling nanotechnology with self assembled block copolymer patterns*, Polymer **44**, 6725 (2003).

[50] D. E. Angelescu, J. H. Waller, R. A. Register, and P. M. Chaikin, *Shear-induced alignment in thin films of spherical nanodomains*, Adv. Mater. **17**, 1878 (2005).

[51] A.C. Arias, N. Corcoran, M. Banach, R.H. Friend, J. D. MacKenzie, and W.T.S. Huck, *Vertically segregated polymer-blend photovoltaic thin-film structures through surface-mediated solution processing*, Appl. Phys. Lett. **80**, 1695 (2002).

[52] E. Sivaniah, y. Hayashi, M. Iino, and T. Hashimoto, *Observation of perpendicular orientation in symmetric diblock copolymer thin films on rough substrates*, Macromolecules **36**, 5894 (2003).

[53] K. Amundson, E. Helfand, D.D. Davis, X. Quan, S.S. Patel, and S.D. Smith, *Effect of electric field on block copolymer microstructure*, Macromolecules **24**, 6547 (1991).

[54] P. Mansky, J. DeRouchey, and T.P. Russel, *Large.area domain alignmen in block copolymer thin films using electric fields*, Macromolecules **31**, 4399 (1998).

[55] T. Thurn-Albrecht, J. DeRouchey, and T.P. Russel, *Overcoming interfacial interactions with electric fields*, Macromolecules **33**, 3250 (2000).

[56] S. Park, D.H. Lee, J. Xu, B. Kim, S.W. Hong, U. Jeong, T. Xu, and T.P. Russell, *Macroscopic 10-terabit-per-square-inch arrays from block copolymers with lateral order*, Science **323**, 1030 (2009).

[57] E. J. W. Crossland, M. Nedelcu, C. Ducat, S. Ludwigs, M.A. Hillmyer, U. Steiner, and H.J. Snaith, *Block copolymer morphologies in dye-sensitized solar cells: probing the photovoltaic structure-function relation*, Nano Lett. **9**, 2813Ű2819 (2009).

[58] I.W. Hamley, J.P.A. Fairclough, A. Ryan, F.S. Bates, and E. Towns-Andrews, *Crystallization of nanoscale-confined diblock copolymer chains*, Polymer **37**, 4425 (1996).

[59] I. W. Hamley, P. Parras, V. Castelletto, R. V. Castillo, A. J. Müller, E. Pollet, P. Dubois, and C. M. Martin, *Melt structure and its transformation by sequential crystallization of the two blocks within poly(L-lactide)-block-poly(epsiv-caprolactone) double crystalline diblock copolymers*, Macromol. Chem. Phys **207**, 941 (2006).

[60] Y.-L. Loo, R.A. Register, and A.J. Ryan, *Modes of crystallization in block copolymer microdomains: breakout, templated, and confined*, Macromol. **35**, 2365 (2002).

[61] Bradley D. Olsen and Rachel A. Segalman, *Self-assembly of rod-coil block copolymers*, Mater. Sci. and Eng. **62**, 37 (2008).

[62] Ulf Stalmach, Bert de Boer, Christine Videlot, Paul F. van Hutten, and Georges Hadziioannou, *Semiconducting diblock copolymers synthesized by means of controlled radical polymerization techniques*, J. Am. Chem. Soc. **122**, 5464 (2000).

[63] M.H. van der Veen, B. de Boer, U. Stalmach, K.I. van de Wetering, and G. Hadziioannou, *Donor-acceptor diblock copolymers based on PPV and C_{60}: Synthesis, thermal properties, and morphology*, Macromolecules **37**, 3673 (2004).

[64] S. Barrau, T. Heiser, F. Richard, C. Brochon, C. Ngov, K. van de Wetering, G. Hadziioannou, D. V. Anokhin, and D. A. Ivanov, *Self-assembling of novel fullerene-grafted donor-acceptor rod-coil block copolymers*, Macromol. **41**, 2701 (2008).

[65] K. Sivula, Z. T. Ball, N. Watanabe, and J. M. J. Frechet, *Amphiphilic diblock copolymer compatibilizers and their effect on the morphology and performance of polythiophene:fullerene solar cells*, Adv. Mater. **18**, 206 (2006).

[66] S. Lindner, S. Hüttner, A. Chiche, M. Thelakkat, and G. Krausch, *Charge separation at self-assembled nanostructured bulk interfaces in block copolmers*, Angew. Chem. Int. Ed. **45**, 3364 (2006).

[67] M. Sommer and M. Thelakkat, *Synthesis, characterization and application of donor-acceptor block copolymers in nanostructured bulk heterojunction solar cells*, Eur. Phys. J. Appl. Phys **36**, 245 (2006).

[68] M. Sommer, S. Lindner, and M. Thelakkat, *Microphase-separated donor-acceptor diblock copolymers: influence of HOMO energy levels and morphology on polymer solar cells*, Adv. Func. Mater. **17**, 1493 (2007).

[69] M. Sommer, A. S. Lang, and M. Thelakkat, *Crystalline-crystalline donor-acceptor block copolymers*, Angew. Chem. Int. Ed. **47**, 7901 (2008).

[70] M. Sommer, S. Hüttner, and M. Thelakkat, *Donor-acceptor block copolymers with nanoscale morphology for photovoltaic*, Adv. Poly. Sci. in print (2010).

[71] B.A. Jones, A. Facchetti, M.R. Wasielewski, and T.J. Marks, *Tuning orbital energetics in arylene diimide semiconductors. Materials design for ambient stability of n-type charge transport*, J. Am. Chem. Soc. **129**, 15259 (2007).

[72] J.E. Anthony, M. Heeney, and B.S. Ong, *Synthetic aspects of organic semiconductors*, MRS Bulletin **33**, 698 (2008).

[73] B.A. Gregg, *The photoconversion mechanism of excitonic solar cells*, MRS Bulletin **30**, 20 (2005).

[74] Z. Chen, V. Stepanenko, V. Dehm, P. Prins, L.D.A. Siebbeles, J. Seibt, P. Marquetand, V. Engel, and F. Würthner, *Photoluminecence and conductivity of self-assembled $\pi - pi$ stacks of perylene bisimide dyes*, Chem. Eur. J. **13**, 436 (2007).

[75] A. Wicklein, A. Lang, M. Muth, and M. Thelakkat, *Swallow-tail substituted liquid crystalline perylene bisimides: Synthesis and thermotropic properties*, J. Am. Chem. Soc. **131**, 14442 (2009).

[76] E.E. Neuteboom, S.C.J. Meskers, E.W. Meijer, and R.A.J. Janssen, *Photoluminescence of Self-organized Perylene Bisimide Polymers*, Macromolecular Chemistry and Physics **205**, 217 (2004).

[77] P. A.J. De Witte, J. Hernando, E.E. Neuteboom, E.M.H.P. van Dijk, S.C.J. Meskers, R. A.J. Janssen, N.F. van Hulst, R.J.M. Nolte, M.F. García-Parajó, and A.E. Rowan, *Synthesis and characterization of long perylenediimide polymer fibers: from bulk to the single-molecule level*, Phys. Chem. B **110**, 7803 (2006).

[78] S. Lindner and M. Thelakkat, *Nanostructres of n-type organic semiconductor in a p-type matrix via self-assembly of block copolymers*, Macromolecules **37**, 8832 (2004).

[79] P.M. Kazmaier and R. Hoffman, *A theoretical study of crystallochromy. Quantum interference effects in the spectra of perylene pigments*, J. Am. Chem. Soc. **116**, 9684 (1994).

[80] K. Balakrishnan, A. Datar, T. Naddo, J. Huang, R. Oitker, M. Yen, J. Zhao, and L. Zang, *Effect of side-chain substituents on self-assembly of perylene diimide molecules: morphology control*, J. Am. Chem. Soc. **128**, 7390 (2006).

[81] H. Sirringhaus, T. Kawase, and R.H. Friend, *High-resolution ink-jet printing of all-polymer transistor circuits*, MRS Bulletin **26**, 539 (2001).

[82] Z. Bao and J. Locklin, in *Organic field-effect transistors*, edited by Z. Bao and J. Locklin (CRC Press, Boca Raton, 2007).

[83] S.M. Sze and K.K. Ng, *Physics of semiconductor devices* (John Wiley & Sons, New York, 2007).

[84] J.N. Haddock, X. Zhang, S. Zheng, Q. Zhang, S.R. Marder, and B. Kippelen, *A comprehensive study of short channel effects in organic field-effect transistors*, Organic Elelectronics **7**, 45 (2006).

Chapter 4

Overview

This thesis deals with the characterisation of optoelectronic properties and the establishment of structure-function relations of electronically active polymeric materials. These polymers are incorporated into block copolymers consisting of donor and acceptor blocks. Both homopolymers and block copolymers are subsequently utilised and characterised in organic photovoltaics (OPV) as well as organic field effect transistors (OFETs). Donor-acceptor block copolymers are promising since both blocks can phase separate by self-assembly into ordered nanostructures, so-called microphases. This feature is important for the efficient operation of bulk heterojunction photovoltaic cells, but also bears interesting new applications for OFETs.

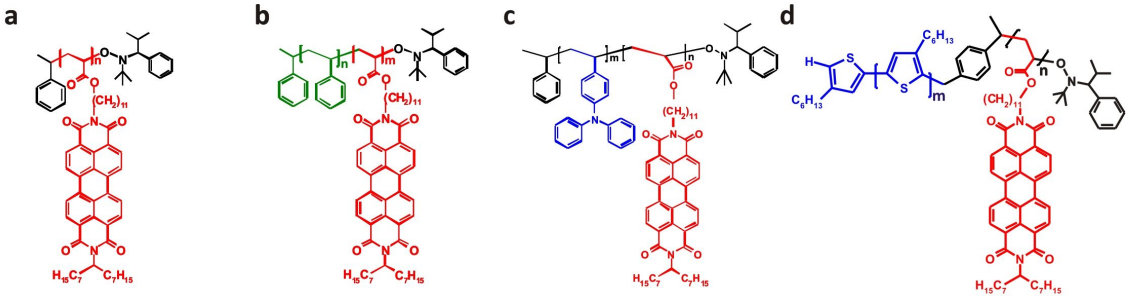

PPerAcr
Homopolymer of poly (perylene bisimide acrylate) (PPerAcr). The perylene bisimides render a side chain crystalline polymer. It features good electron transport capabilities and serves as the acceptor block for all studied heterojunction systems.

PS-*b*-PPerAcr
Block copolymer (BCP) based on an inert block of poly(styrene) (PS) and PPerAcr. It serves as a model BCP for amorphous-side chain crystalline BCP.

PvTPA-*b*-PPerAcr
First fully functionalised donor-acceptor BCP that was incorporated into a photovoltaic device. The BCP is based on an amorphous block of poly (vinyl triphenylamine) (PvTPA) as donor material and PPerAcr as acceptor material.

P3HT-*b*-PPerAcr
Fully functionalised donor-acceptor BCP based on two crystalline blocks of poly(3-hexylthiophene) P3HT and PPerAcr. This polymers achieves the highest external quantum efficienices.

Figure 4.1: Molecular structures of perylene bisimide based polymers and block copolymers.

A poly(perylene bisimide acrylate) (PPerAcr) is chosen as the acceptor material. In this polymer, perylene bisimide units are attached to a polyacrylate backbone. Fig. 4.1 depicts an overview of the block copolymers containing PPerAcr as an acceptor (n-type) polymer block. The perylene bisimides are polymerised to different macroinitiators, for example, an electronically inactive polystyrene (PS) block (Fig. 4.1b) or a donor block of poly(vinyl triphenylamine) (PvTPA, Fig. 4.1c, 4.2b) or conjugated poly(3-hexylthiophenes) (P3HTs, Fig. 4.1d, 4.2c). Perylene bisimide (PBI) is a well-known electron acceptor and electron transporting material. An important property of PBIs is the $\pi-\pi$ interaction of the PBI moieties, which leads to side chain crystallinity

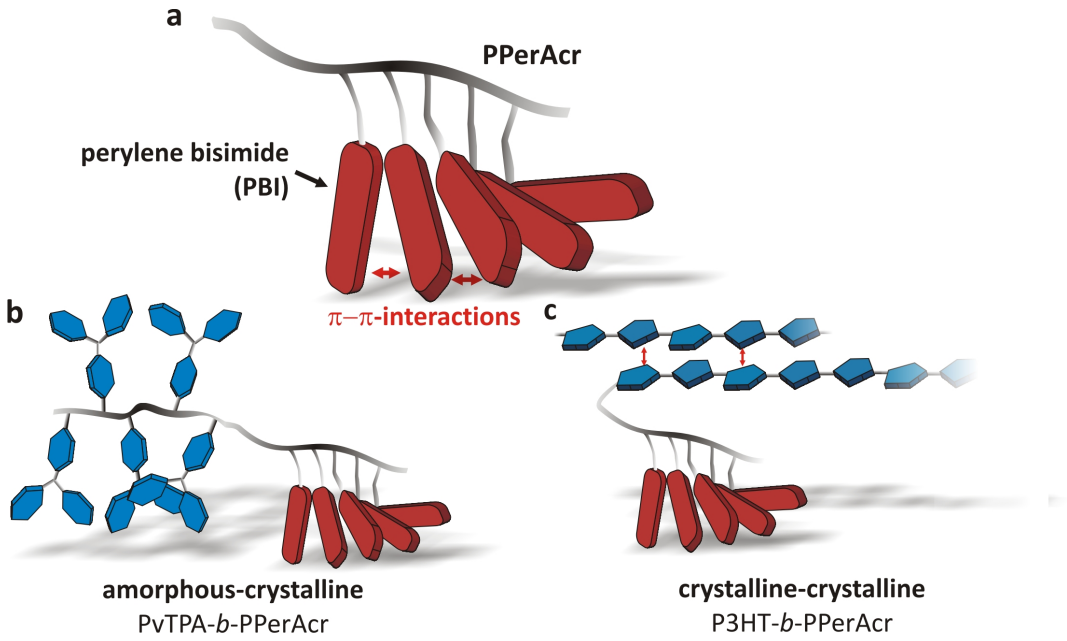

Figure 4.2: a) Poly(perylene bisimide acrylate) PPerAcr is a side-chain crystalline polymer due to the $\pi - \pi$ interactions between the perylene bisimide (PBI) moieties. b) Amorphous-crystalline block copolymer PvTPA-*b*-PPerAcr. c) Double crystalline block copolymer P3HT-*b*-PPerAcr. Poly(3-hexylthiophene) (P3HT) exhibits main chain polymer crystallinity.

of PPerAcr (Fig. 4.1a, 4.2a).

This thesis consists of seven manuscripts that focus on different aspects of these novel materials. Chapter 5 focuses on the n-type transport properties of PPerAcr in OFETs. Chapter 6 investigates in detail the solvent-vapour annealing of PPerAcr and establishes respective annealing procedures. Chapter 7 gives a detailed description of the optical, electronic and structural properties of the perylene bisimide moieties as they are incorporated into polymers and block copolymers with a second amorphous block. OPVs based on block copolymers containing PvTPA are presented as well. The following chapter 8 investigates the charge transport properties of PvTPA and further poly(triarylamines) in OFETs. Another well-known hole transporting donor material is the semi-crystalline polymer poly(3-hexylthiophene) (P3HT). Block copolymers of P3HT-*b*-PPerAcr are in the focus of the subsequent chapters. Chapter 9 demonstrates the application of these double-crystalline block copolymers in OFETs offering adjustable n-type, p-tpye or ambipolar charge transport. Chapter 10 deals with the application of P3HT-*b*-PPerAcr to OPVs and chapter 11 continues by investigating the photophysics of these block copolymers. Additionally, in the annex an outlook towards the use of these materials as a blend compatibiliser is given.

N-type organic field effect transistors from perylene bisimide block copolymers and homopolymers

PPerAcr acts as an acceptor material, i.e. an electron transporting material. Chapter 5 focuses on the characterisation of PPerAcr (Fig. 4.1a) in OFETs. In addition to the homopolymer, we have also characterised the model block copolymer PS-*b*-PPerAcr (Fig. 4.1b). We have processed OFETs in a bottom contact, bottom gate configuration, using gold as both the source and the drain electrodes (Fig. 4.3). After spin-coating the performance of the PPerAcr devices was rather weak, with low charge-carrier mobilities of less than $10^{-5}\,\frac{\mathrm{cm}^2}{\mathrm{Vs}}$ and high threshold voltages. However, after applying an annealing step above the melting temperature of the material, the OFET performance significantly improved. We measured mobilities of up to $10^{-3}\,\frac{\mathrm{cm}^2}{\mathrm{Vs}}$, with low threshold voltages of around 5 V. Thermal annealing enhanced electron transport between the moieties and improved the wetting of the gold electrodes. The results show that in this form polymerised PBIs achieve good charge transport for the rare class of n-type polymers.

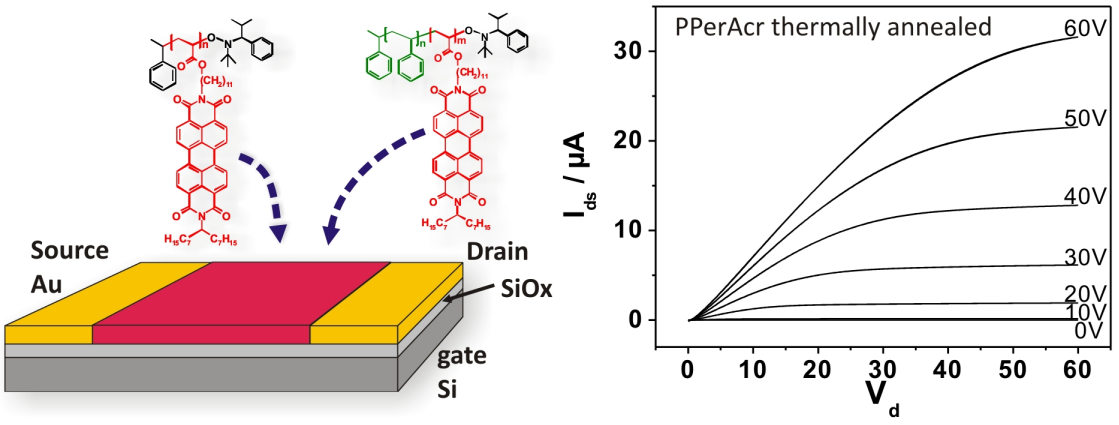

Figure 4.3: n-type OFETs from PPerAcr and PS-*b*-PPerAcr exhibit excellent electron transport and good electron injection from gold electrodes, with mobilites of $\sim 10^{-3}\,\frac{\mathrm{cm}^2}{\mathrm{Vs}}$. The plot depicts the output characteristics of a PPerAcr OFET, thermally annealed after spin-coating. The annealing is essential to obtain an increased PBI aggregation enhancing the charge transport.

We have also processed OFETs from the model BCP PS-*b*-PPerAcr containing 30 wt% polystyrene, which forms a cylindrical morphology. The OFET performance after thermal annealing was almost identical to the pristine PPerAcr. This finding motivates the further incorporation of PPerAcr into block copolymer architectures as an excellent polymeric electron transporter.

Solvent-vapour annealing for organic electronics

Polymer thin films are usually processed from organic solvents. The fast evaporation of low boiling point solvents such as chloroform during spin-coating leads to a kinetic trapping of the polymer chains, far from their thermodynamic melt equilibrium. As a consequence, block copolymers often cannot form highly ordered microphases. In order to induce mobility in the polymer chains, so that phase separation will occur, additional annealing is required. Annealing can be performed either thermally, by increasing the temperature above the glass transition or the melting temperature, or by the controlled introduction of solvent molecules into the polymer films through a solvent-vapour atmosphere.

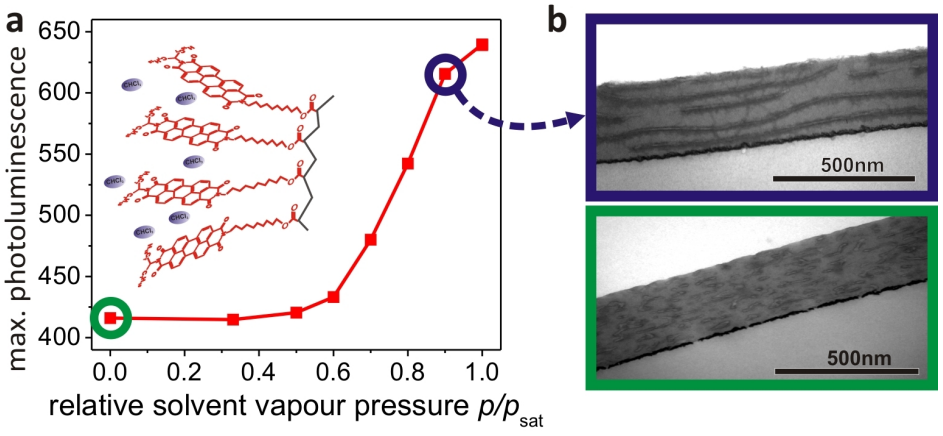

Figure 4.4: a) At a partial vapour pressure of chloroform >0.6, the aggregates of the PDIs become increasingly distorted, which can be seen in the fast rise of the photoluminescence. b) This induces sufficient mobility to the block copolymer chains, which enables phase separation into lamella, as the electron microscopy cross sections show.

Initially, we investigated the effect of solvent vapour exposure on the homopolymer PPerAcr (Fig. 4.1a). The partial vapour pressure of chloroform was carefully controlled and the films of PPerAcr were exposed to this atmosphere. The thickness of the films was measured by ellipsometry and the absorption spectra and photoluminescence were tracked in-situ in specially fabricated chambers. We found that above a certain solvent vapour saturation (i.e. at a certain partial vapour pressure) of $> 60\%$, the strong $\pi - \pi$-aggregates get interrupted by solvent molecules. This is evident from the changes in the absorption spectra, which begin to resemble solution spectra. The enhancement of the photoluminescence is another indication of the decreased aggregation of the perylene bisimide moieties (Fig. 4.4).

Transferring these results to the BCP PvTPA-*b*-PPerAcr (Fig. 4.1c) allowed us to achieve large ordered structures. After solvent-vapour exposure, lamellae of PPerAcr with long-range order assembled parallel to the substrate. These large morphological changes could not be induced by thermal annealing. Furthermore, the low processing temperature prevented the degradation of the temperature-sensitive organic electronic materials. Since π-interactions are prevalent in a wide range of conjugated systems for organic electronics, the methods presented herein offer a way to track the evolution of morphology upon solvent vapour exposure, thereby optimising annealing conditions.

Intermolecular interactions in perylene bisimide polymer architectures

The previous chapter pointed out the effect of intermolecular interactions on polymer dynamics during solvent vapour annealing. However, the intermolecular interactions of the PBI moieties also affect the optical and electronic properties. This chapter investigates the optical and electronic properties of the materials described above in increasingly complex architectures, starting from a low molecular weight model of PBI, to the homopolymer PPerAcr, to amorphous-crystalline block copolymers PS-*b*-PPerAcr and PvTPA-*b*-PPerAcr. The comparison starts with the low molecular weight PBI and its optical properties in solution with the homopolymer PPerAcr. In PPerAcr intermolecular interactions are always prevalent, due to the geometric proximity of these side groups to the polyacrylate backbone. Even at high dilution, the emission is governed by aggregates, indicated by a large red-shift compared to the diluted monomeric species.

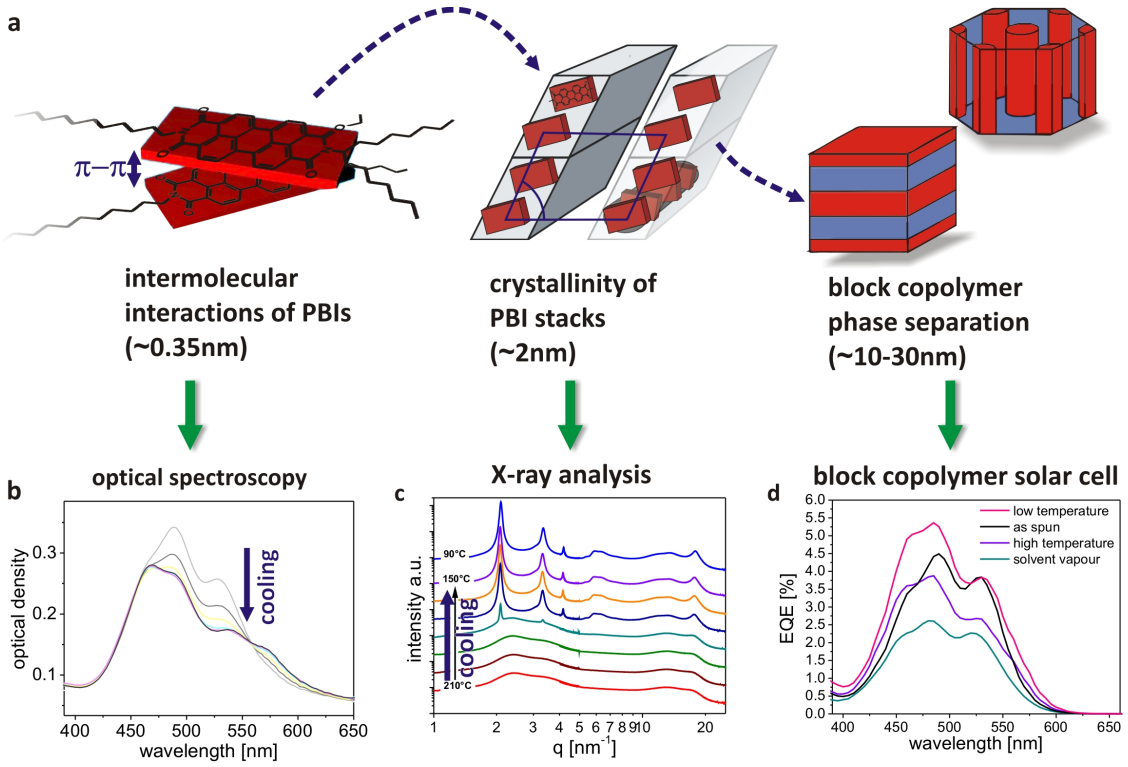

Figure 4.5: a) The incorporation of PBIs into block copolymers leads to hierarchical structures on different length scales: the intermolecular $\pi-\pi$ interactions on a lengthscale of ~0.35 nm, the formation of crystalline stacks of PPerAcr in the range of 2-3 nm and the block copolymer microphase separation up to some tens of nanometers. Different methods are applied to access the different aspects of the hierarchical order. b) The electronic coupling influences the absorption properties, c) X-ray diffraction tracks the crystalline structures and d) OPVs made of the block copolymer with different annealing procedures are compared.

The intermolecular aggregation of the PBI moieties can also be enhanced by thermal annealing. Temperature-dependent X-ray diffraction measurements performed with synchrotron radiation allowed us to track the crystallinity as a function of time

and temperature. The melting temperature of PPerAcr is at 190 °C, however, local rearrangements of the PBI moieties already take place at temperatures as low as 130 °C. Furthermore the crystallinity of PPerAcr, which can be indexed with a 2-dimensional oblique lattice of PBI stacks, depends on the cooling kinetics when the sample is cooled from the melt (>190 °C). A slow cooling rate of 10 $\frac{\mathrm{K}}{\mathrm{min}}$ yields a high crystallinity, i.e. the formation of large PBI aggregates. The X-ray diffraction measurements directly correlate with the absorption spectroscopy measurements performed at the same temperatures. The UV-vis spectra recorded in situ during the recrystallisation process reveal the effect of the operative coupling of the dipole moments in the PBI aggregates. This leads to a low energy feature at 580 nm, but also to a shift of the vibronic features of the absorption, attributed to an intermixing of Frenkel excitons and charge transfer excitons.

Mobility measurements in OFET devices subjected to different annealing procedures show the correlation between aggregate formation and transport properties. The charge carrier mobility is lowest in spin-coated devices at 10^{-5} $\frac{\mathrm{cm}^2}{\mathrm{Vs}}$, but increases by one order of magnitude through annealing below the melting temperature at 160 °C. Annealing above the melting temperature together with a slow cooldown enhances the crystallinity of PPerAcr and enhances the mobility by two orders of magnitude.

The comparison of the block copolymers with an inert block of polystyrene and a donor block of PvTPA yielded similar results for selected annealing methods. Those included as-spun films, solvent-vapour annealed films with and without an additional low temperature treatment (160 °C), as well as only low- and high-temperature treatments (215 °C) with slow and fast cooling rates. With this set of annealing parameters, it is possible to cover a wide range of phenomena, from local rearrangements of the PBI moieties on the intermolecular scale to large scale polymer chain rearrangements. The crucial point is that in these amorphous-crystalline block copolymers, PBI aggregation stays the same even with confinement in a block copolymer microphase.

Finally, the photoluminescence quenching yield of the donor containing block copolymer is related to the actual external quantum efficiencies (EQEs) of photovoltaic devices and their morphology. The highest EQEs are achieved with samples annealed at low temperatures (160°C). The morphology and mobility are optimised there with respect to the interplay of charge carrier mobility, interfacial area and charge percolation.

Organic field effect transistors from triarylamine side-chain polymers

The donor-acceptor block copolymer presented above contained PvTPA as a hole transporter. In this chapter we investigated PvTPA and two other poly(triarylamines) with different electron-rich substituents in a para configuration using OFETs. The molecular structures of PvTPA, PvDMTPA and PvDMTPD are given in Fig. 4.6.

The polymerisation of the triarylamines impedes crystallinity prevalent in its monomeric species. An amorphous state is often desirable when highly homogeneous films are required i.e. in light emitting devices. Furthermore, their thermal properties can be tuned via their molecular weight without changing the electronic properties. This is an important feature for device processing. PvDMTPD exhibited the best OFET performance, whereas PvTPA had the lowest hole carrier mobility. The same trend has been observed in complementary studies of diode devices,* and also in block copolymer solar cells.†

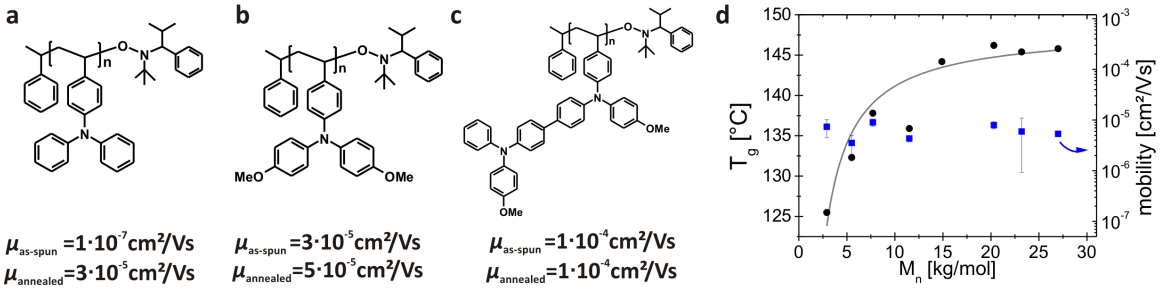

Figure 4.6: OFETs based on triarylamine side-chain polymers. a) poly(vinyl triphenylamine) (PvTPA), b) poly(vinyl dimethoxy-triphenylamine) (PvDMTPA), c) poly(vinyl dimethoxy-triphenyldiamine) (PvDMTPD). Triarylamines are well-known hole transporters and were investigated here as side chains. The polymerisation impedes the crystallisation of the monomers and enables the tuning of the thermal properties without changing the electronic performance: d) The glass-transition temperature depends on the molecular weight, but the mobility stays unaffected.

*E.M. Barea, G. Garcia-Belmonte, M. Sommer, S. Hüttner, H.J. Bolink, M. Thelakkat, Thin Solid Films (2009) , *in print*, doi:10.1016/j.tsf.2009.10.003

†M. Sommer, S. Lindner, and M. Thelakkat, Adv. Func. Mater. **17**, 1493 (2007)

Tunable charge transport using supramolecular self-assembly of nanostructured crystalline block copolymers

The rather weak performance of the triarylamine-based block copolymers in organic solar cells motivated the synthesis of other donor blocks. Poly(3-hexylthiophene) (P3HT) is one of the most ubiquitous hole transporters and used in the currently most efficient organic photovoltaics. P3HT is also a semi-crystalline material that exhibits a lamellar crystalline structure. The P3HT-*b*-PPerAcr therefore features two crystalline polymer blocks – one main-chain and one side chain. The co-existing crystallinity of both blocks affects the resulting charge transport properties.

In chapter 9 we investigate these block copolymers with regard to their charge transport properties and establish a structure-function relation. This is the first time that block copolymers with n- and p-type functionalities have been applied in organic field effect transistors. This offers the possibility of adjusting the charge transport in a single material. We have demonstrated OFETs from three different block copolymer compositions, with an increasing content of PPerAcr from 56 wt%, to 74 wt% and 81 wt%. The electronically active blocks self-assemble into continuous microdomains,

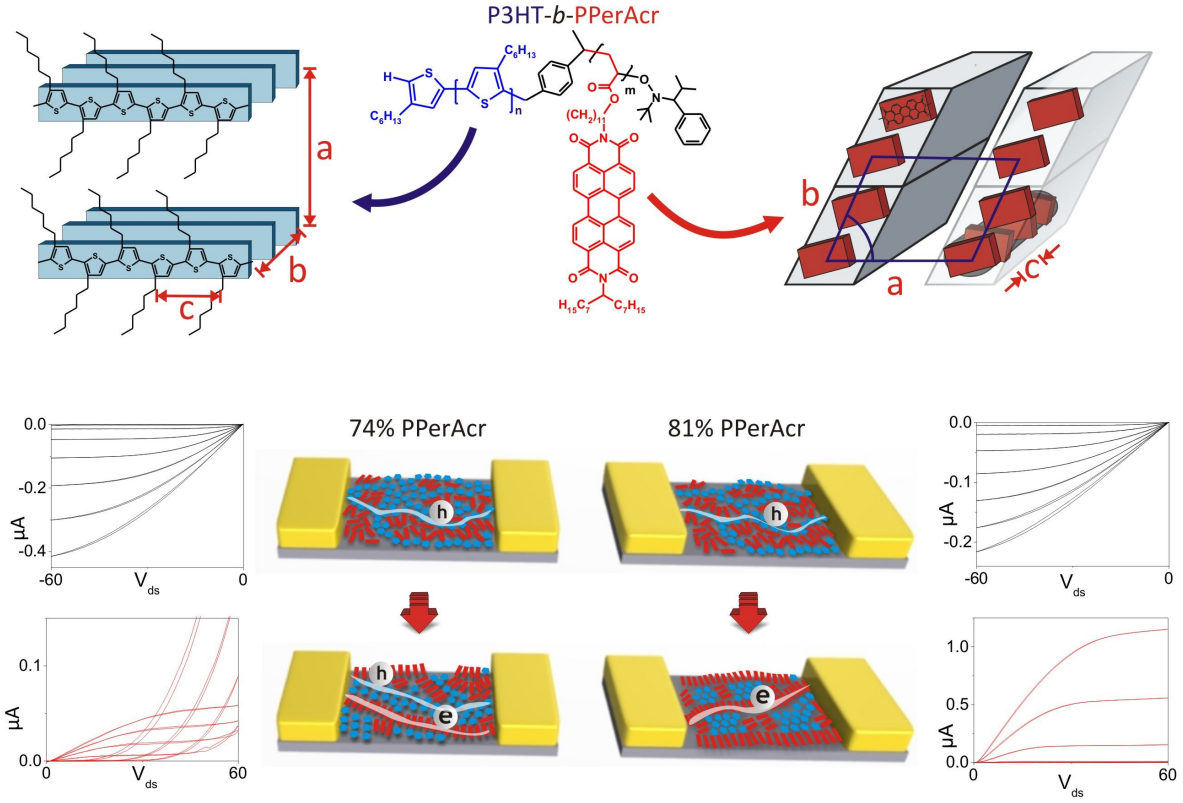

Figure 4.7: Tunable charge transport in P3HT-*b*-PPerAcr OFETs. The upper graph depicts the two co-existing crystalline structures in the block copolymer. The bottom scheme shows the electronically active copolymer subunits that self-assemble into continuous domains, thereby forming percolation channels for both, holes and electrons. The transistor characteristics depend on the selective activation of these percolation networks upon annealing. Depending on the block copolymer composition, the channel polarity switches from p-type to ambipolar or to unipolar n-type transport, respectively.

thereby forming percolation channels for both holes and electrons. The transistor characteristic depends on the selective activation of these percolation networks. We find that initially all block copolymers compositions exhibit unipolar p-type transport after spin coating. After a temperature annealing step above the melting temperature of both crystalline blocks, the OFET remains p-type for 56 wt% PPerAcr, however, the BCP 74 wt% PPerAcr switches to ambipolar transport behaviour, and the 81 wt% PPerAcr switches completely to n-type.

The reason for this switch is the interplay between the crystallinities of the two polymer blocks. Combined small and wide angle X-ray diffraction yielded detailed structural information of these polymers. We found that PPerAcr formed a monoclinic lattice of stacks of perylene bisimides, while P3HT formed lamellar sheets of P3HT chains. The two crystallinities coexisted, as the X-ray measurements demonstrated. Temperature dependent X-ray measurements and differential scanning calorimetry showed that PPerAcr melted first upon heating at approximately 190 °C, followed by P3HT. However, upon cooling PPerAcr re-crystallises first, followed by P3HT, which shows extended undercooling. Therefore, the strong crystallisation of PPerAcr is - depending on its weight percentage - either adding n-type functionality or impeding the p-type percolation in the OFET device completely, switching to a predominantly n-type charge transport.

Both blocks are nevertheless crystalline after the thermal annealing step, as can be seen in the characteristic absorption features. However, the interfacial crystallinity of the P3HT is increasingly affected, as the PPerAcr content increases, leading to a decrease of p-type percolation paths. We probed this phenomenon by time-resolved transient absorption spectroscopy. The characteristic crystalline P3HT feature disappeared at longer time scales (nanoseconds) after a pulsed excitation of P3HT-*b*-PPerAcr. This proves that interfacial charge pairs, which develop as excitons, diffuse to a donor-acceptor interface and do not occupy crystalline P3HT regions.

In most modern digital circuitry, the use of complementary logic components comprising both p- and n-type transistors is essential for stable, power-efficient operation. For organic field-effect transistors the assembly of complementary circuits is, however, often complex and relies on several components and processing steps. The dual charge transport capabilities of block copolymers is especially promising, as the same source drain electrode materials, for example gold, can be used. The transport can be adapted by a one-time annealing process, which opens the way towards simple manufacturing of p-type, n-type and ambipolar transistors based on a single material.

Influence of molecular weight on solar cell performance of double-crystalline donor-acceptor block copolymers.

In this contribution we demonstrate photovoltaic cells based on double-crystalline P3HT-*b*-PPerAcr (Fig. 4.1d). The molecular weight plays a significant role in the device performance. Comparing a BCP based on a 8.9 $\frac{\text{kg}}{\text{mol}}$ block of P3HT with a 17.0 $\frac{\text{kg}}{\text{mol}}$ block, but with the same weight ratio of the two blocks (55 wt% PPerAcr), yielded external quantum efficiencies up to 10 times higher: 31% (25% in average).

The higher molecular weight of P3HT leads to a higher degree of crystallinity and to larger crystals. This can be seen in the higher melting enthalpy and higher melting point. Furthermore, the hole mobility measured in p-type OFETs revealed hole mobility two orders of magnitude higher for the BCP with the long P3HT block of $5 \cdot 10^{-3}$ $\frac{\text{cm}^2}{\text{Vs}}$, compared to $1 \cdot 10^{-5}$ $\frac{\text{cm}^2}{\text{Vs}}$ for the short P3HT block. Nevertheless, the power conversion efficiency was still relatively low at 0.2 %.

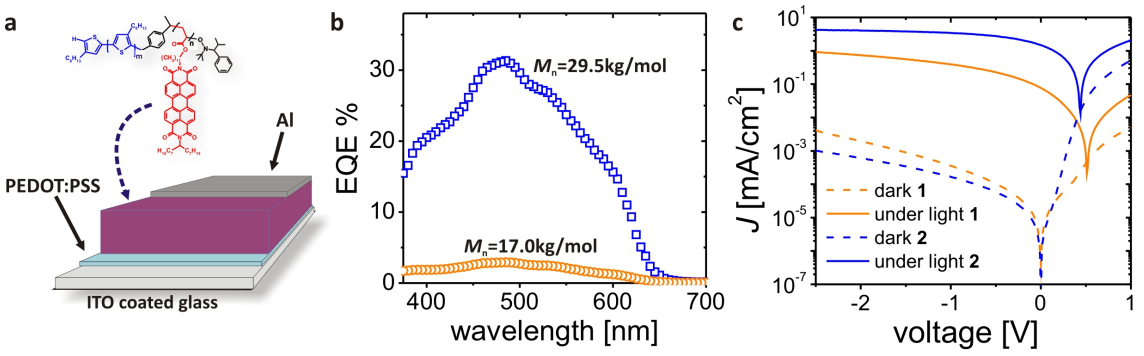

Figure 4.8: a) Different molecular weights of P3HT-*b*-PPerAcr were tested in organic photovoltaic devices. b) External quantum efficiencies (EQEs) up to 31% could be reached with higher molecular weight block copolymers. c) The $J-V$ characteristics of two different molecular weights, but the same block ratio of 55% PPerAcr content.

Photophysics of double-crystalline donor-acceptor block copolymers based on P3HT and perylene bisimide based polymers

The above results are encouraging, since they represent the highest external quantum efficiencies in P3HT and perylene bisimide systems reported so far. We conducted further research in order to obtain a more detailed understanding of this system and to elucidate the actual limitations of P3HT-*b*-PPerAcr in OPV devices. To generate different morphologies and interfacial properties, the two BCPs from the preceding chapter were spin-coated using solvents with different boiling points. This resulted in different P3HT crystallinities, domain sizes and interfacial coarseness. Furthermore, a polymer blend comprised of a binary 1:1 mixture of the homopolymer P3HT and PPerAcr provided the comparison with a macroscopically phase separated donor-acceptor morphology. In addition to the device characterisation, we have employed time-resolved transient absorption spectroscopy, tracking the photophysical processes

from exciton diffusion, to charge generation, charge separation and percolation from a sub-picosecond time scale up to milliseconds.

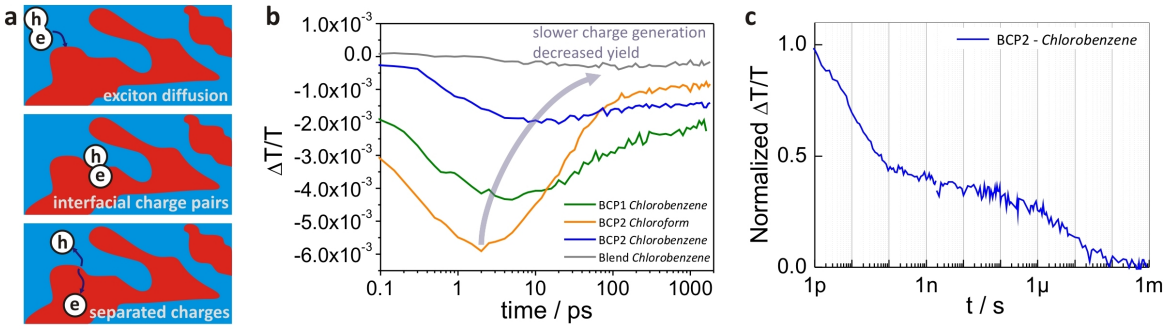

Figure 4.9: a) The domains of P3HT-*b*-PPerAcr are so small that the excitons reach the interface within a picosecond and charge pairs are formed at the interface. An efficient charge pair separation depends on the size and crystallinity of the domains. This enabled more efficient charge separation. b) Charge generation kinetics probed in the photoinduced absorption region. The coarser the donor-acceptor interface and the larger the domains, the slower and the fewer charge pairs are generated at the interface. However, an efficient charge separation occurs only at coarser domains with increased P3HT crystallinity. c) Normalised transient absorption kinetics in the ground state bleach region following pulsed excitation. More than 20% of the initially formed charge pairs are stable up to μs.

As shown in chapter 10, the highest external quantum efficiencies can be achieved from higher molecular weight block copolymers processed from a high boiling point solvent (chlorobenzene). Processing from fast evaporating chloroform or using lower molecular weight block copolymers reduces the amount of charges that can be extracted significantly, even though the initial charge pair formation is higher, due to the larger donor-acceptor interface. In general we observe a rapid charge pair formation in the block copolymers that slows down slightly for larger and more crystalline domains. Those domains instead provide a more efficient charge separation. This can be seen from the fact that in the weakly crystalline samples an applied electric field significantly increases the separation of interfacial charge pairs. There is also a clear difference in the formation of stable charge pairs. The block copolymer (large M_W and processed form chlorobenzene) with the $> 20\%$ EQE shows the stable formation of $\sim 20\%$ initial charge pairs on time scales up to microsceconds, providing more time for separation. Rapid photoinduced charge transfer on a $\sim$ 1 ps timescale and the strong photoluminescence quenching, however, suggest domain sizes significantly below the exciton diffusion length of only a few nanometers. The morphology following spin-coating from chlorobenzene provides a high crystallinity of P3HT, but still does not achieve the expected domain size observed as in bulk samples. The results highlight the importance of P3HT crystallinity at the interface for an enhanced charge separation, but also point out the lack in morphology for an efficient charge percolation.

Annex: Block Copolymers as compatibilisers for binary blends

The small estimated domain sizes in P3HT-*b*-PPerAcr spin-coated films and the observation that binary blends of P3HT and PPerAcr provide a much better fill-factor, supports the approach to compatibilise binary blends with the help of block copolymers. The idea is to optimise the donor-acceptor blend morphology, where the block copolymer gives optimised interfacial ordering, and the blend – an optimised domain size, creating better charge percolation and enhancing the charge separation. In first experiments we increased the loading of the block copolymer into the blend, while keeping the P3HT and PPerAcr ratio constant at 1:1. However, no optimal block copolymer fraction could be found for the 1:1 P3HT:PPerAcr composite and hence aspects for future research are pointed out.

Individual contributions

This thesis consists of seven individual publications. Three are published, one is accepted, one submitted and two further are in preparation and about to be submitted. In the following, the individual contributions of the authors of the following papers are specified. All materials used in this thesis were synthesised in the group of Prof. Mukundan Thelakkat by Michael Sommer or Stefan Lindner, or students under their supervision.

Chapter 5

This work is published in Applied Physics Letters (2008, 92, 093302) under the title:

"N-type organic field effect transistors from perylene bisimide block copolymers and homopolymers."
by Sven Hüttner, Michael Sommer and Mukundan Thelakkat.

I processed the organic field effect transistors, created a setup to characterise them under inert gas conditions and evaluated the data. Michael Sommer synthesised the material and provided the molecular parameters. Mukundan Thelakkat supervised the project and corrected the manuscript.

Chapter 6

This work is published in Soft Matter (2009, 5, 4206-4122) under the title:

"Controlled solvent vapour annealing for polymer electronics."
by Sven Hüttner, Michael Sommer, Arnaud Chiche, Georg Krausch, Ullrich Steiner and Mukundan Thelakkat.

I performed all the described experiments - including the creation and automation of a new and the modification of an exciting setup to perform in-situ ellipsometry and spectroscopy under solvent vapour exposure. The TEM cross sections were imaged with the help of Carmen Kunert. Michael Sommer and Arnaud Chiche were involved in discussions and corrected the manuscript. First Georg Krausch, later Ullrich Steiner and Mukundan Thelakkat supervised the project and corrected the manuscript.

Chapter 7

This manuscript is prepared for submission.

"Intermolecular interactions in perylene bisimide polymer architectures."
by Sven Hüttner, Michael Sommer, Justin Hodgkiss, Panos Keivanidis, Richard Friend, Ullrich Steiner and Mukundan Thelakkat.

I performed all the decribed experiments, except the exciton depolarisation experiments, that were carried out by Justin Hodgkiss who contributed this part. Michael

Sommer provided the electron microscopy images. Panos Keivanidis was involved in discussions and corrected the manuscript as did Michael Sommer. Ullrich Steiner and Mukundan Thelakkat supervised the project and corrected the manuscript.

Chapter 8

This work is published in Applied Physics Letters (2010, 96, 073503) under the title:

"Organic field effect transistors from triarylamine side-chain polymers."
by Sven Hüttner, Michael Sommer, Ullrich Steiner and Mukundan Thelakkat.

I processed the organic field effect transistors, measured the thermal properties and wrote the manuscript. Michael Sommer synthesised the materials, provided the molecular parameters and corrected the manuscript. Ullrich Steiner and Mukundan Thelakkat supervised the project and corrected the manuscript.

Chapter 9

This work is submitted under the title:

"Tunable charge transport using supramolecular self-assembly of nanostructured crystalline block copolymers."
by Sven Hüttner, Michael Sommer, Peter Kohn, Justin Hodgkiss, Thomas Thurn-Albrecht, Richard Friend, Ullrich Steiner and Mukundan Thelakkat.

I processed the organic field effect transistors, characterised the electronic and steady state spectroscopic properties and wrote the manuscript. Peter Kohn was involved in the X-ray diffraction experiments and analysed the data and provided this section and corrected the manuscript. Justin Hodgkiss performed the ultra-fast spectroscopy and edited this section and corrected the manuscript. Michael Sommer synthesised the materials and, characterised their thermal properties. He also corrected the manuscript. Ullrich Steiner and Mukundan Thelakkat supervised the project and corrected the manuscript.

Chapter 10

This work is published in Applied Physics Letters (2009, 95, 183308) under the title:

"Influence of molecular weight on the solar cell performance of double-crystalline donor-acceptor block copolymers."

by Michael Sommer, Sven Hüttner, Ullrich Steiner and Mukundan Thelakkat.

Michael Sommer synthesised the materials and characterised the molecular properties. He was involved in the device fabrication and wrote the publication. I edited the publication and I processed and characterised the presented solar cells and organic field

effect transistors. Ullrich Steiner and Mukundan Thelakkat supervised the project and corrected the manuscript.

Chapter11

This work is prepared for submission under the title:

"Photophysics of double-crystalline donor-acceptor block copolymers from P3HT and perylene bisimide based polymers."
by Sven Hüttner, Justin Hodgkiss, Michael Sommer, Richard Friend, Ullrich Steiner and Mukundan Thelakkat.

I processed the samples, carried out all steady state spectroscopic measurements as well as the electronic characterisation. Justin Hodgkiss performed the time resolved measurements. The manuscript was prepared by both myself and Justin Hodgkiss. Michael Sommer provided the bulk SEM image and corrected the manuscript. Peter Kohn provided the crsytalline structure data. Mukundan Thelakkat and Ullrich Steiner supervised the project and corrected the manuscript.

Chapter12 - Annex

This work is prepared as a basis for further investigations towards the use of:
"Block copolymers as compatibilisers for binary polymer blends."
I performed all experiments. Justin Hodgkiss and Ullrich Steiner were involved in discussions.

Chapter 5

N-type Organic Field Effect Transistors from Perylene Bisimide Block Copolymers and Homopolymers

Sven Hüttner, Michael Sommer, Ullrich Steiner, Mukundan Thelakkat

Angewandte Funktionspolymere, Makromolekulare Chemie I, Universität Bayreuth, Germany

Applied Physics Letters, 92, 093302 (2008)

Abstract

We present organic field effect transistors (OFET) based on solution-processable n-type polymers containing perylene bisimide as pendant groups. The OFET characteristics of a diblock copolymer consisting of polystyrene (PS) and a poly (perylene acrylate) (PPerAcr) blocks and a PPerAcr homopolymer are compared. Thermal annealing improves the OFET performance by 2-3 orders of magnitude, which can be attributed to the improved order and interface properties in the transport layer, arising from the better alignment of the perylene bisimide moieties. Both polymers show excellent n-type performances with electron carrier mobilities of $1.2 \cdot 10^{-3}\,\frac{\mathrm{cm}^2}{\mathrm{Vs}}$ and low threshold voltages of 4-7 V.

Introduction

Air-stable n-type materials are one of the critical material requirements in the field of organic electronics. In contrast to hole conducting materials (p-type), very few n-type materials are known which offer good electron transport properties in combination with high work function electrodes such as gold. Additionally, highly soluble, solution-processable materials are prerequisites for plastic electronics. Low molecular weight perylene bisimide derivatives, also called perylene diimide (PDI) or perylene tetracarboxylic diimide (PTCDI) derivatives are known to be good electron transporting materials[1,2] with electron mobilities of up to $2.1\,\frac{\mathrm{cm}^2}{\mathrm{Vs}}$.[3,4] For polymers containing perylene bisimide moieties values around $10^{-2}\,\frac{\mathrm{cm}^2}{\mathrm{Vs}}$ have been reported,[5] together with a good air stability.[6] Additionally, they show a high absorbance in the visible light and possess long exciton diffusion lengths.[7] The strong $\pi - \pi$ interactions are a key

feature of this material and, depending on the chemical structure, lead to crystallinity or higher hierarchical orders such as the formation of discotic liquid crystals.[8] Therefore, they are suitable for n-type organic field effect transistors[9] as well as for organic heterojunction solar cells.[10] However, the morphology in thin layers plays a key role in device performance. Bulk heterojunction solar cells rely on the distinct structure, where donor and acceptor materials are perpendicular to the electrodes. A large interpenetrating interface between a hole and an electron transporting material is desired, as well as sufficient percolation paths to the electrodes. Organic field effect transistors, on the other hand, use a lateral device geometry, where the charge transport between the source and drain electrode is determined only by a thin layer on top of the gate oxide.[11] Here the alignment of molecules to the substrate and the formation of cocontinuous domains or microcrystals between source and drain can have decisive effects on the device characteristics. Therefore OFET devices give direct information on the influence of morphology on transport properties of a material.

Diblock copolymers are widely known for their ability to form self assembled nanostructures. Here, two different polymer chains are covalently linked to each other. The demixing of the two polymer segments on the one hand, and the molecular connectivity on the other, lead to a nanostructured phase separation, the so-called microphase separation of the block copolymers.[12,13] Depending on the respective volume ratio, interaction parameters of the respective blocks and molecular weight, lamellar, gyroidal, cylindrical and spherical morphologies can be found. Furthermore it has been shown, that directional alignment of these nanostructures can be achieved for example by external fields,[14] shear forces,[15] solvent vapor atmospheres[16] or specific surface interactions. Thus, a morphology which resembles upstanding cylinders of n-type material in the matrix of a p-type material or vice versa may be the perfect structure for bulk heterojunction solar cells.[17] Initial investigations have already been undertaken to use the concept of block copolymer self assembly for organic electronics - both for bulk heterojunction solar cells[10,18] and for transistors.

Moving away from typical amorphous block copolymer systems with no electronic functions - on which it has been extensively reported over the last decades - to block copolymers which carry electronic functionalities, certain obstacles had to be overcome in their synthesis to avoid high polydispersity and to achieve good control over the molecular weight. Furthermore additional effects such as the formation of $\pi-\pi$ stacks and crystallites, as well as a difference in behavior due to the functionalised side groups are only beginning to be investigated.

Results and Discussion

In this paper we investigate the transport characteristics of a novel side chain perylene bisimide homopolymer poly (perylene bisimide acrylate) and a novel perylene bisimide block copolymer, polystyrene-*block*-poly(perylene bisimide acrylate) in OFET devices. Fig. 5.1a shows the molecular structure of the perylene bisimide acrylate polymer (PPerAcr). The synthesis is described elsewhere and the LUMO level of PPerAcr is

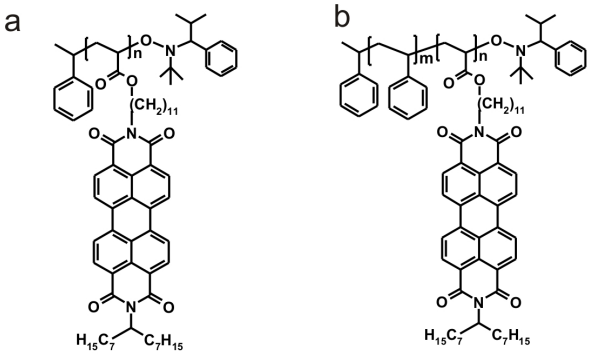

Figure 5.1: Chemical structures of the polymers: a) Poly (perylene bisimide acrylate) (PPerAcr), b) Diblock copolymer polystyrene-*block*-poly(perylene bisimide acrylate)

reported as 3.6 eV.[10] The perylene bisimide groups are linked to a polyacrylate backbone via a C11 spacer. The other end of the perylene bisimide carries a C15 swallow-tail substituent. The homopolymer PPerAcr has a melting point at around 190 °C. The crystallinity is caused by the strong $\pi - \pi$ interactions, also referred to as $\pi - \pi$ stacking, of the perylene bisimide groups, leading to a crystallinity of the sidechains.[19] The weight-average molecular weight of PPerAcr is 30.9 kg/mol with a polydispersity of 1.86. The block copolymer PS-*block*-PPerAcr (5.1b) consists of PPerAcr (70 wt%) and of polystyrene (30 wt%) blocks. Its overall molecular weight is 37.9 kg/mol with a polydispersity of 1.52. The block copolymer exhibits features from both components - the glass transition of the polystyrene which is around 100 °C and the melting point of the perylene bisimide acrylate groups at 189 °C indicating the presence of phase separated domains in bulk.[20]

For the transistor substrates we used heavily n-doped silicon wafers with a common gate contact carrying a 200 nm thermally grown gate oxide layer. The source and drain contacts were lithographically patterned Au interdigitating electrodes. The substrates were cleaned and then exposed to hexamethyldisilazane (HMDS) vapour for approximately 3 h in order to silanise the substrates, rendering the dielectric surface hydrophobic. After the HMDS exposure the substrates were rinsed again with isopropanol. The polymers were spin-cast from a 1.5 wt% chloroform solution. This procedure and all subsequent device annealing and device characterization steps were carried out in a glove box in inert gas. The transistors were characterised using a HP4155A semiconductor parameter analyser. Tab. 5.1 summarises the respective mobilities,* threshold voltages† and on/off ratios. All processed devices show only a very weak performance with threshold voltages around 20 V directly after spin casting. Fig. 5.2b and Fig. 5.2d show the output and transfer characteristics of an as spun PPerAcr thin film transistor. That changes dramatically after annealing the samples at 210 °C for 60 min, which is above the melting temperature of PPerAcr of 190 °C. The threshold voltage drops significantly to 6.8 V, while the current and charge carrier mobility both increase by two orders of magnitude. Thus electron transport mobilities

*The mobility ţ has been calculated using the gradual channel approximation $\partial I_d/\partial V_g = \mu C_i W/L$, where C_i is the capacitance, W the gate width and L the gate length of the transistor.

†The threshold voltage V_{th} has been determined through the intercept of a line fit through the linear part in the $\sqrt{I_{ds}}$ vs. V_g plot with the V_g axis.

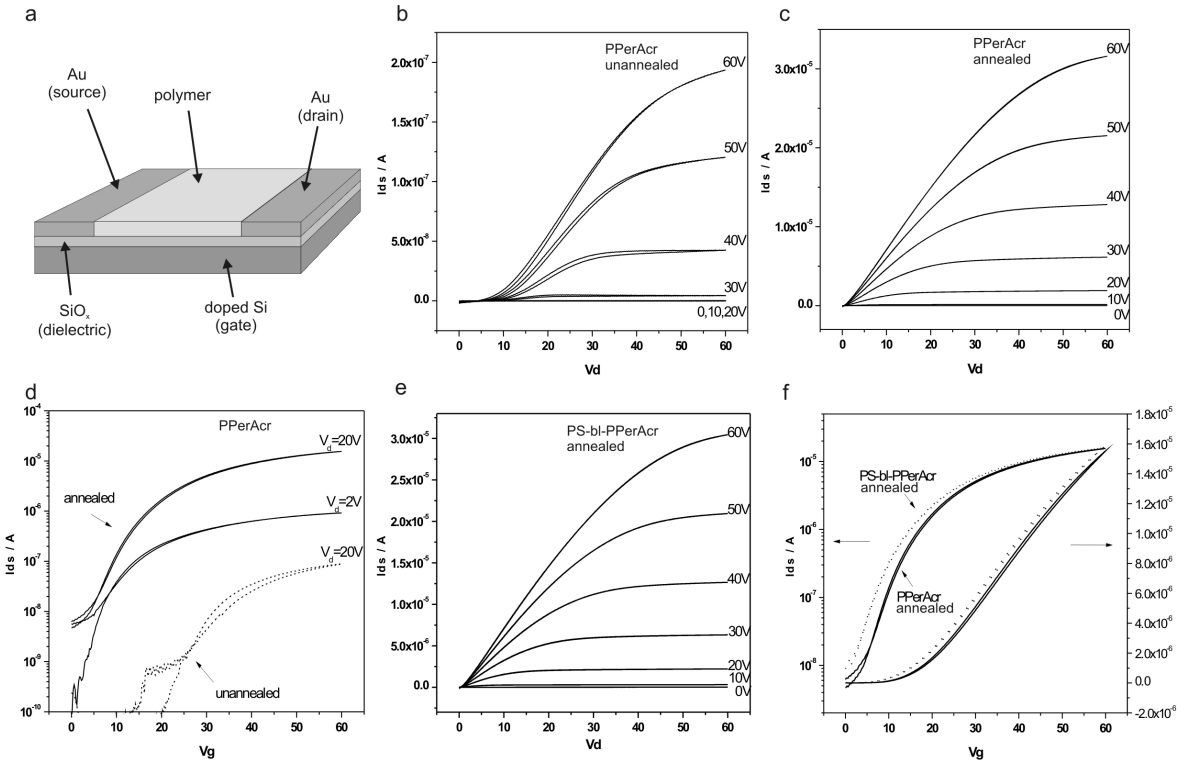

Figure 5.2: a) Schematic of a bottom gate OFET, b) output characteristics measured forwards and backwards of the as spun homopolymer PPerAcr, c) output characteristics of the annealed homopolymer PPerAcr showing no hysteresis, d) comparison of the transfer characteristics between unannealed (dashed line) and annealed homopolymer PPerAcr, e) output characteristics of the annealed block copolymer PS-*b*-PPerAcr, f) transfer characteristics of the block copolymer (dashed line) and the homopolymer (solid line) showing almost identical results.

Table 5.1: OFET parameters of homopolymer and block copolymer devices: electron mobility μ, threshold voltage V_{Th} and the On/Off ratio.

Polymer	$\mu[\frac{\mathrm{cm}^2}{\mathrm{Vs}}]$	V_{th}	On/Off
PPerAcr (as spun)	$9.6 \cdot 10^{-6}$	21.8 V	$3.7 \cdot 10^2$
PPerAcr (annealed)	$1.2 \cdot 10^{-3}$	6.8 V	$3.3 \cdot 10^4$
PS-*block*-PPerAcr (as spun)	$3.5 \cdot 10^{-6}$	24.9 V	$1.0 \cdot 10^2$
PS-*block*-PPerAcr (annealed)	$1.2 \cdot 10^{-3}$	4.1 V	$1.8 \cdot 10^3$

of up to $1.2 \cdot 10^{-3}\,\frac{\mathrm{cm}^2}{\mathrm{Vs}}$ were achieved for a device made of PPerAcr with a channel length of 10 μm and a width of 10 mm. The output and transfer characteristics of a thermally annealed device are illustrated in Fig. 5.2c and Fig. 5.2d.

In the same way we characterised the devices based on the block copolymer PS-*block*-PPerAcr containing 30 wt% PS. Surprisingly both materials, the pristine homopolymer and the block copolymer, show almost identical performances. The diblock copolymer also shows the same weak performance just after spin casting (not shown here), but after thermal annealing the output (Fig. 5.2e) and transfer characteristics

(Fig. 5.2f) are almost identical to those of the homopolymer PPerAcr. The block copolymer shows an even lower threshold voltage of 4.1 V After the annealing step both polymers show a fast onset of the linear regime in their output characteristics with increasing source drain voltage indicating a low contact resistance to the gold electrodes. The annealing step also increases the on/off-ratio by almost two orders of magnitude and the initial hysteresis, which was seen with respect to the forward and backward scans, has vanished.

These results suggest that the perylene bisimides moieties possess a favourable interaction with the substrate after annealing, since the charge transport in OFETs takes place only in a thin layer channel of some nanometers above the gate oxide. In the case of the block copolymer this means that the microdomains of the perylene bisimide containing block go down to the substrate during the annealing process. This phenomenon is widely known and originates from the strong surface interaction with one of the blocks.[21] The morphology in the OFET films of the block copolymer was studied using scanning electron microscopy (SEM). The top view SEM image (Fig. 5.3) clearly shows lying cylinders with diameters of around 15 nm and domain spacings of 20-25 nm. The film thickness is around 150 nm, which means that the visualised morphology appears at the polymer-air interface, a couple of domain spacings above the substrate interface. The preferred interaction of PPerAcr with the substrate is not visible from the top, however all electrical characterizations are indicative of this behavior. Furthermore the annealing process seems to lead to an optimised alignment of the perylene bisimides units within the microdomain itself resulting in a high electron transport mobility. This finding is even more impressive considering that PS (30 wt% in block copolymer) does not contribute to the charge transport at all. Generally in blends, copolymers and block copolymers, the charge carrier mobility decreases with dilution of the active components by an amorphous component.[22,23] Only in semicrystalline multicomponent systems a device performance improvement has been reported in diluted systems.[24]

In the case of PS-*block*-PPerAcr, the electron carrier mobility remains the same as that in the homopolymer, due to possible morphological advantages resulting from the stacking of the bisimide units in a confined geometry. Annealing causes significant changes both in the electrical properties as well as in the morphology of these thin films, as demonstrated in SEM images of the block copolymer before and after annealing steps. Only after thermal treatment does the block copolymer show a distinct phase separation. The reason for this is that during film preparation from chloroform, which is a fast evaporating low boiling point solvent, the polymer chains are not given sufficient time to rearrange and therefore high order in the film is not achieved. This affects both, the phase separation itself, and the intermolecular interaction of the perylene bisimide moieties leading to high order.

Conclusion

We conclude that new perylene bisimide polymers - a homopolymer and a diblock copolymer- show an outstanding n-type performance with high electron transport mobilities, low threshold voltages and good electron injection from gold electrodes. A ther-

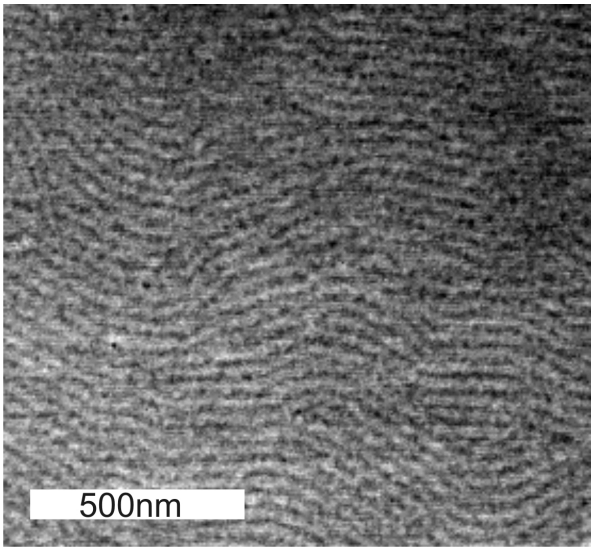

Figure 5.3: SEM top view image of an annealed PS-*block*-PPerAcr transistor. The block copolymer forms lying cylinders of PPerAcr (bright) in a matrix of polystyrene (dark) on the surface.

mal annealing step improves drastically the device performance. The charge transport properties are maintained in a block copolymer exhibiting cylindrical microdomains, where one block consists of insulating polystyrene with a content of 30 wt%. These results are promising not only for the further application of polymerised perylene bisimides as an electron transporting material, but also to develop novel multifunctional materials, the charge transport properties of which can be well optimised in the respective microdomains of an ordered block copolymer. Thus the capability of block copolymers with distinct control of the morphology on a nanometer scale and extended charge transport pathways throughout the bulk, which lead to excitonic solar cells with a nanostructured bulk heterojunction[10,25] can also open the door to ambipolar transistors,[26] which is the current scope of our research.

Acknowledgement

We acknowledge the financial support from projects SFB 481 (DFG) and EUROCORES ORGANISOLAR (ESF). SH thanks Universität Bayern e.V. for the financial support in the form of a scholarship of the Bayerische Graduiertenförderung.

Bibliography

[1] Z. An, J. Yu, Jones, S. S.C.and Barlow, S.and Yoo, B. Domercq, P. Prins, L.D.A. Siebbeles, B. Kippelen, and S.R. Marder, *High electron mobility in roomtemperature discotic liquid-crystalline perylene diimides*, Advanced Materials **17**, 2580 (2005).

[2] J.H. Oh, S. Liu, Z. Bao, R. Schmidt, and F. Würthner, *Air-stable n-channel organic thin-film transistors with high field-effect mobility based on N,N[prime]-bis(heptafluorobutyl)-3,4:9,10-perylene diimide*, Appl. Phys. Lett. **91**, 212107 (2007).

[3] R. J. Chesterfield, J. C. McKeen, C. R. Newman, P. C. Ewbank, D. A. daSilva Filho, J.-L. Brédas, L. L. Miller, K. R. Mann, and C. D. Frisbie, *Organic thin film transistors based on n-alkyl perylene diimides: charge transport kinetics as a function of gate voltage and temperature*, Phys. Chem. B **108**, 19281 (2004).

[4] S. Tatemichi, M. Ichikawa, T. Koyama, and Y. Taniguchi, *High mobility n-type thin-film tranisotrs based on N,N'-ditridecyl perylene diimide with thermal treatments*, Appl. Phys. Let. **89**, 112108 (2006).

[5] X. Zhan, Z. Tan, B. Domercq, Z. An, X. Zhang, S. Barlow, Y. Li, D. Zhu, B. Kippelen, and S.R. Marder, J. Am. Chem. Soc. **129**, 7246 (2007).

[6] M. Ling, M. Erk, P.and Gomez, M. Koenemann, J. Locklon, and Z. Bao, *Air-stable n-channel organic semiconductors based on perylene diimide derivatives whithout strong electron withdrawing groups*, Advanced Materials **19**, 1123 (2007).

[7] B.A. Gregg, *Excitonic solar cells*, J. Phys. Chem. B **107**, 4688 (2003).

[8] C.W. Struijk, A.B. Sieval, J. E.J. Dakhorst, M. van Dijk, P. Kimkes, R.B.M. Koehorst, H. Donker, T.J. Schaafsma, S.J. Picken, A.M. van de Craats, J.M. Warman, H. Zuilhof, and E.J.R. Sudhölter, *Liquid crystalline perylene diimides: architecture and charge carrier mobilities*, J. Am. Chem Soc. **122**, 11057 (2000).

[9] P.R.L. Malenfant, C.D. Dimitrakopoulos, J.D. Gelorme, L.L. Kosbar, and T.O. Graham, *N-type organic thin-film transistor with high field-effect mobility based on a N,N'-dialkyl-3,4,9,10-perylene tetracarboxylic diimide derrivative*, Appl. Phys. Lett. **80**, 2517 (2002).

[10] S. Lindner, S. Hüttner, A. Chiche, M. Thelakkat, and G. Krausch, *Charge separation at self-assembled nanostructured bulk interfaces in block copolmers*, Angew. Chem. Int. Ed. **45**, 3364 (2006).

[11] H. Sirringhaus, *Device physics of solution-processed organic fiel-effect transistors*, Advanced Materials **17**, 2411 (2005).

[12] G.H. Fredrickson and F.S. Bates, *Dynamics of block copolymers: theory and experiment*, Annu. Rev. Mater. Sci. **26**, 501 (1996).

[13] C. Park, J. Yoon, and E.L. Thomas, *Enabling nanotechnology with self assembled block copolymer patterns*, Polymer **44**, 6725 (2003).

[14] T. Thurn-Albrecht, R. Steiner, J. DeRouchey, C.M. Stafford, E. Huang, M. Bal, M. Tuominen, C.J. Hawker, and T.P. Russell, *Nanoscopic templates from oriented block copolymer films*, Adv. Mater. **12**, 787 (2000).

[15] D. E. Angelescu, J. H. Waller, R. A. Register, and P. M. Chaikin, *Shear-induced alignment in thin films of spherical nanodomains*, Adv. Mater. **17**, 1878 (2005).

[16] K. Fukunaga, T. Hashimoto, H. Elbs, and G. Krausch, *Self-assembly of a lamellar ABC triblock copolymer thin film*, Macromol. **35**, 4406 (2002).

[17] G.A. Buxton and N. Clarke, *Predicting structure and property relations in polymeric photovoltaic devices*, Physical Review B **74**, 085207 (2006).

[18] G. Hadziioannou, *Semiconducting block copolymers for self-assembled photovoltaic devices*, MRS Bulletin **27**, 456 (2002).

[19] S.M. Lindner, N. Kaufmann, and M. Thelakkat, *Nanostructured semiconductor block copolymers: $\pi - \pi$ stacking, optical and electrochemical properties*, Organic Electronics **8**, 69 (2007).

[20] M. Sommer, S. Hüttner, S. Wunder, and M. Thelakkat, *Electron-conducting block copolymers: morphological, optical, and electronic properties*, Adv. Mater. **20**, 2523 (2008).

[21] C. Harrison, P. M. Chaikin, D.A. Huse, R.A. Register, D.H. Adamson, A. Daniel, E. Huang, P. Mansky, T.P. Russell, C.J. Hawker, D.A. Egolf, I.V. Melnikov, and E. Bodenschatz, *Reducing substrate pinning of block copolymer microdomains with a buffer layer of polymer brushes*, Macromol. **33**, 857 (2000).

[22] G. Sauvé and R. D. McCullough, *High field-effect mobilities for dibock copolymers of poly(3-hexylthiophene) and poly(methyl acrylate)*, Adv. Mater. **19**, 1822 (2007).

[23] A. Babel and S.A. Jenekhe, *Morphology and field-effect mobility of charge carriers in binary belnds of poly(3-hexylthiophene) with poly[2-methoxy-5-(2–ethylhexoxy)-1,4-phenylenevinylene] and polystyrene*, Macromolecules **37**, 9835 (2004).

[24] S. Goffri, C. Müller, N. Stingelin-Stutzmann, D.W. Breiby, C.P. Radano, J.W. Andreasen, R. Thompson, R.A.J Janssen, M.M. Nielsen, P. Smith, and H. Sirringhaus, *Multicomponent semiconducting polymer systems with low crystallization-induced percolation threshold*, Nature Materials **5**, 950 (2006).

[25] M. Sommer, S. Lindner, and M. Thelakkat, *Microphase-separated donor-acceptor diblock copolymers: influence of HOMO energy levels and morphology on polymer solar cells*, Adv. Func. Mater. **17**, 1493 (2007).

[26] C. Rost, S. Karg, and W. Riess, *Ambipolar light-emitting organic field-effect transistor*, Appl. Phys. Let. **85**, 1613 (2004).

Chapter 6

Controlled Solvent Vapour Annealing for Polymer Electronics

Sven Hüttner[a,b], Michael Sommer[a], Arnaud Chiche[a,c], Georg Krausch[a,d], Ullrich Steiner[b] and Mukundan Thelakkat[a]
a) Angewandte Funktionspolymere, Makromolekulare Chemie I, Universität Bayreuth, Germany
b) Cavendish Laboratory, University of Cambridge, United Kingdom
c) DSM Material Science Centre, Geleen, The Netherlands
d) Johannes Gutenberg Universität Mainz, Germany

Soft Matter, 5, 4206-4211 (2009)

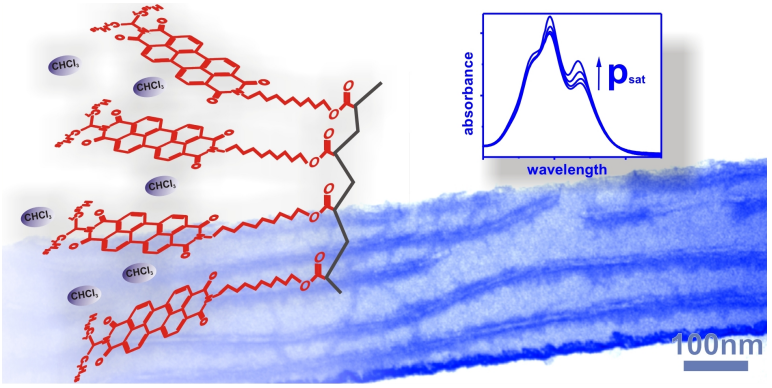

Abstract

Solvent vapour annealing (SVA) is demonstrated as an attractive method to anneal polymer blend and block copolymer thin films at low temperatures. This is especially suitable for organic electronics, where sensitive materials with strong intermolecular interactions are used. We demonstrate the effect of solvent vapour exposure on film properties of a perylene bisimide acrylate (PPerAcr) side chain polymer with strong crystallinity at the perylene bisimide moieties. We record the film thickness, light absorption and fluorescence as function of the relative solvent vapour pressure. At a certain threshold of relative solvent vapour pressure, we observe a disruption of the $\pi - \pi$ stacking, which is responsible for the perylene bisimide crystallisation. This leads to an increased polymer chain mobility and therefore to changes in the film morphology. The results are applied to a film of a donor-acceptor block copolymer

carrying PPerAcr segments, and the influence of solvent annealing on the nanoscale morphology is demonstrated.

Introduction

The field of organic electronics has enjoyed increasing interest over the past decade. Organic light emitting diodes, field effect transistors and solar cells have a promising future, with some products already commercially available. Both, low molecular weight systems or polymeric materials are used in organic electronic devices. Polymers typically offer an easy processability from solution, potentially paving the way for low cost and large area applications.

Bulk heterojunction solar cells, for example, consist of two components, an acceptor and a donor material. A distinct phase morphology of the two components is required in order to guarantee efficient charge separation combined with sufficient charge percolation to the electrodes. This is important because of the limited diffusion length of the photogenerated excitons of only several nanometres. Charge separation only takes place at the donor-acceptor interface because of the low permittivity of organic materials. A general approach to achieve an interpenetrating network of the donor and the acceptor material is blending the two materials. The most common method to produce such films is spin casting. Depending on the solubility and the boiling point of the solvent, film formation takes place within several seconds, freezing-in a non-equilibrium morphology of a polymer blend.[1] The detailed demixing process during film processing therefore determines the internal structure of binary polymeric thin films. The morphology always plays the decisive role in such devices since it has a large effect on several essential properties such as charge transport, charge separation and recombination.

Post annealing steps are therefore often applied in order to alter or induce the desired phase separation. This can be done either by temperature annealing, where the polymer film is heated above its glass transition or melting temperature,[2,3] or by solvent vapour annealing (SVA).[4,5] Alternatively, co-solvent spin casting can be used, where a high boiling point solvent is mixed with a low boiling point solvent.[6] All of these methods increase the polymer chain mobility, giving the system sufficient time to modify its morphology towards its thermodynamic equilibrium. This provides a path for the polymer blend to evolve towards an advantageous morphology. Once a desired morphology is obtained, the system is "frozen" to prevent further changes. Solvent vapour annealing involves the exposure of the cast film to a solvent atmosphere under controlled conditions. The film swells by solvent take-up, causing an increase in polymer chain mobility similar to temperature-annealing above the melting or glass transition temperature. SVA has the advantage that it can be done at room temperature, significantly reducing the risk of thermal degradation of the material.

Perylene bisimides (PBI) are well-known stable electron transporting materials. Extensive research has been performed on low molecular weight perylene bisimides derivatives, and their application in organic field effect transistors, photovoltaic cells, and photo-detectors has been demonstrated.[7–9] Various derivatives of PBI have been synthesised, in which the molecular packing is altered by different substituents. This

leads to a variation in the physical properties such as melting temperature, solubility in organic solvents, liquid crystal formation, and charge carrier transport. For example, high electron mobilities of up to 0.1 $\frac{\mathrm{cm}^2}{\mathrm{Vs}}$ were reported for low molecular weight PBIs.[10] The $\pi-\pi$ interaction between the perylene bisimide cores strongly influences the optical properties of the PBI moieties. This is due to p-orbital overlap causing the formation of one-dimensional aggregates.[11] As a consequence, charge transfer excitons are produced in addition to Frenkel excitons, which give rise to new spectral features. The magnitude of coupling of these levels to the ground state is determined by the relative orientation of the corresponding dipole moments.[12]

Absorption and fluorescence spectroscopy directly probes the stacking of the PBI. SVA affects PBI stacking, which has been shown by studies on low molecular weight PBIs.[13] Polymers containing perylene bisimide groups are attractive because they can be processed from solution.[14,15] Recently, we demonstrated excellent electron mobilities of up to $10^{-3}\frac{cm^2}{Vs}$ of the side-chain PBI polymer poly(perylene bisimide acrylate (PPerAcr) as shown in Fig. 6.1a.[16,17] One reason for the high electron mobility are the strong intermolecular interactions between adjacent PBI moieties bound to the polymer backbone, leading to side-chain crystallinity.

A further advantage of PPerAcr arises from the ability to incorporate this polymer into covalently linked block copolymers.[17–19] The generic microphase separation of flexible copolymers includes spherical, cylindrical, lamellar, and gyroidal morphologies, depending on the relative block lengths.[20] The self-assembly of these structures are highly regular with domain sizes on the 10-nm scale. The long-ranged interconnectivity of some of these microphases makes block copolymers very attractive for applications in organic photovoltaics (OPVs).[21] We have reported on the herein presented donor-acceptor block copolymer in its application in OPVs, with PPerAcr acting as the acceptor polymer and poly(triphenylamine) (PvTPA) as the donor segment.[22,23] These

Table 6.1: Molecular weights, composition, and thermal properties.

Polymer	$M_n[\frac{kg}{mol}]$	PDI	PPerAcr wt.-%	T_g [°C]	T_m [°C]
PPerAcr	18.7	1.47	100		190
PvTPA-*b*-PPerAcr	37.7	1.97	78.9	150	198

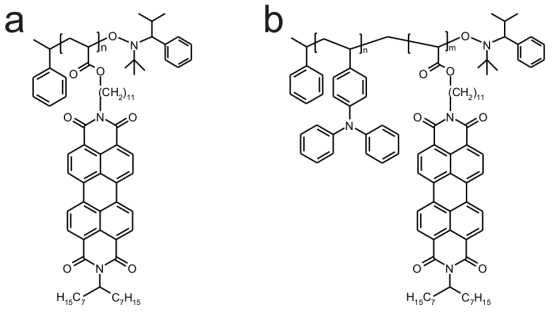

Figure 6.1: Molecular structures of a) poly(perylene bisimide acrylate) (PPerAcr) homopolymer and of b) poly(vinyltriphenylamine)-*b*-poly(perylene bisimide acrylate) (PvTPA-*b*-PPerAcr) block copolymer.

fully functionalised block copolymers are interesting because they achieve a higher control over the morphology compared to a similar polymer blend. Furthermore, block copolymers possess a "melt thermodynamic equilibrium" that is the desired final morphology. But because the viscosity of complex polymers is typically rather high, this thermodynamic equilibrium morphology is often only slowly reached.[24] Temperature annealing often involves high temperatures (around 210 °C for PPerAcr). Prolonged annealing times at high temperatures may cause thermal degradation of these materials which is particularly harmful for electronically active materials. More specifally, the PvTPA-*b*-PPerAcr block copolymer used in this study is not directly comparable to classical amorphous-amorphous block copolymers due to the presence of the side chain crystalline PPerAcr block. Rather, such a system might be compared to semi-rod-coil block copolymers[25] or to rod-coil block copolymers. Rod-coil block copolymers show a further complexity in their microphase morphology, because the conformational entropy is influenced stronlgy by the stiffer chain topology[26] and because of specific interactions between the conjugated moieties. In particular, the competition between microphase separation and crystallisation leads to a rich phase behaviour, which is not fully understood.

Here, we show that SVA at room temperature is a promising alternative for the control of the microphase separated morphology in these systems. We apply controlled SVA on thin films of the homopolymer PPerAcr (Fig. 1a). We show how the optical properties of PPerAcr change during exposure to chloroform vapour. First, the film thickness of PPerAcr homopolymer was tracked in situ by ellipsometry as a function of the partial solvent vapour pressure. To understand the molecular processes occurring during the solvent vapour exposure, the absorption and fluorescence were also measured as a function of the partial vapour pressure. These results were then related to morphological changes in thin films of the block copolymer PvTPA-*b*-PPerAcr (Fig. 6.1b), which were investigated by cross-sectional transmission electron microscopy (TEM). A comparison between thermal annealing and SVA demonstrates the superior control over the copolymer microphase morphology by solvent vapor annealing in terms of morphology control and long-range order.

Experimental

The synthesis of PPerAcr and PvTPA-*b*-PPerAcr is described elsewhere[18] and details of the molecular properties are listed in Tab. 6.1. Thin films of PPerAcr were prepared by spin casting from chloroform solutions of different concentrations onto clean silicon wafers, resulting in film thicknesses between 126 nm and 145 nm. The films were loaded into a small chamber with optically flat windows on both sides at an angle of 65° with respect to the chamber base, allowing ellipsometric measurements at 65° of samples that were exposed to a solvent vapour (Fig. 6.2a). The saturation of the solvent vapour was controlled by using two streams of nitrogen gas, one of which was passed through a washbottle filled with chloroform, causing the chloroform saturation of this stream. The two streams were mixed and introduced into the sample chamber. The flow rates of both streams were controlled by two electronic mass flow controllers (MKS). The precise adjustment of the relative flow rates controlled the relative solvent vapour pressure $\frac{p}{p_{sat}}$

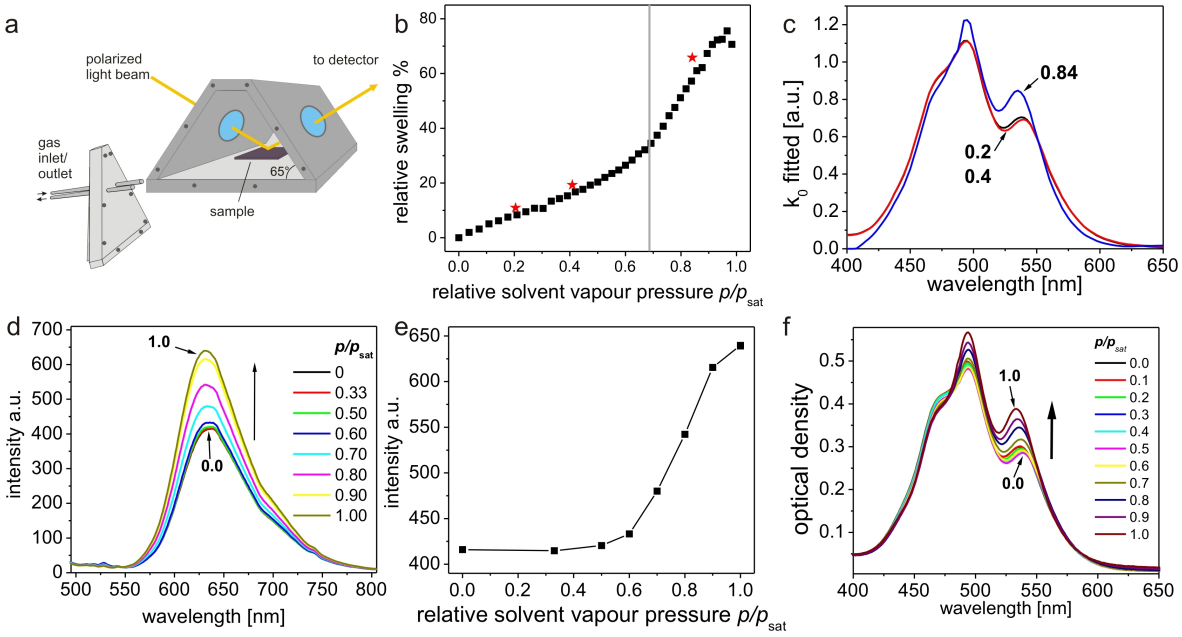

Figure 6.2: a) Schematic setup of the solvent chamber and direction of the incident light beam. b) Ellipsometric measurement of the relative swelling of a PPerAcr thin film upon solvent vapour exposure at different relative solvent vapour pressures exposed for 400 s at each measurement point. The stars indicate the measurements taken by the spectroscopic ellipsometer for which the absorption spectrum was recalculated. The gray line indicates a cross over point at $\frac{p}{p_{sat}} = 0.68$. c) Recalculated absorbance from spectroscopic ellipsometry for data recorded at $\frac{p}{p_{sat}} = 0.20$, 0.40, and 0.84 relative chloroform vapour pressure (stars in b) and normalised to the isosbestic point at 482 nm. d) Fluorescence emission during solvent vapour exposure. The arrow indicates increasing p/psat. e) Maximum fluorescence intensity at 630 nm vs. solvent vapour saturation. The small difference in the cross-over point compared to b) originates from the different chamber geometries. f) Absorption spectra recorded by an UV/Vis spectrometer during solvent vapour exposure. The arrow indicates increasing optical density at 530 nm with increasing relative solvent vapour pressure.

in fine increments from 0.00 to 1.00, that corresponds to a solvent vapour saturation from 0-100%. The temperatures of the solvent reservoir and the sample chamber were kept at the same temperature of 21 °C by separate temperature controllers. While this setup yields quantitative, reproducible results, measurements taken above $\frac{p}{p_{sat}} = 0.9$ solvent saturation have larger inaccuracies in the partial solvent vapour pressure because of a possible condensation of the solvent in the tubes or on the chamber walls.

Ellipsometry measurements were carried out using a Sentech 850 spectroscopic ellipsometer using the 400 nm to 900 nm wavelength range. SpectraRay Software, using a layer model of silicon, a 2.2 nm siliconoxide layer, a Cauchy layer to fit the polymer film and air was used to analyse the ellipsometry data. The Cauchy layer model fitted a layer model to the data by varying the layer thickness d, the refractive index in 0th and 3rd order, and the 1st order absorbance. Fits were carried out using only the data between 650 nm and 900 nm where light absorption is negligible. Additional ellipsometric measurements were carried out with a Nanofilm EP3-SE imaging nulling ellipsometer at three different wavelengths, 769.8 nm, 810.7 nm, and 833.4 nm.

UV-Vis spectra were acquired in two different ways. The spectroscopic data from the ellipsometer were analysed by a point to point fit for the absorbance in a range from 400 nm to 650 nm, keeping the thickness constant at a value that was determined by a previous fit. In addition, absorption spectra were recorded using a Hewlett-Packard 8453 diode array UV-Vis spectrometer, with the sample in a sealed chamber allowing the acquisition of absorption spectra in transmission during in-situ solvent vapour exposure. Photoluminescence spectra were obtained using a Cary Eclipse Fluorimeter (Varian Inc.). A chamber with two quartz glass windows at a 90° angle was used for measurements in a solvent vapour atmosphere. The excitation wavelength was 470 nm.

For TEM sample preparation, block copolymer thin films were spin-cast from a 2.7 wt.% chloroform solution at 2000 rpm, resulting in approximately 235 nm thick films. A thin layer of platinum was sputtered onto the samples as a diffusion barrier and the films were placed onto an epoxy resin. After the epoxy was cured, the silicon substrate was fractured off in liquid nitrogen, so that the film remained on the epoxy resin. Cross sectional cuts (approximately 50 nm thick) were obtained using a Leica Ultramicrotome, and were picked up on gold grids. The specimens were then stained for 15 min in a RuO4 vapour and imaged with a Zeiss 902 TEM at 80 kV.

Results and Discussion

First, spin coated films of PPerAcr were investigated in terms of their swelling behaviour during chloroform vapour annealing as a function of the relative vapour saturation. The geometry of the sample chamber and the incident beam is depicted in Fig. 6.2a. Fig. 6.2b shows the evolution of the film thickness as a function of the relative solvent vapour saturation. The relative vapour pressure was stepwise increased from 0.00 to 1.00, pausing for 400 s at each step to equilibrate the polymer film before each ellipsometric measurement. The resulting swelling curve in Fig. 6.2b shows two swelling regimes, with a relatively low solvent take-up for low solvent vapour pressures, and a strong swelling close to nearly saturated chloroform atmospheres. The linear approximations of the two regimes indicate a cross-over at approximately $\frac{p}{p_{sat}} = 0.68$. Generic amorphous polymers, in comparison, obey a swelling[24] according to the Flory Huggins theory. The Flory-Huggins equation[27] gives a quantitative description of the swelling of amorphous polymer films:

$$\ln \frac{p}{p_{sat}} = \chi \cdot \phi_p^2 + \ln(1 - \phi_p) + (1 - \frac{1}{N})\phi_p, \tag{6.1}$$

where $\frac{p}{p_{sat}}$ is the partial vapour pressure, corresponding to the relative vapour saturation of the solvent in a carrier gas. $\phi_0 = \frac{d_0}{d}$ describes the ratio between the initial film thickness d_0 and the swollen film thickness d. N is the number of monomers and is the Flory Huggins parameter, describing the interaction of a monomer unit with the respective solvent molecules. The equation above is based on a simplified model, assuming a homogeneous solvent absorption. It has been found that the solvent absorption depends on the film thickness and a concentration gradient may form.[28] Nevertheless, a

measurement of the film thickness during solvent vapour exposure quantifies the solvent - polymer interaction.[24] In the presented case, this Flory Huggins description only holds for amorphous polymers, where monomer-monomer interactions are not taken into account. These assumptions are hardly met by PPerAcr, which exhibits side-chain crystallinity and has low values of N ($N \approx 23$). We anticipate that only the alkyl substituents are responsible for the swelling of the thin film for $\frac{p}{p_{sat}} < 0.6$.

This assumption is supported by the spectroscopic data shown in Fig. 6.2c-f. The increase in fluorescence with increasing chloroform vapour saturation in Fig. 6.2d and 2e mirrors the variation observed in the ellipsometry data. The spectra in Fig. 6.2d are dominated by a broad peak at 630 nm which stems from the presence of PBI aggregates.[11] This peak is always dominant, even in highly diluted solutions of the polymer. Qualitatively, the intensity of the emission is related to the extent and quality of the aggregates, with better organised aggregates showing a higher photoluminescence quenching due to non-radiative recombination pathways.[13] The small variation in photoluminescence for relative solvent vapour pressures below 0.6 indicates that the PBI stacks are little affected by the swelling. The strong increase in fluorescence above relative vapour pressures of 0.6 is indicative of a change in PBI stacking. This leads to the conclusion that the solvent is taken up only by the alkyl substituents for $\frac{p}{p_{sat}} < 0.6$.

The organisation of the PBI moieties also affects the absorption spectra, reflecting the coupling of the transition dipole moments of each molecule site. Kazmaier et al. showed in theoretical calculations that the coupling is dependent on the lateral translation of the molecule with respect to its neighbours.[12] In the case of symmetrically substituted PBIs with two branched alkyl chains - similar to PPerAcr - a rotational offset of 45° has been determined by molecular dynamic simulations.[29] These relative changes in the stacking and stacking quality are also visible in the absorption spectra of PPerAcr. Fig. 6.2c and 6.2f show the absorption spectra of PPerAcr, measured as a function of the relative solvent vapour pressure. The absorption curve consists of three broad main features at 470 nm, 494 nm, and 537 nm. These features and the broad linewidth are the result from operative intermolecular interactions that convolute Frenkel-exciton transitions with charge transfer excitons.[30] Above a relative solvent vapour pressure of $\frac{p}{p_{sat}} > 0.6$, the relative changes in the oscillator strength of the three vibronic transitions are significant upon a change in partial chloroform vapour pressure. The spectra in Fig. 6.2c are normalised to the isosbestic point at 482 nm, which stays unaffected as it can be seen in the directly recorded absorption spectra in Fig. 6.2f. With increasing solvent vapour saturation, the peak at 470 nm decreases and the peak at 537 nm increases, accompanied by a slight blueshift from 537 nm to 533 nm. The opposite is observed when the sample is temperature annealed, pointing towards an improvement in PBI aggregation. The absorption data therefore also indicates a loss in the quality of stacking at relative vapour pressures above 0.6.

This observed effect is useful since it provides a way to determine the appropriate solvent vapour annealing conditions for block copolymer films containing PPerAcr. This is particularly relevant because the microphase morphology of spin-cast block copolymer films is often quenched far from equilibrium by the fast solvent evaporation. Clearly, morphology changes which involve a rearrangement of the perylene bisimide moieties are only possible for $\frac{p}{p_{sat}} > 0.6$. The block coplymer PvTPA-*b*-PPerAcr shows the same changes in absorbance and fluorescence upon solvent swelling as does the

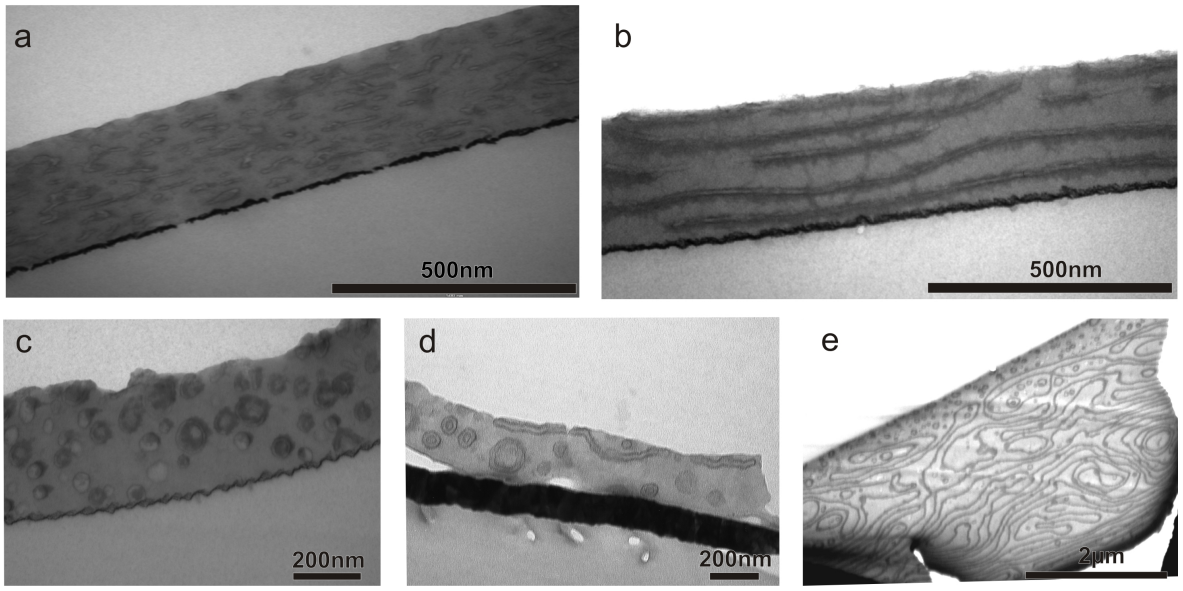

Figure 6.3: Transmission electron microscopy (TEM) cross sections of PvTPA-*b*-PPerAcr thin films. a) As spun. b) Solvent vapour annealed film at a saturation of $\frac{p}{p_{sat}} = 0.9$ for 90 min. c) The relative solvent vapour pressure of $\frac{p}{p_{sat}} \approx 0.6$ leads to poorly defined domains with a vesicle-like morphology. d) Thermal annealing at 210 °C for 18 h under nitrogen results in similar vesicle-like features. e) Solvent vapour annealing at $\frac{p}{p_{sat}} = 0.9$ for 16 h leads to the dewetting of the thin film.

homopolymer. This indicated that the stacking of the perylene moeities is unaffected by the presence of the additional PvTPA block (see supplementary information Fig. 6.5).

The change in morphology upon solvent annealing was further investigated by cross-sectional TEM. Fig. 6.3a shows an example of a cross section of PvTPA-*b*-PPerAcr block copolymer films after spincoating from chloroform. Disordered (dark) PPerAcr domains are finely interdispersed in a bright PvTPA matrix. After SVA for 90 min at 0.9 relative solvent vapour pressure the block copolymer reorganises into very long and ordered lamellae, as shown in Fig. 6.3b. The parallel orientation is induced by the preferential wetting of the polar SiO_2 substrate by one of the blocks, most likely PvTPA. This effect is commonly observed in lamellar block copolymers.[31] The PPerAcr lamellae have a thickness of around 20 nm and extend over several micrometres. The outstanding long-range connectivity and the lamellar width are photovoltaically favourable, simultaneously meeting the requirements imposed by the short exciton diffusion length and the charge transport across the entire device. The in-plane orientation of the lamellae is, however, not ideal. Optimal charge carrier percolation to the electrodes requires an orientation of the microstructure perpendicular to the substrate. While the feasibility of a perpendicular orientation has been demonstrated for cylinder-forming amorphous block-copolymers using electric fields,[32] neutral surfaces[33] or patterned substrates,[34,35] the modification of lamellar copolymer morphologies from their in-plane orientation is more difficult.

Prolonged thermal annealing (18 h, 210 °C) did not result in a lamellar morphology with a long-ranged connectivity of each phase, but isolated, round structures were observed in the cross-sectional TEM images of Fig. 6.3d. In the absence of three-

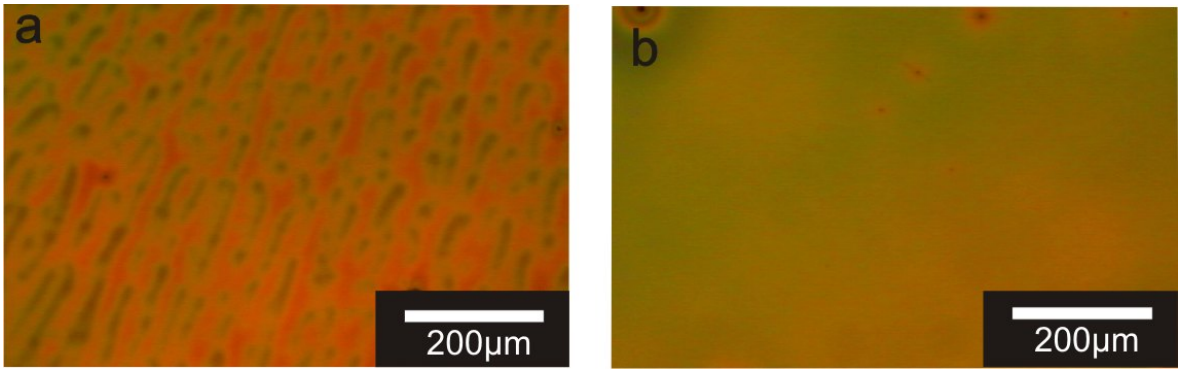

Figure 6.4: Optical microscopy images of a thin film before (a) and after (b) solvent vapour annealing. The solvent vapour removes and flattens the thin film instabilities that can occur during the spin-coating process.

dimensional information it appears that the disordered structure of Fig. 6.3a has assembled into a vesicle-like morphology. Fig. 6.3c shows a similar morphology which was obtained after SVA for 90 min at low relative solvent vapour pressures $\frac{p}{p_{sat}} < 0.6$. The comparison of Fig. 6.3b and 6.3c leads to the conclusion that that the polymer chain mobility was too low and the intermolecular interactions were too strong in as cast films to allow a long-ranged rearrangements of the block copolymer microdomains. The $\pi - \pi$ interactions are thus more reduced in solvent vapour swollen films, thereby approximating the copolymer closer to a generic coil-coil morphology.

Extensive SVA or a relative solvent vapour pressure of $\frac{p}{p_{sat}} = 1$ introduces even more solvent molecules into the film and further enhances the polymer chain mobility. However, an overall lowering of the film viscosity enables the dewetting of the entire film from the substrate. This effect is possibly enhanced by condensation of solvent onto the sample. Fig. 6.3e shows a cross section of such a dewetted film. The lamellar disorder presumably arises from the film flow during dewetting. This experiment illustrates the need for accurate control of the solvent vapour saturation and time during the annealing of the morphology of PvTPA-*b*-PPerAcr films, but also for polymer films in general.

Finally, we have examined the overall appearance of spin-cast PvTPA-b-PPerAcr films. Fig. 6.4 shows optical microscopy images of films before and after SVA treatments. After spin coating from chloroform solution (Fig. 6.4a), the film surface was inhomogeneous on the micrometer scale. During SVA, the film flattened to a smooth surface (Fig. 6.4b), comparable to earlier work.[36] While the details of the surface instability during spin-coating were not further investigated, film surface undulations are often observed when spin-coating from low boiling point solvents. A possible explanation for this has been given by de Gennes.[37] The surface perturbation of the strong concentration gradient that forms across the film during spin coating can lead to lateral Maringoni-stresses which drive the formation of convection rolls. Importantly, however, Fig. 6.4 illustrates that SVA significantly improves the overall film quality, which is one of the prerequisites for device manufacture.

Conclusion

In conclusion we showed that a sufficient solvent vapour concentration during SVA leads to a disruption of the $\pi - \pi$ stacking of the PBI moieties in PPerAcr. This effect was monitored in-situ by ellipsometric and spectroscopic measurements. The disruption of the aggregates led to an increase in photoluminescence and to a change in the relative oscillator strengths reflected in the absorption spectra. As a consequence, we were able to demonstrate that sufficient polymer chain mobility is introduced to PPerAcr by the disruption of PBI stacking. When this type of treatment was applied to thin films of a donor-acceptor block copolymer PvTPA-*b*-PPerAcr, the enhanced chain mobility led to the formation of long, uninterrupted lamellar microdomains. We expect that the method presented here is of general applicability to semiconductor polymer thin films since it induces a high degree of chain mobility at low temperatures and provides precise control of the annealing conditions.

Acknowledgement

We acknowledge the financial support from the European network "PolyFilm" under RTN-6, German Research Council (DFG) project SFB 481 and ESF Eurocores ORGANISOLAR project. S.H. thanks Universität Bayern e.V. for the financial support in the form of a scholarship of the Bayerische Graduiertenförderung and Elitenetzwerk Bayern (ENB) for their support.

Supplementary Information

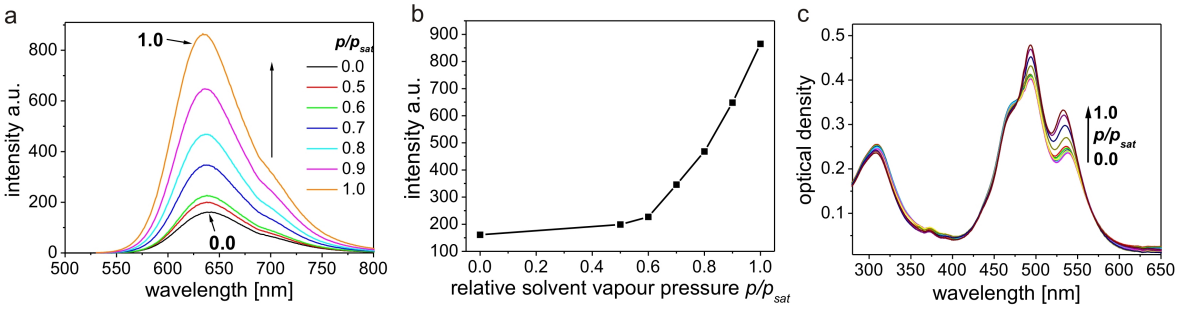

Figure 6.5: Optical properties of the PvTPA-*b*-PPerAcr block copolymer. a) Fluorescence emission as a function of the relative chloroform vapour pressure $\frac{p}{p_{sat}}$. The fluorescence of the block copolymer is strongly quenched due to the presence of the PvTPA donor material, resulting in a less pronounced shape of the fluorescence curve compared to the homopolymer in Fig. 6.2d. b) Maximum fluorescence intensity at 630 nm vs. relative solvent vapour pressure. f) Absorption spectra recorded by an UV/Vis spectrometer during solvent vapour exposure. The arrow indicates increasing optical density at 530 nm with increasing relative solvent vapour pressure. The peak at 310 nm corresponds to the absorption of the PvTPA block. Overall, the perylene bisimide block shows a very similar behaviour compared to the homopolymer.

Bibliography

[1] S. Y. Heriot and R. A. L. Jones, *An interfacial instability in a transient wetting layer leads to lateral phase separation in thin spin-cast polymer-blend films*, Nat. Mater. **4**, 782 (2005).

[2] W. Ma, C. Yang, X. Gong, K. Lee, and A.J. Heeger, *Thermally stable, efficient polymer solar cells with nanoscale control o fthe interpenetrating network morphology*, Adv. Func. Mater. **15**, 1617 (2005).

[3] F. Padinger, R.S. Rittberger, and N.S. Sariciftci, *Effects of postproduction treatment on plastic solar cells*, Adv. Funct. Mater. **13**, 85 (2003).

[4] S. Miller, G. Fanchini, Y.-Y. Lin, C. Li, C.-W. Chen, W.-F. Su, and M. Chhowalla, *Investigation of nanoscale morphologicl changes in organic photovoltaics during solvent vapor annealing*, J. Mater. Chem. **18**, 306 (2008).

[5] Yun Zhao, Zhiyuan Xie, Yao Qu, Yanhou Geng, and Lixiang Wang, *Solvent-vapor treatment induced performance enhancement of pol(3-hexylthiophene):methanofullerene bulk-heterojunction photovoltaic cells*, Appl. Phys. Lett. **90**, 043504 (2007).

[6] A.R. Campbell, J.M. Hodgkiss, S. Westenhoff, I.A. Howard, R.A. Marsh, C.R. McNeill, R.H. Friend, and N.C. Greenham, *Low-temperature control of nanoscale morphology for high performance polymer photovoltaics*, Nanolett. **8**, 3942 (2008).

[7] B. A. Jones, M. J. Ahrens, M.-H. Yoon, A. Facchetti, T. J. Marks, and M. R. Wasielewski, *High-mobility air-stable n-type semiconductors with processing versatility: dicyanoperylene-3,4:9,10-bis(dicarboximides)*, Angew. Chem. **116**, 6523 (2004).

[8] L. Schmidt-Mende, A. Fechtenkötter, K. Müllen, E. Moons, R.H. Friend, and J.D. MacKenzie, *Self-organized discotic liquid crystals for high-efficiency organic photovoltaics*, Science **293**, 1119 (2001).

[9] B.A. Gregg, *The photoconversion mechanism of excitonic solar cells*, MRS Bulletin **30**, 20 (2005).

[10] B.A. Jones, A. Facchetti, M.R. Wasielewski, and T.J. Marks, *Tuning orbital energetics in arylene diimide semiconductors. Materials design for ambient stability of n-type charge transport*, J. Am. Chem. Soc. **129**, 15259 (2007).

[11] Z. Chen, V. Stepanenko, V. Dehm, P. Prins, L.D.A. Siebbeles, J. Seibt, P. Marquetand, V. Engel, and F. Würthner, *Photoluminecence and conductivity of self-assembled $\pi - pi$ stacks of perylene bisimide dyes*, Chem. Eur. J. **13**, 436 (2007).

[12] P.M. Kazmaier and R. Hoffman, *A theoretical study of crystallochromy. Quantum interference effects in the spectra of perylene pigments*, J. Am. Chem. Soc. **116**, 9684 (1994).

[13] P.E. Keivanidis, I.A. Howard, and R.H. Friend, *Intermolecular interactions of perylene diimides in photovoltaic blend of fluorene copolymers: disorder effects on photophysical properties, film morphology and device efficiency*, Adv. Func. Mater. **18**, 3189 (2008).

[14] X. Zhan, Z. Tan, B. Domercq, Z. An, X. Zhang, S. Barlow, Y. Li, D. Zhu, B. Kippelen, and S.R. Marder, J. Am. Chem. Soc. **129**, 7246 (2007).

[15] Zhihua Chen, Yan Zheng, He Yan, and Antonio Facchetti, *Naphthalenedicarboximide- vs Perylenedicarboximide-based copolymers. Synthesis and semiconducting properties in bottom-gate n-channel organic transistors*, J. Am. Chem. Soc. **131**, 8 (2009).

[16] S. Hüttner, M. Sommer, and M. Thelakkat, *n-type organic field effect transistors from perylene bisimide block copolymers and homopolymers*, Appl. Phys. Lett. **92**, 093302 (2008).

[17] M. Sommer, S. Hüttner, S. Wunder, and M. Thelakkat, *Electron-conducting block copolymers: morphological, optical, and electronic properties*, Adv. Mater. **20**, 2523 (2008).

[18] S. Lindner and M. Thelakkat, *Nanostructres of n-type organic semiconductor in a p-type matrix via self-assembly of block copolymers*, Macromolecules **37**, 8832 (2004).

[19] M. Sommer, A. S. Lang, and M. Thelakkat, *Crystalline-crystalline donor-acceptor block copolymers*, Angew. Chem. Int. Ed. **47**, 7901 (2008).

[20] G.H. Fredrickson and F.S. Bates, *Dynamics of block copolymers: theory and experiment*, Annu. Rev. Mater. Sci. **26**, 501 (1996).

[21] G.A. Buxton and N. Clarke, *Predicting structure and property relations in polymeric photovoltaic devices*, Physical Review B **74**, 085207 (2006).

[22] S. Lindner, S. Hüttner, A. Chiche, M. Thelakkat, and G. Krausch, *Charge separation at self-assembled nanostructured bulk interfaces in block copolmers*, Angew. Chem. Int. Ed. **45**, 3364 (2006).

[23] M. Sommer, S. Lindner, and M. Thelakkat, *Microphase-separated donor-acceptor diblock copolymers: influence of HOMO energy levels and morphology on polymer solar cells*, Adv. Func. Mater. **17**, 1493 (2007).

[24] H. Elbs and G. Krausch, *Ellipsometric determination of Flory-Huggins interaction parameters in solution*, Polymer **45**, 7935 (2004).

[25] T. Hayakawa and S. Horiuchi, *From Angstroms to micrometers: self-organized hierarchical structure within a polymer film*, Angew. Chem. Int. Ed. **42**, 2285 (2003).

[26] Bradley D. Olsen and Rachel A. Segalman, *Self-assembly of rod-coil block copolymers*, Mater. Sci. and Eng. **62**, 37 (2008).

[27] P.J. Flory, *Principles of polymer chemistry*, 9th edition ed. (Cornell University Press, Ithaca, 1975).

[28] M. Mukherjee, Amarjeet Singh, J. Daillant, Alain Menelle, and F. Cousin, *Effect of solvent-polymer interaction in swelling dynamics of ultrathin polyacrylamide films: A neutron and x-ray reflectivity study*, Macromol. **40**, 1073 (2007).

[29] V. Marcon, J. Kirkpatrick, W. Pisula, and D. Andrienko, *Supramolecular structure of perylene tetracarboxdiimides*, Phys. Stat. Sol. (b) **5**, 245 (2008).

[30] A. J. Ferguson and T. S. Jones, *Photophysics of PTCDA and Me-PTCDI thin films: effects of growth temperature*, J. Phys. Chem. B **110**, 6891 (2006).

[31] U. Steiner, J. Klein, E. Eiser, A. Budkowski, and L.J. Fetters, *Complete wetting from polymer mixtures*, Science **13**, 1126 (1992).

[32] T. Thurn-Albrecht, J. DeRouchey, and T.P. Russel, *Overcoming interfacial interactions with electric fields*, Macromolecules **33**, 3250 (2000).

[33] P. Mansky, Y. Liu, E. Huang, T.P. Russell, and C. Hawker, *Controlling Polymer-Surface Interactions with Random Copolymer Brushes*, Science **275**, 1458 (1997).

[34] L. Rockford, Y. Liu, P. Mansky, and T. P. Russell, *Polymers on nanoperiodic, heterogeneous surfaces*, Phys. Rev. Lett. **82**, 2602 (1997).

[35] M.J. Fasolka, D.J. Harris, and A.M. Mayes, *Observed substrate topography-mediated lateral patterning of diblock copolymer films*, Physical Review Letters **79**, 3018 (1997).

[36] Mitchell Anthamatten, Stephan A. Letts, and Robert C. Cook, *Controlling surface roughness in vapor-deposited poly(amic acid) films by solvent-vapor exposure*, Langmuir **20**, 6288 (2004).

[37] P.G. de Gennes, *Instabilities during the evaporation of a film: Non-glassy polymer + volatile solvent*, Eur. Phys. J. E **6**, 421 (2001).

Chapter 7

Intermolecular Interactions in Perylene Bisimide Polymer Architectures

Sven Hüttner,[a,b] Michael Sommer,[b] Justin Hodgkiss,[a,c] Panos Keivanidis,[a,d] Ullrich Steiner,[a] Mukundan Thelakkat[b]

a) Cavendish Laboratory, University of Cambridge, United Kingdom
b) Makromolekulare Chemie I, Universität Bayreuth, Germany
c) MacDiarmid Institute, Vicotria University of Wellington, New Zealand
d) Department of Physics, Imperial College London, United Kingdom

Abstract

This work focuses on a set of perylene bisimide (PBI) based homo- and block copolymers, able to serve as model materials in the study of self-organising properties of PBI moieties. The possibility of utilising the films of these block copolymers as photoactive components in organic photovoltaic devices is addressed by detailed spectroscopic and structural characterisation studies. The tendency of these compounds to self-organise in the solid state is addressed in a step-wise fashion by increasing the complexity of the chemical structure, from a monomer (Per), to a polymer of poly(perylene bisimide acrylate) (PPerAcr), to a block copolymer with an inert polystyrene block (PS-*b*-PPerAcr), and finally to a block copolymer carrying a donor block of poly(vinyl triphenylamine) (PvTPA-*b*-PPerAcr). The PBI moieties exhibit strong $\pi - \pi$ interactions, affecting the optical and electronic properties, but also its semi-crystalline structure. The factors that dictate the extent of mesoscopic order in PPerAcr films are discussed based on in-situ temperature-dependent small and wide angle X-ray scattering, combined with absorption spectroscopy. Evidence for long range order is presented for these superstructures when appropriate thermal processing protocols are adapted, which improve the electron charge carrier mobility. The formation of longer aggregates is related to a decrease in the photoluminescence and a prolonged exciton polarisation anisotropy measured by time resolved transient absorption spectroscopy.

Further, modified patterns of hierarchical organisation in the solid state are found when block-units of electronically inactive polystyrene (PS) are linked to PPerAcr (PS-*b*-PPerAcr). Block copolymer morphologies such as lamellae and cylinders could be identified by small angle X-ray scattering depending on the block copolymer

composition. The mesoscopic order and the optical properties of the PBI moieties stay unaffected by the confinement in these microphases. The effect of annealing regarding the interplay between morphological order and intermolcuar packing of the PBIs was studied.

Finally, photovoltaic active PPerAcr-*b*-PvTPA block copolymers are obtained when the PS block is replaced by the conducting poly(vinyl triphenylamine). The photovoltaic performance of PvTPA-*b*-PPerAcr, however, strongly depends on both, the crystallinity and the morphology of a donor-acceptor system. The crystallinity can be increased locally by thermal annealing already below its melting temperature, increasing the electron mobility as well as the external quantum efficiency.

Introduction

Perylene bisimide (PBI) derivatives have attracted attention for their application in organic electronics for a long time. They show a broad and intensive absorption in the visible light spectrum and they combine good n-type charge transport properties with a high air stability.[1,2] These features make PBIs outstanding candidates for n-type organic semiconductors. Intensive research has been undertaken towards their applications in thin film transistors, photovoltaic devices and detectors.[3,4] PBIs have been synthetically modified in various ways from low molecular weight molecules that often exhibit liquid crystalline behaviour[5,6] to polymerised derivatives,[7–9] opening up new possibilities for the morphology control in polymer solar cells.

Bulk heterojunction solar cells, for example, rely on a distinct morphology between a donor and an acceptor material. Excitons created by photoabsorption in one of the materials separate into charges at the donor-acceptor interface. The ideal donor-acceptor morphology is determined by two seemingly contradictory conditions. On the one hand the exciton diffusion length is only a few nanometres, requiring short distances between donor and acceptor domains, while on the other hand as much light as possible should be absorbed which requires thicker layers. In addition, each of the semiconducting phases should have continuous percolation paths to the electrodes. Conventional devices use a phase separated blend of donor and acceptor materials with the attempt to create a sufficiently fine bicontinuous network[10] by the adjustment of the phase separation kinetics of the two materials. This can be obtained through the use of the right solvents, cosolvents,[11] as well as additional thermal annealing[12] or solvent vapour annealing procedures.[13] High levels of morphological control in organic photovoltaics are sought to be achieved by the self-assembling properties of donor acceptor (D-A) block copolymers. Conventional block copolymers consist of two different polymers that are covalently linked. In block copolymers, the interplay between molecular connectivity and immiscibility leads to the spontaneous formation of ordered microdomains of molecular dimensions. Depending on the volume ratio of the respective blocks, a range of different morphologies can be found, including spherical, lamellar, cylindrical and gyroidal structures.[14,15] Those structures are highly regular and form via self-assembly during the annealing processes of the material.

The potential of the block copolymer strategy for organic photovoltaics has been recognised earlier.[16] However, replacing amorphous, non-functional copolymer blocks

with electronically functional blocks is far from trivial. A number of obstacles had to be overcome in their synthesis to avoid high polydispersity and to achieve good control over the molecular weight.[17] Furthermore, the $\pi-\pi$ interactions of conjugated systems or the rigidity of conjugated polymers[18] complicate the thermodynamics and the phase separation kinetics of block copolymers. Fully functionalised D-A block copolymers with suitable electronic functions, sufficient solubility in common organic solvents and the ability to microphase separate, are therefore rare. Recently, a number block copolymer architectures with poly(perylene bisimide acrylate) (PPerAcr) as electron acceptor have been synthesized, most notably amorphous-crystalline D-A block copolymers with a poly(triarylamine) donor block and a side chain perylene bisimide (PPerAcr) acceptor block, and crystalline-crystalline D-A block copolymers with poly(3-hexylthiophene) as donor and PPerAcr as acceptor segment.[9,19–22] In these partially or double-crystalline block copolymers, the competing crystallisation and microphase separation lead to a complex phase behaviour.[23] This paper focuses on the structural and electronic properties of PPerAcr as a homopolymer and in combination with amorphous polymer blocks.

$\pi-\pi$ interactions are a main characteristic of PBIs which lead to the formation of supramolecular aggregates, crystallites or liquid crystals.[6,24,25] Thereby the material properties can be altered without changing the perylene bisimide core, just by replacing the attached substituents at the imide position. The substituents determine physical properties such as the melting temperature, solubility, crystallinity or liquid crystalline behaviour. The electro-optical properties of the aggregates are also directly affected since they are determined by the relative stacking of the perylene bisimide cores. The electronic properties of single PBI-moieties, however, do not change upon substitution at the imide position, which is due to the wavefunction's nodes localised at the imide groups.[26,27]

The optical properties of isolated PBI are characterised by Frenkel excitons (FE) - excited states that are localised at the molecule. The strong $\pi-\pi$ interactions between the perylene bisimide moieties enable their close packing. A different orientation, position or distance modifies the coupling of the transition dipole-moments resulting in a change of the spectral properties,[26] which causes the formation of charge transfer excitons.[28] These are excited states localised at two neighbouring molecules, self-trapped charge transfer states (CT_{ST}), or dimers. Furthermore, molecules have been synthesised with additional groups attached to the bay positions of the molecule[1] leading to a twist of the flat perylene bisimide core and to changes in the electronic properties.[29]

With the numerous synthetic and theoretical studies of monomeric forms of perylene bisimides on the one hand, and the exciting but complex supramolecular structures of perylene bisimide containing block copolymers[30] on the other hand, this study attempts to bridge the gap between monomeric PBIs and PBI containing block copolymers. We investigate systematically how the photophysical properties of PBI moieties evolve with increasing complexity of the polymeric architecture, in which the PBIs are incorporated. Starting from a monomeric, branched, and symmetrically substituted low molecular weight perylene bisimide (Per), we continue with a side-chain crystalline perylene bisimide homopolymer (PPerAcr), where aggregation occurs already in a single polymer chain. This is followed by the study of three block copolymers which elucidates the effect of confinement on the photophysics of PBI in block

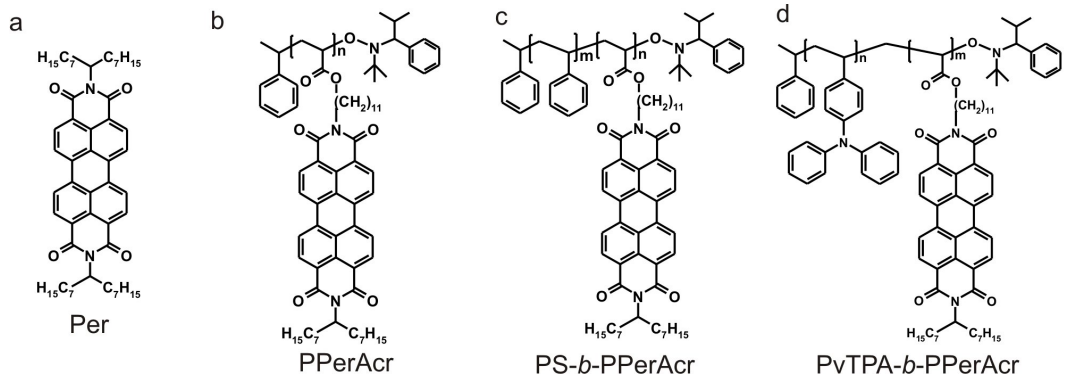

Figure 7.1: a) Low molecular weight model (Per); b) Side chain polymerised poly(perylene bisimide acrylate) (PPerAcr) c) Block copolymer of an inert block of polystyrene (PS) and PPerAcr (PS-*b*-PPerAcr). d) Fully functionalised block copolymer with poly(vinyl triphenylamine) as a donor block and PPerAcr as an acceptor block.

Table 7.1: Molecular weight, block ratio, polydispersity (PDI) and thermal properties.[9,21]

Material	$M_n\left[\frac{\text{g}}{\text{mol}}\right]$	PDI	wt.% PPerAcr	$T_g[^\circ C]$	$T_m[^\circ C]$
Per	803				130
PPerAcr	30 900	1.86	100	–	193
PS-*b*-PPerAcr I	37 900	1.52	70	100	189
PS-*b*-PPerAcr II	43 100	1.78	65	105	192
PvTPA-*b*-PPerAcr	40 420	1.50	86.0	150	198

copolymer domains. Two block copolymers carry an electronically inactive polystyrene block (PS) and a PPerAcr block. Different molecular weights of the PPerAcr block result in either a cylindrical (PS-*b*-PPerAcr I) or a lamellar block copolymer morphology (PS-*b*-PPerAcr II). The third block copolymer consists of a poly (vinyl triphenylamine) donor block which is covalently connected to PPerAcr (PvTPA-*b*-PPerAcr), resulting in charge transfer between donor and acceptor upon excitation. The PvTPA-*b*-PPerAcr block copolymer exhibits a lamellar morphology. The photophysics of all these materials are investigated in solution and in thin films. Finally, photovoltaic devices are constructed from PvTPA-*b*-PPerAcr using several annealing protocols. The resulting changes of the PBI interactions are correlated with their photoluminescence quenching efficiency and external quantum efficiencies of photovoltaic devices.

The chemical structures of the molecules are shown in Fig. 7.1 and their corresponding material properties are given in Tab. 7.1. Fig.7.1a shows the low molecular weight PBI derivative used in this study (Per). This molecule consists of a PBI core, symmetrically substituted with branched C15 alkyl groups. An isotropic phase is observed above 130 °C and a narrow monotropic liquid crystalline phase occurs on cooling between 119 and 106 °C as studied by differential scanning calorimetry (DSC).[6] The alkyl side groups guarantee excellent solubility e.g. in chloroform.

The homopolymer and block copolymers were prepared via nitroxide mediated radical polymerisation (NMRP) of a polymerisable PBI monomer perylene bisimide acrylate (PerAcr) (Fig. 7.1b). The repeat units of this polymer carry the same branched C15 alkyl group at one imide position and a linear alkyl group at the other imide posi-

tion. The synthetic procedures of the homo- and block copolymers have been described in previous publications.[9,31] The number of repeat units is approximately 28 resulting in a molecular weight of 30.9 $\frac{\text{kg}}{\text{mol}}$. The polymer exhibits one melting temperature of 193 °C which is higher than in Per. This already shows that the spatial freedom of the PBI moieties is more restricted through the covalent linkage to the poly acrylate backbone.

The PS-*b*-PPerAcr block copolymers (Fig. 7.1c) with polystyrene as the first block are synthesised using PS macroinitiators of different molecular weights, whereas the PPerAcr weight fraction was roughly held constant (Fig. 7.1c). PS-*b*-PPerAcr I has a total molecular weight of 37.9 $\frac{\text{kg}}{\text{mol}}$ and a polydispersity index of 1.52 and contains 70 wt% PPerAcr. The glass transition temperature T_g and the melting temperature T_m are 100 and 189 °C, respectively. PS-*b*-PPerAcr II has a molecular weight of 43.1 $\frac{\text{kg}}{\text{mol}}$, a polydispersity of 1.78 and 65 wt% PPerAcr. The T_g and the T_m are 105 and 192 °C, respectively.

The PvTPA-*b*-PPerAcr block copolymer (Fig. 7.1d), consists of a block of poly (vinyl triphenylamine) (PvTPA) and a block of PPerAcr, with M_n=40.4 $\frac{\text{kg}}{\text{mol}}$, a PPerAcr weight fraction of 86% and a polydispersity of 1.5. Two thermal transitions occur, a T_g due to the amorphous PvTPA at 150 °C and a T_m due to PPerAcr at 198 °C. Triphenylamine is a hole transporting material and serves as an electron donor site. Thus, this block copolymer features both, donor and acceptor functionalities and can therefore be applied in bulk heterojunction solar cells as previously demonstrated.[32] This specific block copolymer exhibits a lamellar morphology.[13]

Results and discussion

Spectroscopy in solution

Optical spectroscopy of Per in solution gives a first insight into the interactions of the PBIs. Fig. 7.2a shows an absorption and emission spectrum (at 470 nm excitation) of the model monomer Per in a diluted chloroform solution (10^{-5} M). The spectra exhibit an electronic transition from the ground state $S_0 - S_1$ with its well-resolved vibronic levels. The emission is quasi-symmetric to the absorption and exhibits a classical Stokes shift. The absorption is not concentration dependent (in the concentration range of 10^{-3} to 10^{-7} $\frac{\text{mol}}{\text{l}}$), but the emission is, as shown in the inset of Fig. 7.2. The spectral overlap of the emission and absorption spectra leads to reabsorption with the result that the high energy peak becomes less pronounced with increasing concentration. The low molecular weight perylene bisimide shows no aggregation in solution in the observed concentration range, owing to the good solubility in chloroform solution.

The spectra change drastically once the solvent is withdrawn (Fig. 7.2c). In a spin-coated film the intermolecular interactions are dominant. The $\pi - \pi$ interactions lead to the formation of aggregates with an intermolecular distance of ~ 0.35 nm.[33] This is sufficiently close for the p-orbitals to overlap in such a way that charge transfer excitons are significantly produced in addition to Frenkel excitons (FE). The peak that developed at 550 nm (2.26 eV) has been identified to be of charge-transfer exciton origin, as demonstrated for example by Bulovic et al.[34] The mixing of the charge-transfer (CT) excitons and the Frenkel excitons is suggested to lead to new transition dipole

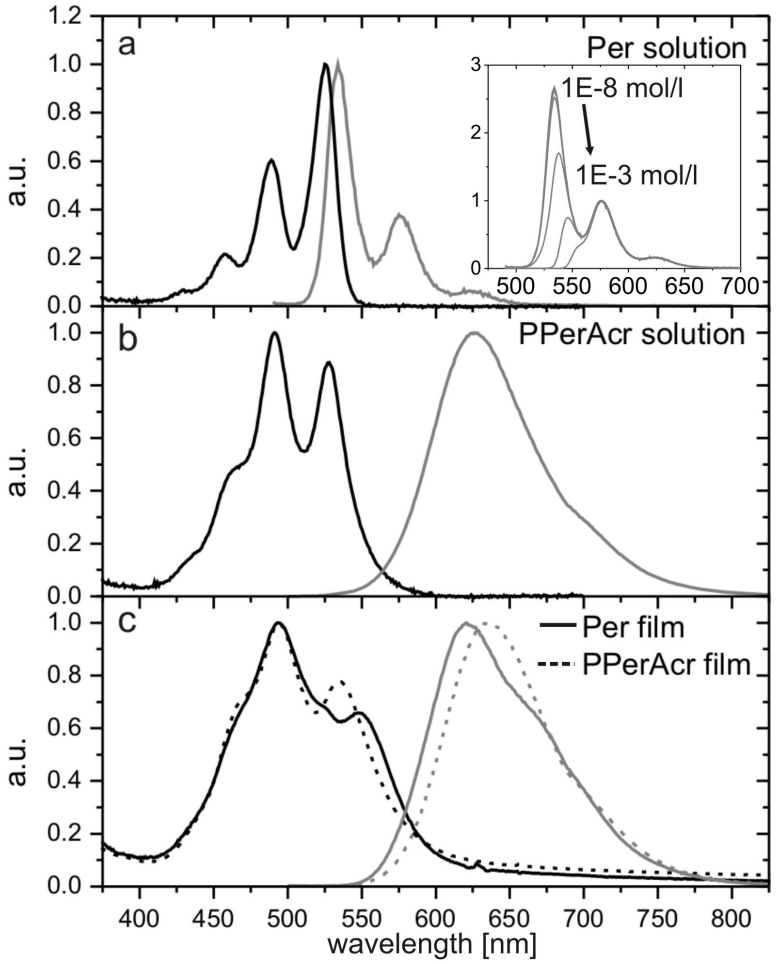

Figure 7.2: a) Absorption and emission of Per model monomer in $10^{-5}\,\mathrm{M}$ and $10^{-8}\,\mathrm{M}$ chloroform solution, respectively. The emission spectra is concentration dependent (inset) and the first vibronic level decreases with a bathochromic shift. The inset shows the emission spectra in a concentration range of $10^{-8}\,\mathrm{M}$ to $10^{-3}\,\mathrm{M}$. b) Absorption and emission spectra of PPerAcr in solution ($10^{-6}\,\mathrm{M}$). The emission is dominated by the formation of aggregates shifting the maximum to 635 nm and broadening to lower energies. c) Absorption and emission spectra of low molecular weight Per (solid line) and homopolymer PPerAcr (broken line) in a spin-coated film. The absorption spectra broadens and new spectral features develop. The emission spectra corresponds to the aggregate's emission, with a more pronounced red shift of PPerAcr.

components.[35] Ferguson and Jones describe this as a combination of contributions from a self-trapped CT state and further low energy bands.[36] They also consider the broadening at around 496 nm (2.5 eV) caused by CT-FE, whereby the vibronic progressions of the Frenkel excitons, which are located on isolated molecules, are dominant. The broadening of the absorption spectra, the appearance of new features and a wide low energy tail has also been observed in various compounds of perylene bisimide.

The homopolymer PPerAcr in solution shows a different spectrum compared to Per (Fig. 7.2b). The perylene side groups are always in proximity to each other since they are all bound to a polymer backbone. The consequence is that molecular

coupling is always present in the polymer: The spectrum is broadened and the clear vibronic splitting vanishes due to the formation of intermixed states. The spectrum of the spin-coated polymer film (Fig. 7.2c) resembles mostly the spectrum of the spin-coated monomer film however with a more elaborate bathochromic shift of the feature at 549 nm (2.2 6eV). It is evident, that spectral features owing to charge transfer states are more pronounced in the Per than in the PPerAcr. The intermolecular packing is enhanced in the low molecular weight molecule due to its small size and symmetrical shape.

The fluorescence of Per in solution is completely distinct from the emission of PPerAcr in solution and from Per and PPerAcr in thin films. While the symmetric progressions in absorption are resolved for Per in solution, PPerAcr and the thin films of Per show only one, bathochromic shifted, broad peak at 635 nm (1.95eV) with a small feature at 700 nm (1.77 eV). These spectra resemble those typically observed for excimers - excited states that are localised on two moieties. Würthner et al. suggest that an excited perylene bisimide moiety can induce structural and energetic reorganisation processes with the neighbouring unexcited moiety leading to a relaxed state that has an energetically lower emission.[5]

X-ray diffraction and opto-electrical properties of PPerAcr

The crystallinity and the aggregation of the perylene bisimide units is strongly influenced by the sample processing. In order to investigate the effect of different sample preparation, we performed X-ray scattering experiments at different temperatures and after several annealing procedures. Crystalline PPerAcr, obtained by slow cooling ($\sim 10\,\frac{\mathrm{K}}{\mathrm{min}}$ from the melt (Fig. 7.3b-VIa) shows features of the $\pi-\pi$ stacking of the perylene bisimide moieties of 0.35 nm at $q = 17.8\,\mathrm{nm}^{-1}$. The crystalline perylene bisimide forms an oblique 2-d lattice with lattice parameters of $a = 3.5\,\mathrm{nm}$ and $b = 2.2\,\mathrm{nm}$ meeting at an angle of $\alpha = 60.5\,^{\circ}$. The first order peaks are indicated in Fig. 7.3b-VIa followed by higher order peaks in the $q = 5 - 8\,\mathrm{nm}^{-1}$ range and a broad amorphous halo originating from the alkyl chains ($q = 9 - 16\,\mathrm{nm}^{-1}$). The extend of the crystallinity depends on the kinetics and the temperature of the annealing procedure which is investigated here. Fig. 7.3a shows a temperature profile used in in-situ X-ray measurements, where selected data is shown in Fig. 7.3b. The series starts with a bulk that has been exposed to chloroform solvent vapour for some hours before the start of the measurements. The fast evaporation of the solvent molecules when drying the sample leads to a disrupted structure that gives rise to a broad maximum between $q = 2 - 4\,\mathrm{nm}^{-1}$. When the sample is heated to a temperature still below the melting temperature first rearrangements of amorphous parts take place and cold crystallisation occurs at temperatures as low as 130 °C (not shown here). The temperature was then kept constant at 160 °C for ten minutes. Fig. 7.3b-II and III show the development of the spectra during this time period. Interestingly, an additional weak feature at $q = 1.2\,\mathrm{nm}^{-1}$ appears in films that where never heated over T_m. This feature cannot be assigned to the suggested oblique 2-d lattice and we attribute this to a non-equilibrium structure with a structure size of 5.2 nm since this feature is not prevalent when the sample is recrystallised from the melt. Local intermolecular rearrangements among the perylene bisimide moieties into larger and ordered crystalline structures occur below the

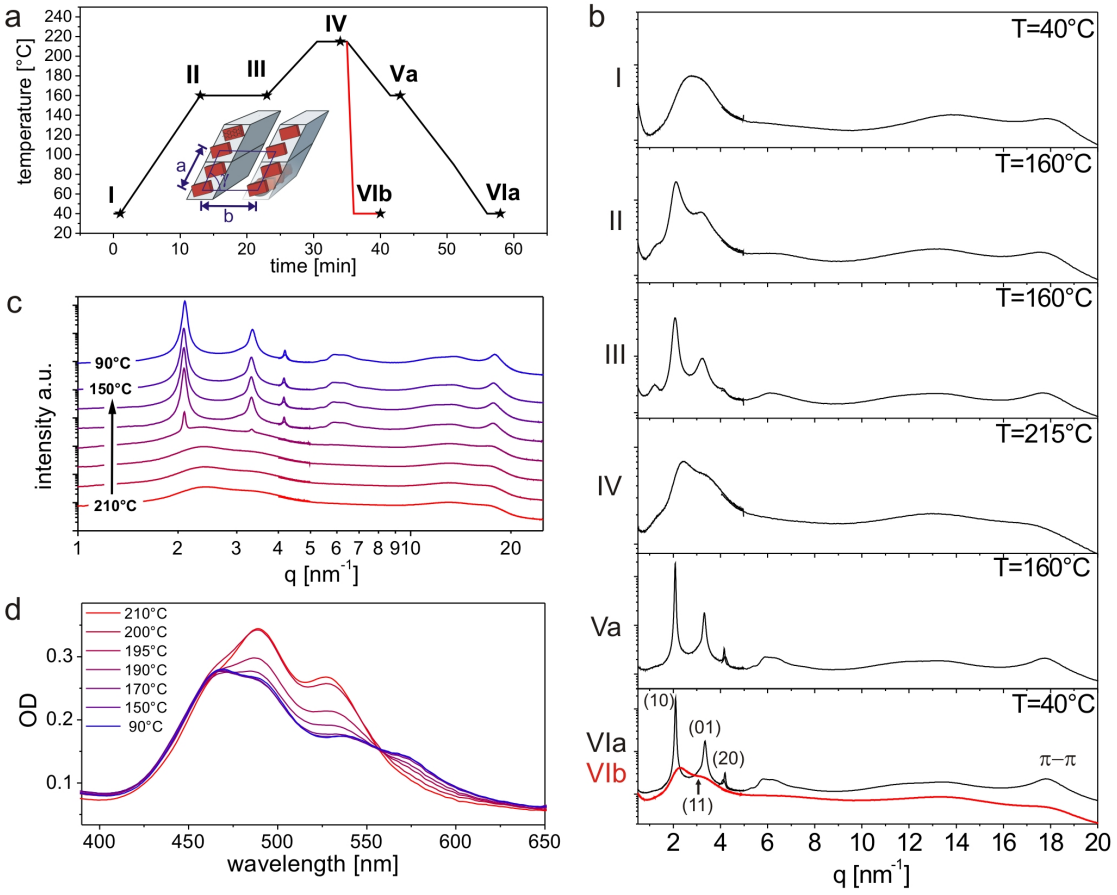

Figure 7.3: Temperature dependent X-ray and absorption spectroscopy measurements of PPerAcr. a) Temperature profile of the sample run. The stars indicate the points at which X-ray spectra of b) were taken. b) Combined small and wide angle X-ray spectra from PPerAcr at selected temperatures: (I) after solvent vapour exposure at 40 °C; (II) at 160 °C; (III) after holding at 160 °C for 10 min; (IV) at 215 °C, where PPerAcr is molten; (Va) at 160 °C after cooling from the melt at $10\,\frac{\mathrm{K}}{\mathrm{min}}$; (VIa) at 90 °C, which is identical to the measurement at 40 °C after cooling it further down from 160 °C at a rate of $10\,\frac{\mathrm{K}}{\mathrm{min}}$ (black line); (VIb) at 40 °C after fast cool down (red curve). c) Selected X-ray measurements during cooling from the melt and d) corresponding absorption spectra taken from thin films at the same temperatures. The recrystallisation is visible by the appearance of sharp features in the X-ray spectra and also by the enhanced formation of charge-transfer states.

melting temperature. PPerAcr melts at ∼193 °C and the crystalline features disappear as shown the Fig. 7.3b-IV. The peak for the intermolecular stacking disappears and a broad halo replaces the distinct crystalline features. The kinetics of recrystallisation determines the degree of crystallinity depending on the cooling rate.

A qualitative comparison of the peak widths yields information about the long range order in the bulk. Fig. 7.3b-Va and VIa show the recrystallised PPerAcr which was cooled at a rate of $10\,\frac{\mathrm{K}}{\mathrm{min}}$, where the highest crystallinity was observed. Fig. 7.3c shows intermediate steps of the cooling process and the corresponding absorption spec-

tra of a PPerAcr film (Fig. 7.3d). Upon cooling, the vibronic transitions decrease in oscillator strength together with a systematic increase of the low energy charge transfer feature with an isosbestic point at 558 nm. This provides direct experimental proof of the previously suggested correlation between oscillator strength at 590 nm and crystallinity.[36,37] Fast quenching from the melt with rates $> 10\,\frac{\mathrm{K}}{\mathrm{s}}$, where the sample is quickly cooled on a metal block results in frozen-in amorphous material with the spectral signature of the melt, shown in Fig. 7.3b-VIb (red curve). Note that the cooling rate of the quenched X-ray samples that were supported on an aluminum holder were much higher than those on the glass substrates used for the spectroscopic measurements because of the 290 times higher thermal conductivity of aluminum.

The degree of aggregation not only influences the optical absorption, but also the charge transport. We measured field effect transistors of PPerAcr after a range of annealing methods similar as presented in previously.[38] These measurements allow to extract a value for the charge carrier mobility. The value calculated from field effect transistor measurements usually overestimates the bulk charge carrier mobility, but it offers a reliable and simple method to compare the different annealing methods, i.e. the effect of perylene bisimide aggregation on the transport characteristics. The details of the transistor measurements can be found in the supplementary information. The mobility – as determined from the OFET saturation regime – is as low as $10^{-5}\,\frac{\mathrm{cm}^2}{\mathrm{Vs}}$ and a similar value was found for solvent vapour annealed samples ($6.5 \cdot 10^{-6}\,\frac{\mathrm{cm}^2}{\mathrm{Vs}}$). Additional thermal annealing leads to a strong increase of the mobility. After a low temperature annealing at 160°C, the as spun sample and the previously solvent vapour annealed sample reached mobilities of $9.9 \cdot 10^{-4}\,\frac{\mathrm{cm}^2}{\mathrm{Vs}}$ and $6.8 \cdot 10^{-4}\,\frac{\mathrm{cm}^2}{\mathrm{Vs}}$, respectively. The thermally annealed sample at 215°C followed by fast quenching reached mobilities up to $10^{-5}\,\frac{\mathrm{cm}^2}{\mathrm{Vs}}$ and those quenched slowly reach even higher mobilities of approximately $1.2 \cdot 10^{-3}\,\frac{\mathrm{cm}^2}{\mathrm{Vs}}$. Thus, an enhanced aggregation of the perylene bisimides, is important for the charge transport. The charge carrier mobility scales with the crystallinity, i.e. the extend of the PBI-stacks.

The observations in the charge carrier transport prompted us also to investigate the dynamics of optical excitations in the perylene polymer materials. We carried out transient absorption (TA) measurements in order to probe these dynamics. Fig. 7.4 shows the differential transmission spectrum of the PPerAcr homopolymer on a timescale of 200 fs - 1.9 ns following excitation with a 490 nm, 80 fs excitation pulse. The spectrum is dominated by photoinduced absorption ($\Delta T/T < 0$) for wavelengths beyond 580 nm ($\lambda_{mx} = 730\,\mathrm{nm}$). On the blue edge of the spectra, the photoinduced absorption overlaps with bleaching features ($\Delta T/T > 0$) at wavelengths corresponding to ground-state absorption into PBI aggregates ($\lambda_{max} = 496, 550\,\mathrm{nm}$). As expected, no stimulated emission is observed in the wavelength region where luminescence is observed ($\lambda_{max} = 635\,\mathrm{nm}$) because PBI aggregation increases the radiative lifetime of excitons, corresponding to a low stimulated emission cross-section. These spectral features are consistent with previous TA investigations of PBI aggregates.[39] Thermally annealing the film resulted in no observable difference in the TA spectra, however this measurement is not ideally suited to reveal information about the orientational ordering within PBI aggregates.

Our interest in ordering of PBIs in PPerAcr prompted us to extend the TA

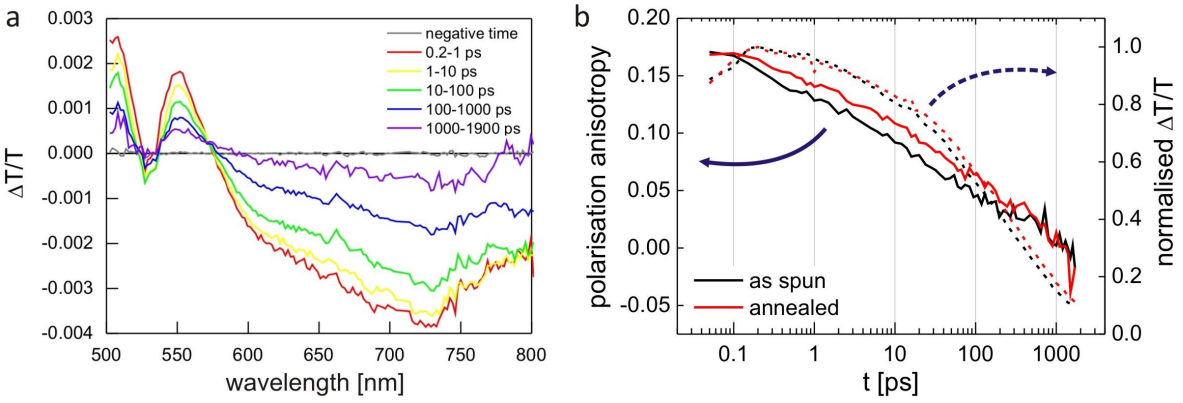

Figure 7.4: a) Transient absorption spectra of PPerAcr for different time ranges after excitation. The negative values of $\Delta T/T$ indicate the region of photoinduced absorption that develops after exciton formation. b) Time dependent polarisation anisotropy of an as-spun (blue) and an annealed (red) film of PPerAcr shows that the anisotropy increases, caused by the better packing of the perylene bismides after thermal annealing. The dashed line shows the normalised corresponding transient absorption integrated from 700-750 nm.

measurements to include polarisation resolution. In this experiment, a linearly polarised excitation pulse initially generates an anisotropic distribution of excitations. The delayed probe pulse is split into two simultaneously detected polarisation channels (parallel and perpendicular with respect to the excitation pulse) to resolve the anisotropy decay associated with excitations migrating to regions with differently orientated chromophores.[40] Polarisation anisotropy dynamics are a powerful probe of the motion of optical excitations and of the morphology that they encounter, particularly in materials where motion is not associated with a spectral shift.[41–43] Fig. 7.4b shows polarisation resolved TA kinetics for a pristine film of the PPerAcr homopolymer (solid black curve) compared with a thermally annealed film (solid red curve), which was kept for 10 min at 215 °C followed by slow cooling at 10 $\frac{\mathrm{K}}{\mathrm{min}}$. The samples were probed in the photoinduced absorption region at 800 nm. The initial polarisation anisotropy level is $r = 0.17$ - considerably lower than the maximum value of 0.4 expected for a chromophore with parallel transition dipole moments in the ground and excited states prior to depolarisation.[44] The initial loss of polarisation anisotropy could be accounted for if the photoinduced absorption probed at 800 nm has a transition dipole moment polarised 38° relative to the ground state absorption at the excitation wavelength of 490 nm.* Interchain absorption bands are indeed found to have significant transition dipole moment intensity out of the molecular plane.[41] Additionally, exciton localisation has been demonstrated to cause ultra-fast depolarisation following absorption into interchain aggregate states.[45] The polarisation anisotropy decay is strongly dispersive in all cases and significantly faster in the case of the pristine film of PPerAcr (black curve, $t_{1/2} = 15$ ps) than in the thermally annealed films of PPerAcr film (red curve, $t_{1/2} = 30$ ps). For comparison, the polarisation anisotropy is found to decay substantially faster in a disordered film of poly(9,9'-dioctylfluorene-co-benzothiadiazole)

*Using the equation extracting transition dipole moment shift using the initial and final polarisation anisotropy values r_i and r_f; $\Theta = \cos^{-1}(\pm\sqrt{\frac{r_i+2r_f}{3r_i}})$[44]

($t_{1/2} = 5\,\mathrm{ps}$), corresponding to a loss of polarisation anisotropy in just a few exciton hops.[46] We attribute the prolonged polarisation anisotropy to orientational ordering of PPerAcr. The slower anisotropy decay in thermally annealed films is consistent with an enhancement of orientational ordering compared with the pristine film of PPerAcr. We note that polarisation anisotropy decay is significantly faster than the population decay in all cases (dashed curves, $t_{1/2} \approx 100 - 200\,\mathrm{ps}$), which shows that polymeric PBI aggregates still have enough orientational disorder for excitations to depolarise within their lifetimes.

Block copolymer morphologies

Further, the different degrees of structural order and intermolecular interplay was investigated for different block copolymer architectures of perylene bisimide. The block copolymer PS-*b*-PPerAcr that confines the perylene domains in its nanostructured morphology within the polystyrene domains. The fully functionalised block copolymer PvTPA-*b*-PPerAcr which offers the next higher degree of complexity where the electronically non-active polystyrene block has been replaced by PvTPA acting as a donor polymer. Fig. 7.5 shows small angle X-ray scattering measurements (SAXS) and corresponding transmission electron microscopy (TEM) images for two different molecular weight fractions of PS-*b*-PPerAcr and of PvTPA-*b*-PPerAcr. As mentioned above, different morphologies can be achieved by a variation the volume ratio of the blocks. PS-*b*-PPerAcr I shows a hexagonal cylindrical morphology, whereas PS-*b*-PPerAcr II shows a lamellar morphology. The SAXS pattern of PvTPA-*b*-PPerAcr is not very well resolved, only exhibiting a broad first order peak that indicates a rather large domain sizes of around 50 nm. The TEM image in Fig. 7.5c shows a that the domains are not aligned explaining the missing of higher order peaks, but the PPerAcr (dark) seems to form long connected sheet-like strucutres.

In summary, these material systems exhibit hierarchical orders on three different length-scales: the intermolecular $\pi - \pi$ stacking (0.35 nm), the mesoscopic ordering of 1-d aggregates into a 2-dimensional oblique lattice (2-3 nm) and the formation of microphases ($\sim 15 - 20\,\mathrm{nm}$).

Annealing and optical spectroscopy of homo- and block copolymer films

The results above prompted us to investigate the spectroscopic behaviour in thin films of the three PPerAcr-containing polymers. The thin films were processed by spin-coating. One consequence of spin-coating is that molecules and polymers are kinetically trapped on their way to a thermodynamic equilibrium as the solvent evaporates. Annealing methods such a temperature annealing[37] and solvent vapour annealing[13,47,48] introduce mobility to the molecules so that they can rearrange. Annealing is not only decisive for the intermolecular packing of the PBIs, but also on a macroscopic scale, meaning the morphology of a polymer blend or block copolymer. Therefore annealing is a critical step for the processing of bulk heterojunction solar cells, where donor and acceptor materials are blended together. Annealing followed by quenching of polymer blends usually attempts to arrest a certain morphology during the process of phase separation. The thermodynamic melt equilibrium is expected to result in too large, micrometre-

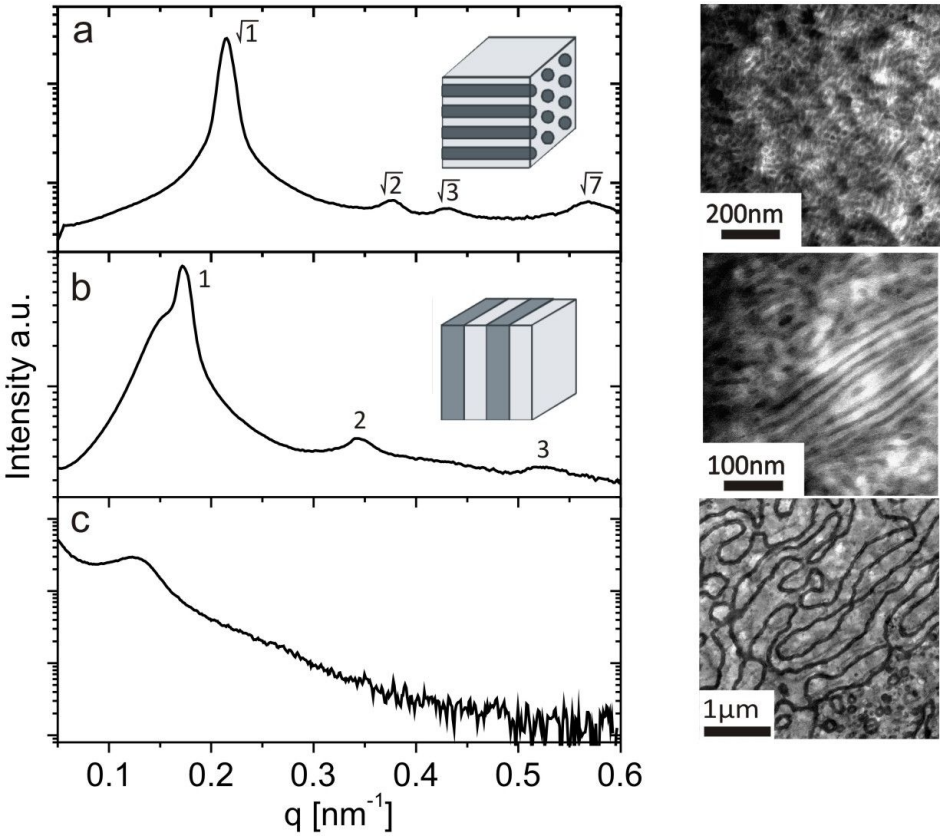

Figure 7.5: Small angle X-ray scattering in a $\frac{Counts}{q^2} - q-$plot and corresponding transmission electron microscopy images of a) PS-*b*-PPerAcr I. The diffraction peaks relative to the first peak of $\sqrt{1}, \sqrt{3}, \sqrt{4}, \sqrt{7}, ...$ indicate a hexagonal arranged cylinders with a lattice constant of 29.9 nm. b) PS-*b*-PPerAcr II exhibits a lamellar morphology with a d-spacing of 36.9 nm. c) PvTPA-*b*-PPerAcr only shows a broad first order peak. The TEM image shows a sheet-like structures without any higher order. (PPerAcr are the dark domains.)

sized domains. This is different to block copolymers, where the melt equilibrium is microphase separated with domain sizes of some tens of nanometres. In the following, we present the photophysical effects of several annealing procedures: after annealing at 160 °C and at 215 °C with fast and slow ($\sim 10 \frac{\mathrm{K}}{\mathrm{min}}$) quenching, as well as after solvent vapour annealing and solvent vapour annealing followed by an additional annealing step at 160 °C. These selected procedures cover a broad range of structures with hierarchical morphologies from an intermolecular to a nanoscopic level.

Spin-coating – in particular from low boiling point solution – not only results in non-equilibrium morphologies, but also affects the intermolecular stacking of the PBI moieties as mentioned above. Solvent vapour annealing induces additional mobility to the polymer chains, so that they can phase separate towards their thermodynamic equilibrium as presented in Chap. 6 resulting in large morphological changes.[13] However, the fast withdrawal of the solvent molecules after stopping the annealing procedure is similar to the spin-coating procedure and a extended intermolecular aggregation of PBI is suppressed. We therefore introduced an additional 160 °C annealing step, permitting the PBIs to rearrange as demonstrated above. Furthermore we annealed the samples

at 215 °C – above the melting temperature, enabling the rearrangement of the entire polymer chain. The samples were either cooled down slowly with $\sim 10\,\frac{\mathrm{K}}{\mathrm{min}}$ or quenched quickly on a metal block under nitrogen flow.

Fig. 7.6 compares the absorption spectra and fluorescence quantum efficiencies (PLQE) of the different polymers before and after solvent or temperature annealing.

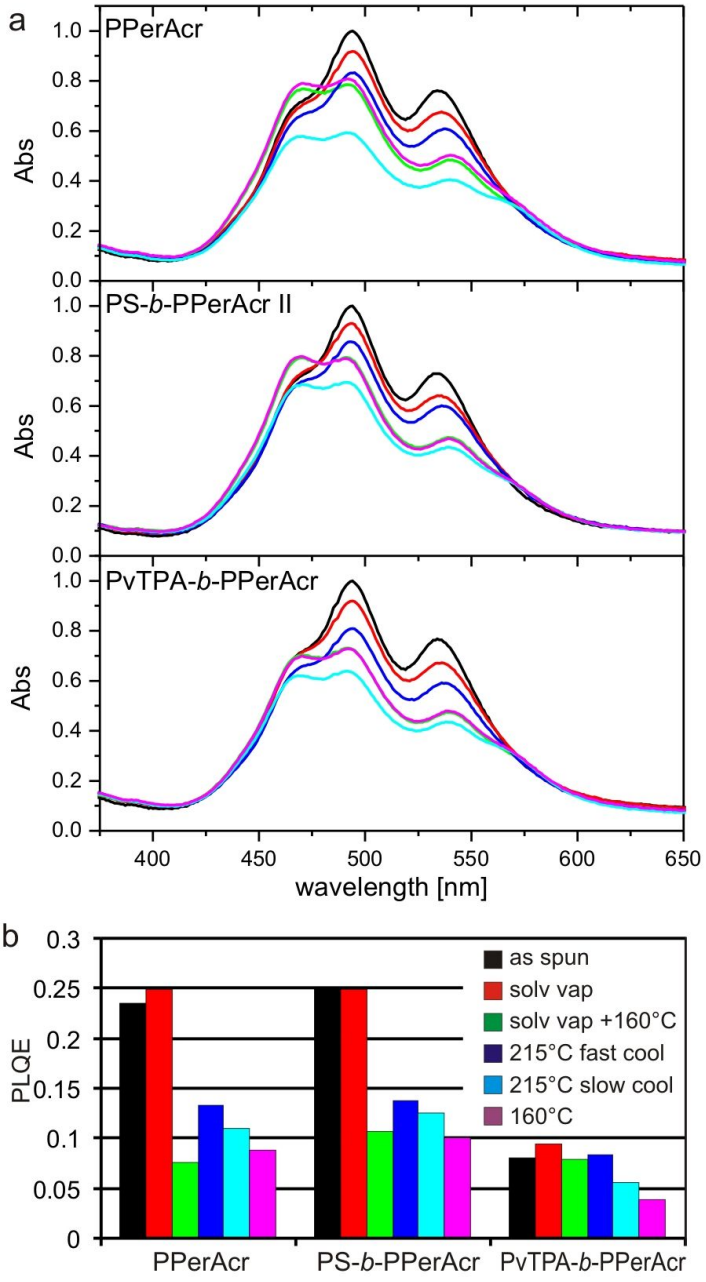

Figure 7.6: Absorption spectra of spin-coated polymer films after different annealing methods. (black: as spun, red: solvent vapour annealed (solv vap), green solvent vapour annealed and low temperature (solv vap + 160°C), blue: high temperature annealed followed by fast quenching (215°C fast cool), cyan: high temperature annealed followed by slow cooling (215°C slow cool), magenta: low temperature annealed (160°C). b) Photoluminescence quantum efficiencies (PLQE) of the samples presented in a).

All films were approximately 100 nm thick. PS-*b*-PPerAcr II exhibits the same PLQE as PS-*b*-PPerAcr I and therefore is not plotted for clarity. The samples were excited in the spectral region where light is absorbed exclusively by the the PPerAcr block at 488 nm - the PvTPA absorption is centered around 315 nm. As-spun and solvent vapour annealed films are very similar in their spectra due to the quick withdrawal of solvent in both cases. This causes a disrupted aggregation of the PBI units as shown above. However, the morphology regarding the microphase separation changes by solvent vapour annealing as we will show later.

The absorption spectra show largest changes upon temperature annealing in all three polymers - PPerAcr, PS-*b*-PPerAcr I and PvTPA-*b*-PPerAcr even for temperatures below the melting temperature of the Perylene bisimide block. As seen above the temperature annealing step increases the formation of PBI aggregates leading to a relative shift in the oscillator strengths: the first at 535 nm and second at 496 nm spectral feature decrease, while the third at 470 nm increases relatively in strength. Temperature annealing steps result in a larger quenching of the photoluminescence as shown in Fig. 7.6b. The pristine homopolymer PPerAcr as well as PS-*b*-PPerAcr show an enhanced quenching of the photoluminescence and a PLQE reduction to 30% of its original value. The formation of larger aggregates enhances the propensity of non-radiative decay pathways. The reduction of photoluminescence is coherent with the observed enhancement in crystallinity as described in Fig. 7.3 and in an enhancement in the oscillator strength of the low energy absorption peak.[37] The similar behaviour of both polymers show, that the confinement of the perylene domains within an amorphous matrix – either in cylinders or in lamellae – does not influence the optical properties and the $\pi - \pi$ interactions between the perylene moieties. They stay unaffected, confirming the picture of perylene stacks within the 2-dimensional oblique lattice. The charge transport of the two polymers also confirms this model. Previously, we have reported, that the mobility and device performance in thermally annealed PPerAcr organic field effect transistors and those based on PS-*b*-PPerAcr I are identical at $10^{-3}\,\frac{\mathrm{cm}^2}{\mathrm{Vs}}$.[38] In both cases the mobility increases by two orders of magnitude from $10^{-5}\,\frac{\mathrm{cm}^2}{\mathrm{Vs}}$ in the as-spun organic field effect transistors. The mobility of the low temperature annealed samples increased also by almost two orders of magnitude (see supplementary information for measurements and details) and confirms the correlation between crystallinity, photoluminescence quenching, and charge carrier mobility. The solvent vapour annealed films show the same optical characteristics as spin-coated films due to the quick solvent withdrawal in both cases.

The photoluminescence of the donor-acceptor block copolymer PvTPA-*b*-PPerAcr is strongly quenched due to charge transfer. The presence of the donor material leads to an efficient charge separation of the photogenerated excitons so that the photoluminescence quantum efficiency (PLQE) is only around 3.5%. The emission of the solvent vapour annealed sample increases (compared to a decrease in the other materials). The reason for this are the morphological changes and the decrease of interfacial area between the donor and acceptor materials, which will be discussed in the following section. In order to estimate the photoluminescence quenching yield (ϕ_p) and the charge transfer yield in the block copolymer PvTPA-*b*-PPerAcr, we compare the PLQE with the lamellar PS-*b*-PPerAcr II and calculate the ϕ_p as: $\phi_p =$

$1 - \mathrm{PLQE}_{\mathrm{PvTPA}-b-\mathrm{PPerAcr}}/\mathrm{PLQE}_{\mathrm{PS}-b-\mathrm{PPerAcr}}$. The as-spun films show a yield of 69%, indicating the relative number of excitons that are quenched at the interface by charge transfer. The yield of the 160 °C annealed films is around 60% and thus comparable to the as spun films. Since 160 °C is below the melting temperature of the polymer, annealing does not affect the block copolymer morphology. The loss in the charge transfer yield can be attributed to local rearrangement in the packing of the PBI moieties that result in the formation of enlarged PBI crystallites as already seen in Fig. 7.2b-III. The excitons are likely to be trapped in the aggregates, where they decay before reaching the interface.[49] Both, the reduction in the photoluminescence and the increase in the charge carrier mobility are strongly related to the crystallinity, but these may be also competing parameters for the solar cell performance.

Devices and morphology

The morphology of the donor and acceptor phases plays a crucial role in bulk heterojunction solar cells. In order to relate these to the spectroscopic and structural results organic photovoltaic devices from the PvTPA-*b*-PPerAcr block copolymer were processed and characterised by cross-sectional transmission electron microscopy (TEM). Fig. 7.7a shows a cross section of a spin-coated film of this block copolymer after spin-coating. Microphase separation with very small domain sizes of the PPerAcr in the matrix of the donor material was observed. Longer-range equilibration did not take place because of the fast evaporation of the solvent. Solvent vapour annealing changes the morphology to a long-ranged ordered lamellar morphology (Fig. 7.7b). The formation of the larger domains leads to a reduction in interface, which in return leads to a slight increase of the photoluminescence. The quantitative measurements also show that annealing at 160 °C leads to a higher PL quenching due to the additional improvement of molecular order in the aggregates. Annealing at 210 °C and solvent

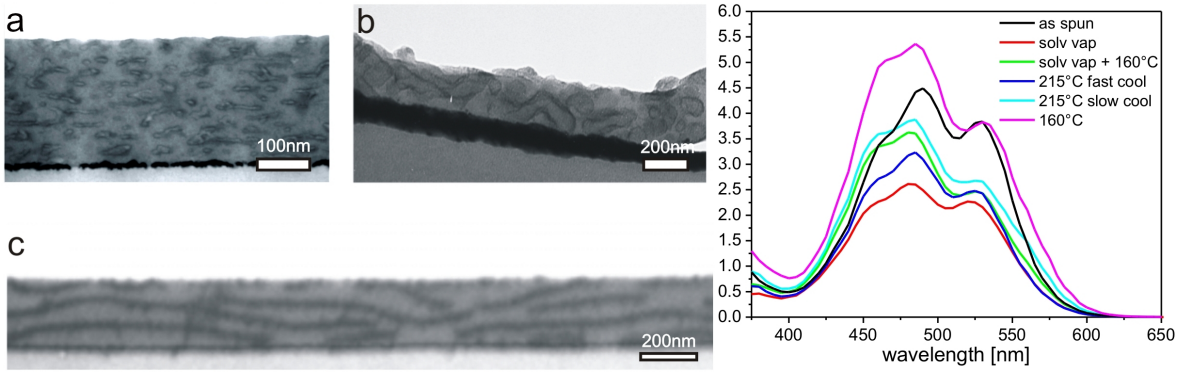

Figure 7.7: Cross sectional TEM of thin films of PvTPA-*b*-PPerAcr spin-coated from a 3.0 wt% solution, a) as-spun – showing a finely dispersed morphology, b) after thermal annealing at 210 °C. The morphology roughens and larger domains tend to form, however the mobility of the polymer-chains stays low for long annealing times (4 h). c) Solvent vapour annealing introduces a high mobility in the polymer chains so that lange range phase separation takes place, leading to a lamellar structure oriented parallel to the substrate surface. d) External quantum efficiency (EQE) of devices made of PvTPA-*b*-PPerAcr after different annealing processes.

vapour annealing involve much larger morphological changes, which reduce the donor-acceptor interface. The duration of thermal processing of PvTPA-*b*-PPerAcr at 210 °C is crucial for the resulting mesostructure of the material in the bulk. Fig. 7.7b shows TEM images of films annealed at 210°C for 4 h, revealing only a coarsening of the as-spun morphology. The melt viscosity of those complex molecules is high and therefore several hours may be required. Short annealing times mainly affect the intermolecular stacking. Long annealing times of ($\sim$ 20 h) were detrimental for the performance of the material.

In order to see the effects of the different annealing methods on the photovoltaic performance, device from the donor-acceptor polymer PvTPA-*b*-PPerAcr were prepared. Fig. 7.7d shows the external quantum efficiencies (EQE) of the devices. This block copolymer exhibits a relatively low EQE. Possible reasons for that are the low charge carrier mobility[50] and the lower HOMO level of PvTPA.[19] Block copolymers using polythiophenes for example result in much higher quantum efficiencies over 25%.[30] Since the thiophene block is a crystalline block as well, it would introduce another degree of complexity and is demonstrated elsewhere (Chap. 11). The as-spun film reaches maximum EQE values at around 4.5%.

Solvent vapour annealing decreases the EQE by almost a factor of 2. Temperature annealing also reduces the device performance, except the annealing at 160 °C. Annealing leads to changes in both – in the microphase morphology and intermolecular changes in the degree of PBI aggregation. It seems that the formation of larger aggregates leads to a decrease in the photocurrent. Similar observations have been made using low molecular weight perylene diimides.[37] Annealing above the melting temperature and solvent vapour annealing are also able to induce morphological changes. Fig. 7.7a shows a cross-section of a spin-coated block copolymer film. The effect on the morphological changes of solvent vapour annealing and temperature annealing have been reported previously (Chap. 6).[13] The morphology consists of a nanostructured phase separation on the order of some tens of nanometres. The chloroform solvent evaporated very quickly during the spin coating process, so that a longer ranged ordered phase separation could not develop and the morphology was kinetically frozen-in. The domains exhibit a certain lateral orientation stemming from two mechanisms, the preferential surface wetting of one of the blocks, leading to a lateral phase separation and the sheer forces during spin-coating. During solvent vapour annealing the film swells and the absorbed solvent molecules enable the molecule chains to rearrange. The result is shown in Fig. 7.7c. Long lamellae form, that arrange parallel to the interface. A parallel oriented morphology is not the optimal device morphology for solar cells, and a perpendicular orientation would offer an optimum percolation.[51,52] A perpendicular orientation can be achieved for example by the application of electric fields, provided that there is a sufficient difference in the dielectric constant of the two polymer blocks.[53]

The temperature annealed samples exhibit an increased stacking of the perylene bisimide moieties. This is favourable for the charge transport increasing the charge carrier mobility up to two orders of magnitude. This is consistent with the increased photoluminescence quenching. Trapped excitons, however, lead to a smaller charge generation yield and can cause the decrease of the EQE. Devices annealed at 160 °C seem to balance out these two effects and show an increase in the EQE, reaching peak

values of 5.5%. A negative effect on the device performance is observed in samples annealed above the melting temperature. These results show that only local improvements of the PBI aggregates result in better EQEs than in samples that were thermally annealed above the melting temperature and show larger, more defined aggregates as confirmed by the X-ray studies above. The solvent vapour annealed devices decreased in EQE due to morphological disadvantages and can be increased by an enhancement of intermolecular aggregation through thermal annealing at 160 °C (Fig. 7.7d).

Conclusion

We have investigated the molecular order and morphology of PBIs that are linked to a polymer back-bone. Three different polymer architectures were used, a homopolymer, a block copolymer, where one block is an inert polystyrene block and a block copolymer with a donor material – PvTPA. The degree of the intermolecular packing is strongly dependent on the sample preparation and annealing. Thermal annealing enhances the crystallinity in an identical fashion for all polymers. An improvement of the aggregation can take place already below the melting temperature. The cooling rate determines the kinetics and degree of recrystallisation. The crystallinity can be locally increased by annealing below the actual melting temperature. In all investigated materials – the homopolymer as well as both block copolymers – the perylene bisimide aggregation is unaffected by the surrounding confinement. The PBI moieties stack in a 2-dimensional oblique lattice, which is unchanged upon incorporation into block copolymers that consist of another amorphous block. The optoelectronic properties of the three materials are directly linked to the packing of the perylene bisimide moieties. A correlation between the appearance of a low energy feature at 580 nm in the absorption spectra with the crystallisation of the PBI moieties is given. Better aggregation leads to an enhanced formation of charge transfer transitions that overlay with the vibronic transitions. The enhanced aggregation also results in a higher exciton anisotropy and an enhanced charge carrier mobility and a larger photoluminescence quenching.

Different annealing methods affect both, the morphology on a length scale of some tens of nanometers and the intermolecular crystalline packing. This complex interplay is demonstrated in photovoltaic devices based on PvTPA-*b*-PPerAcr block copolymers. The largest photocurrents were achieved with an annealing step below the melting temperature. Solvent vapour annealing, instead, causes large changes in the polymer morphology but oriented parallel to the substrate precluding charge percolation. The results show the predominant effect of intermolecular interactions in perylene bisimide derivatives. The fact that these are independent of the different polymer morphologies is important for a further development of perylene bisimide based polymeric materials offering favourable processing and morphology properties.

Experimental

Thin film preparation and annealing

Thin films were prepared by spin coating from a 0.5 wt% chloroform solution of the material at 2000 rpm onto quartz glass. Temperature annealing was carried out on a hotplate under nitrogen flow. The solvent vapour annealing procedure is described elsewhere.[13]

Steady-state spectroscopy

The materials were investigated in solution and in films. The absorption of the solutions was measured with a Cary Eclipse UV-vis spectrometer (Varian Inc) and the films with a Hewlett-Packard 8453 diode array spectrometer. The fluorescence was measured in both cases with a Cary Eclipse Fluorimeter (Varian Inc). For the emission spectra, the samples were excited at 470 nm. The fluorescence data was corrected by the respective absorbance at 470 nm. The photoluminescence quantum efficiency (PLQE) was determined as described previously.[54] The measurements were carried out using an Ar-Laser at 474 nm, a nitrogen-purged integrating sphere and a diode array spectrometer.

Small and wide angle X-ray scattering

Combined small and wide angle X-ray scattering measurements were carried out at the ESRF in Grenoble, beamline ID02. The samples were prepared on thin glass substrates. The polymer was pressed into a 0.6 mm hole of a metal disc that served as a support for the material. The samples were annealed in this configuration. Temperature dependent measurements were carried out with a Linkam hotstage that was mounted in the beam path. The samples were measured at different temperatures under an inert gas atmosphere.

Transmission electron microscopy (TEM)

The TEM cross sections of thin films were prepared by sputtering a Pt diffusion barrier onto the films. The films were glued to epoxy resin and then frozen off their substrate with liquid nitrogen. The cross sections were prepared by using a Leika microtome. The block copolymer films were stained domains in vapour of RuO_4 for 10 min for contrast enhancement.

Device preparation and characterisation

ITO coated glass served as device substrates. These were cleaned and oxygen plasma etched for 10 min before covering with a layer of PEDOT:PSS. The PvTPA-*b*-PPerAcr block copolymer was spin cast from a 0.8 wt% chloroform solution at 2000 rpm. A roughly 60 nm thick counter electrode of Al was evaporated. The latter two steps were carried out in a glovebox under nitrogen atmosphere. The devices were sealed with epoxy before characterisation. The photocurrents were measured using a Keithley

237 source-measure unit. The external quantum efficiency spectra (EQE) were measured by illuminating the devices with a tungsten lamp (80 W) using a single-grating monochromator.

Transient absorption spectroscopy and exciton anisotropy measurements

The setup for transient absorption (TA) spectroscopy has been described elsewhere.[40,46,55] Briefly, a 1-kHz train of 60 fs pulses (800 μJ/pulse, $\lambda_0 = 800$ nm) is split; a portion is used to pump a TOPAS optical parametric amplifier to tune the excitation pulses, and a further portion of the 800 nm beam is used directly as a probe in the case of the TA anisotropy measurements, or used to pump a home-built broadband non-collinear optical parametric amplifier (NOPA)[40] for broadband TA spectra. The probe beam is delayed relative to the excitation beam via a mechanical delay stage before overlapping with the excited region of the film. In the spectral measurements, the probe beam is spectrally resolved and digitised for each laser pulse. The excitation beam is chopped at 500 Hz such that the transmission of alternate probe pulses can be compared to obtain the spectrally resolved differential transmission as a result of excitation, and temporal dynamics are compiled by collecting spectra for a range of relative probe delay times (typically ∼150 points are distributed from -10 to 2000 ps). For polarisation anisotropy measurements, we separated s and p polarisations of the 800 nm probe beam with a cube polariser and detected the $\Delta T/T$ signals with polarisation parallel and perpendicular to the excitation source simultaneously using separate photodiodes in addition to a reference photodiode to reduce shot-to-shot noise. Samples were contained in a vacuum chamber ($\sim 10^{-5}$ mbar) during TA measurements.

Acknowledgement

We acknowledge the European Synchrotron Radiation Facility for provision of synchrotron radiation facilities and we would like to thank M. Stuecky for assistance in using beamline ID02. The authors thank M. Kolle and H. Schoberth for their support during the X-ray measurements and P. Kohn for his help and discussions. We acknowledge the financial support from the European network "PolyFilm" under RTN-6 and the German Research Council (DFG) project SFB 481. S.H. thanks Universität Bayern e.V. for the financial support in the form of a scholarship of the Bayerische Graduiertenförderung and the Elitenetzwerk Bayern (ENB) for their support. JMH and RHF wish to acknowledge a grant from the U.K. Engineering and Physical Sciences Research Council (EPSRC).

Supplementary information

Field effect transistor measurements on PPerAcr

We have characterised the electronic properties of PPerAcr by organic filed effect transistors. As a substrate served a highly p-doped silicon waver that carried a 250 nm thick gate oxide layer as well as interdigitating source drain contacts made of gold. The measured transistors had a gate length of $L = 10\,\mu$m and a width of $W = 10\,$mm. The substrates were cleaned carefully, plasma etched and silanised in hexamethyldisilazane (HMDS) vapour. The polymer films were spin-coated from a 0.8 wt% chloroform solution.

Fig. 7.8 shows the corresponding transfer and output characteristics of the OFET measurements and the extracted device parameters are given in Tab. 7.2. A comparison of the as spun sample and the annealed sample that has been slowly cooled at a rate of $\sim 10\,\frac{\mathrm{K}}{\mathrm{min}}$ were presented previously.[38] The mobility increases with a better crystallinity. All temperature annealed samples show an increase by two orders of magnitude compared to the as spun or solvent vapour treated OFETs. The threshold voltages V_{th} decreases significantly in the 215 °C thermal annealed OFETs. This is related to the contact resistance which improves as soon as the polymer is heated above its melting temperature. Quantitatively this can be seen in the straight rise of the current in the output characteristics. Thus the samples annealed at 160 °C shows an increase in the mobility, but still an inhibited charge injection. Annealing at 215 °C renders conformational changes in the polymer chains and the perylene bisimide units towards the gold interface respectively.

Table 7.2: OFET parameters based on PPerAcr

processing	μ_{sat} $[\frac{\mathrm{cm}^2}{\mathrm{Vs}}]$	V_{th} [V]	on/off ratio
as spun	$4.3 \cdot 10^{-5}$	28.0	10^2
solvent vapour	$4.3 \cdot 10^{-6}$	30.7	10^2
solvent vapour and 160 °C	$6.8 \cdot 10^{-4}$	23.2	10^4
215 °C fast cool	$9.9 \cdot 10^{-4}$	11.8	10^5
215 °C slow cool	$1.5 \cdot 10^{-3}$	7.3	10^5
160 °C	$9.9 \cdot 10^{-4}$	30.7	10^5

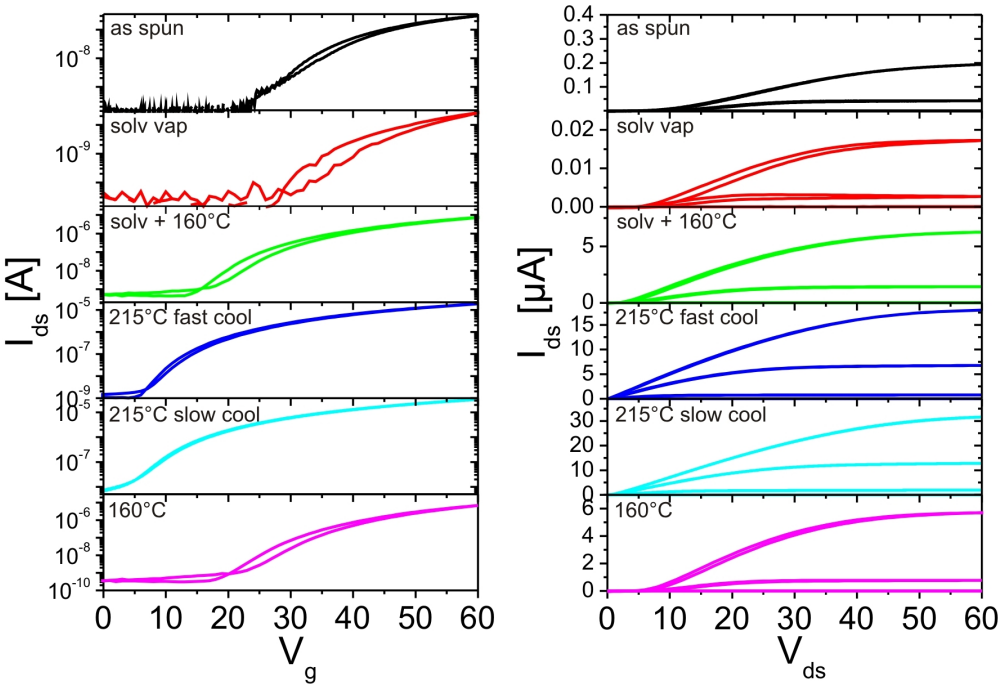

Figure 7.8: Transfer (left) and output (right) characteristics of OFETs after different annealing methods. (black: as spun, red: solvent vapour annealed (solv vap), green solvent vapour annealed and low temperature (solv vap + 160°C, blue: high temperature and fast quenching (215°C fast cool), cyan: high temperature and slow cool down (215°C slow cool), magenta: low temperature annealing (160°C). The transfer characteristics were measured at a source-drain voltage $V_{ds} = 60\,\mathrm{V}$. The output characteristics were measured at gate biases of $V_g = 0, 20, 40, 60\,\mathrm{V}$.

Bibliography

[1] B.A. Jones, A. Facchetti, M.R. Wasielewski, and T.J. Marks, *Tuning orbital energetics in arylene diimide semiconductors. Materials design for ambient stability of n-type charge transport*, J. Am. Chem. Soc. **129**, 15259 (2007).

[2] J.E. Anthony, M. Heeney, and B.S. Ong, *Synthetic aspects of organic semiconductors*, MRS Bulletin **33**, 698 (2008).

[3] L. Schmidt-Mende, A. Fechtenkötter, K. Müllen, E. Moons, R.H. Friend, and J.D. MacKenzie, *Self-organized discotic liquid crystals for high-efficiency organic photovoltaics*, Science **293**, 1119 (2001).

[4] B.A. Gregg, *The photoconversion mechanism of excitonic solar cells*, MRS Bulletin **30**, 20 (2005).

[5] Z. Chen, V. Stepanenko, V. Dehm, P. Prins, L.D.A. Siebbeles, J. Seibt, P. Marquetand, V. Engel, and F. Würthner, *Photoluminecence and conductivity of self-assembled $\pi - pi$ stacks of perylene bisimide dyes*, Chem. Eur. J. **13**, 436 (2007).

[6] A. Wicklein, A. Lang, M. Muth, and M. Thelakkat, *Swallow-tail substituted liquid crystalline perylene bisimides: Synthesis and thermotropic properties*, J. Am. Chem. Soc. **131**, 14442 (2009).

[7] E.E. Neuteboom, S.C.J. Meskers, E.W. Meijer, and R.A.J. Janssen, *Photoluminescence of Self-organized Perylene Bisimide Polymers*, Macromolecular Chemistry and Physics **205**, 217 (2004).

[8] P. A.J. De Witte, J. Hernando, E.E. Neuteboom, E.M.H.P. van Dijk, S.C.J. Meskers, R. A.J. Janssen, N.F. van Hulst, R.J.M. Nolte, M.F. García-Parajó, and A.E. Rowan, *Synthesis and characterization of long perylenediimide polymer fibers: from bulk to the single-molecule level*, Phys. Chem. B **110**, 7803 (2006).

[9] S. Lindner and M. Thelakkat, *Nanostructres of n-type organic semiconductor in a p-type matrix via self-assembly of block copolymers*, Macromolecules **37**, 8832 (2004).

[10] G. Yu, J. Gao, J. Hummelen, F. Wudl, and A. Heeger, *Polymer photovoltaic cells: enhanced efficiencies via a network of internal donor-acceptor heterojunctions*, Science **270**, 1789 (1995).

[11] A.R. Campbell, J.M. Hodgkiss, S. Westenhoff, I.A. Howard, R.A. Marsh, C.R. McNeill, R.H. Friend, and N.C. Greenham, *Low-temperature control of nanoscale morphology for high performance polymer photovoltaics*, Nanolett. **8**, 3942 (2008).

[12] F. Padinger, R.S. Rittberger, and N.S. Sariciftci, *Effects of postproduction treatment on plastic solar cells*, Adv. Funct. Mater. **13**, 85 (2003).

[13] S. Hüttner, M. Sommer, A. Chiche, G. Krausch, U. Steiner, and M. Thelakkat, *Controlled solvent vapour annealing for polymer electronics*, Soft Matter **5**, 4206 (2009).

[14] F.S. Bates and G.H. Fredrickson, *Block copolymer thermodynamics: theory and experiment*, Annu. Rev. Phys. Chem. **41**, 525 (1990).

[15] C. Park, J. Yoon, and E.L. Thomas, *Enabling nanotechnology with self assembled block copolymer patterns*, Polymer **44**, 6725 (2003).

[16] Ulf Stalmach, Bert de Boer, Christine Videlot, Paul F. van Hutten, and Georges Hadziioannou, *Semiconducting diblock copolymers synthesized by means of controlled radical polymerization techniques*, J. Am. Chem. Soc. **122**, 5464 (2000).

[17] M. Sommer, S. Hüttner, and M. Thelakkat, *Donor-acceptor block copolymers with nanoscale morphology for photovoltaic*, Adv. Poly. Sci. in print (2010).

[18] Y. Tao, B.D. Olsen, V. Ganesan, and R.A. Segalman, *Domain size control in self-assembling rod-coil block copolymers and homopolymer blends*, Macromolecules **40**, 3320 (2007).

[19] M. Sommer and M. Thelakkat, *Synthesis, characterization and application of donor-acceptor block copolymers in nanostructured bulk heterojunction solar cells*, Eur. Phys. J. Appl. Phys **36**, 245 (2006).

[20] M. Sommer, S. Lindner, and M. Thelakkat, *Microphase-separated donor-acceptor diblock copolymers: influence of HOMO energy levels and morphology on polymer solar cells*, Adv. Func. Mater. **17**, 1493 (2007).

[21] M. Sommer, A. S. Lang, and M. Thelakkat, *Crystalline-crystalline donor-acceptor block copolymers*, Angew. Chem. Int. Ed. **47**, 7901 (2008).

[22] M. Sommer, S. Hüttner, U. Steiner, and M. Thelakkat, *Influence of molecular weight on the solar cell performance of double-crystalline donor-acceptor block copolymers*, Appl. Phys. Lett. **95**, 183308 (2009).

[23] Peter Kohn, Michael Sommer, Sven Hüttner, Mukundan Thelakkat, and Thomas Thurn-Albrecht, *Crystallization induced phase separation in poly(3-hexyl thiophene)-block-poly(perylene bisimide acrylate) donor-acceptor block copolymer*, in preparation .

[24] F. Würthner, C. Thalacker, S. Diele, and C. Tschierske, *Fluorescent J-type aggregates and thermotropic columnar mesophases of perylene bisimide dyes*, Chem. Eur. J. **10**, 2245 (2001).

[25] F. Würthner, Z. Chen, V. Dehm, and V. Stepanenko, *One-dimensional luminescent nanoaggregates of perylene bisimides*, Chem. Comm. **11**, 1188 (2006).

[26] P.M. Kazmaier and R. Hoffman, *A theoretical study of crystallochromy. Quantum interference effects in the spectra of perylene pigments*, J. Am. Chem. Soc. **116**, 9684 (1994).

[27] K. Balakrishnan, A. Datar, T. Naddo, J. Huang, R. Oitker, M. Yen, J. Zhao, and L. Zang, *Effect of side-chain substituents on self-assembly of perylene diimide molecules: morphology control*, J. Am. Chem. Soc. **128**, 7390 (2006).

[28] J. Seibt, P. Marquetand, Volker Engel, Z. Chen, V. Dehm, and F. Würthner, *On the geometry dependence of molecular dimer spectra with an application to aggregates of perylene bisimide*, Chem. Phys. **328**, 354 (2006).

[29] B. A. Jones, M. J. Ahrens, M.-H. Yoon, A. Facchetti, T. J. Marks, and M. R. Wasielewski, *High-mobility air-stable n-type semiconductors with processing versatility: dicyanoperylene-3,4:9,10-bis(dicarboximides)*, Angew. Chem. **116**, 6523 (2004).

[30] M. Sommer, S. Huettner, and M. Thelakkat, *Semiconductor block copolymers for photovoltaic applications*, J. Mater. Chem. **20**, 10788 (2010).

[31] M. Sommer, S. Hüttner, S. Wunder, and M. Thelakkat, *Electron-conducting block copolymers: morphological, optical, and electronic properties*, Adv. Mater. **20**, 2523 (2008).

[32] S. Lindner, S. Hüttner, A. Chiche, M. Thelakkat, and G. Krausch, *Charge separation at self-assembled nanostructured bulk interfaces in block copolmers*, Angew. Chem. Int. Ed. **45**, 3364 (2006).

[33] S.M. Lindner, N. Kaufmann, and M. Thelakkat, *Nanostructured semiconductor block copolymers: $\pi - \pi$ stacking, optical and electrochemical properties*, Organic Electronics **8**, 69 (2007).

[34] V. Bulovic, P.E. Burrows, S.R. Forrest, J.A. Cronin, and M.E. Thompson, *Study of localized and extended excitons in 3,4,9,10-perylenetetracarboxylic dianhydride (PTCDA). 1. Spectroscopic properties of thin films and solutions*, Chem. Phys. **210**, 1 (1996).

[35] M. Hoffmann, K. Schmidt, T. Fritz, T. Hasche, V.M. Agranovich, and K. Leo, *The lowest energy Frenkel and charge-transfer excitons in quasi-one-dimensional structures: application to MePTCDI and PTCDA crystals*, Chem. Phys. **258**, 73 (2000).

[36] A. J. Ferguson and T. S. Jones, *Photophysics of PTCDA and Me-PTCDI thin films: effects of growth temperature*, J. Phys. Chem. B **110**, 6891 (2006).

[37] P.E. Keivanidis, I.A. Howard, and R.H. Friend, *Intermolecular interactions of perylene diimides in photovoltaic blend of fluorene copolymers: disorder effects on photophysical properties, film morphology and device efficiency*, Adv. Func. Mater. **18**, 3189 (2008).

[38] S. Hüttner, M. Sommer, and M. Thelakkat, *n-type organic field effect transistors from perylene bisimide block copolymers and homopolymers*, Appl. Phys. Lett. **92**, 093302 (2008).

[39] Tomoaki Yago, Yoshiaki Tamaki, Akihiro Furube, and Ryuzi Katoh, *Self-trapping limited exciton diffusion in a monomeric perylene crystal as revealed by femtosecond transient absorption microscopy*, Phys. Chem. Chem. Phys. **10**, 4435 (2008).

[40] S. Westenhoff, I.A. Howard, J.M. Hodgkiss, K.R. Kirov, H.A. Bronstein, C.K. Williams, N.C. Greenham, and R.H. Friend, *Charge recombination in organic photovoltaic devices with high open-circuit voltages*, J. Am. Chem. Soc. **130**, 13653 (2008).

[41] Y.-S. Huang, S. Westenhoff, I. Avilov, P. Sreearunotha, J.M. Hodgkiss, C. Deleener, R.H. Friend, and D. Beljonne, *Electronic structures of interfacial states formed at polymeric semiconductor heterojunctions*, Nat. Mater. **7**, 483 (2008).

[42] Thuc-Quyen Nguyen, Junjun Wu, Vinh Doan, Benjamin J. Schwartz, and Sarah H. Tolbert, *Control of energy transfer in oriented conjugated polymer-mesoporous silica composites*, Science **288**, 652 (2000).

[43] Benjamin J. Schwartz, *Conjugated polymers as molecular materials: How chain conformation and film morphology influence energy transfer and interchain interactions*, Annu. Rev. Phys. Chem. **54**, 141 (2003).

[44] B. Valeur, *Molecular Fluorescence Ch. 5.* (Wiley-VCH Verlag GmbH, Weinheim, 2002).

[45] M. H. Chang, M. J. Frampton, H. L. Anderson, , and L. M. Herz, *Intermolecular interaction effects on the ultrafast depolarization of the optical emission from conjugated polymers*, Phys. Rev. Lett. **98**, 027402 (2007).

[46] J.M. Hodgkiss, G. Tu, S. Albert-Seifried, W.T.S. Huck, and R.H. Friend, *Ion-induced formation of charge-transfer states in conjugated polyelectrolytes*, J. Am. Chem. Soc. **131**, 8913 (2009).

[47] B.A. Gregg, *Evolution of photophysical and photovoltaic properties of perylene bis(phenethylimide) films upon solvent vapor annealing*, J. Phys. Chem. **100**, 852 (1996).

[48] Giovanna de Luca, Andrea Liscio, Fabian Nolde, Luigi Monsu, Scolaro, Vincenzo Palermo, Klaus Müllen, and Paolo Samori, *Self-assembly of discotic molecules into mesoscopic crystals by solvent-vapourannealing*, Soft Matter **4**, 2064 (2008).

[49] S. Foster, C.E. Finlayson, P.E. Keivanidis, Y.-S. Huang, I. Hwang, R.H. Friend, M.B.J. Otten, L.-P. Lu, E. Schwartz, R.J.M. Nolte, and A.E. Rowan, *Improved performance of perylene-based photovoltaic cells using polyisocyanopeptide arrays*, Macromol. (2009).

[50] S. Hüttner, M. Sommer, U. Steiner, and M. Thelakkat, *Organic field effect transistors from triarylamine side-chain polymers*, Appl. Phys. Lett. **in print**, (2010).

[51] G.A. Buxton and N. Clarke, *Predicting structure and property relations in polymeric photovoltaic devices*, Physical Review B **74**, 085207 (2006).

[52] C. Groves, R.A. Marsh, and N.C. Greenham, *Monte Carlo modeling of geminate recombination in polymer-polymer photovoltaic devices*, J. Chem Phys. **129**, 114903 (2008).

[53] T. Thurn-Albrecht, J. DeRouchey, and T.P. Russel, *Overcoming interfacial interactions with electric fields*, Macromolecules **33**, 3250 (2000).

[54] J.C. deMello, H.F. Wittmann, and R.H. Friend, *An improved experimental determination of external photoluminescence quantum efficiency*, Adv. Mater. **9**, 230 (1997).

[55] F. Laquai, A.K. Mishra, K.Müllen, and R.H. Friend, *Amplified spontaneous emission of poly(ladder-type phenylene)s - The influence of photophysical properties on ASE thresholds*, Adv. Funct. Mater. **18**, 3265 (2008).

Chapter 8

Organic Field Effect Transistors from Triarylamine Side-Chain Polymers

Sven Hüttner[a,b], Michael Sommer[a], Ullrich Steiner[b] and Mukundan Thelakkat[a]

a) Angewandte Funktionspolymere, Makromolekulare Chemie I, Universität Bayreuth, 95440 Bayreuth, Germany.
b) Cavendish Laboratory, University of Cambridge, United Kingdom.

Applied Physics Letters 96, 073503 (2010)

Abstract

We present a comparative study of organic field effect transistors (OFET) based on amorphous side-chain p-type polymers obtained from controlled radical polymerization. The side-chain moieties consist of different triarylamines such as triphenylamine (TPA), dimethoxytriphenylamine (DMPTA), and dimethoxytriphenyldiamine (DMTPD). The DMTPD-based polymer shows the highest OFET performance with mobilities of $10^{-4}\,\frac{\mathrm{cm}^2}{\mathrm{Vs}}$. Furthermore we show that the electrical properties are independent of the molecular weight due to the all-amorphous character of these side-chain polymers.

Introduction

The development and synthesis of new semiconductor materials have caused large advances in the field of organic electronics. Materials based on triarylamines (TAA) became a major class of hole conductors. Well-defined, low molecular weight materials such as star-shaped molecules, spiro-compounds and dendrimers on the one hand, as well as side-chain and main-chain polymers on the other hand have been developed.[1] Originally, they were used for xerographic applications,[2] but the further synthetic advancement of triarylamine derivatives towards good hole-transporters extended their application, especially to organic light emitting diodes (OLEDs).[3] In addition, bulk heterojunction solar cells[4] and solid state dye sensitized solar cells[5,6] have been realised with these donor materials. In view of their respective applications, the electro-optical properties such as the HOMO level (highest occupied molecular orbital) can be chemically tuned via substitution of the phenyl rings with electron-rich or electron-deficient groups. Furthermore, the physical properties such as crystallinity, solubility, melting

temperature or glass transition temperature can be controlled at the the same time. One major parameter that is inherently important for all electro-optical applications is the charge carrier mobility. High charge carrier mobilities for this class of materials have been reported for amorphous low molecular weight derivatives at $10^{-2}\,\frac{\mathrm{cm}^2}{\mathrm{Vs}}$ using time of flight (ToF) measurements.[7]

Amorphous polymers often show a low charge carrier mobility since a strong cooperative intermolecular interaction is disturbed and a large energetic disorder is prevalent.[8] This is not necessarily the case for polytriarylamines, where the low molecular weight materials and the polymers exhibit appreciably high mobilities in their amorphous state.[1] Polymers comprised of TAA were demonstrated as fully conjugated molecules, with the TAA moiety as part of the conjugated main-chain,[9] non-conjugated main-chain polymers,[10,11] or side-chain polymers[12–14] with the triarylamine group attached to a polymer backbone. Side-chain polymers are rather comparable to their low molecular weight analogs in terms of the electronic properties, but they possess a high solubility and the mechanical and thermal properties of a polymer. For such materials, the molecular weight is not expected to have a large influence on the electronic properties, which is in contrast to semi-crystalline conjugated polymers such as poly(3-hexylthiophene).[15]

There are various methods to access the electrical properties of a material. The charge carrier mobility can be measured for example by time of flight,[2,7] dark injection space-charge-limited current,[16] organic field effect transistors, admittance spectroscopy or microwave Hall measurements. The first three methods are among the most commonly used techniques for organic electronic materials. A comparative study of these methods with phenylamines was recently published.[17]

Recently, we have investigated a variety of amorphous-crystalline donor-acceptor block copolymers as active layers in photovoltaic cells. We showed that a variation in the substitution pattern of the triphenylamine unit gave rise to large differences in the photovoltaic performance of the block copolymers.[18] While several causes have been identified for this, the influence of charge carrier mobility was not analyzed for these materials.Here we report on organic field-effect transistors (OFETs) with a series of differently substituted amorphous side-chain poly(triarylamines) as the active layer. In addition, we show that the molecular weight does not influence the charge carrier mobility due to the amorphous nature of the polymers. The synthesis of the triarylamine polymers is reported elsewhere.[13,14,18] We investigated three different polymers, namely poly(vinyltriphenylamine) (PvTPA), poly(vinyldimethoxytriphenylamine) (PvDMTPA), and poly(vinyldimethoxy-triphenyldiamine) (PvDMTPD) (see Fig. 8.1a-c). Tab. 8.1 shows the physical and thermal properties of these polymers. All the polymers are amorphous and have a glass transition temperature ranging from 130 to 175 °C. PvTPA has a HOMO level of 5.24 eV, that decreases to 4.96 eV for PvDMTPA and PvDMTPD as determined earlier by cyclic voltammetry.[18]

Results and Discussion

We processed OFET devices in a bottom gate bottom contact geometry (Fig. 8.1d) and compared the resulting device characteristics. The charge carrier mobility μ can

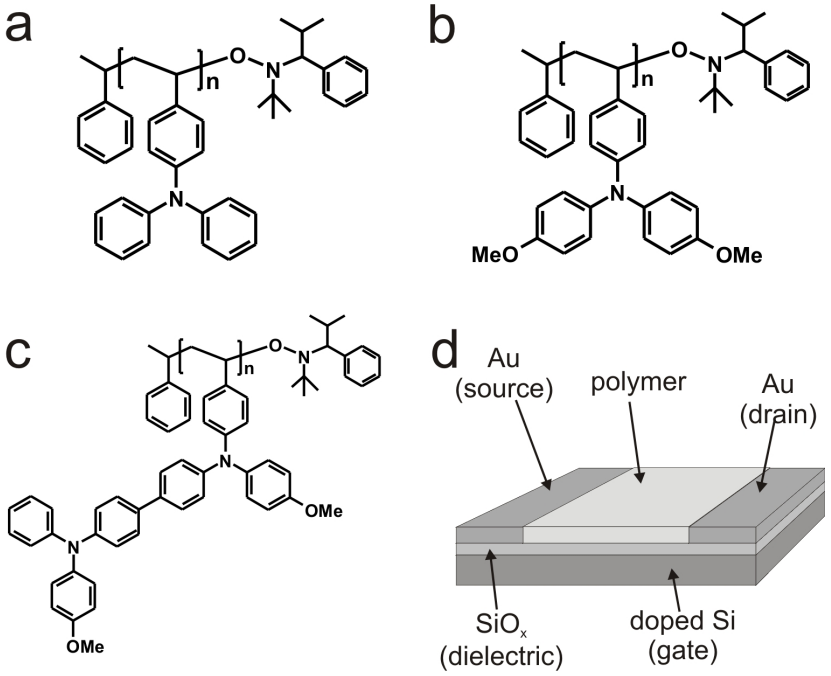

Figure 8.1: Molecular structures of the polymers, a) poly(vinyltriphenylamine) PvTPA, b) poly(vinyldimethoxytriphenylamine) PvDMTPA, c) poly(vinyldimethoxytriphenlydiamine) PvDMTPD, d) schematic of a bottom gate bottom contact OFET architechture.

be extracted in the saturation region of the transfer characteristics as:

$$I_d = \frac{W}{L}\mu_{sat}C_i(V_g - V_{th})^2, \tag{8.1}$$

where W is the gate width, L the gate length, C_i the silicon oxide capacitance and V_{th} the threshold voltage. The transistor substrates were prepared and silanized with hexamethyldisilazane (HMDS) according to published procedures.[19] The polymers were spin cast from a 1.9 wt% toluene solution. This procedure and all subsequent device annealing and device characterization steps were carried out in a glove box under inert gas atmosphere. The transistors were characterized using a HP4155A and a HP4156B semiconductor parameter analyzer.

As spin-cast samples of PvTPA showed a very weak performance, with high threshold voltages, small on-off ratios and low charge carrier mobilities. Annealing the sample at approximately 15 °C above its T_g caused a significant increase in the performance leading to greater than tenfold drain currents and a charge carrier mobility of around $3 \cdot 10^{-5}\,\frac{\mathrm{cm}^2}{\mathrm{Vs}}$. The threshold voltage was still quite high at -37 V. The output and transfer characteristics are shown in Fig. 8.2. The polymers PvDMTPA and PvDMTPD, each carrying two methoxy groups showed a different behaviour. After spin-coating, both the PvDMTPA and the PvDMTPD showed a significantly better performance compared to PvTPA, which did not improve significantly after thermal annealing above T_g. Both materials showed low threshold voltages between -4 to -5 V. Annealing shifted the threshold voltage to higher values of -12 to -13 V. We assume this due to conformational changes in the polymer and an altered spatial ordering of

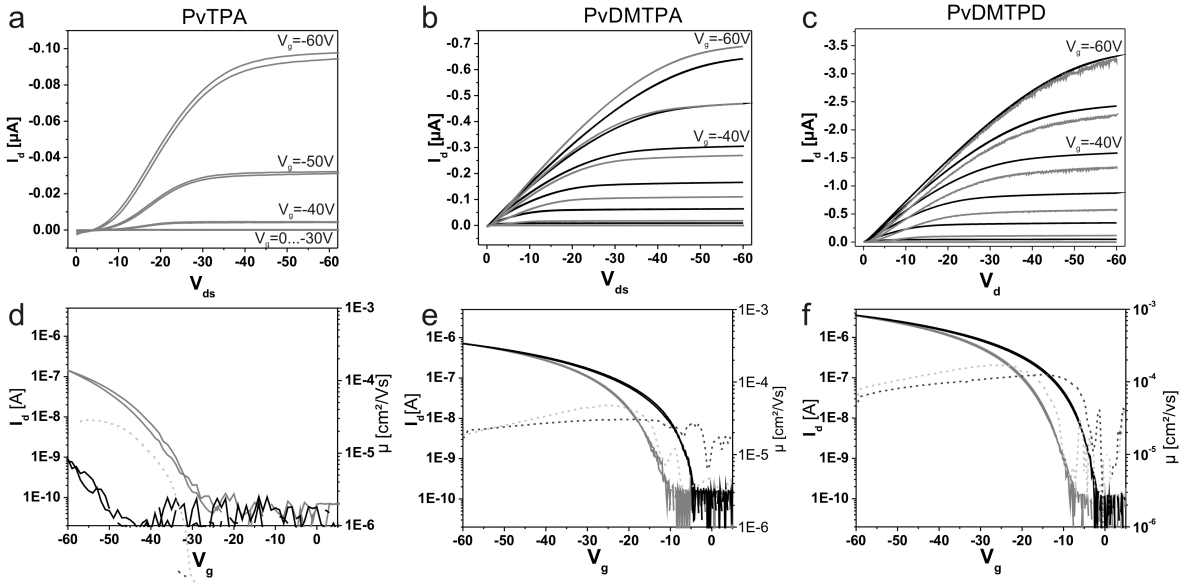

Figure 8.2: The upper graphs show the output characteristics with $V_g = 0\,\mathrm{V}$ to -60 V in steps of -10 V. d-f) The bottom graphs show the transfer characteristics of PvTPA, PvDMTPA and PvDMTPD for $V_{ds} = -60\,\mathrm{V}$. The black lines correspond to the as spun polymers and the grey lines to the annealed transistors. The dashed lines show the first derivative in units of the charge carrier mobility as calculated from the saturation region.

Table 8.1: OFET characteristics of homopolymer and block copolymer devices.

	PvTPA	PvDMTPA	PvDMTPD
M_n (kg/mol)	15.8	23.6	22.4
T_g (°C)	143.6	146.2	174.5
HOMO (eV)[14]	5.24	4.96	4.96
μ_{sat} as spun ($\frac{\mathrm{cm}^2}{\mathrm{Vs}}$)	$1 \cdot 10^{-7}$	$3 \cdot 10^{-5}$	$1 \cdot 10^{-4}$
V_{th} as spun (V)	-45.1	-4.3	-4.1
on/off spun	$4 \cdot 10^{1}$	$2.5 \cdot 10^{2}$	$1.6 \cdot 10^{3}$
μ_{sat} annealed ($\frac{cm^2}{Vs}$)	$3 \cdot 10^{-5}$	$5 \cdot 10^{-5}$	$1 \cdot 10^{-4}$
V_{th} annealed (V)	-35.2	-13.2	-12.1
on/off annealed	$6 \cdot 10^{2}$	$4 \cdot 10^{2}$	$2 \cdot 10^{3}$
W / L	10 mm / 10 μm	10 mm / 10 μm	10 mm / 7.5 μm

the polar methoxy groups towards the gate dielectric. The PvDMTPD was superior in terms of its charge carrier mobility and on-off ratio. The PvDMTPA had a mobility $\mu_{sat} = 5 \cdot 10^{-5}\,\frac{\mathrm{cm}^2}{\mathrm{Vs}}$ and an on-off ratio of 10^2, while PvDMTPD exhibited a mobility of $\mu_{sat} = 1.2 \cdot 10^{-4}\,\frac{\mathrm{cm}^2}{\mathrm{Vs}}$ and an on-off ratio of 10^3. The superior charge carrier mobility of PvDMTPD is in line with previous findings on the solar cell performance of poly(triarylamine) based block copolymers.[18] Furthermore, the contact resistance of PvDMTPA and PvDMTPD was very low, whereas PvTPA showed a significant contact resistance, as can be seen in the slow rise of the output characteristics. We tentatively propose that spatial ordering of the methoxy groups at the dielectric interface might cause the difference in contact resistance. Changes in the OFET performance before

and after annealing have generally been attributed to morphological and spatial ordering, but also to changes in the energetic disorder at the interface introduced by local polarization.[20] The latter possibility can be rather excluded since the interface itself stays unaffected. The dimethoxy groups seem to have an effect after annealing as both materials show a significant increase in their threshold voltage. The polar methoxy groups may conform to the dielectric interface that way that a significant increase of the threshold voltage is induced. This is not observed in pure PvTPA which contains no substituents. Here, a large contact resistance is observed, that affects the overall extracted charge carrier mobility.[21]

The way of processing thin films - such as spin coating and thermal or solvent annealing can have a large effect on the conformation of amorphous polymer chains. Latest investigations on spincoated polystyrene show that spin coated films are far away from bulk equilibrium.[22] The increase in performance of PvTPA after annealing may be related to a better packing of the triphenylamine moieties and the higher degree of freedom that is conserved with unsubstitued triphanlyamine moieties. Low molecular weight TPA without substituents shows a strong crystallinity[23] where even by very fast quenching with liquid nitrogen no amorphous glassy state could be achieved.[24] The introduction of substituents rather supports the formation of an amorphous phase. Large efforts have been made in order to synthesise amorphous compounds and molecular glasses of triarylamines.[3] In the case of the side chain poly(vinyltriarylamine)s presented here, only amorphous states have been observed. The reason for that is the non-planar conformation of the TPA core that hinders a crystalline packing when attached to a polymer backbone. PvDMTPA and PvDMTPD contain much bulkier side groups compared to PvTPA which is a possible explanation for the only minor changes in charge transport before and after annealing. Therefore changes upon annealing are rather expected at unsubsituted triphenylamine side chains - where the small molecule counterpart shows an extensive crystallinity.

In order to study the effect of the molecular weight on the device performance, we prepared OFET devices using polymers with different molecular weights. As an example, we considered a PvDMTPA series with different molecular weights. The PvDMTPA blocks with well-defined molecular weights between 3 and 30 $\frac{\mathrm{kg}}{\mathrm{mol}}$ and fairly low polydispersities between 1.1 and 1.2 were synthesised via nitroxide mediated radical polymerization by varying the initiator to monomer ratio in analogy to previously published procedures.[18] It is not expected that the charge carrier mobility of amorphous polymers significantly depends on the molecular weight, however, to the best of our knowledge, no report exists in the literature explicitly addressing this question. As shown in Fig. 8.3, the charge carrier mobility of PvDMTPA of around $10^{-5}\,\frac{\mathrm{cm}^2}{\mathrm{Vs}}$ does not change with molecular weight within the margin of error. The lowest threshold voltage ranges between -4 and -9 V, which is attributed to batch to batch differences. Thus, the electronic properties of the polymers have not changed, but only the chain length. This is different from the case of conjugated polymers, where the polymer length has a direct influence on the electronic properties determined by the average conjugation length and chain packing.[15]

These amorphous polymers have the advantage of unchanged electronic properties, while the physical properties such as the glass transition temperature T_g, do scale with molecular weight. Fig. 8.3b shows the T_g as a function of the molecular weight.

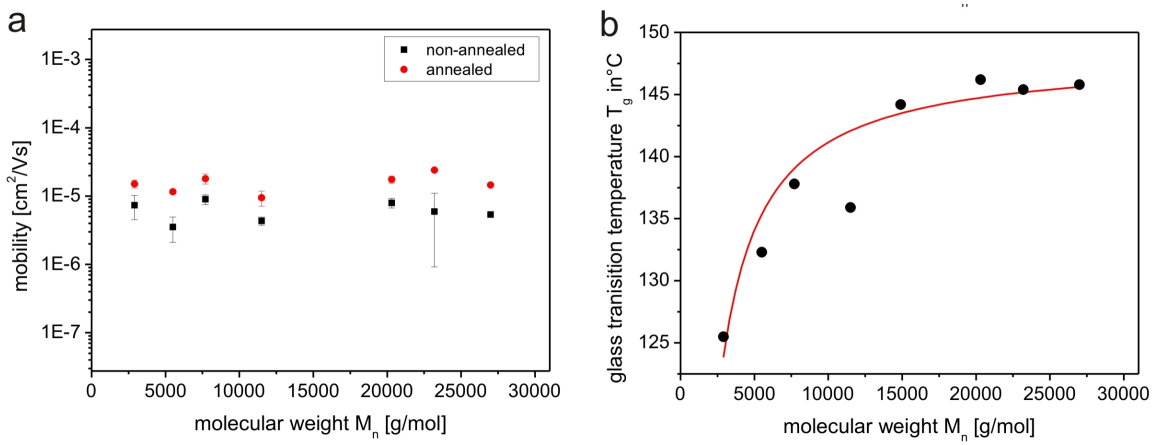

Figure 8.3: a) Charge carrier mobility of PvDMTPA as a function of the molecular weight. The black squares show the as spun transistors and the red circles show the mobilities for annealed transistors. b) Glass transition temperature T_g of PvDMTPA as a function of the molecular weight. The red curve shows an asymptotic fit according to Fox and Flory. The T_g for $M_n = 11.5\,\frac{\mathrm{kg}}{\mathrm{mol}}$ shows a certain inconsistency due to a double peak in the $\tan\delta$ curve (see supplementary information.)

We deteremined the T_g by dynamic mechanical analysis (DMA) measurements using a Triton DS6000 Thermal Analyser. The T_gs were determined as the peak value of $\tan\delta$ at an actuation frequency of 1 Hz, where $\tan\delta$ is the phase difference between the store modulus G' and the loss modulus G'' (see supplementary information). This method for determining T_g results in slightly higher values compared to differential scanning calorimetry (DSC) measurements, but the extraction of the $\tan\delta$ peak value was very reliable for small amounts of polymers.[25] In agreement with Flory and Fox, the glass transition temperature shows an asymptotic behaviour: $T_g = T_{inf} - \frac{K}{M_n}$, where we found T_{inf}=148.2 °C and K = $70.8 \cdot 10^5 \frac{g}{mol}$. The T_g varies from 125 °C for the lowest molecular weight of 2900 $\frac{g}{mol}$ and rises quickly to a saturation value at around 145 °C for polymers with more than 20 $\frac{\mathrm{kg}}{\mathrm{mol}}$. Thus, by varying the molecular weight, it is possible to adjust the physical properties to the needs of the processing conditions without changing the electronic properties.

To conclude, we have investigated the charge carrier mobilities of side-chain triarylamine polymers PvTPA, PvDMTPA and PvDMTPD with differently substituted triarylamine units. PvDMTPD bearing triphenyldiamine units demonstrated the best performance in terms of charge carrier mobility, threshold voltage and on-off ratio Furthermore we used PvDMTPA as an example to show that the charge carrier mobility is independent of the molecular weight while the thermal properties are not. The independence of the molecular weight is different to conjugated polymers such as polyhexylthiophene (P3HT), where the molecular weight influences the conjugation length but also morphological properties such as the formation of crystalline domains together and the interconnectivity of those. Thus they offer an excellent possibility to adjust the glass transition temperature through the molecular weight and also take a direct influence on the phase separation when blended with an acceptor material.

Acknowledgement

We acknowledge the financial support from the European network "PolyFilm" under RTN-6 and the German Research Council (DFG) project SFB 481. The authors are grateful to K. Neumann for help in synthesis of PvDMTPA. S.H. thanks Universität Bayern e.V. for the financial support in the form of a scholarship of the Bayerische Graduiertenförderung and the Elitenetzwerk Bayern (ENB) for their support.

Supplementary Information

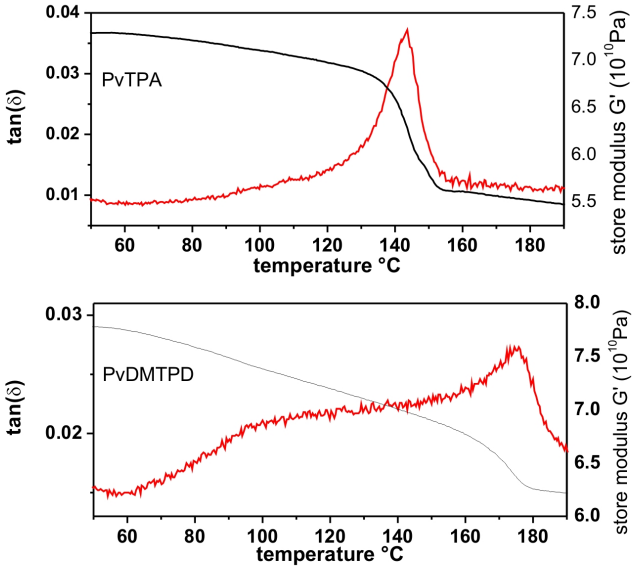

Figure 8.4: $\tan\delta$ and store modulus G' as a function of the temperature. The upper graph shows PvTPA and the lower PvDMTPD.

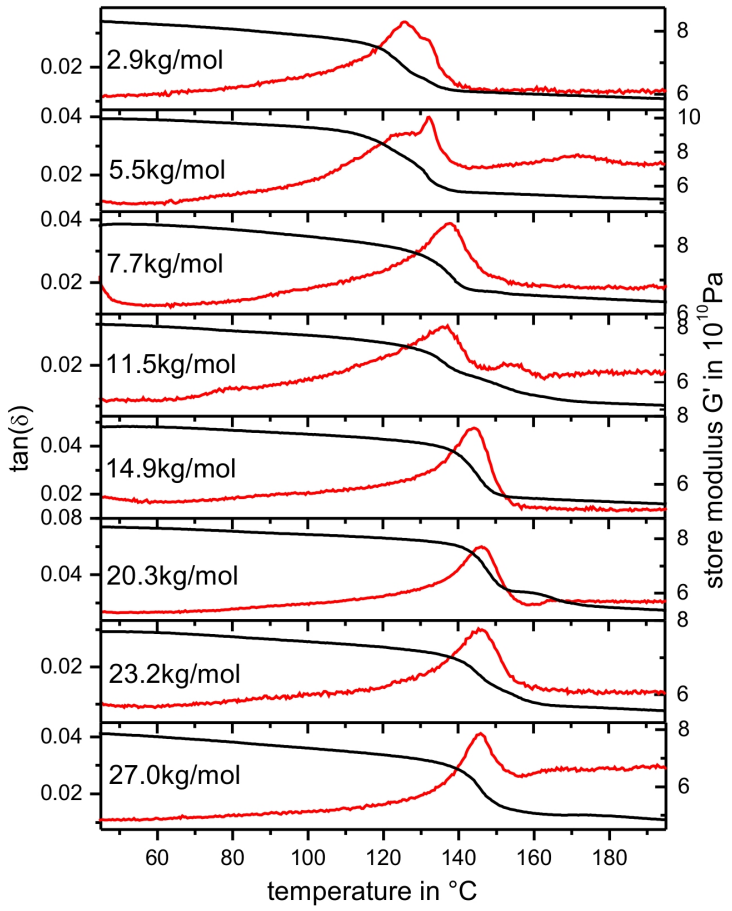

Figure 8.5: $\tan\delta$ and store modulus G' as a function of the temperature for PvDMTPA for different molecular weights.

Bibliography

[1] M. Thelakkat, *Star-shaped, dendrimeric and polymeric triarylamines as photoconductors and hole transport materials for electro-optical applications*, Macromol. Mater. Eng. **287**, 442 (2002).

[2] Paul M. Borsenberger and David S. Weiss, *Organic photoreceptors for imaging systems* (Marcel Dekker Inc., New York, 1993).

[3] Yasuhiko Shirota and Hiroshi Kageyama, *Charge carrier transporting molecular materials and their applications in devices*, Chem. Rev. **107**, 953 (2007).

[4] S. Lindner, S. Hüttner, A. Chiche, M. Thelakkat, and G. Krausch, *Charge separation at self-assembled nanostructured bulk interfaces in block copolmers*, Angew. Chem. Int. Ed. **45**, 3364 (2006).

[5] U. Bach, D. Lupo, P. Comte, J. E. Moser, F.Weissörtel, J. Salbeck, H. Spreitzer, and M. Grätzel, *Solid-state dye-sensitized mesoporous TiO2 solar cells with high photon-to-electron conversion efficiencies*, Nature **395**, 583 (1998).

[6] J. E. Kroeze, N. Hirata, L. Schmidt-Mende, C. Orizu, S. D. Ogier, K. Carr, M. Grätzel, and J. R. Durrant, *Parameters influencing charge separation in solid-state dye-sensitized solar cells using novel hole conductors*, Adv. Funct. Mater. **16**, 1832 (2006).

[7] P.M. Borsenberger, L. Pautmeier, and H. Bässler, *Charge transport in disordered molecular solids*, J. Chem. Phys. **94**, 5447 (1991).

[8] I. I. Fishchuk, A. K. Kadashchuk, H. Bässler, and D. S. Weiss, *Nondispersive charge-carrier transport in disordered organic materials containing traps*, Phys. Rev. B **66**, 205208 (2002).

[9] Y. Ohsawa, M. Ishikawa, T. Miyamoto, Y. Murofushi, and M. Kawai, *Electrically conducting polytriphenylamines*, Synth. Met. **18**, 371 (1987).

[10] M. Thelakkat, J. Hagen, D. Haarer, and H.-W. Schmidt, *Poly(triarylamine)s - synthesis and application in electroluminescent devices and photovoltaics*, Synth. Met. **102**, 1125 (1999).

[11] K. R. Haridas, J. Ostrauskaite, M. Thelakkat, M. Heim, R. Bilke, and D. Haarer, *Synthesis of low melting hole conductor systems based on triarylamines and application in dye sensitized solar cells.*, Synth. Met. **121**, 1573 (2001).

[12] Erika Bellmann, Sean E. Shaheen, Robert H. Grubbs, Seth R. Marder, Bernard Kippelen, and Nasser Peyghambarian, *Organic two-layer light-emitting diodes based on high-Tg hole-transporting polymers with different redox potentials*, Chem. Mater. **11**, 399 (1999).

[13] S. Lindner and M. Thelakkat, *Nanostructres of n-type organic semiconductor in a p-type matrix via self-assembly of block copolymers*, Macromolecules **37**, 8832 (2004).

[14] M. Sommer and M. Thelakkat, *Synthesis, characterization and application of donor-acceptor block copolymers in nanostructured bulk heterojunction solar cells*, Eur. Phys. J. Appl. Phys **36**, 245 (2006).

[15] R. Joseph Kline, Michael D. McGehee, Ekaterina N. Kadnikova, Jinsong Liu, Jean M. J. Fréchet, , and Michael F. Toney, *Dependence of regioregular poly(3-hexylthiophene) film morphology and field-effect mobility on molecular weight*, Macromol. **38**, 3312 (2005).

[16] V. D. Mihailetchi, J. Wildeman, and P.W. M. Blom, *Space-charge limited photocurrent*, Phys. Rev. Lett. **94**, 126602 (2005).

[17] C. H. Cheung, K. C. Kwok, S. C. Tse, and S. K. So, *Determination of carrier mobility in phenylamine by time-of-flight, dark-injection, and thin film transistor techniques*, J. Appl. Phys. **103**, 093705 (2008).

[18] M. Sommer, S. Lindner, and M. Thelakkat, *Microphase-separated donor-acceptor diblock copolymers: influence of HOMO energy levels and morphology on polymer solar cells*, Adv. Func. Mater. **17**, 1493 (2007).

[19] S. Hüttner, M. Sommer, and M. Thelakkat, *n-type organic field effect transistors from perylene bisimide block copolymers and homopolymers*, Appl. Phys. Lett. **92**, 093302 (2008).

[20] J. Veres, S.D. Ogier, S.W. Leeming, D.C. Cupertino, and S. Mohialdin Khaffaf, *Low-k insulators as the choice of dielectrics in organic field effect transistors*, Adv. Funct. Mater. **13**, 199 (2003).

[21] L. Bürgi, T.J. Richards, R.H. Friend, and H. Sirringhaus, *Close look at charge carrier injection in polymer field-effect transistors*, J. Appl. Phys. **94**, 6129 (2003).

[22] D.R. Barbero and U. Steiner, *Nonequilibrium polymer rheology in spin-cast films*, Phys. Rev. Lett. **102**, 248303 (2009).

[23] A.N. Sobolev, V.K. Belsky, I.P. Romm, N.Yu. Chernikova, and E.N. Guryanova, *Structural investigation of the triaryl derivatives of the group V elements. IX. Structure of triphenylamine, C18H15N*, Acta. Crystallogr., Sect. C: Cryst. Struct. Commun. **41**, 967 (1985).

[24] Y. Shirota, *Organic materials for electronic and optoelectronic devices*, J Mater Chem. **10**, 1 (2000).

[25] P.J. Brown, D.S. Thomas, A. Köhler, J.S. Wilson, J.-S. Kim, C.M. Ramsdale, H. Sirringhaus, and R.H. Friend, *Effect of interchain interactions on the absorption and emission of poly(3-hexylthiophene)*, Phys. Rev. B **67**, 064203 (2003).

Chapter 9

Tunable Charge Transport using Supramolecular Self-assembly of Nanostructured Crystalline Block Copolymers

Sven Hüttner[a,b], Michael Sommer[a], Justin Hodgkiss[b,c], Peter Kohn[d], Thomas Thurn-Albrecht[d], Ullrich Steiner[b], Mukundan Thelakkat[a]

a) Angewandte Funktionspolymere, Makromolekulare Chemie I, Universität Bayreuth, Germany.
b) Cavendish Laboratory, University of Cambridge, United Kingdom.
b) Experimentelle Polymerphysik, Martin-Luther-Universität Halle-Wittenberg, Germany.
c) MacDiarmid Institute for Advanced Materials and Nanotechnology, Victoria University of Wellington, New Zealand

Abstract

Electronically functionalised block copolymers, combining covalently linked p-type and n-type blocks, show switching behaviour of charge transport in organic field effect transistors (OFETs). The electronically active subunits self-assemble into continuous microdomains in a nanoscale regime, thereby forming percolation channels for holes or electrons or both depending on the composition and processing conditions. Here, we establish a charge transport - morphology relation for donor-acceptor block copolymers with two crystalline blocks. The n-type and p-type blocks self-assemble into two-dimensional lattices of $\pi - \pi$ stacks and main chain polymer lamella, respectively, over a broad composition range. Controlling the crystallization preferences of the two blocks by thermal annealing allows control over the OFET polarity. Depending on the block ratio, the charge transport can be tuned from p-type to n-type or p-type to ambipolar, respectively. The impact of nanostructured phase separation is further delineated by X-ray diffraction, time resolved spectroscopy and scanning electron microscopy studies.

Introduction

Block copolymers will play a major role in many nanotechnology applications because of their scope for well-defined 3-dimensional self-assembly on the nanometer scale.[1] In

the simplest case, diblock copolymers consist of two covalently linked polymers. Predictable self-assembled nanostructures result from the tendency of the two blocks to phase separate whilst remaining attached to each other. The self-assembling properties of block copolymers have inspired widespread application especially in thin film technology such as nanostructured templates.[2,3]

Complementary circuits involving coupled p- and n-type transistors form the basis of efficient and logic circuits,[4] which has proven its success in inorganic CMOS technology. The development of complementary circuitry in organic electronics is an inevitable step for the future of organic circuitry and different approaches have been demonstrated: Circuitry based on ambipolar organic semiconductors have previously been demonstrated by employing a combination of high- and low work-function metal electrodes in order to achieve dual charge injection into a single semiconductor.[5] Alternatively, a combination of n-type and p-type materials can support dual charge transport using electrodes of a single metal. In analogy with bulk heterojunction solar cells, ambipolar OFET devices have been fabricated by co-evaporation of small molecules or solution processing a mixture of n-type and p-type polymers.[6,7] In polymer blends, the morphology plays a crucial role in determining the device properties due to the requirement for each electronic component to contact the source and drain electrodes and form sufficient percolation paths for each of the charge carriers. The blend morphology is typically optimised through processing conditions - by adjusting the blend ratio, solvents or annealing conditions. However, the resulting blend morphologies are non-equilibrium structures that are kinetically trapped during the phase separation process. Additionally, the electronic functionality of a given conjugated material in a blend is often linked to its crystallinity, which is difficult to influence within the constraints of a non-equilibrium, kinetically trapped structures.

Another strategy is to combine the functional molecular donor (D) and acceptor (A) units in one macromolecule, either as alternating copolymer as -$[DA]_n$- or in a diblock copolymer with covalently bound segments as $[D]_n$-*block*-$[A]_m$. $[DA]_n$ conjugated polymers with a low bandgap have been synthesised. These materials exhibit an intrinsically ambipolar charge transport.[8,9] $[D]_n$-block-$[A]_m$ copolymers consisting of separate, covalently linked D and A polymer chains can self-assemble into bicontinuous domains for p-type and n-type charge transport. They bridge the gap between $[DA]_n$ materials[10,11] and donor acceptor blends. In these block copolymers, polymer crystallinity of each domain, which is important for the charge transport, can be combined with a well-defined interconnectivity of both domains.

Equilibrium nanostructured morphologies of diblock copolymers with two amorphous blocks are well known,[12] but morphologies in block copolymers with rod-like units[13] or crystallisable blocks are much more complicated to predict.[14–16] Nevertheless, the covalent bond between the donor- and acceptor sub-chains always ensures nanoscale heterogeneity, and together with the control of the crystallisation preferences, offers potential new device processing possibilities.

Here we report on the first organic field effect transistors realised with fully functionalised diblock copolymers and demonstrate the relationship between composition, crystallinity and charge transport. More importantly, the charge transport in the OFETs can be set from p-type to ambipolar or from p-type to n-type device characteristics in one single material depending on the block-ratios. This potentially

a

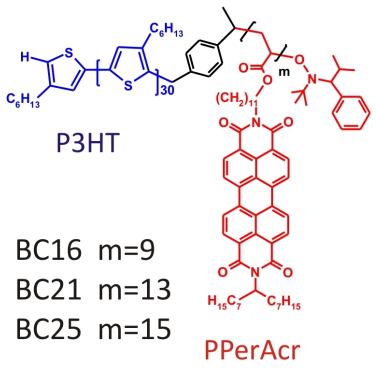

compound	M_n [kg/mol] polydispersity	wt.-% PPerAcr	PPerAcr		P3HT	
			a, b, γ [nm]	c [nm]	a [nm]	b, c [nm]
PPerAcr	23 / 1.71	100	a=3.086 b=2.196 γ=81.2°	0.354	-	-
P3HT	8.9 / 1.12	0	-	-	1.754	0.766
BC 16	16.1 / 1.25	55.7	a=3.078 b=2.206 γ=80.9°	0.365	1.798	0.766
BC 21	20.6 / 1.31	73.7	a=2.987 b=2.096 γ=79.5°	0.365	1.791	0.768
BC 25	24.8 / 1.53	81.4	a=2.988 b=2.105 γ=79.5°	0.363	1.785	0.764

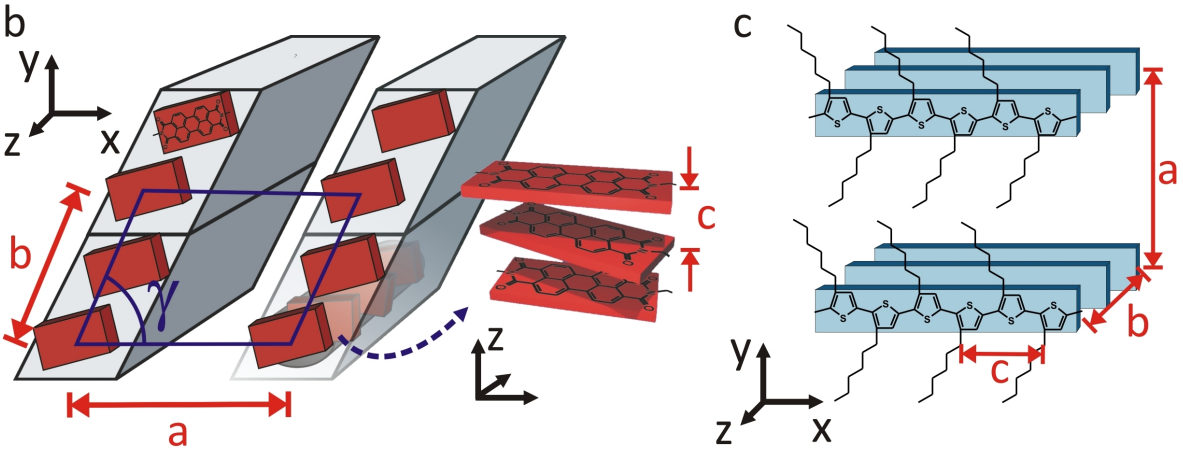

Figure 9.1: a) Molecular structure of the block copolymer P3HT-b-PPerAcr. The table shows the properties of the homopolymers and block copolymers together with the unit cell dimensions (at T =90 °C). Sketch of the crystalline structure of PPerAcr (b) and P3HT (c).

opens new possibilities for the design of complementary electronic elements by simple solution processing of a single component. We have studied a series of diblock copolymers, BC16, BC21 and BC25, comprising regioregular poly(hexylthiophene) (P3HT) and poly(perylene bisimide acrylate) (PPerAcr) subchains in different volume ratios.[17] The chemical structure, the overall molecular weight M_n, the polydispersity (PDI) and the composition are given in Fig. 9.1. P3HT is a ubiquitous hole transporter (donor material) that is amongst the most effective polymers in organic photovoltaics and OFETs, owing to field effect hole mobilities up to 0.1 $\frac{cm^2}{Vs}$.[18,19] The crystalline structure of P3HT is well known[20,21] (Fig. 9.1c). Perylene bisimides (PBIs) are one class of n-type materials (acceptor material) that combine promising electronic properties with good air stability. Low molecular weight PBIs have shown electron mobilities as large as 2.1 $\frac{cm^2}{Vs}$ in evaporated thin films.[22,23] Furthermore, attachment of side chains at the imide groups renders them soluble in common organic solvents and an alteration of the intermolecular packing without changing the delocalised π-electron system within the PBI core.[24] Alkyl substituents can be used to induce the formation of one-dimensional columnar PBI aggregates.[25,26] We have recently reported a polymerised form of this

PBI (PPerAcr) that exhibits electron mobilities of $10^{-3}\,\frac{\mathrm{cm}^2}{\mathrm{Vs}}$ and good electron injection from gold electrodes.[27] The latter fact is important since the higher LUMO levels of other n-type materials usually necessitate low work function metals such as aluminium, calcium or magnesium as electrodes, which would not allow hole injection into P3HT. The demonstrated block copolymer OFETs use solely one electrode material - gold - with good injection properties for holes and electrons.

Results and Discussion

Before we will demonstrate the OFET properties which are thin film devices, we firstly present some fundamental X-ray characterization of the nanostructured bulk material. The relative composition of the block copolymers merely affects the crystal structure, while the relative crystallinity is strongly influenced. This is an important property which will influence the charge transport i.e. the formation of nanoscopic percolation paths. We studied the temperature-dependent structure formation in the homopoly-

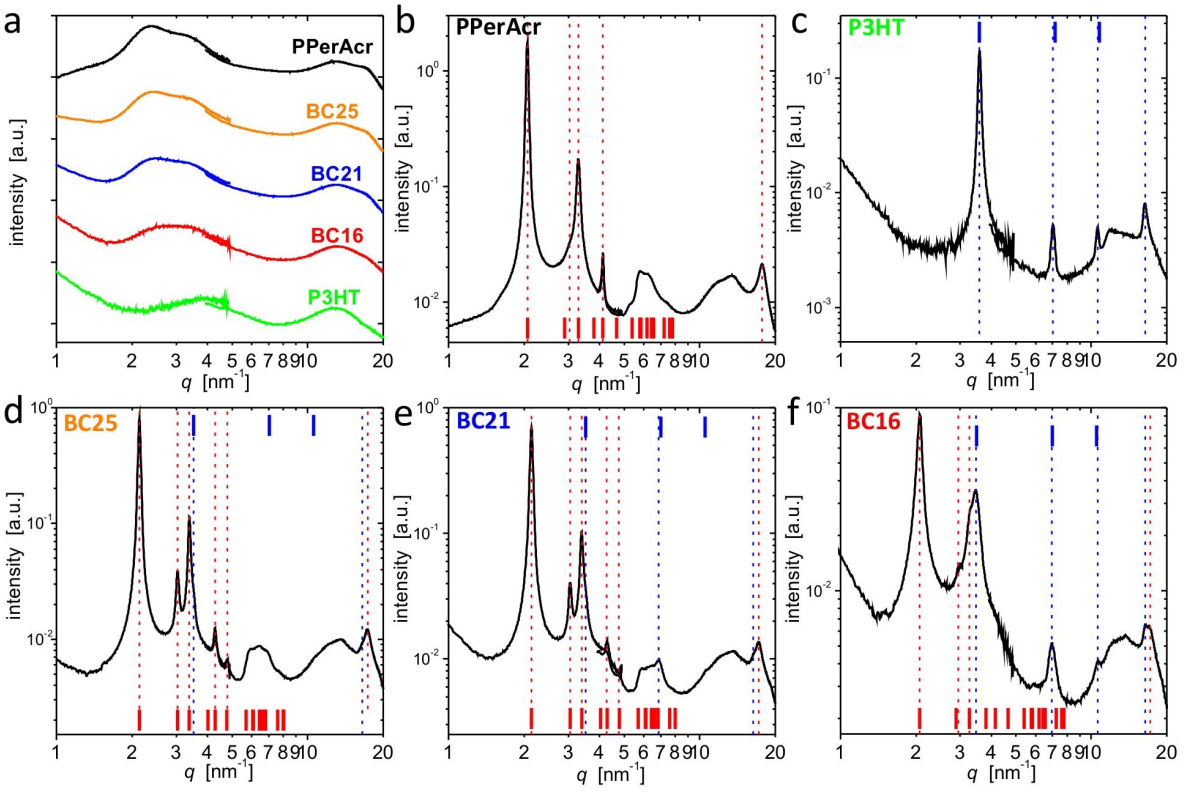

Figure 9.2: Radially averaged SAXS/WAXS patterns of bulk samples. a) At high temperatures $T = 210\,^{\circ}\mathrm{C}$ all the samples are molten and do not show any Bragg-reflections; the curves are offset for clarity. During cooling the PPerAcr- and P3HT-parts of the diblock copolymers crystallise and Bragg-reflections appear: b) to f) show the corresponding patterns at $T = 90\,^{\circ}\mathrm{C}$ for the different samples as indicated in the graphs. The dashed lines correspond to peak positions obtained by fitting Lorentz-functions to the data, red: PPerAcr, blue: P3HT. The red (PPerAcr) and blue (P3HT) bars correspond to expected peak positions for the lattice parameters given in Fig. 9.1a.

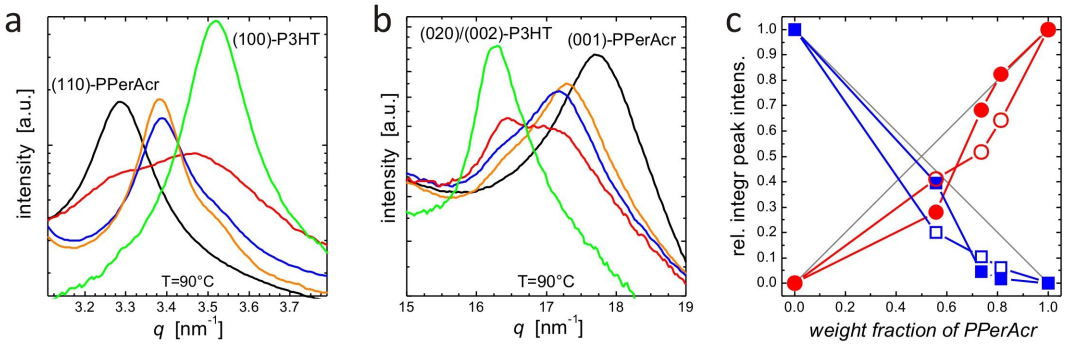

Figure 9.3: a) Overlap of the *(110)* PPerAcr reflection and the the *(100)* P3HT reflection. For BC21 and BC25 the *(110)* PPerAcr reflection is slightly shifted due to a little different unit cell and the *(100)* P3HT reflection is still visible as a shoulder at $\sim 3.5\,\frac{1}{\mathrm{nm}}$ b) Change of the overlapping *(020)/(002)*-reflection of the P3HT-crystallites and the *(001)*-reflection of PPerAcr with copolymer composition (colors as in Fig. 9.2a). b) Integrated Bragg-reflection intensities normalised to the homopolymer values as a function of PPerAcr-content. Open symbols correspond to *(020)/(002)*-reflection of P3HT (blue squares) and *(001)*-reflection of PPerAcr (red circles) and filled symbols represent the integrated intensities of the *(100)*-reflection of P3HT (squares) and PPerAcr (circles), respectively.

mers and the block copolymers using X-ray scattering by slowly cooling from the molten state (Fig. 9.2a). The PPerAcr homopolymer (Fig. 9.2b, schematic in Fig. 9.1b) shows a crystallisation of the PBI cores into stacks with a π-stacking distance of $c = 0.354\,\mathrm{nm}$ (X-ray reflection at $q = 17.75\,\mathrm{nm}^{-1}$). These stacks arrange on 2-d lattices (Fig. 9.1b). We find good agreement of the observed Bragg reflections (red dashed lines in Fig. 9.2b) with the reflections expected for a 2-d oblique lattice with parameters $a = 3.086\,\mathrm{nm}$, $b = 2.196\,\mathrm{nm}$ and $\gamma = 81.2°$ (red bars in Fig. 9.2b). The number of PBI cores per unit cell can be estimated by assuming that the overall density is not much smaller than $1\,\frac{\mathrm{g}}{\mathrm{cm}^3}$. Thus a value for the density of $1.14\,\frac{\mathrm{g}}{\mathrm{cm}^3}$ is obtained by dividing the mass of two PPerAcr monomers (molar mass per monomer: $825\,\frac{\mathrm{g}}{\mathrm{mol}}$) by the volume of the unit cell ($V = abc\sin\gamma$).[28] Having 2 PBIs per unit cell, the comparison of the lattice parameter b with the molecular dimension of the PBI core lead us to suggest a lamellar packing as shown in Fig. 9.1. Consistent with this arrangement, the (010) reflection is strongly suppressed by the formfactor of the unit cell and only a weak shoulder is visible in Fig. 9.2b at $3\,\mathrm{nm}^{-1}$. For the block copolymers the unit cell structure slightly changes leading to a clearly visible (010) reflection mainly attributed to the slight change in γ.

Fig. 9.2c shows evidence for the crystallinity of P3HT. The first three reflections correspond to the $(h00)$-reflections for h = 1,2,3 with $a = 1.754\,\mathrm{nm}$ (cf. Fig. 9.1b). The reflection at $q = 16.41\,\mathrm{nm}^{-1}$ is a convoluted reflection of the inter- and intrachain stacking (b- and c-direction) with the corresponding Miller indices $(020)/(002)$. The values for lattice parameters a and b/c (determined at $T = 90\,°\mathrm{C}$) are in close agreement with the lamellar packing reported in the literature.[29]

Having thus identified the signatures of the PPerAcr- and P3HT homopolymer lattices, we have studied the series of asymmetric block copolymers which have PPerAcr-weight fractions of 55.7% (BC16), 73.7% (BC21) and 81.4% (BC25). The molecular weight of the P3HT-block was $8.9\,\frac{\mathrm{kg}}{\mathrm{mol}}$ in all cases. After crystallization from

the melt (same thermal treatment as for the homopolymers), the scattering patterns in Fig. 9.2d-f closely resemble a combination of the Bragg reflections in Fig. 9.2b,c, though small changes in the unit cell parameters were observable (Fig. 9.1a). The signature of both crystal structures in these patterns (red and blue dashed lines and Fig. 9.3) provides clear evidence that phase separation occurs in all three block copolymers. The covalent linkage of both blocks ensures a nanoscopic phase separation. Indeed probing the charge generation dynamics by ultra-fast spectroscopy as shown below, the estimated domain sizes range below 10 nm which is consistent with the molecular dimensions of the blocks (estimated contour length of the P3HT block of approx. 11.6 nm). (Additional scanning electron microscopy images on the nanoscopic phase separation are given in the supplementary information.)

The separated crystals of donor- and acceptor- units demonstrate the potential applicability of these block copolymers in devices. Fig. 9.3a,b show compilations the 5 polymers of a) the (*110*) PPerAcr reflection and the (*110*) P3HT reflection, and b) the q-range where the (*020*)/(*002*)-reflection of the P3HT-crystals and the (*001*)-reflection and the PPerAcr-crystals appear. Though the P3HT reflections in Fig. 9.2a,b for higher PPerAcr content appeared only as weak shoulders, we tried to estimate the change in P3HT crystallinity as a function of PPerAcr content by considering the respective peak intensities (Fig. 9.3c). At higher PPerAcr content the P3HT crystallinity seemed to be lower than expected from a linear scaling. This indicates that part of the P3HT chains were not able to crystallise and frustrated by PPerAcr crystallisation.

The competing crystallisation behaviour can be used to adjust the charge carrier properties in an OFET device. The polymer was spin-coated from chloroform solution onto bottom gate, bottom contact OFET substrates. Despite the higher PPerAcr weight fraction compared to the P3HT content, we found that all block copolymers exhibited p-type character after spin coating. Fig. 9.4 shows the OFET output characteristics for devices made with the three copolymers. All as-spun films (Fig. 9.4a-c) show typical unipolar hole transport, even the block copolymer with a PPerAcr weight content of 81% PPerAcr. The overall drain-source current I_{ds} decreases slightly with increasing PPerAcr content presumably indicating an increasing lateral disruption of hole-conducting channels. The contact resistance was low in all cases, as indicated by the linear raise of drain source current I_{ds} for applied voltages $V_{ds} < 0$. Fig. 9.5a-c (black lines) show the transfer characteristics measured for these p-type devices. The measurements indicate hole injection from the drain electrode, leading to decreasing output characteristics with increasing gate voltages. Hole mobilities of around $10^{-5}\,\frac{\mathrm{cm}^2}{\mathrm{Vs}}$ were extracted in the saturation regime. P3HT homopolymer can exhibit hole mobilities which are magnitudes higher, however the low molecular weight fraction of the block is strongly limiting the maximal achievable mobilities.[30] Electron injection was observed in some of the devices only at very high drain-source voltages. These results indicated that only the P3HT component forms sufficiently interconnected domains to support the creation of a channel from source to drain in spin-cast films. Since the thiophene units are part of a conjugated polymer chain that favors both, interchain and intrachain charge transport,[19,31] the formation of interconnected percolation paths for holes is less constrained than the electron conduction pathways formed by the intermolecular π-orbital overlap of the tethered PBI moieties. Additionally, the weight percentage of the PBI block do not resemble the real content of PBI electronic moieties

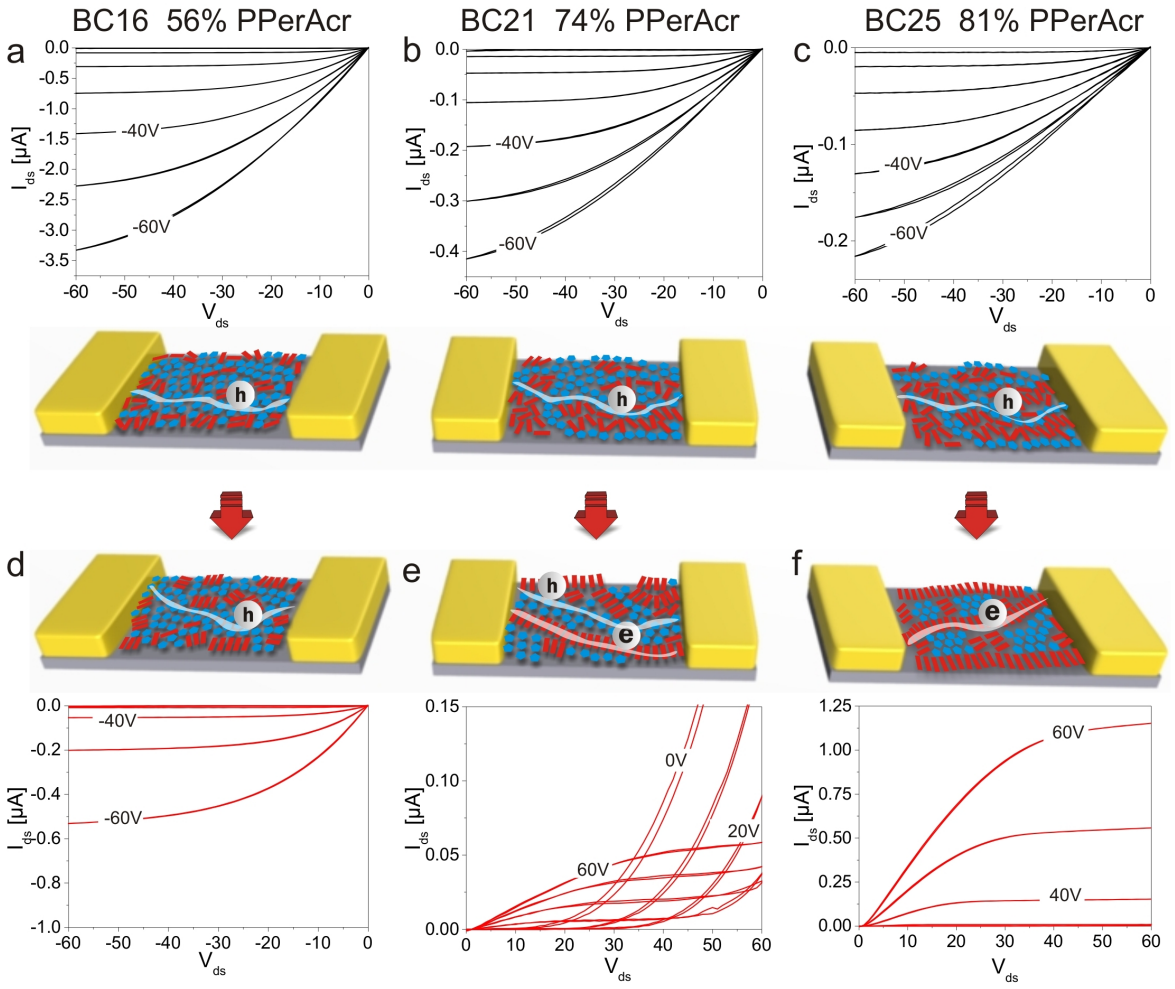

Figure 9.4: a-f) Output characteristics of OFETS made from BC16, BC21, BC25 before annealing (a-c, black curves) and after annealing (d-f, red curves). The gate voltage V_g was varied from 0 to 60 V in steps of 10 V. Before annealing all transistors show unipolar p-type character, whereas after annealing ambipolar transport was observed for BC21 and unipolar n-type transport for BC25. Schematics of the thermally induced structure-function transition in block copolymer OFETs are shown inbetween the output graphs. Before annealing (upper sketch) P3HT forms hole percolation paths between the source and drain electrode. After cooling from melt (lower sketch), n-type percolation paths dominate and the transistor switches to ambipolar or n-type behaviour.

due to high dilution caused by substituents, which are necessary for solubility. The percolation path formation is also influenced by the fast drying during the spin-coat process which freezes in non-equilibrium structures.

After a thermal annealing step at 225°C (above the melting temperature of both components, Fig. 9.2a) for 15 min and cooling down at 10 $\frac{\mathrm{K}}{\mathrm{min}}$ (similar to the X-ray studies), the OFET properties changed drastically depending on the block copolymer composition. After annealing (Fig. 9.4d-f), BC16 retains p-type behaviour but with slightly reduced currents and an increased threshold voltage for hole accumulation V_{ThH}. In the case of BC21 (Fig. 9.4b,e), an ambipolar character was found, with both, holes and electrons accumulating in the channel. The most significant transi-

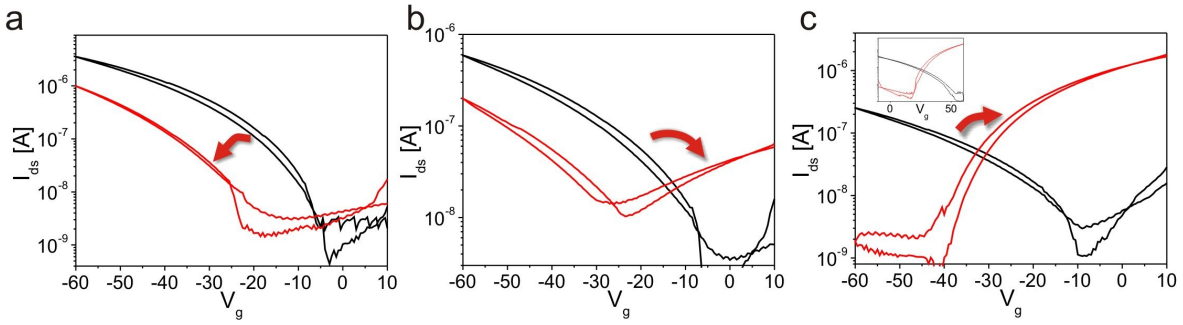

Figure 9.5: Transfer characteristics of the block copolymer transistors measured in p-type configuration at $V_{ds} = -60\,\mathrm{V}$. The black and red curves show the as-spun annealed devices, respectively. a) BC16 remains unipolar p-tpye, b) BC21 shows ambipolar properties, and c) BC25 switches to unipolar n-type after annealing. The inset of c) shows the transfer characteristic of BC25 measured in n-type configuration. (For additional output and transfer characteristics see supplementary information (Fig. 9.7, Fig. 9.8).

tion occurred for BC25, the block copolymer containing the highest PPerAcr content (Fig. 9.4c,f). Upon thermal annealing, the polarity switched entirely from a p-type to n-type behaviour.

Fig. 9.5a-c show the transistor transfer characteristics before and after annealing. The extracted hole mobilities from the OFETs in saturation before annealing account for $10^{-5}\,\frac{\mathrm{cm}^2}{\mathrm{Vs}}$. The P3HT hole mobilities are relatively small, which is related to the short P3HT block length.[32]. The electron mobilities for the annealed BC21 and BC25 are around $10^{-5}\,\frac{\mathrm{cm}^2}{\mathrm{Vs}}$, which is two orders below the mobility of the pristine homopolymer.[27] The ambipolar character of the annealed BC21 transistor is clearly evident in its characteristic V-shaped transfer characteristic (Fig. 9.5b), caused by the injection of electrons via the drain electrode, while measuring in p-type configuration (see supplementary information). Fig. 9.5c shows the complete switch from a p-type to an n-type behaviour of the device upon annealing and only a marginally small injection of holes is noticeable.

We identify two main reasons for the switching in transistor characteristics upon annealing. Firstly, the fact that both p- and n-type polymer segments are covalently connected means that the scope of the phase separation is constrained to the nanometer length scale. Thus, both polymer segments are in close proximity to the gate dielectric interface and are potentially able to form field-effect charge carrier channels. The second reason is the interplay of the crystallisation behaviour of the two polymers - the main chain crystallinity of P3HT and the side chain crystallinity of PPerAcr. Thermal annealing enables the PBIs units to rearrange sufficiently into $\pi - \pi$ stacks building up the 2-d lattice causing enhanced intramolecular electronic coupling. However, the crystallinity of PPerAcr possibly improves at the expense of the crystallinity (compare discussion of Fig. 9.3c) and connectivity of P3HT domains. In the case of the BC21, the interconnectivity and crystallinity of both components was sufficiently high so that electron as well as hole percolation paths could form, leading to an ambipolar device. The OFET properties of BC25 were dominated by the formation of percolating PPerAcr stacks after annealing. The X-ray analysis carried out on bulk samples of the block copolymers support this observed evolution of the crystalline domains during annealing

(Fig. 9.10).

An alternative explanation of the change in transistor characteristics upon annealing involves the possible build-up of a PPerAcr wetting layer on the gate, displacing the P3HT domains further into the bulk of the film. In order to test this hypothesis X-ray photoelectron spectra (XPS) of the bottom surface (in contact with the gate) of the block copolymer films were carried out. No significant differences between the as-spun and the annealed samples were observed. On the other hand, a comparison of the XPS-spectra of the homopolymers, PPerAcr and P3HT shows significant differences in the relative signals of N and O that are contained in PPerAcr and S that is contained in P3HT only (supplementary information Fig. 9.11).

Directly resolving the morphology at the gate oxide interface is not simple as the domains are on the edge or beyond the resolution of standard scanning electron microscopy or scanning probe microscopy. In the latter case, for example, the stiffness of both blocks strongly limits a possible phase contrast. Only extensive solvent vapour annealing of the samples provides a sufficient contrast in SEM (see supporting information Fig. 9.12). In order to substantiate the above findings and to obtain an indirect access to the nanoscopic structure of the material, we also employed several complementary spectroscopic methods to investigate the evolution of crystallinity in thin films. The overlap of the π-orbitals within crystals of conjugated materials causes morphology-dependent changes in transition dipole moments and therefore in optical absorption and emission spectra. The degree of aggregation can be assessed by comparing the relative intensities of vibronic bands. For PBI, the relative intensities of vibronic bands at 490 and 540 nm can be considered to estimate the effect of aggregation.[33] Fig. 9.6a shows the absorption spectra of the two homopolymers P3HT and PPerAcr after spincoating and after thermal annealing for 10 min at 225°C followed by cooling down at 10 $\frac{\mathrm{K}}{\mathrm{min}}$. Absorption spectroscopy confirms the favorable aggregation of PBI moieties after thermal annealing. The main spectral changes of PPerAcr after thermal annealing are the suppression of higher energy absorption combined with the emergence of a low energy shoulder (see change in relative intensities of vibronic bands). The improved perylene bisimide aggregation decreases the oscillator strength of transitions to higher vibronic levels, whereas the new low energy features are attributed to charge transfer states and mixed Frenkel-charge transfer states.[34] A general feature of crystalline P3HT films is the strength of the 0-0 vibronic band at 610 nm which is indicative of extended planarised chains.[35,36] The P3HT homopolymer shows marginal enhancement of this vibronic band for the annealed film compared to the as-spun film. Fig. 9.6b shows the absorption spectra of the block copolymers. For the as-prepared sample (solid lines), little difference is seen among the three block copolymers. The absorption spectra are broadly described as a weighted average of the homopolymer spectra according to their respective weight ratios. However, the suppression of the P3HT 0-0 vibronic feature in the block copolymers is clear evidence that the presence of the PPerAcr block disrupts the full crystallization of P3HT. Thermal annealing induces similar spectral changes in the absorption spectra of block copolymers as observed in the constituent homopolymers (Fig. 9.6a). The suppression of higher energy absorption features is accompanied by the growth of lower energy absorption peaks as the crystallinity of both blocks improves. The spectral shifts on annealing are clearly dominated by the increased crystallization of the PPerAcr component, explaining the

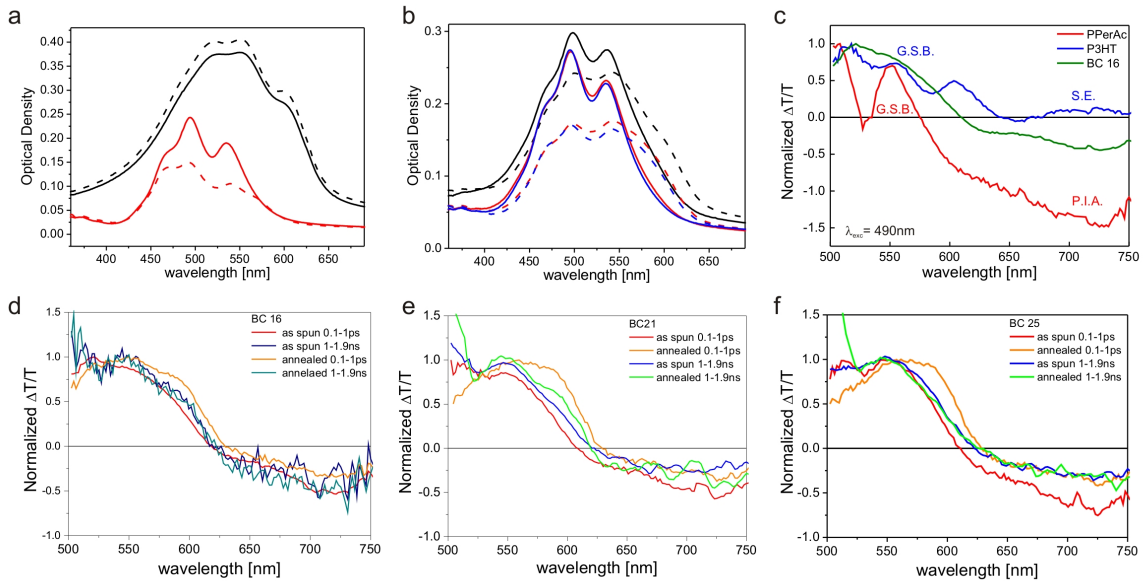

Figure 9.6: a) and b) UV-Vis spectra of the as spun (solid line) and annealed (broken line) film. a) comprises the homopolymers P3HT (black) and PPerAcr (red). b) shows the block copolymer samples with BC16 (black), BC21 (red), BC25 (blue). c) to f) Transient absorption spectroscopy data. c) shows representative TA spectra of the homopolymers taken within the first picosecond after excitation. A positive change in the transmission $\Delta T/T$ indicates a goundstate bleach (GSB) or a stimulated emission (SE), whereas a negative change indicates photo induced absorption (PIA). The broad PIA peaked at 730 nm is associated with excitons in PPerAcr, consistent with other photophysical studies of perylene diimides.[37] d - f) compare the photoinduced absorption for block copolymer BC16 (d), BC21 (e) and BC25 (f) right before and after annealing on sub-ps and ns timescales. Thermal annealing results in some ordering of P3HT, as evident by the enhanced GSB in the 0-0 region at 610 nm for the sub-ps exciton spectra, however ordering is disrupted at the interfaces with the PPerAcr block, as evident from the invariance of interfacial charge pair spectra recorded at 1-1.9 ns.

observed switching behaviour of polymers with the highest content of PPerAcr.

In addition to absorption spectroscopy which provides a picture of the overall changes in crystallinity throughout the films, transient absorption (TA) spectroscopy was employed to extract information about nanoscale morphological changes in the vicinity of interfaces. A detailed discussion of the TA data is provided elsewhere.[38] As is typical for nanostructured donor-acceptor systems, photoexcitation results in the formation of interfacial charge pairs, with holes and electrons in the P3HT and PPerAcr moieties, respectively. The information gained by TA spectroscopy is based upon spectral signatures of crystallinity for excitons (the primary excitation, formed throughout the film) compared with charge pairs (formed at later times, localised near donor-acceptor interfaces).

Fig. 9.6d-f shows the effect of annealing on excitonic spectra (recorded at $t \approx 0.1-1$ ps delay) and interfacial charge spectra ($t \approx 1-1.9$ ns) for the block copolymers. At $t \approx 0.1-1$ ps delay (red and orange curves), the spectra largely represent a weighted average of excitonic spectra of both homopolymers, which are shown in Fig. 9.6c. At

$\lambda < 620\,\text{nm}$, the positive $\Delta T/T$ signal is dominated by ground-state bleaching (GSB) of the P3HT chromophore and corresponds to the ground state absorption spectrum. Analogous to the ground state absorption spectra, bleaching of the 0-0 peaks at 610 nm is suppressed in the as-spun films (red curves, Fig. 9.6d-f). We are able to assign the $t \approx 1 - 1.9\,\text{ns}$ TA spectra to interfacial charge pairs based on the strong photovoltaic response of the material and the persistence of the spectra on time scales that far exceed exciton lifetimes.[38]

The TA spectra shown beyond $t \approx 1 - 1.9\,\text{ns}$ in Fig. 9.6d-f exhibit photoinduced absorption at $\lambda > 630\,\text{nm}$ (attributed to charges in both phases) and ground-state bleaching at $\lambda < 630\,\text{nm}$ (largely corresponding to the P3HT chromophore). As was the case for exciton TA spectra, the vibronic structure of the P3HT-based bleach signal can be interpreted on the basis of the crystallinity of polymer chains occupied by excitations.

The close resemblance of the charge pair spectra obtained before (blue curves) and after (green curves) thermal annealing, and the suppression of GSB intensity in the 610 nm region with higher PPerAcr content clearly show that P3HT is increasingly disordered at the interfaces where charge pairs are detected.

Since the time scale of exciton diffusion limited charge generation (i.e. formation of charge transfer states) is directly related to the size of domains, we can extract nanometer-scale morphological parameters on a length scale that is not resolved by electron microscopy.[39,40] The population of charge pairs peaks within just 2 ps, as ascertained from the growth of the photoinduced absorption at 700 nm.*[38] The short timescale reflects the close proximity of most P3HT regions to an interface less than 10 nm.Thus, after spincoating the domains are considerably smaller than those expected for thermodynamical equilibrium structures (e.g. obtained after extensive annealing). On 15 min thermal annealing, the kinetics of charge transfer for all samples remain unchanged. This clearly indicates that the domain sizes do not change considerably during the device annealing procedure. This is also consistent with the complete quenching of emissive P3HT excitons in photoluminescence measurements.[38] Comparable as seen in the bulk crystallinity (Fig. 9.3c), an increasing content of PPerAcr influences the subsequent crystallisation of P3HT, so that a higher content of PPerAcr is sufficient to severely disrupt the connectivity of P3HT networks hence to suppress p-type transport. The TA on a longer time scale (nanoseconds) probes the interfacial character as only long lived charge transfer states can be detected and proofs the decreasing P3HT crystallinity with higher PPerAcr content.

Conclusion

In conclusion, we have demonstrated a series of double-crystalline block copolymers that comprise a hole transporting P3HT block (p-type) and an electron transporting PPerAcr block (n-type). The n-type block self-aggregates into a nanoscopic two dimensional lattice comprised of PPerAcr stacks and the p-type block consisting of

*In addition to charge pairs, PPerAcr-based excitons also exhibit absorption at 700 nm. However, the growth of absorption at 700 nm cannot be attributed to energy transfer from P3HT to PPerAcr because the P3HT-based ground-state bleach is retained on this timescale.

P3HT crystallises in its well-known lattice. The interplay of the crystallinity and the block sizes determine the formation of percolating paths that lead to either p-type, n-type or ambipolar behaviour. Directly after solution processing, which results in a non-equilibrium morphology, only the P3HT phase provides sufficiently interconnected pathways. This is the case for all the block copolymers inclusive BC16, where it comprises only 19 wt% of the film. A thermal annealing step enhances the formation of crystalline PPerAcr domains that favor n-type transport. In return, these may impede the formation of interconnected P3HT pathways. Depending on the composition of the block copolymer, the devices switched from unipolar hole transport to ambipolar or unipolar electron transport in a single material.

These results demonstrate the versatility of fully functionalised block copolymers as a new class of materials for the application in organic thin film transistors. Broadening the range of supramolecular structures of P3HT-*b*-PPerAcr is feasible by different annealing methods such as solvent annealing,[41] or by further changing the block size. Locally focused thermal annealing by laser is under current investigation and yields towards the selective switching of transistors on the substrate. The covalent linkage of the two blocks preserves the nanoscopic structure also after extensive annealing procedures and therefore the block copolymers are expected to provide robust systems regarding the annealing parameters for device fabrication. We believe that these results will inspire further efforts towards complementary electronic applications based on supramolecular assembly of materials with multiple electronic functionalities.

Methods

The polymers were dissolved in waterfree chloroform 0.7-1 wt% solution and spincast on the respective substrates at 2000 RPM. For the OFETs we used lithographically prepatterned substrates. The drain and source contacts were interdigitating gold electrodes with gate lengths of 10 μm and gate widths of 20 mm. Highly n-doped silicon wafer with a 300 nm thick silicon oxide layer was used as the gate dielectric. Prior to spincoating the polymer, the substrates were solvent and plasma cleaned and then subsequently silanised by HMDS vapour for approximately 3 h. The transistors were measured with a HP4155A or HP4155B parameter analyzer. All OFET preparation and characterization steps were carried out in a glovebox under nitrogen atmosphere. The charge carrier mobility μ was extracted in the saturation region of the transfer characteristics using $I_d = \frac{W}{L}\mu_{sat}C_i(V_g - V_{Th})^2$, where W is the gate width, L the gate length, C_i the silicon oxide capacitance and V_{th} the threshold voltage.

X-ray diffraction was measured at the ESRF Synchrotron in Grenoble at Beamline ID02. The energy of the X-rays was 12.54 keV. The sample consisted of polymer powder which was pressed into holes of Aluminium discs with holes of 0.8 mm diameter and a thickness of 1 mm. The thermal measurements where carried out at 10 $\frac{\mathrm{K}}{\mathrm{min}}$ under inert gas atmosphere. Two detectors were used simultaneously to cover a wide q range overlapping at $\sim 1\,\mathrm{nm}^{-1}$. Para-bromo benzoic acid was used to calibrate the detectors. The measurements were corrected by empty cell measurements.

X-ray photoelectron spectra (XPS) of the bottom side of the block copolymer films. Films were prepared on silicon oxide coated silicon wafers using the same proce-

dure as for the organic field effect transistors. A protective platinum layer was sputtered on top and an epoxy resin was glued to that. The silicon substrate was then removed from the film and the resin by liquid nitrogen, so that the bottom of the polymer film was exposed and could be analyzed by XPS (Perkin Elmer PHI-5600). The complete delamination of the film was assured by optical investigation of the initial silicon oxide substrates.

For the spectroscopic measurements, the polymers were spincoated onto spectrosil quartz glass. The UV-Vis measurements were carried out with a Hewlett-Packard 8453 diode array spectrometer. The setup for transient absorption (TA) spectroscopy is described elsewhere.[42–44] Briefly, a 1-kHz train of 60 fs pulses (800 μJ/pulse, $\lambda_0 = 800$ nm) is split; a portion used to pump a TOPAS optical parametric amplifier to tune the excitation pulses, and a further portion of the 800-nm beam is used to pump a home-built broadband non-collinear optical parametric amplifier (NOPA)[42] for broadband TA spectra. The probe beam is delayed relative to the excitation beam via a mechanical delay stage before overlapping with the excited region of the film. In the spectral measurements, the probe beam is spectrally resolved and digitised for each laser pulse. The excitation beam is chopped at 500 Hz such that the transmission of alternate probe pulses can be compared to obtain the spectrally resolved differential transmission as a result of excitation, and temporal dynamics are compiled by collecting spectra for a range of relative probe delay times (typically ∼150 points are distributed from -10 to 2000 ps). Samples were contained in a vacuum chamber ($\sim 10^{-5}$ mbar) during TA measurements.

Acknowledgement

We acknowledge the European Synchrotron Radiation Facility for provision of synchrotron radiation facilities and we would like to thank M. Stuecky for assistance in using beamline ID02. The authors thank M. Kolle and H. Schoberth for their support during the x-ray measurements. We also thank Prof. Dr. Jürgen Rühe group, IMTEK, Freiburg for the XPS measurements. We acknowledge the financial support from the European network "PolyFilm" under RTN-6 and the German Research Council (DFG) project SFB 481 and SPP1355. S.H. thanks Universität Bayern e.V. for the financial support in the form of a scholarship of the Bayerische Graduiertenförderung and the Elitenetzwerk Bayern (ENB) for their support. JMH and RHF wish to acknowledge a grant from the U.K. Engineering and Physical Sciences Research Council (EPSRC).

Supplementary information

Complete set of output and transfer characteristics

For completeness we present here the output characteristics that have been measured as a p-type ($V_g = 0, -10, -20, -30, -40, -50 - 60\,\mathrm{V}$ and $V_{ds} = 10.. - 60\,\mathrm{V}$) and an n-type device ($V_g = 0, 10, 20, 30, 40, 5060\,\mathrm{V}$ and $V_{ds} = -10..60\,\mathrm{V}$) (Fig. 9.7). If a device exhibits n-type character while it is measured under no gate bias, hole injection occurs from the drain electrode. This leads to a current that decreases with an increases gate bias. Fig. 9.8 shows a complete set of the transfer characteristics before and after annealing. The ambipolar character of the annealed BC21 transistor is clearly evident in its characteristic V-shaped transfer characteristic (Fig. 9.8b). Considering the p-type transfer regime, where the drain voltage was kept at $V_{ds} = -60\,\mathrm{V}$, holes are injected from the source electrode for $V_g < V_{ThH}$. For $V_g - V_{ds} > V_{ThE}$ the drain electrode was more positive than the threshold voltage for electron injection V_{ThE}, so that electrons are injected from the drain electrode. For the n-type regime, the same considerations apply with opposite signs. Fig. 9.8c shows the switch from a p-type to an n-type behaviour of the device upon annealing. The as-spun device exhibited marginal electron injection at positive voltages, but the threshold voltage for electron injection is very high and not significant as shown by the n-type transfer characteristic of the as spun film.

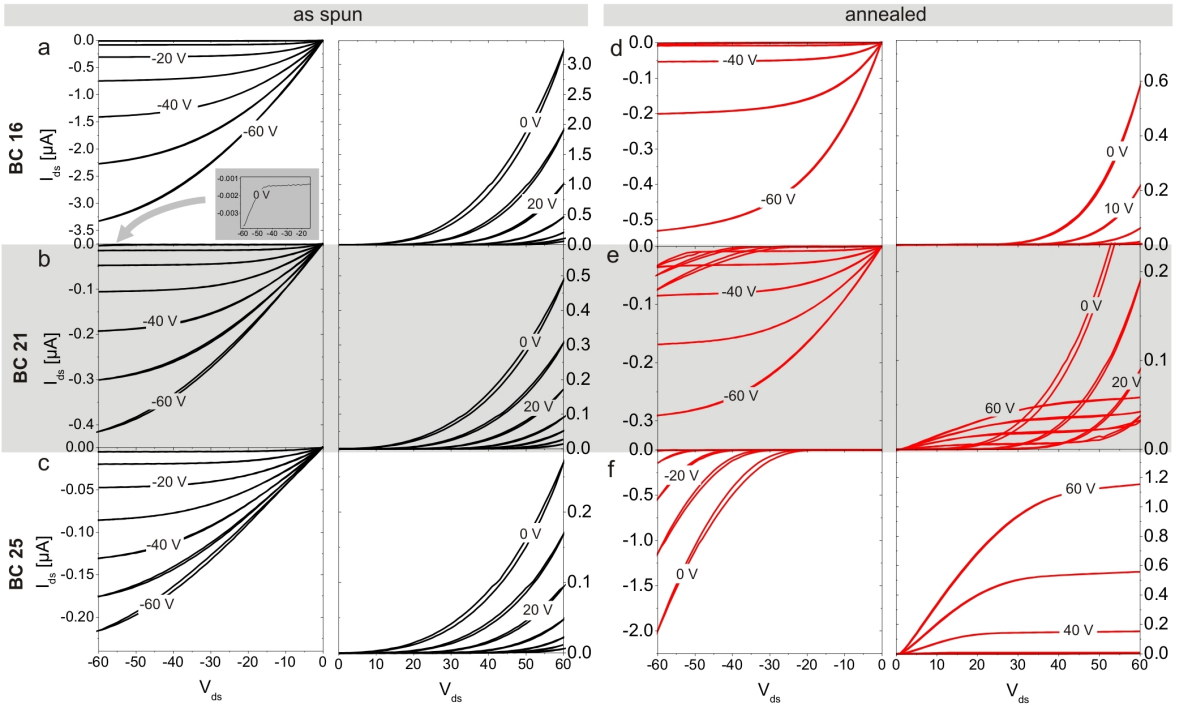

Figure 9.7: Output characteristics measured under p-type (left) and n-tpye (right) conditions before annealing (left) and after annealing (right). The gate voltage V_g is changed stepwise by 10 V from 0 to -60 V (for p-type, left) and from 0 to 60 V (for n-type, right).

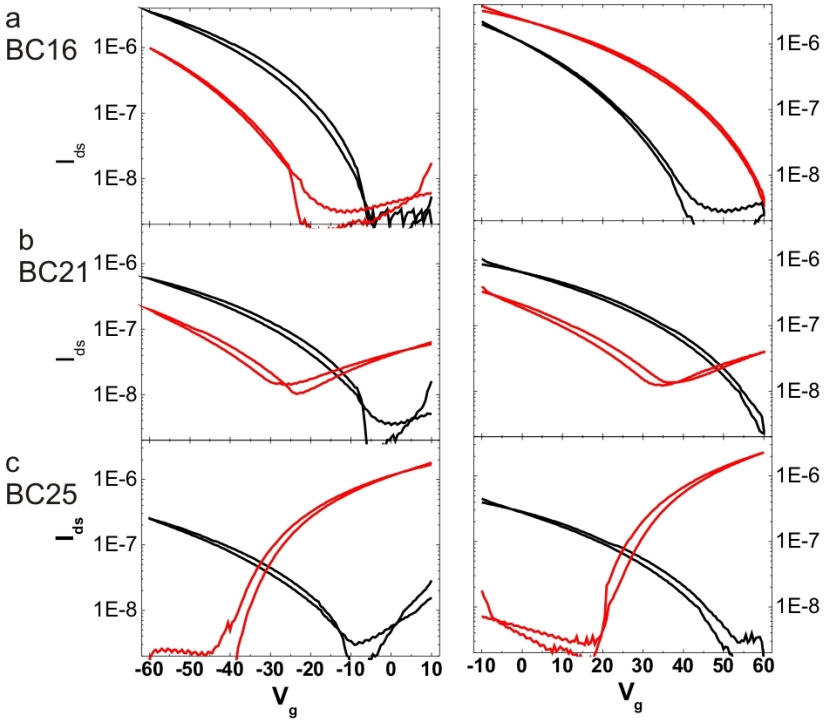

Figure 9.8: Transfer characteristics measured under p-type (left) and n-tpye (right) conditions before annealing (black) and after annealing (red). The source drain voltage V_{ds} was kept at -60 V and (for p-type, left) and at 60 V, respectively (for n-type, right).

Thermal analysis of P3HT-*b*-PPerAcr block copolymers

Differential scanning calorimetry (DSC) measurements were carried out at heating and cooling rates of 10 $\frac{\mathrm{K}}{\mathrm{min}}$ under nitrogen using a Perkin Elmer Diamond DSC (Fig. 9.9.

The occurrence of a positive or negative enthalpy change indicates the event of

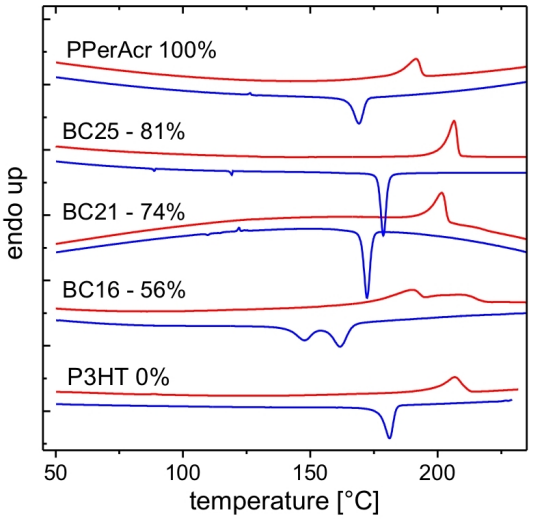

Figure 9.9: Differential scanning calorimetry (DSC). The graph shows the second heating and third cooling cycle with a rate of 10 $\frac{\mathrm{K}}{\mathrm{min}}$.

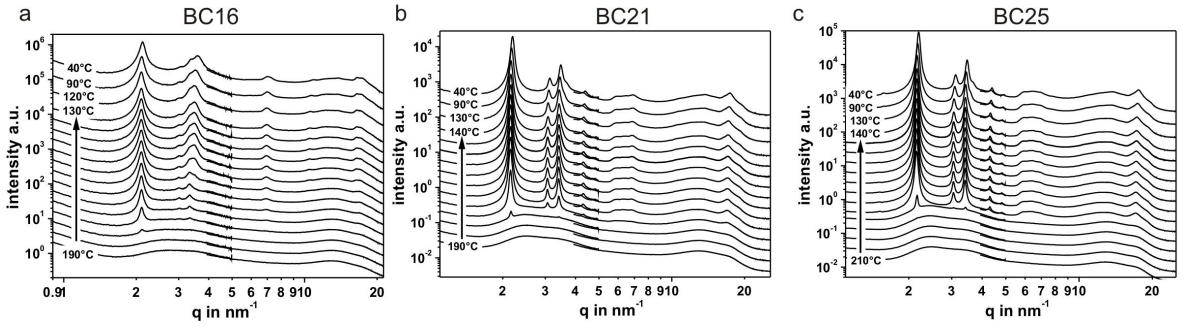

Figure 9.10: X-ray diffraction upon cooling the block copolymer samples from a melt at a rate of $10\,\frac{\mathrm{K}}{\mathrm{min}}$ for a) BC16, b) BC21 and c) BC25. The PPerAcr crystallises has the lower melting temperature compared to P3HT, but also re-crystallises first, disturbing the formation of long range ordered P3HT, which gets becomes and more pronounced with increasing PPerAcr content.

melting or freezing, respectively. Figure S3 shows the first cooling curve and the second heating curve. The P3HT homopolymer, which also served as the macroinitiator for the block copolymers, exhibits a T_m of 211 °C and a ΔH_m of $13.1\,\frac{\mathrm{J}}{\mathrm{g}}$. Homopolymer PPerAcr melts at 191 °C and has a melting enthalpy of $9.8\,\frac{\mathrm{J}}{\mathrm{g}}$. BC16 shows two melting transitions at 190 °C and 211 °C as it is typical for a phase separated block copolymer. The transitions are similar to the respective homopolymer temperatures, whereby the P3HT block ($T_m = 211\,°\mathrm{C}$) melts after the PPerAcr block ($T_m = 190\,°\mathrm{C}$). The cooling curve of BC16 shows two recrystallisations at 162 °C and 148 °C. The block copolymer with a slightly longer PPerAcr block (BC17) shows also these two transitions however, the enthalpy of the first crystallization (at 162 °C) increases with increasing PPerAcr length, as does the first melting peak. This suggests that PPerAcr melts first, but also crystallises first on cooling, explaining how the crystallisation of PPerAcr can happen at the expense of P3HT crystallinity. This increased undercooling of one of the crystalline blocks has been observed in block copolymers, where the melting transistors are close to each other. With increasing block length of PPerAcr, the PPerAcr crystallisation/recrystallisation becomes more and more dominant. For BC21 and BC25 only one major enthalpic change attributed to the PPerAcr overlaying the P3HT is detectable.

Complementary to the thermal analysis, X-ray diffraction spectra during the cooling process. This way, the evolution of the crystallinity can be tracked directly, showing the primary crystallisation of PPerAcr (Fig. 9.10).

X-ray photoelectron spectroscopy

The interpretation of OFET results - where charge transport occurs within a thin layer above the dielectric layer - in the context of bulk morphologies requires further experimental efforts to justify correlation. Therefore, preferential surface wetting effects of one of the blocks during spincoating were investigated using x-ray photoelectron spectroscopy (XPS). A switched surface wetting of BC25 could not be proven, since the XPS data of the interfacing side of the polymer film to the substrate did not indicate any significant domain enrichment of one of the blocks before and after thermal annealing. This has to be taken into account, since the wetting properties of polymers strongly depend on the surrounding environment.[45]

Fig. 9.11 shows the relative atomic compositions of C, O, Si and S as determined by XPS. No significant differences between the as spun and the annealed BC25 could be resolved. The spectra of the homopolymers PPerAcr and P3HT show that there are significant differences in the relative signals of N and O that are contained in PPerAcr and S that is contained in P3HT only. Cracks in the delaminated film caused the small amount of oxygen in the control sample P3HT (<1%).

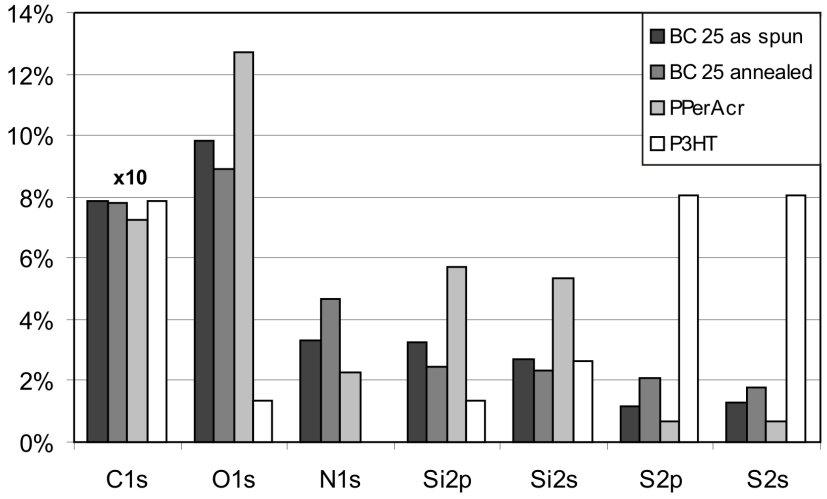

Figure 9.11: Relative atomic compositions of C, O, Si and S have been resolved by XPS.

Scanning electron microscopy

In order to give real image of the phase separation of the block copolymers, images taken with a scanning electron microscope are presented in Fig. Fig. 9.12. The images were obtained films that were extensively annealed under chloroform solvent vapour. This procedure only allowed to obtain a proper phase contrast between the two blocks. Whereas electronically solvent vapour annealed devices behaved similar to as spun devices, the surface morphology exhibits a more pronounced phase separation, that rather corresponds to the block copolymer equilibrium morphology.

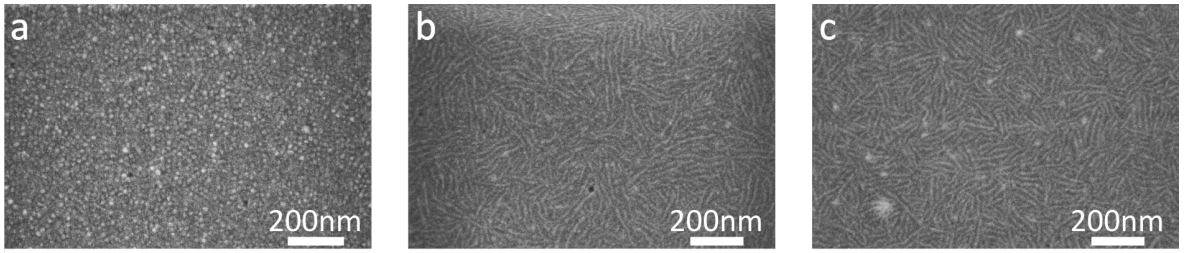

Figure 9.12: Scanning electron microscopy images of chloroform vapour annealed samples of a) BCP16, b) BCP21, c) BCP25. The bright phase represents the PPerAcr block. The phase separation is in the order of $\sim$ 15 nm.

Transient absorption spectroscopy

As Fig. 9.6d-f shows the the spectra recorded at $t \approx 0.1 - 1$ ps delay and $t \approx 1 - 1.9$ ns, Fig. 9.13 shows the respective kinetics integrated over a spectral range of 590 to 610 nm. This range covers the 0-0 vibronic transition of ordered and aggregated (i.e. crystalline) P3HT.

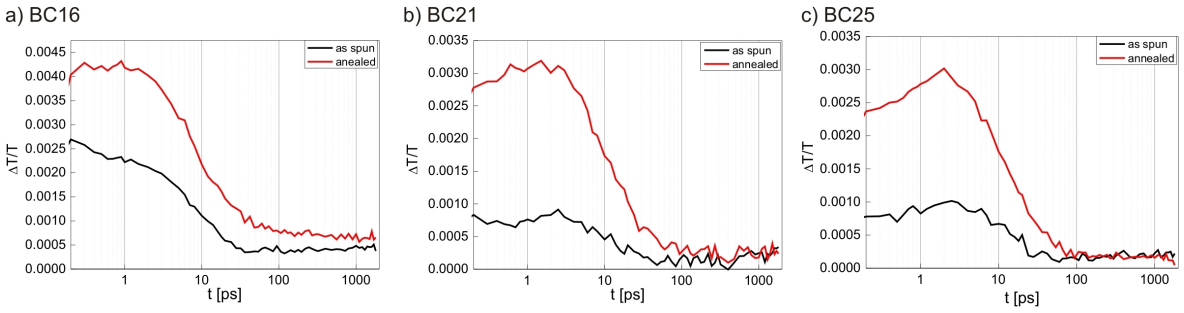

Figure 9.13: TA kinetics integrated over a spectral range of 590 to 610 nm for all three block copolymers before (black) and after (red) annealing.

Bibliography

[1] C. Park, J. Yoon, and E.L. Thomas, *Enabling nanotechnology with self assembled block copolymer patterns*, Polymer **44**, 6725 (2003).

[2] C. Tang, E.M. Lennon, G.H. Fredrickson, E.J. Kramer, and C.J. Hawker, *Evolution of block coplmyer lithography to highly ordered square arrays*, Science **322**, 429 (2008).

[3] S. Park, D.H. Lee, J. Xu, B. Kim, S.W. Hong, U. Jeong, T. Xu, and T.P. Russell, *Macroscopic 10-terabit-per-square-inch arrays from block copolymers with lateral order*, Science **323**, 1030 (2009).

[4] B. Crone, A. Dodabalapur, Y. Lin, R. Filas, Z. Bao, A. LaDuca, R. Sarpeshkar, H. Katz, and W. Li, *Large-scale complementary integrated circuits based on organic transistors*, Nature **403**, 521 (2000).

[5] J. Cornil, J.-L. Brédas, J. Zaumseil, and H. Sirringhaus, *Ambipolar transport in organic conjugated materials*, Adv. Mater. **19**, 1791 (2007).

[6] C. Rost, S. Karg, and W. Riess, *Ambipolar light-emitting organic field-effect transistor*, Appl. Phys. Let. **85**, 1613 (2004).

[7] M.A. Loi, C. Rost-Bietsch, M. Murgia, S. Karg, W. Riess, and M. Muccini, *Tuning optoelectronic properties of ambipolar organic light-emitting transistors using a bulk-heterojunction approach*, Adv. Funct. Mater. **16**, 41 (2007).

[8] T.T. Steckler, X. Zhang, J. Hwang, R. Honeyager, S. Ohira, X.-H. Zhang, A. Grant, S. Ellinger, S.A. Odom, D.l Sweat, D.B. Tanner, A.G. Rinzler, S. Barlow, J.-L. Brédas, B. Kippelen, S.R. Marder, and J.R. Reynolds, *A spray-processable, low bandgap, and ambipolar donor-acceptor conjugated polymer*, J. Am. Chem. Soc. **131**, 2824 (2009).

[9] F. S. Kim, X. Huo, M. D. Watson, and S. A. Jenekhe, *High-mobility ambipolar transistors and high-gain inverters from a donor-acceptor copolymer semiconductor*, Adv. Mater. **21**, (2009).

[10] Th. B. Singh, S. Günes, N. Marjanovic, N. S. Sariciftci, and R. Menon, *Correlation between morphology and ambipolar transport in organic field-effect transistors*, J. Appl. Phys. **97**, 114508 (2005).

[11] Antonio Cravino and N.S. Sariciftci, *Molecules as bipolar conductors*, Nature Mater. **2**, 360 (2003).

[12] F.S. Bates and G.H. Fredrickson, *Block copolymer thermodynamics: theory and experiment*, Annu. Rev. Phys. Chem. **41**, 525 (1990).

[13] Bradley D. Olsen and Rachel A. Segalman, *Self-assembly of rod-coil block copolymers*, Mater. Sci. and Eng. **62**, 37 (2008).

[14] I.W. Hamley, J.P.A. Fairclough, A. Ryan, F.S. Bates, and E. Towns-Andrews, *Crystallization of nanoscale-confined diblock copolymer chains*, Polymer **37**, 4425 (1996).

[15] Shuichi Nojima, Kazunori Kato, Satoru Yamamoto, and Tamaichi Ashida, *Crystallization of block copolymers. 1. Small-angle x-ray scattering study of a .epsilon.-caprolactone-butadiene diblock copolymer*, Macromol. **25**, 2237 (1992).

[16] Y.-L. Loo, R.A. Register, and A.J. Ryan, *Modes of crystallization in block copolymer microdomains: breakout, templated, and confined*, Macromol. **35**, 2365 (2002).

[17] M. Sommer, A. S. Lang, and M. Thelakkat, *Crystalline-crystalline donor-acceptor block copolymers*, Angew. Chem. Int. Ed. **47**, 7901 (2008).

[18] H. Sirringhaus, P. J. Brown, R. H. Friend, M. M. Nielsen, K. Bechgaard, B. M. W. Langeveld-Voss, A. J. H. Spiering, R. A. J. Janssen, E. W. Meijer, P. Herwig, and D. M. de Leeuw, *Two-dimensional charge transport in self-organized, high-mobility conjugated polymers*, Nature **401**, 685 (1999).

[19] J.-F. Chang, B. Sun, D. W. Breiby, M. M. Nielsen, T. I. Sölling, M. Giles, I. McCulloch, and H. Sirringhaus, *Enhanced mobility of poly(3-hexylthiophene) transistors by spin-coating from high-boiling-point solvents*, Chem. Mater. **16**, 4772 (2004).

[20] S. Hugger, R. Thomann, T. Heinzel, and T. Thurn-Albrecht, *Semicrystalline morphology in thin films of poly(3-hexylthiophene)*, Colloid. Polym. Sci. **282**, 932 (2004).

[21] Z. Wu, A. Petzold, T. Henze, T. Thurn-Albrecht, R.H. Lohwasser, M. Sommer, and M. Thelakkat, *Temperature and molecular weight dependent hierarchical equilibrium structures in semiconducting poly(3-hexylthiophene)*, Macromolecules **43**, 4646 (2010).

[22] R. J. Chesterfield, J. C. McKeen, C. R. Newman, P. C. Ewbank, D. A. daSilva Filho, J.-L. Brédas, L. L. Miller, K. R. Mann, and C. D. Frisbie, *Organic thin film transistors based on n-alkyl perylene diimides: charge transport kinetics as a function of gate voltage and temperature*, Phys. Chem. B **108**, 19281 (2004).

[23] S. Tatemichi, M. Ichikawa, T. Koyama, and Y. Taniguchi, *High mobility n-type thin-film tranisotrs based on N,N'-ditridecyl perylene diimide with thermal treatments*, Appl. Phys. Let. **89**, 112108 (2006).

[24] H. Langhals, S. Demmig, and H. Huber, *Rotational barriers in perylene fluorescent dyes*, Spectrochim. Acta Part A **44A**, 1189 (1988).

[25] F. Würthner, C. Thalacker, S. Diele, and C. Tschierske, *Fluorescent J-type aggregates and thermotropic columnar mesophases of perylene bisimide dyes*, Chem. Eur. J. **10**, 2245 (2001).

[26] F. Würthner, Z. Chen, V. Dehm, and V. Stepanenko, *One-dimensional luminescent nanoaggregates of perylene bisimides*, Chem. Comm. **11**, 1188 (2006).

[27] S. Hüttner, M. Sommer, and M. Thelakkat, *n-type organic field effect transistors from perylene bisimide block copolymers and homopolymers*, Appl. Phys. Lett. **92**, 093302 (2008).

[28] Shunji Ito, Mike Wehmeier, J. Diedrich Brand, Christian Kübel, Rebekka Epsch, J. P. Rabe, and Klaus Müllen, *Synthesis and self-assembly of functionalized hexa-peri-hexabenzocoronenes*, Chem. Eur. J. **6**, 4327 (2001).

[29] K. Tashiro, K. Ono, Y. Minagawa, M. Kobayashi, T. Kawai, and K. Yoshino, *Structure and thermochromic solid-state phase transition of poly(3-alkylthiophene)*, J. of Polym. Sci: Part B: Polym. Phy. **29**, 1223 (1991).

[30] M. Sommer, S. Hüttner, U. Steiner, and M. Thelakkat, *Influence of molecular weight on the solar cell performance of double-crystalline donor-acceptor block copolymers*, Appl. Phys. Lett. **95**, 183308 (2009).

[31] R. Joseph Kline, Michael D. McGehee, Ekaterina N. Kadnikova, Jinsong Liu, Jean M. J. Fréchet, , and Michael F. Toney, *Dependence of regioregular poly(3-hexylthiophene) film morphology and field-effect mobility on molecular weight*, Macromol. **38**, 3312 (2005).

[32] A. Zen, M. Saphiannikova, D. Neher, J. Grenzer, S. Grigorian, U. Pietsch, U. Asawapirom, S. Janietz, U. Scherf, I. Lieberwirth, and G. Wegner, *Effect of molecular weight on the structure and crystallinity of poly(3-hexylthiophene)*, Macromol. **39**, 2162 (2006).

[33] S.M. Lindner, N. Kaufmann, and M. Thelakkat, *Nanostructured semiconductor block copolymers: $\pi - \pi$ stacking, optical and electrochemical properties*, Organic Electronics **8**, 69 (2007).

[34] M. Hoffmann, K. Schmidt, T. Fritz, T. Hasche, V.M. Agranovich, and K. Leo, *The lowest energy Frenkel and charge-transfer excitons in quasi-one-dimensional structures: application to MePTCDI and PTCDA crystals*, Chem. Phys. **258**, 73 (2000).

[35] Frank C. Spano, *Modeling disorder in polymer aggregates: The optical spectroscopy of regioregular poly(3-hexylthiophene) thin films*, J. Chem. Phys. **122**, 234701 (2005).

[36] J. Clark, C. Silva, R.H. Friend, and F.C. Spano, *Role of intermolecular coupling in the photophysics of disordered organic semiconductors: aggregate emission in regioregular polythiophene*, Phys. Rev. Let. **98**, 206406 (2007).

[37] Tomoaki Yago, Yoshiaki Tamaki, Akihiro Furube, and Ryuzi Katoh, *Self-trapping limited exciton diffusion in a monomeric perylene crystal as revealed by femtosecond transient absorption microscopy*, Phys. Chem. Chem. Phys. **10**, 4435 (2008).

[38] S. Hüttner, J. Hodgkiss, M. Sommer, R.H. Friend, U. Steiner, and M. Thelakkat, *Charge dynamics in donor-acceptor block coplymers based on poly(perylene bisimide acrylate) and poly thiophene*, submitted .

[39] A.R. Campbell, J.M. Hodgkiss, S. Westenhoff, I.A. Howard, R.A. Marsh, C.R. McNeill, R.H. Friend, and N.C. Greenham, *Low-temperature control of nanoscale morphology for high performance polymer photovoltaics*, Nanolett. **8**, 3942 (2008).

[40] S. Westenhoff, I.A. Howard, and R.H. Friend, *Probing the morphology and energy landscape of blends of conjugated polymers with sub-10 nm resolution*, Phys. Rev. Lett. **101**, 016102 (2008).

[41] S. Hüttner, M. Sommer, A. Chiche, G. Krausch, U. Steiner, and M. Thelakkat, *Controlled solvent vapour annealing for polymer electronics*, Soft Matter **5**, 4206 (2009).

[42] S. Westenhoff, I.A. Howard, J.M. Hodgkiss, K.R. Kirov, H.A. Bronstein, C.K. Williams, N.C. Greenham, and R.H. Friend, *Charge recombination in organic photovoltaic devices with high open-circuit voltages*, J. Am. Chem. Soc. **130**, 13653 (2008).

[43] J.M. Hodgkiss, G. Tu, S. Albert-Seifried, W.T.S. Huck, and R.H. Friend, *Ion-induced formation of charge-transfer states in conjugated polyelectrolytes*, J. Am. Chem. Soc. **131**, 8913 (2009).

[44] F. Laquai, A.K. Mishra, K.Müllen, and R.H. Friend, *Amplified spontaneous emission of poly(ladder-type phenylene)s - The influence of photophysical properties on ASE thresholds*, Adv. Funct. Mater. **18**, 3265 (2008).

[45] U. Steiner, J. Klein, E. Eiser, A. Budkowski, and L.J. Fetters, *Complete wetting from polymer mixtures*, Science **13**, 1126 (1992).

Chapter 10

Influence of Molecular Weight on the Solar Cell Performance of Double-Crystalline Donor-Acceptor Block Copolymers

Michael Sommer[a], Sven Hüttner[a,b], Ullrich Steiner[b] and Mukundan Thelakkat[a]

a) Makromolekulare Chemie I, Universität Bayreuth, Germany.
b) Cavendish Laboratory, University of Cambridge, United Kingdom.

Applied Physics Letters, 95, 183308 (2008)

Abstract

We investigate the influence of the molecular weight of double-crystalline donor-acceptor block copolymers comprised of poly(3-hexylthiophene) P3HT as donor and poly(perylene bisimide acrylate) PPerAcr as acceptor segments on the device performance of polymer solar cells. Two block copolymers 1 and 2 exhibiting different molecular weights but the same composition are compared. Block copolymer 2 with the higher molecular weight shows an improvement in the hole carrier mobility μ_{OFET} of more than two orders of magnitude, and an improvement in the external quantum efficiency EQE of one order of magnitude reaching 31%, which is the highest reported value for a block copolymer system.

Introduction

Substantial research progress has been made in the field of solution-processed organic photovoltaic cells (OPVs) over the last decade.[1,2] In such devices, the active layer morphology has been shown to be crucial to the device performance.[3–5] State-of-the-art OPVs mostly employ blends of conjugated polymers as donor and fullerene derivatives as acceptor materials, which have already attained high power conversion efficiencies of $\sim 4-6\%$.[6–8] Perylene bisimides (PBI) are promising acceptor materials due to their absorption in the visible region and their tendency to crystallise.[9,10] In general, a phase separation of the donor and acceptor material on a nanoscale is needed to separate charges efficiently, thereby addressing the conflict of the relatively large optical absorption length ($\sim$100 nm) and the short exciton diffusion length ($\sim$10 nm). Polymer blends comprised of low molecular weight PBIs and conjugated polymers such

as poly(3-hexylthiophene) P3HT give rise to uncontrolled crystallization of PBI, and hence lead to a reduction in the interfacial area, hindered charge transport, and moderate device performance.[11] One possible approach to solve this is the use of polymers with PBI units in the main chain.[12] Yet, macrophase separation generally occurring in polymer-polymer blends is a drawback in terms of controlling the size and shape of the interfacial area. Block copolymers (BCPs) microphase separate into well-defined periodic nanostructures due to the interplay of covalent connectivity and demixing of the two polymer segments[13], and therefore are expected to guarantee distinct charge transport pathways for both holes and electrons.[14] Indeed, the concept of fully functionalised BCPs comprised of amorphous donor blocks and side-chain crystalline perylene bisimide acceptor segments has demonstrated that co-continuous morphologies with domain sizes commensurate to the exciton diffusion length can be obtained while PBI crystallization is confined to microdomains.[15–17] This approach has recently been extended to double-crystalline BCPs comprised of P3HT and side chain crystalline PBI blocks by our group and others.[18–20]

Here, we report on the photovoltaic properties of these double-crystalline BCP systems. Two BCPs poly(3-hexylthiophene)-*b*-poly(perylene bisimide acrylate) P3HT-*b*-PPerAcr 1 and 2, which possess the same composition but differ in molecular weight by a factor of 2, are compared in single component single layer solar cells (Fig. 10.1).

Results and discussion

The synthesis of P3HT-*b*-PPerAcr 1 was reported recently.[18] A batch of the high molecular weight BCP 2 with exactly the same composition was synthesised analogously for this comparative study here. 1 and 2 exhibit molecular weights of 16.1 and 29.5 $\frac{kg}{mol}$ (de-

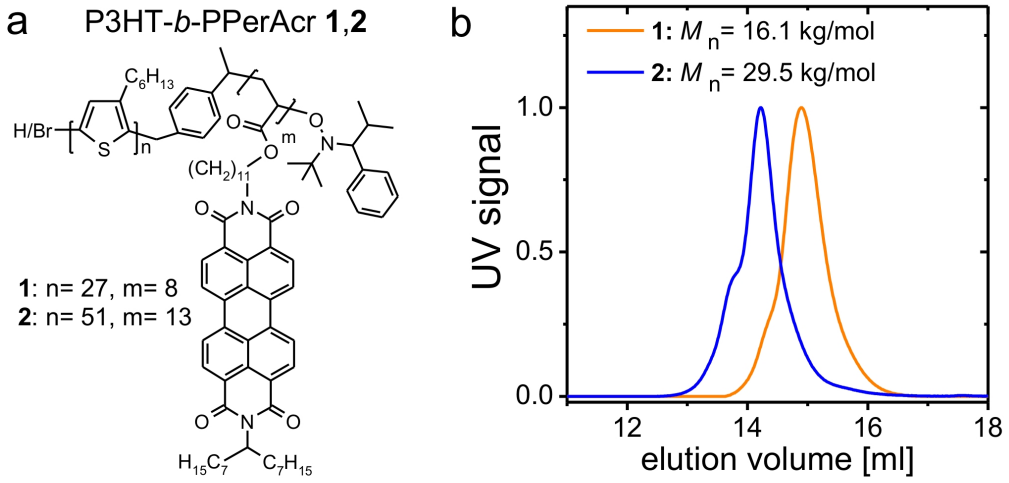

Figure 10.1: a) Chemical structure of poly(3-hexylthiophene)-*b*-poly(perylene bisimide acrylate) P3HT-*b*-PPerAcr 1 and 2. (b) SEC curves showing the difference in molecular weight. The composition is maintained at 55 wt.% PPerAcr.

termined by SEC in THF using polystyrene standards), and very low polydispersities of 1.25 and 1.15, respectively. The molecular weights of the P3HT segments in 1 and 2 are 8.9 and 17.0 $\frac{kg}{mol}$, respectively. The content of PPerAcr (determined by 1H-NMR) is maintained at 55 wt.% in both BCPs. Since the charge carrier mobility of P3HT films depends on the molecular weight considerably, we assumed such a dependence to be of importance here as well.[21,22] The absorption profiles of 1 and 2 in films spun from chlorobenzene are depicted in Fig. 10.2a.

The common characteristic P3HT homopolymer absorption at 610 nm arising from interchain exciton delocalization[23] is visible in both block copolymers, however the intensity at 610 nm is higher for 2, which indicates a higher degree of P3HT crystallinity.[24] Apart from this difference, the similar UV-vis profiles of both block copolymers guarantee that the same amount of light is absorbed in the devices. Solar cells were fabricated using the device structure ITO/PEDOT:PSS/active layer/Al. The best devices were obtained by spin coating solutions of 15 mg BCP in 1ml chlorobenzene at 700 r/min, giving a film thickness of ∼60 nm. Using these parameters, a maximum

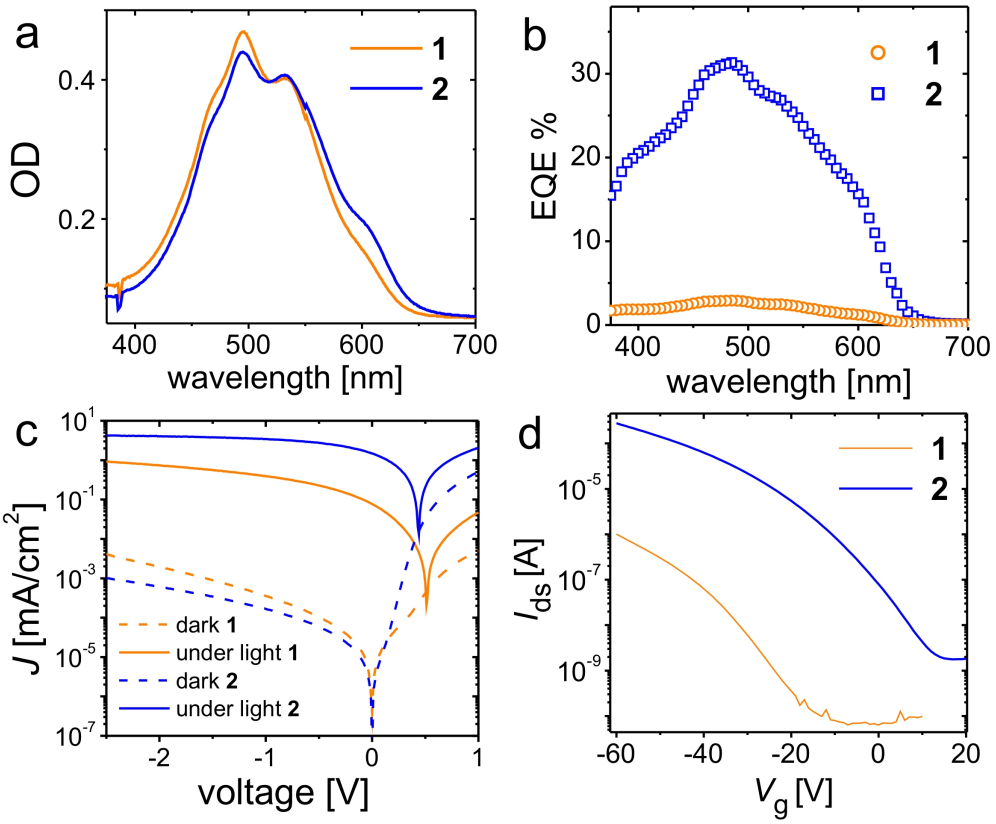

Figure 10.2: Optical and electrical properties of 1 (orange) and 2 (blue). The color code is equal for all plots. a) Optical densities of thin films spin cast from chlorobenzene. b) External quantum efficiency (EQE). c) $J-V$-curves measured in the dark (dashed lines) and under AM 1.5G conditions (100 $\frac{mW}{cm^2}$, solid lines). d) OFET transfer characteristics of 1 and 2 after spin coating from chloroform in bottom-gate bottom-contact devices with gold electrodes.

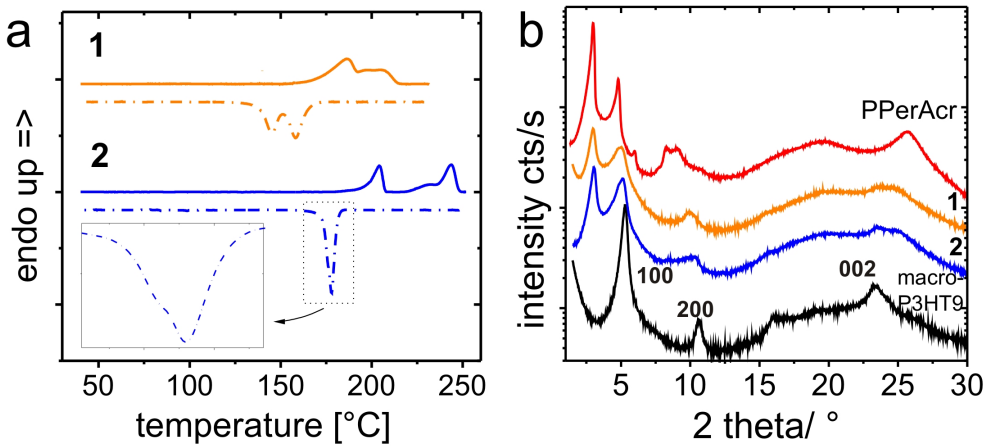

Figure 10.3: Crystallinity of P3HT-*b*-PPerAcr 1 and 2. a) Differential scanning calorimetry at 10 K/min under nitrogen. The second heating (solid lines) and second cooling curves (dashes-dots) are shown. The inset enlarges the recrystallization peak of 2. b) X-ray scattering of 1 (orange), 2 (blue), P3HT macroinitiator (black), and PPerAcr homopolymer (red). Curves are offset in y-direction.

external quantum efficiency (EQE) of 31 % at 495 nm was obtained for 2. The average values measured from 16 solar cells resulted in an $EQE_{max} = 25\,\%$, $J_{SC} = 1.14\,\frac{\mathrm{mA}}{\mathrm{cm}^2}$, $V_{OC} = 0.40\,\mathrm{V}$, fill factor $FF = 27.6\,\%$ and 0.10 %. Additional post production treatments of devices made from 2 such as chloroform vapor annealing[25] or thermal annealing did not lead to further improvements in the external quantum efficiency. Devices with 1 as the active layer yielded EQE peak values of 3% only (Fig. 10.2b). The corresponding $J-V$-characteristics are shown in Fig. 10.2c. P3HT-*b*-PPerAcr 1 with a molecular weight of 16.1 $\frac{kg}{mol}$ gave very low short circuit currents J_{SC} around 0.08 $\frac{mA}{cm^2}$ and open circuit voltages V_{OC} of 0.51 V, resulting in poor power conversion efficiencies of 0.007 %. Block copolymer 2 with a molecular weight of 29.5 $\frac{kg}{mol}$ again shows a drastic improvement; a J_{SC} of 1.5 $\frac{mA}{cm^2}$ and a power conversion efficiency of 0.2 % are observed. The fill factor also increases from 0.17 to 0.25, and the open circuit voltage V_{OC} was 0.44 V. Organic field effect transistors (OFETs) with a bottom-gate bottom-contact configuration and gold electrodes using 1 and 2 as active layers both show p-channel behaviour (Fig. 10.2d). The hole carrier mobility μ_h of 2 after spin coating is $5 \cdot 10^{-3}\,\frac{\mathrm{cm}^2}{\mathrm{Vs}}$, while the OFET device made of block copolymer 1 only shows a mobility of $3 \cdot 10^{-5}\,\frac{\mathrm{cm}^2}{\mathrm{Vs}}$. Thus, BCP 2 with the higher molecular weight exhibits an improvement of the EQE by one order of magnitude in solar cells, and an improvement of the hole carrier mobility by more than two orders of magnitude compared to BCP 1.

Differential scanning calorimetry (DSC) and X-ray scattering (XRD) experiments are used to investigate the phase behaviour and to explain the huge difference in the device parameters of 1 and 2. The DSC curve of 1 shows two endotherms at 190 °C and 211 °C that are ascribed to the melting of PPerAcr and P3HT, respectively (Fig. 10.3).

On cooling, PPerAcr crystallises first at 162 °C followed by P3HT at 148 °C. This

is evidenced by the crystallization peak at 162 °C, intensity increasing with increasing PPerAcr weight fraction. In the heating curve of 2, two endotherms are observed at 204 °C and 244 °C, corresponding to PPerAcr and P3HT, respectively. Note that the difference in the melting temperatures of 2 is larger than of 1. The single peak in the cooling curve of 2 at 178 °C entails the crystallization of both, P3HT and PPerAcr. The magnification of this peak reveals a small shoulder at 176 °C (see inset of Fig. 10.3a), arising from PPerAcr. Hence, crystallization of P3HT and PPerAcr occurs almost simultaneously in BCP 2. The larger distance between the two melting points and the coincidence of the two crystallizations in 2 are caused by the strong dependence of the melting and crystallization temperature of P3HT on its molecular weight.[26] Note that the thermal behaviour of P3HT causes a fundamental difference in the thermal properties of 1 and 2: On cooling from the melt, PPerAcr crystallises first in 1, while simultaneous crystallization of the two blocks occurs in 2. The different block lengths of P3HT in 1 and 2, together with the varying behaviour of crystallization, finally give rise to different degrees of P3HT crystallinity, as can be tracked by the melting enthalpies ΔH_m. ΔH_m(P3HT) is 15.4 $\frac{J}{mol}$ for 2, but only 10.3 $\frac{J}{mol}$ for 1. Qualitatively, the lower degree of P3HT crystallinity in 1 is also visible from the different optical densities at 610 nm (Fig. 10.2a).[24] In addition, the higher melting point of 244 °C of the P3HT segment in 2 depicts larger P3HT domains compared to those in 1, which melt at 211 °C. A larger domain size in turn should favor charge percolation and obviously is responsible for the improved hole transport in BCP 2. Indeed, a similar dependence has been observed in amorphous-crystalline block copolymers, in which improvements of the OPV device performance with molecular weight were ascribed to better charge percolation due to microphase separation.[27]

Conclusion

Further investigation of the crystalline nature of P3HT-*b*-PPerAcr is accomplished using X-ray diffraction of thermally annealed powders (Fig. 10.3b). Both P3HT-macroinitiators exhibited very similar diffraction patterns. As a typical example, the XRD pattern of 1 is shown in Fig. 10.3b. The known (100), (200) and (002) reflections of lamellar stacks of P3HT are observed at 2θ values of 5.3 °, 10.6 °, 16.1 °, and 23.4 °, respectively, in agreement with reported values.[28,29] In the PPerAcr homopolymer two strong Bragg reflections appear at 2θ values of 3.0 ° and 4.8 °, respectively. These result from a two-dimensional lattice formed by stacks of the PBI units of PPerAcr where the individual stacks are separated by the alkyl groups. An additional reflection at $2\theta = 25.6$ ° indicates the $\pi - \pi$ distance of 0.35 nm between two PBI moieties within one stack. The two BCPs 1 and 2 feature the reflections of the individual homopolymers and hence, stacks of P3HT and PPerAcr coexist here. A comparison of the intensities $(100)_{P3HT}/(2\theta = 3.0\,^\circ)_{PPerAcr}$ and $(002)_{P3HT}/(2\theta = 25.6\,^\circ)_{PPerAcr}$ yields higher values for 2, which is indicative of a higher degree of P3HT crystallinity. These results are in accordance with the higher degree of P3HT crystallinity of 2 observed in the absorption spectrum (Fig. 10.2a) and in the DSC curves (Fig. 10.3a).

Acknowledgement

Financial support by the Deutsche Forschungsgemeinschaft (SFB 481, SPP 1355), and the Polyfilm EU Research Training Network is gratefully acknowledged. S.H. acknowledges a scholarship of the Bayerische Graduiertenförderung. The authors are indebted to P. Kohn and T. Thurn-Albrecht, University of Halle, for fruitful discussions, and to R. H. Friend for the opportunity to use the solar cell preparation and characterization facilities.

Bibliography

[1] Serap Günes, Helmut Neugebauer, and Niyazi Serdar Sariciftci, *Conjugated polymer-based organic solar cells*, Chem. Rev. **107**, 1324 (2007).

[2] Gilles Dennler, Markus C. Scharber, and Christoph J. Brabec, *Polymer-fullerene bulk-heterojunction solar cells*, Adv. Mater. **21**, 1323 (2009).

[3] Harald Hoppe and Niyazi Serdar Sariciftci, *Morphology of polymer/fullerene bulk heterojunction solar cells*, J. Mater. Chem. **16**, 45 (2006).

[4] Mariano Campoy-Quiles, Toby Ferenczi, Tiziano Agostinelli, Pablo G. Etchegoin, Youngkyoo Kim, Thomas D. Anthopoulos, Paul N. Stavrinou, Donal D. C. Bradley, and Jenny Nelson, *Morphology evolution via self-organization and lateral and vertical diffusion in polymer: fullerene solar cell blends*, Nat. Mater. **7**, 158 (2008).

[5] A.R. Campbell, J.M. Hodgkiss, S. Westenhoff, I.A. Howard, R.A. Marsh, C.R. McNeill, R.H. Friend, and N.C. Greenham, *Low-temperature control of nanoscale morphology for high performance polymer photovoltaics*, Nanolett. **8**, 3942 (2008).

[6] W. Ma, C. Yang, X. Gong, K. Lee, and A.J. Heeger, *Thermally stable, efficient polymer solar cells with nanoscale control o fthe interpenetrating network morphology*, Adv. Func. Mater. **15**, 1617 (2005).

[7] Gang Li, Vishal Shrotriya, Jinsong Huang, Yan Yao, Tom Moriarty, Keith Emery, and Yang Yang, *High-efficiency solution processable polymer photovoltaic cells by self-organization of polymer blends*, Nat. Mater. **4**, 864 (2005).

[8] Martijn M. Wienk, Mathieu Turbiez, Jan Gilot, and René A. J. Janssen, *Narrow-bandgap diketo-pyrrolo-pyrrole polymer solar cells: The effect of processing on the performance*, Adv. Mater. **20**, 2556 (2008).

[9] L. Schmidt-Mende, A. Fechtenkötter, K. Müllen, E. Moons, R.H. Friend, and J.D. MacKenzie, *Self-organized discotic liquid crystals for high-efficiency organic photovoltaics*, Science **293**, 1119 (2001).

[10] P.E. Keivanidis, I.A. Howard, and R.H. Friend, *Intermolecular interactions of perylene diimides in photovoltaic blend of fluorene copolymers: disorder effects on photophysical properties, film morphology and device efficiency*, Adv. Func. Mater. **18**, 3189 (2008).

[11] J. J. Dittmer, E. A. Marseglia, and R. H. Friend, *Electron trapping in dye/polymer blend photovoltaic cells*, Advanced Materials **12**, 1270 (2000).

[12] Zhan'ao Tan, Erjun Zhou, Xiaowei Zhan, Xiang Wang, Yongfang Li, Stephen Barlow, and Seth R. Marder, *Efficient all-polymer solar cells based on blend of tris(thienylenevinylene)-substituted polythiophene and poly[perylene diimide-alt-bis(dithienothiophene)]*, Appl. Phys. Lett. **93**, 073309 (2008).

[13] F.S. Bates and G.H. Fredrickson, *Block copolymer thermodynamics: theory and experiment*, Annu. Rev. Phys. Chem. **41**, 525 (1990).

[14] G.A. Buxton and N. Clarke, *Predicting structure and property relations in polymeric photovoltaic devices*, Physical Review B **74**, 085207 (2006).

[15] S. Lindner and M. Thelakkat, *Nanostructres of n-type organic semiconductor in a p-type matrix via self-assembly of block copolymers*, Macromolecules **37**, 8832 (2004).

[16] S. Lindner, S. Hüttner, A. Chiche, M. Thelakkat, and G. Krausch, *Charge separation at self-assembled nanostructured bulk interfaces in block copolmers*, Angew. Chem. Int. Ed. **45**, 3364 (2006).

[17] M. Sommer, S. Lindner, and M. Thelakkat, *Microphase-separated donor-acceptor diblock copolymers: influence of HOMO energy levels and morphology on polymer solar cells*, Adv. Func. Mater. **17**, 1493 (2007).

[18] M. Sommer, A. S. Lang, and M. Thelakkat, *Crystalline-crystalline donor-acceptor block copolymers*, Angew. Chem. Int. Ed. **47**, 7901 (2008).

[19] Q. Zhang, A. Cirpan, T.P. Russel, and T. Emrick, *Donor-acceptor poly(thiophene-block-perylene diimide) copolymers: synthesis and solar cell fabrication*, Macromolecules **42**, 1079 (2009).

[20] S. Rajaram, P.B. Armstrong, B.J. Kim, and J.M.J. Fréchet, *Effect of addition of a diblock copolymer on blend morphology and performance of poly(3-hexylthiophene):perylene diimide solar cells*, Chem. Mater. **21**, 1775 (2009).

[21] R. Joseph Kline, Michael D. McGehee, Ekaterina N. Kadnikova, Jinsong Liu, Jean M. J. Fréchet, , and Michael F. Toney, *Dependence of regioregular poly(3-hexylthiophene) film morphology and field-effect mobility on molecular weight*, Macromol. **38**, 3312 (2005).

[22] Jui-Fen Chang, Jenny Clark, Ni Zhao, Henning Sirringhaus, Dag W. Breiby, Jens W. Andreasen, Martin M. Nielsen, Mark Giles, Martin Heeney, and Iain McCulloch, *Molecular-weight dependence of interchain polaron delocalization and exciton bandwidth in high-mobility conjugated polymers*, Phys. Rev. B **74**, 115318 (2006).

[23] J. Clark, C. Silva, R.H. Friend, and F.C. Spano, *Role of intermolecular coupling in the photophysics of disordered organic semiconductors: aggregate emission in regioregular polythiophene*, Phys. Rev. Let. **98**, 206406 (2007).

[24] U. Zhokhavets, T. Erb, G. Gobsch, M. Al-Ibrahim, and O. Ambacher, *Relation between absorption and crystallinity of poly(3-hexylthiophene)/fullerene films for plastic solar cells*, Chem. Phys. Lett. **418**, 347 (2006).

[25] S. Hüttner, M. Sommer, and M. Thelakkat, *n-type organic field effect transistors from perylene bisimide block copolymers and homopolymers*, Appl. Phys. Lett. **92**, 093302 (2008).

[26] A. Zen, M. Saphiannikova, D. Neher, J. Grenzer, S. Grigorian, U. Pietsch, U. Asawapirom, S. Janietz, U. Scherf, I. Lieberwirth, and G. Wegner, *Effect of molecular weight on the structure and crystallinity of poly(3-hexylthiophene)*, Macromol. **39**, 2162 (2006).

[27] Simon King, Michael Sommer, Sven Huettner, Mukundan Thelakkat, and Saif A. Haque, *Charge separation and recombination in self-organizing nanostructured donorŰacceptor block copolymer films*, J. Mater. Chem. **19**, 5436 (2009).

[28] T. J. Prosa, M. J. Winokur, Jeff Moulton, Paul Smith, and A. J. Heeger, *X-ray structural studies of poly(3-alkylthiophenes): an example of an inverse comb*, Macromol. **25**, 4364 (1992).

[29] S. Hugger, R. Thomann, T. Heinzel, and T. Thurn-Albrecht, *Semicrystalline morphology in thin films of poly(3-hexylthiophene)*, Colloid. Polym. Sci. **282**, 932 (2004).

Chapter 11

Photophysics of Double-Crystalline Donor-Acceptor Block Copolymers containing P3HT and Perylene Bisimide based Polymers

Sven Hüttner[a,b], Justin Hodgkiss[a,c], Michael Sommer[b], Richard H. Friend[a], Ullrich Steiner[a], Mukundan Thelakkat[b]

a) Cavendish Laboratory, University of Cambridge, United Kingdom
b) Angewandte Funktionspolymere, Makromolekulare Chemie I, Universität Bayreuth, 95440 Bayreuth, Germany
c) MacDiarmid Institute, Victoria University of Wellington, New Zealand

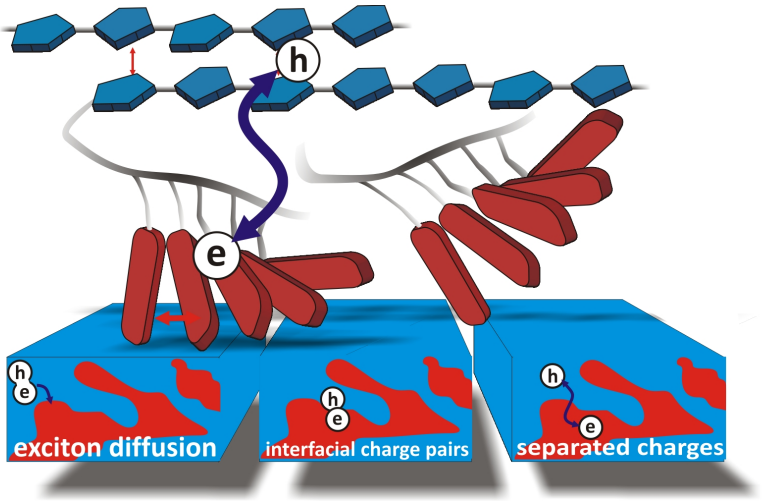

Abstract

Block copolymers are well known for their self-assembled highly ordered phase separation on a nanometer scale. These morphologies would correspond to ideal morphologies in bulk heterojunction solar cells. We investigated the photophysical properties of a double-crystalline donor acceptor block copolymer consisting of poly(3-hexylthiophene) (P3HT) and a polymerised perylene bisimide (PPerAcr). In addition to the structural and electronic characterization of photovoltaic devices, time resolved transient absorption spectroscopy (TAS) was employed to investigate the processes from exciton creation, diffusion and dissociation. Based on the observed kinetics, the struc-

ture size of the photoactive layer can be estimated as being smaller than the exciton diffusion length, accessing length scales that are beyond the resolution of electron microscopy. The block copolymer system resolves photoinduced charge transfer on a ∼1 ps timescale. Together with a high photoluminescence quenching this suggests small and highly inter-dispersed donor-acceptor interfaces induced by the covalent linkage of the blocks and a rapid solvent evaporation during film processing. The variation of solvents and of the copolymer molecular weight allowed to control the interfacial structure, coarseness and interfacial crystallinity. High boiling point solvents and higher molecular weights of P3HT provide the basis of crystalline P3HT/PPerAcr interfaces. This leads to high levels of long-lived charge pairs that are more easily separated under an applied electric field.

Introduction

Diblock copolymers offer a platform to realise the ideal nanoscale morphology for organic photovoltaic (OPV) devices[1] - all from a single solution processing step. The two components of a diblock copolymer phase separate during film formation, but due to their covalent linkage, the size of the separating domains is constrained. In amorphous block copolymers, predictable morphologies ranging from lamellae to cylinders, gyroids and spheres self-assemble as determined by the volume ratio of the two blocks.[2] These highly ordered morphologies correspond to their thermodynamic equilibria and offer domain sizes on the order of tens of nanometers, limited by the radius of gyration of each polymer block in the case of purely amorphous block copolymers.[3] Where the two blocks are electron donor and acceptor materials, the resulting nanomorphologies can balance the multiple lengthscale constraints that govern the efficiency of OPVs, including i) the exciton diffusion length (usually 5-10 nm),[4–6] ii) the geminate charge capture radius (can exceed 15 nm in low dielectric materials),[7] and iii) the need for bicontinuous networks throughout the active layer for charges to reach to the electrodes.

We and others reported on block copolymer OPVs that combine perylene bisimide acceptor blocks[8,9] and P3HT donor blocks.[10–12] P3HT is amongst the most effective polymers used in OPVs[5,13–15] and organic field effect transistors,[16–18] which has been linked to its propensity to form highly crystalline lamellae. Perylene bisimides form crystalline stacks, offering high electron mobilities (up to 2.1 $\frac{cm^2}{Vs}$ in the case of evaporated small molecules[18,19] 10^{-3} $\frac{cm^2}{Vs}$ in the case of side chain poly(perylene bisimide acrylate)[20]). The energy levels of perylene bisimides are suitably positioned to facilitate a photovoltaic response when combined with P3HT[21] and other conjugated polymers,[22] however, the lack of control over morphology in these blends results in modest photovoltaic efficiencies. Recently we and others demonstrated that the favourable electronic properties of perylene bisimides can be harnessed in an easily processable form when they are tethered to a polymer backbone.[20,23]

Despite the attractive possibilities of block copolymer OPVs, the best power conversion efficiency achieved by this are to date below 1% is substantially lower than single junction binary blend devices (over 7%[24]). Moreover, the photovoltaic responses observed for different block copolymer OPVs with similar compositions are widely variable. This suggests that efficient block copolymer OPVs may only be realised on the

Table 11.1: Molecular weight and composition ratios of the block copolymers and blends..

Polymer	M_n (total) (kg/mol)	M_n (P3HT) (kg/mol)	weight ratio P3HT-*b*-PPerAcr
BCP1	16.1	8.9	44% - 56%
BCP2	29.5	17.0	45% - 55%
Blend	$\sim$ 50 / 30.9		50% / 50%

basis of an understanding of their photophysical and electronic properties that goes beyond classic models of block copolymer nanomorphology. Crystallinity is one critical parameter whose influence is not accounted for in standard block copolymer models. Not only does crystallinity impose a more complex phase behaviour on block copolymers,[25] the photovoltaic response of organic materials is strongly dependent on the nature and strength of supramolecular interactions and packing,[26,27] with some degree of crystallinity usually being favoured. Charge separation efficiencies are found to be remarkably sensitive to the molecular structure at interfaces,[18] yet the competing assembly preferences of two different materials inevitably leads to disruption of interfacial order.

Here, we present a detailed examination of the photovoltaic response and photophysical properties of double crystalline donor-acceptor diblock copolymers. The material (Fig. 11.1) is comprised of a poly(3-hexylthiophene) (P3HT) donor block coupled to a poly(perylene bisimide acrylate) (PPerAcr) acceptor block. As summarized in Tab. 11.1, BCP1 and BCP2 contain a 45 wt% P3HT block and 55wt% PPerAcr with two different molecular weights of 16.7 $\frac{\text{kg}}{\text{mol}}$ (BCP1) and 29.1 $\frac{\text{kg}}{\text{mol}}$ (BCP2). For comparison, blends of homopolymers of P3HT and PPerAcr have also been assessed. The synthesis of these materials is presented elsewhere.[10]

Employing block copolymers with two different molecular weights, combined with different film preparation routes allows us to widely vary the crystallinity and interfacial structure. By employing a combination of structural, photophysical and electronic measurements for films and devices prepared from P3HT-*b*-PPerAcr block

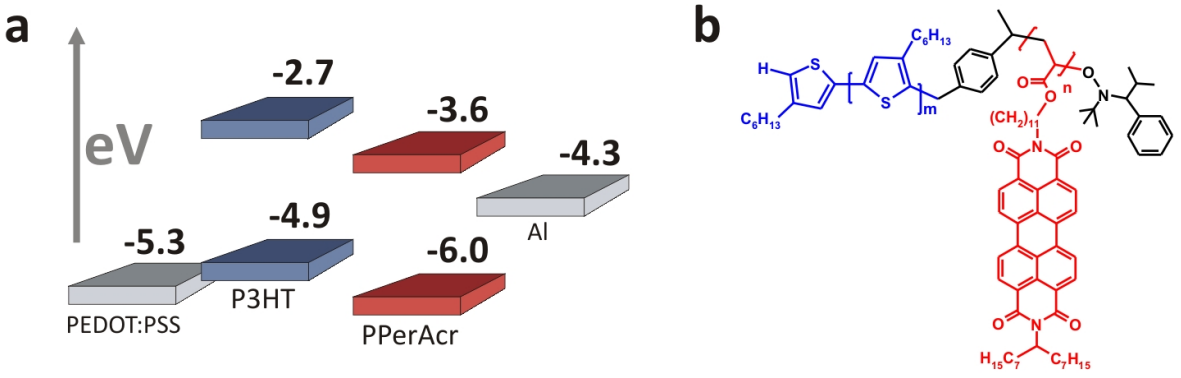

Figure 11.1: a) HOMO and LUMO levels of the block copolymer and the electrodes as used in the organic photovoltaic devices. b) Molecular structure of the investigated donor-acceptor block copolymer P3HT-*b*-PPerAcr consisting of a donor block of poly(3-hexylthiophene) (P3HT - blue) and poly(perylene bisimide acrylate) (PPerAcr - red).

copolymers, we are able to elucidate the requirements to optimise donor-acceptor block copolymer devices.

Results and Discussion

Fig. 11.2a shows the absorption spectra of the homopolymers P3HT and PPerAcr and the block copolymer BCP2. P3HT exhibits well resolved vibronic structure with significant intensity in the 0-0 band at 610 nm. This feature is associated with planarised chains which allows the chains to crystallise in a lamella structure[28–30] and interchain delocalization of the excitons.[31] Therefore, this feature is a clear indication for the prevalence of crystalline packing of P3HT chains.[17] PPerAcr contains side chains of perylene bisimide moieties that are connected to the poly(acrylate) backbone via an alkyl spacer. The flat perylene bisimide cores undergo strong $\pi - \pi$ interactions. The coupling of the π orbitals leads to a mixing of Frenkel excitons with charge transfer excitons.[32] Enhanced aggregation of the perylene bisimide leads to a relative increase of the feature at 465 nm as well as in the low energy tail at approximately 580 nm (Chap. 7). The absorption spectra of the series of block copolymers are well represented by a linear combination of the two homopolymer spectra weighted by their molecular weight ratios (see supplementary information). The slight divergence of block copolymer absorption spectra from the linear combination of homopolymers is most pronounced in the 610 nm region and is clearly dependent on film preparation. Since the intensity of the 610 nm peak is a signature of P3HT crystallinity (vida supra), we find that crystallinity is markedly suppressed when the block copolymer film forms rapidly (via spin coating from the low boiling point solvent chloroform (CF) ($T_{B.P.} = 61\,^{\circ}\mathrm{C}$). On the other hand, film formation is sufficiently slow when cast from chlorobenzene (CBZ) ($T_{B.P.} = 131\,^{\circ}\mathrm{C}$) that a high level of crystallinity is achieved within P3HT phases. In a similar manner it is possible to recover the P3HT crystallinity by subsequent solvent vapour annealing or temperature annealing steps (data not shown).

The microphase separation of double crystalline block copolymers is dissimilar to that of pure amorphous ones. We report elsewhere that P3HT and PPerAcr domains are in fact two coexisting crystalline regions whose hierarchical structures are driven by strong $\pi - \pi$ stacking, as evident from X-ray measurements (see suppl. information Fig. 11.8).[33,34] The perylene bisimide moieties form one dimensional stacks which assemble into an oblique 2-dimensional lattice. P3HT forms a crystalline lamellae. The crystallisation of both blocks has a significant effect on the phase separation of the block copolymer as the estimated order-disorder transition temperature of the block copolymer phase separation is below the crystallisation temperature. The consequence is that the crystallization of the blocks induces a lamellar phase separation with domain spacings of around 15 nm as observed in the bulk which is discussed in detail elsewhere.[34] However this does not necessarily reflect the morphology directly after spincoating or shorter annealing times, nor does it reflect the energetic landscape experienced by most optical excitations. In the following sections, we refine the P3HT-*b*-PPerAcr copolymer morphology model via photophysical and photovoltaic measurements.

Strong optical absorption derived from both PPerAcr and P3HT chromophores (Fig. 11.2a) leads to exciton photogeneration in both phases. When intrachain ex-

citons diffuse to a donor-acceptor interface, the energy-level offset across the heterojunction induces the formation of non-emissive interfacial charge transfer states and ultimately free charge carriers. As a consequence, the photoluminescence quantum efficiency (PLQE) is strongly quenched in films of the block copolymers compared with individual homopolymers (PLQE (P3HT) $\sim$ 4%) , PLQE (PPerAcr) $\sim$20%). Films of BCP2 spincoated from CBZ result only in a PLQE of only 1%, the CF processed films are even lower at 0.8%. Block copolymers spincoated from CF (BCP2-CF) or with the lower molecular weight (BCP1-CBZ) result in barely quantifiable PLQEs of less than 0.1%. Strong PLQE quenching in the block copolymers illustrates that donor-acceptor interfaces are assembled on lengthscales considerably shorter than the exciton diffusion lengths of the individual materials. The analysis of PL quenching highlights the particularly finely interspersed donor-acceptor morphology that results in films that dry rapidly (cast from CF) and films comprised of the low molecular weight block copolymer (BCP1). In these cases, the phase separated nanomorphology is clearly beyond the image resolution of the force microscopy or electron microscopy. The PLQE recovers to around 7% in the blend of homopolymers cast from CBZ, confirming the much finer donor-acceptor morphology of donor-acceptor block copolymers.

Quantitative analysis of PL quenching must be balanced by consideration of the spectral composition. The PL spectra of block copolymer films are dominated by PPerAcr emission (λ_{max}=637 nm) with a minor contribution of P3HT emission (λ_{max}=717 nm) (Fig. 11.2b). A broad feature at 580 nm seems to be always prevalent, which we attribute to amorphous P3HT chains based on the comparable spectral position of PL measured in P3HT solutions.[35] One might expect that efficient resonant energy transfer would cause PL spectra of block copolymer films to be dominated by emission from the lowest energy chromophore, in this case ordered regions of P3HT. Emission from disordered P3HT chains is not usually detectable solid films of P3HT

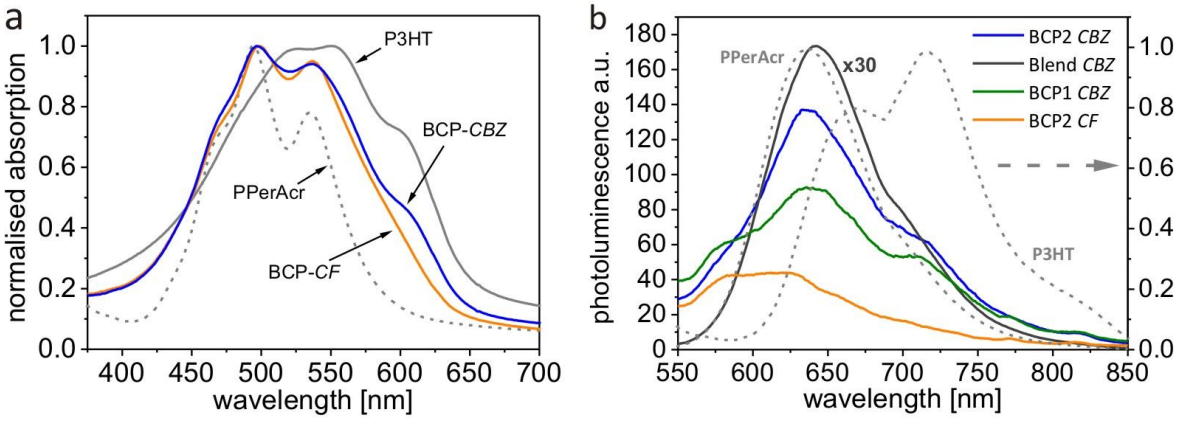

Figure 11.2: a) Absorption spectra of the used materials. The BCPs are equivalent to a linear superposition of the homopolymer spectra with a 48%-P3HT and 52%-PPerAcr ratio (suppl. inf. – Fig. 11.10). The P3HT crystallinity is strongly reduced in the block copolymer BCP2 when spin coated from chloroform resulting in a decrease of the 610 nm feature. b) Photoluminescence (PL) spectra excited at 490 nm. The blend is scaled down by a factor of 30. The homopolymers PPerAcr and P3HT (grey, dotted) are shown on a normalised scale (right axis).

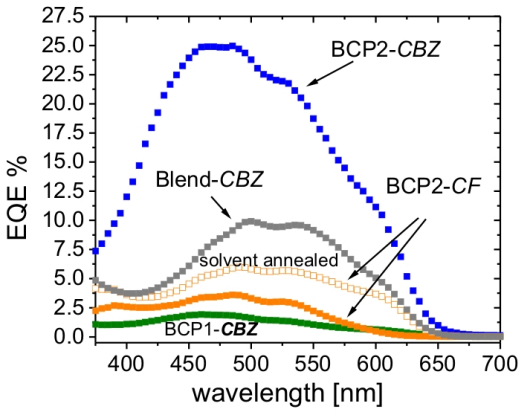

Figure 11.3: Power action spectra displaying the external quantum efficiency (EQE) of the tested material composites measured under short circuit conditions.

for this reason.[29] The relative suppression of emission from ordered P3HT in films of block copolymers is consistent with the disrupted crystallinity of P3HT induced by the presence of interfaces. The PL spectra suggest that excitons are frequently generated on PPerAcr and disordered P3HT chains that are too isolated to energy transfer to ordered P3HT domains. Secondly, the higher inherent PLQEs of PPerAcr and disordered P3HT chromophores compared with ordered P3HT further enhances their relative contribution to PL.[36] Notwithstanding, the high levels of PL quenching in all cases points to high yields of charge photogeneration.

Despite the higher yields of charge generation seen for finely distributed donor-acceptor interfaces, the quantum efficiency of subsequent charge extraction is known to favour somewhat coarser morphologies where the geminate charge pairs are able to escape their mutual Coulombic attraction.[16,35] Fig. 11.3 shows the external quantum efficiency (EQE) spectra of photovoltaic devices whose active layers were comprised of block copolymers of two different molecular weights, and each processed from both low- and high boiling point solvents. Devices whose active layer is processed from chloroform (BCP2-CF) only reach an EQE of 3.6%, or only 2.9% in the case of the low molecular weight block copolymer (BCP1-CBZ). As described previously,[10] maximum EQEs of over 25% are achieved using BCP2 with a 'high' molecular weight P3HT block and spincoating from a high boiling-point solvent (CBZ). A blend of the two constituent homopolymers results in peak EQEs of around 10% when processed under the same conditions. The superior EQEs found through use of a single block copolymer demonstrate the success of this approach in producing nanomorphologies that achieve the optimal balance of exciton-to-charge conversion and charge extraction.

The EQE values stated above were determined under short circuit conditions. Application of a large negative bias assists the field-induced separation of interfacial charge pairs and provides a sufficient driving force for the separation of charges that would otherwise remain trapped at interfaces, particularly in films with a high interfacial area. Fig. 11.4b shows the photocurrent measured under lower light intensity ($28\,\frac{\mathrm{mW}}{\mathrm{cm}^2}$) to avoid space charge effects. The chloroform processed device (BCP2-CF) exhibits a much lower short circuit current J_{SC}. Upon application of a strong reverse

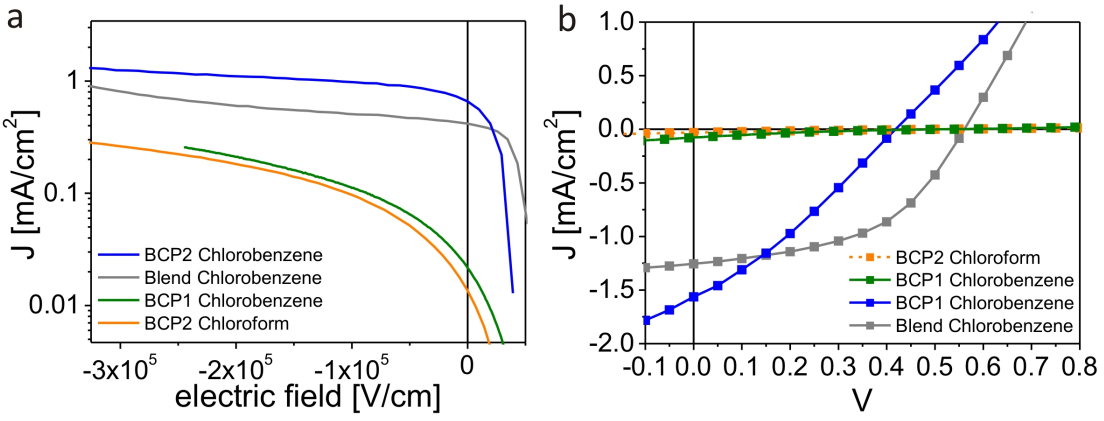

Figure 11.4: a) $J-V$ characteristics under lower intensity illumination ($28\ \frac{\mathrm{mW}}{\mathrm{cm}^2}$ and strong applied electric field caused by an applied bias. Charge pairs generated in BCP1-CBZ and BCP2-CF that are only separated with the help of an electric field result in a current, which increases by one order of magnitude before it starts to saturate. In contrast, the blend and the BCP2-CBZ device show efficient charge separation already at zero electric field (i.e. short circuit current). b) $J-V$ characteristics of the tested organic photovoltaic devices with simulated sunlight at AM 1.5, $100\ \frac{\mathrm{mW}}{\mathrm{cm}^2}$.

Table 11.2: Device parameters of photovoltaic characterization: Open circuit voltage V_{OC}, short circuit current J_{SC}, fill factor FF, power conversion efficiency η, external quantum efficiency EQE, photolumincescence quantum efficiency PLQE from quantitative fluorescence measurements and hole mobilities μ_h estimated from hole only devices using a space charge limited current expression (see supplementary information).

Device	V_{OC} [V]	J_{SC} $[\frac{\mathrm{mA}}{\mathrm{cm}^2}]$	FF	η	PLQE	EQE_{max}	μ_h (SCLC)
BCP 2 CF	0.50	0.03	0.20	0.003%	0.71%	3.6%	$10^{-10}\ \frac{\mathrm{cm}^2}{\mathrm{Vs}}$
BCP 2 CBZ	0.42	1.56	0.30	0.20%	1.19%	25%	$10^{-6}\ \frac{\mathrm{cm}^2}{\mathrm{Vs}}$
BCP 1 CBZ	0.51	0.07	0.17	0.007%	0.76%	2%	$10^{-8}\ \frac{\mathrm{cm}^2}{\mathrm{Vs}}$
Blend CBZ	0.56	1.25	0.49	0.35%	6.85%	10%	$10^{-6}\ \frac{\mathrm{cm}^2}{\mathrm{Vs}}$

bias, the photocurrent increases by one order of magnitude, highlighting the charge population that is otherwise lost to geminate recombination in the chloroform processed device. On the other hand, in the BCP2-CBZ devices or the homopolymers blend devices, the photocurrent is already close to saturation under short circuit conditions. Photoconductivity may be prevalent as well, but has to be considered mainly at high reverse bias.[37]

Fig. 11.4b shows the corresponding $J-V$ curves measured under AM 1.5, $100\ \frac{\mathrm{mW}}{\mathrm{cm}^2}$ simulated solar illumination and Tab. 11.2 compiles the analysed device parameters. In spite of the superior short circuit photocurrent exhibited by BCP2, its reduced fill factor (FF) and open circuit voltage (V_{OC}) decrease its overall power conversion efficiency ($\eta = 0.20\%$) compared with the blend of homopolymers ($\eta = 0.35\%$). The devices BCP2-CF or BCP1-CBZ exhibit substantially lower power conversion efficiencies, at

$\eta = 0.003\%$ and $\eta = 0.007\%$, respectively. The observed trend in PCEs is inversely correlated with the interfacial area and suppression of crystallinity inferred for the series of block copolymer films from UV-visible absorption and PL measurements.

The morphology dependence of field-induced charge separation is supported by analysis of charge carrier mobilities in the devices. Substituting the aluminum cathodes for higher workfunction gold contacts turns the devices into hole-only diodes and permits an estimation of hole charge carrier mobilities by fitting the space charge limited currents (supplementary information).[38] The BCP2-CBZ devices show hole mobilities of around $10^{-6}\,\frac{\mathrm{cm}^2}{\mathrm{Vs}}$. The hole mobilities are reduced by two orders of magnitude in the case of BCP1-CBZ ($10^{-8}\,\frac{\mathrm{cm}^2}{\mathrm{Vs}}$), consistent with the trends observed for the same materials incorporated in OFET devices.[10] The hole mobilities of BCP2-CF OPV devices are suppressed by 4 orders of magnitude to $10^{-10}\,\frac{\mathrm{cm}^2}{\mathrm{Vs}}$. Such a large difference is not paralleled in OFET devices, highlighting the geometrical factors that can also couple to film morphologies to influence charge mobilities.

The observed reduction in charge mobilities for the various block copolymer OPV devices reflects the combined effects of higher interfacial areas and reduced crystallinity. The crystallinity of P3HT is known to play a crucial role in the performance of block copolymer OPV devices[10] and P3HT/fullerene blend devices,[39] with crystalline nanostructures supporting considerably higher hole mobilities. Importantly, it is the local charge mobilities caused by crystallinity in the vicinity of heterojunction interfaces that has the biggest effect over field-induced charge separation.[7] While the series of absorption spectra clearly demonstrates that the crystallinity of the P3HT component is strongly affected by the interfacial area, absorption spectroscopy or X-ray scattering does not distinguish between chains at interfaces and in the bulk.

By employing transient absorption (TA) spectroscopy as a direct probe of the nature and dynamics of photoexcitations generated in films as a function of different processing conditions, we are able to directly probe the formation and properties of interfacial states, including the crystallinity of interfacial polymer chains. Fig. 11.5a and 11.5b show the TA dynamics for the constituent homopolymers in order to establish the spectral features and dynamics in the absence of heterojunctions for charge separation. For of P3HT (Fig. 11.5a), the series of TA spectra are dominated by bleaching ($\Delta T/T > 0$) of the ground-state (GS) absorption at $\lambda < 650\,\mathrm{nm}$ as observed in the UV-vis spectra (Fig. 11.2a). Accordingly, a vibronic progression is clearly resolved in the ground-state bleaching (GSB) signal. The prominence of the 0-0 band at 610 nm shows that excitations occupy P3HT chains adopting a planar chain conformation and packed in ordered lamellae. The positive $\Delta T/T$ signal observed in the region of $\lambda = 650 - 750\,\mathrm{nm}$ coincides with the weak photoluminescence from P3HT and is thus attributed to stimulated emission (SE) from P3HT excitons. No photo-induced absorption (PIA) signals ($\Delta T/T < 0$) are seen within the probed wavelength range. The signal exhibits a non-exponential decay with a half-life of $\sim 100\,\mathrm{ps}$, and the bleaching features display a dynamic red-shift as excitons migrate towards more extended chains and delocalise. In the case of PPerAcr, the spectra are dominated by a broad photo-induced absorption signal at $\lambda_{max} = 720\,\mathrm{nm}$, with a sharp GSB feature at $\lambda = 550\,\mathrm{nm}$ and further bleaching evident on the blue edge of the spectrum. These features are consistent with aggregated PPerAcr chromophores,[40] and the spectrum

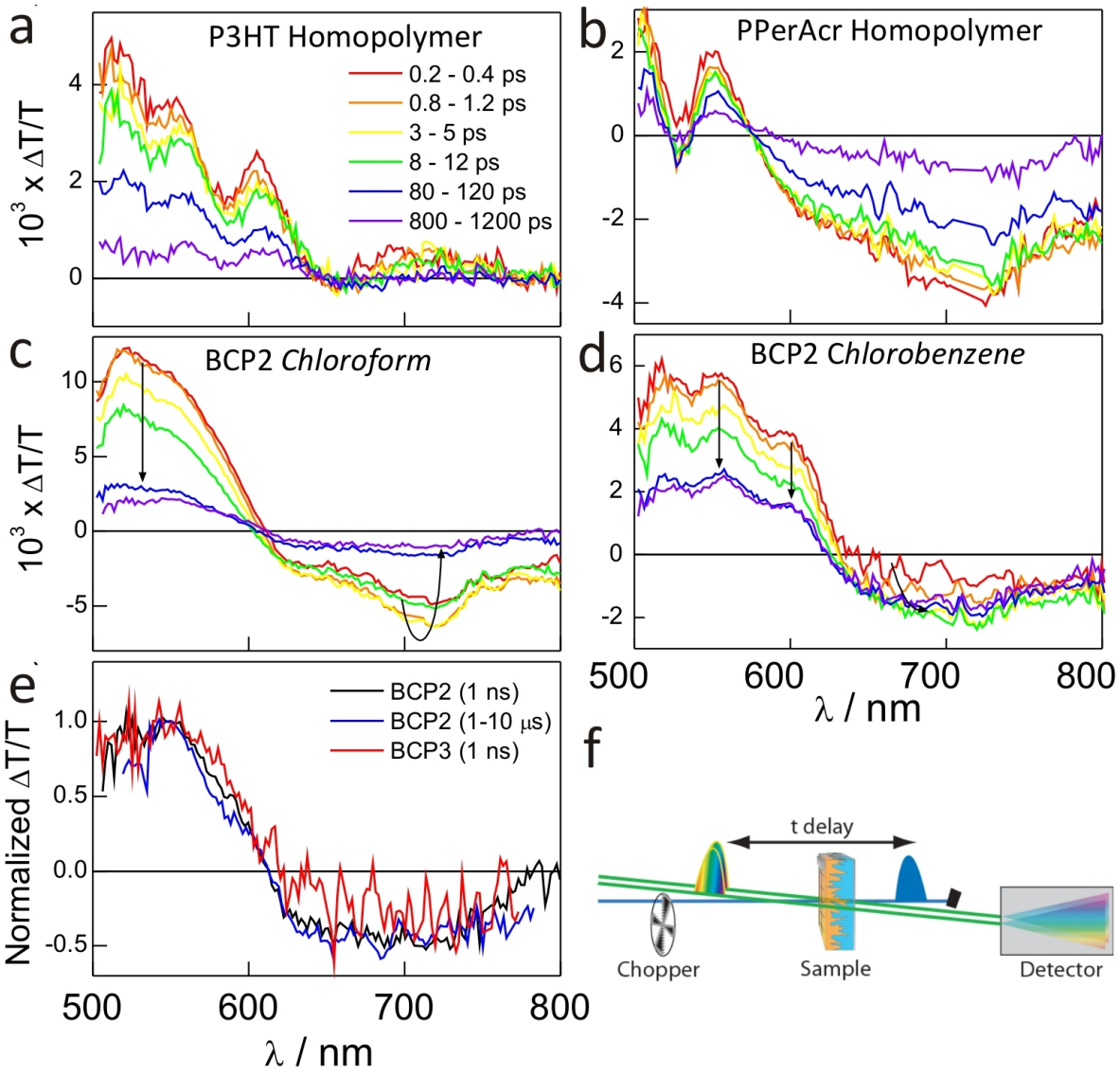

Figure 11.5: Time evolution of transient absorption (TA) spectra in thin films of a) P3HT homopolymer, b) PPerAcr homopolymer, c) BCP2-CF and d) BCP2-CBZ. The color scheme for the integrated time ranges is shown in a). e) Normalised TA spectra for thin films of the BCP2 diblock copolymer at probe delays of 1 ns and 1-10 μs and the BCP3 (81%-PPerAcr) diblock compolymer at a probe delay of 1 ns. A 490-nm, 60-fs pulsed excitation with a fluence of 2-4 $\cdot$ 10^{14} $\frac{\text{photons}}{\text{cm}^2}$ was used to obtain all spectra except the μs timescale spectra, which employed 532 nm, 600 ps excitation at the same fluence (see experimental section for details).

decays dispersively with a half-life of $\sim$ 100 ps.

Fig. 11.5c shows the TA dynamics for a film of BCP2-CF. The earliest TA spectrum (200-400 fs, red curve) exhibits a GS bleach at $\lambda < 600$ nm and an absorption feature centered at 720 nm – each being distinct excitonic features of the constituent P3HT and PPerAcr homopolymers, respectively. A weighted sum of the constituent TA spectra might be expected for the diblock copolymer since UV-visible absorption spectra show that 490 nm excitation light is strongly absorbed (48% P3HT and 52% PPerAcr) by both chromophores (suppl. inf. – Fig. 11.10). However, in contrast to the

TA spectra of the homopolymers, the diblock copolymer clearly lacks vibronic structure in the P3HT GS bleaching region. Specifically, the lack of bleaching intensity in the 0-0 band at 610 nm is strong evidence that connection of the PPerAcr block disrupts the preferred chain planarity and lamellar packing in the P3HT block for a film of BCP2-CF as already pointed out in Fig. 11.2a. Within the next picosecond (orange curve), the TA spectrum of the diblock copolymer is seen to enhance its photoinduced absorption intensity beyond 620 nm, while the GS bleaching region remains unchanged. By referring to the reference spectra of the homopolymers, we can rule out an energy transfer process of the following facts: i) Energy transfer from P3HT* to PPerAcr would be associated with *decreased* GS bleaching at $\lambda < 600$ nm on a commensurate timescale with an *increased* photoinduced absorption beyond 620 nm, and ii) Energy transfer from PPerAcr* to P3HT would lead to *increased* GS bleaching at $\lambda < 600$ nm and *decreased* photoinduced absorption beyond 620 nm. This is not the case for P3HT-*b*-PPerAcr block copolymers. Instead, we attribute the spectral dynamics on a 1-ps timescale to the conversion of P3HT-based excitons to interfacial charge pairs, thus retaining the P3HT GS bleach, while introducing charge-based photoinduced absorption in the region where P3HT excitons have a weak SE. Instead, we attribute the spectral dynamics on a 1-ps timescale to the conversion of P3HT-based excitons to interfacial charge pairs, thus retaining the P3HT GS bleach, while introducing a rather flat PIA feature beyond 620 nm from a combination of electrons in PPerAcr and holes in P3HT, consistent with previous TA studies of charges in these materials.[41,42] Charge generation could also proceed via PPerAcr excitons, however if this was the dominant mechanism then we would expect the P3HT-based GS bleach to *increase* concomitantly with charge generation. There appears to be a population of PPerAcr excitons still present on slightly longer timescales, based on the survival of the 720 nm PIA peak in the 8-12 ps spectrum. This observation is consistent with the traces of PPerAcr emission seen in PL spectra (Fig. 11.2b). Combinations of energy transfer processes preceding a much faster charge transfer step are also likely to occur, but if the intermediates are short-lived, this mechanism is spectroscopically indistinguishable from direct charge generation.

The assignment of rapid charge pair formation is supported by comparison with normalised TA spectra shown in Fig. 11.5e. The close resemblance of TA spectra for two diblock copolymers with a vastly different P3HT and PPerAcr ratio (BCP2 contains 55%-PPerAcr and BCP3 contains 81%-PPerAcr) is consistent with an interfacial state rather than a mixture of states localised in each domain type. Moreover, the survival of the TA spectral features on the microsecond timescale is consistent with charges and not singlet excitons. Finally, the detection of photogenerated charges is quantitatively consistent with the photocurrent measurements. Based on the magnitude of the GS bleach at 1 ns compared to the initial signal 300 fs, we constrain the yield of excitations that could contribute to photocurrent to <20%. The corresponding chloroform-processed OPV devices have a peak short-circuit external quantum efficiencies of 3.6% (Fig. 11.3) (higher under reverse bias, Fig. 11.4a), suggesting that a large fraction of the excitations detected beyond the disappearance of excitons must be charges. This also suggests that triplet excitons do not play a significant role. Triplets have been demonstrated to form in high yields via recombination of interfacial charge-transfer states in material blends where this is thermodynamically favourable.[43–45] In the case of P3HT-*b*-PPerAcr, the

interfacial charge transfer state is estimated to be close in energy to triplet excitons in P3HT based on an estimated driving force of 0.6 eV for charge transfer from the P3HT singlet exciton compared with the range of exchange energies found for ordered P3HT (0.45 eV)[46] and an extensive range of amorphous conjugated polymers (0.7 eV).[47]

We are also able to use these spectral signatures to resolve the timescale of charge transfer. The population of charge pairs peaks within just 3 ps for the chloroform-processed film, as ascertained from the growth of the PIA signal at 700 nm. This fast timescale is consistent with the lack of photoluminescence and reflects a finely-interdispersed phase separation. This assertion may seem at odds with the $\sim$ 15 nm phase separation predicted by the composition of the block copolymer. The two measurements are reconciled on the basis of the assumption of incomplete phase separation resulting from rapid film drying after processing. This interpretation is consistent with other investigations on the dependence of film drying time on phase separation,[36] and with the spectroscopic observation that P3HT chains are disordered in the BCP2-CF films.

Fig. 11.5d shows the evolution of TA spectra for a BCP2-CBZ film which was measured under identical conditions as a BCP2-CF film. There are several striking differences in the TA spectral evolution. The prominence of the GS bleach of the 0-0 vibronic peak at 610 nm is clear evidence that excitations occupy ordered P3HT and corresponds to the changes in the UV-vis absorption spectrum. Whereas UV-visible absorption spectroscopy provides a picture of the average P3HT crystallinity in the film, TA spectroscopy can yield information about ordering in the vicinity of interfaces where charges are formed. The retention of the 610 nm peak beyond the timescale of charge generation shows that interfaces occupied by charge pairs are considerably better ordered when films are cast from chlorobenzene compared to chloroform. The TA spectra support our previous assertion that enhanced interfacial ordering plays a crucial role in facilitating the initial separation of charge pairs and accounts for considerably higher photovoltaic efficiencies observed when films are processed from a higher molecular weight and chlorobenzene, BCP2-CBZ.

The rate of charge generation, as assessed from the growth of the photoinduced absorption feature at 700 nm, is compared for each of the block copolymers spin-coated from different solvents and for the blend of homopolymers in Fig. 11.6a. A clear trend is observed: the charge population peaks at later times for CBZ processed films compared with those processed from CF, and likewise for high vs. low molecular weight block copolymers. The peak charge population is later still in the polymer blend of homopolymers. Since excitons must diffuse to an interface prior to generating charges, a slower rate of charge generation is consistent with a larger phase separation and cleaner interfaces.[36] A parallel trend is observed in the magnitude of the peak charge population, with earlier absorption peaks being associated with higher yields of charge generation, consistent with PLQE trends. We note that exciton-charge annihilation can also operate to complicate the quantitative analysis of charge generation kinetics at this excitation density.[43] Consistent with the GSB kinetics, only $\sim$ 20% of the maximum charge population (peaked at $\sim$ 2 ps) is found to survive beyond 100 ps in the chloroform-processed film, suggesting that a rapid phase of geminate charge recombination operates across the disordered interfaces of chloroform-processed block copolymer films.

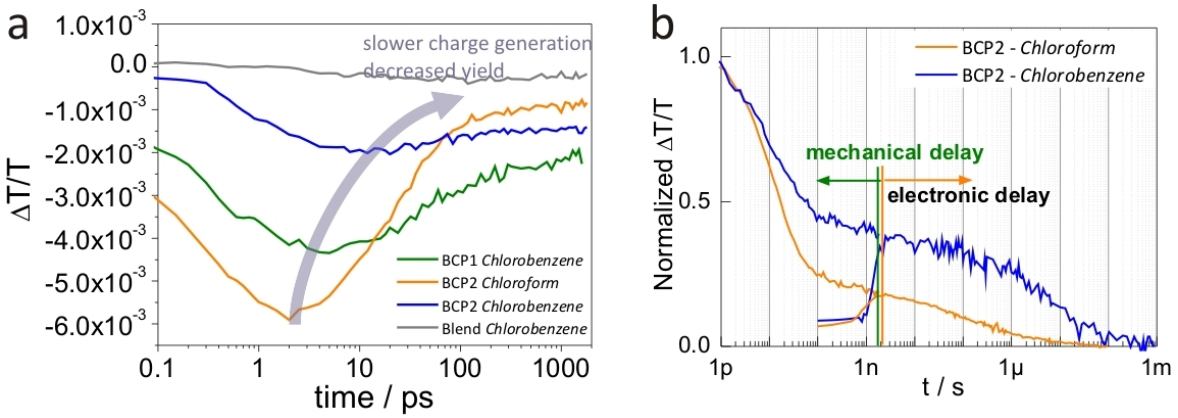

Figure 11.6: a) Charge generation kinetics probed in the photoinduced absorption region ($\lambda_{probe} = 700 - 750\,\mathrm{nm}$) for BCP1, BCP2 as well as for the blend of P3HT / PPerAcr. The coarsening of the donor-acceptor interface causes a slower charge pairs generation at the interface and decrease in the overall number. However, efficient charge separation occurs only for sufficiently coarse domains with a high P3HT crystallinity. b) Normalised TA kinetics in the GS bleach region ($\lambda_{probe} = 530 - 570\,\mathrm{nm}$) for thin films of BCP2-chlorobenzene (blue curve) and BCP2-chloroform (red curve) on timescales of 1 ps - 1 ms following pulsed excitation. This plot was obtained by splicing the normalised kinetics obtained on sub-ns timescales (using mechanically-delayed 60-fs pulses) and longer timescales (with electronically delayed 600-ps excitation pulses).

The comparison of the TA dynamics in the GS bleaching regions reveals that P3HT ordering is also associated with a significantly higher level of charges surviving beyond the nanosecond timescale. We were able to resolve the dynamics of charge recombination on longer timescales by synchronizing a Q-switched Nd:YVO_4 excitation laser with the femtosecond probe via an electronic delay generator. Fig. 11.6b shows the normalised GS recovery kinetics for films of BCP2 processed from CBZ and CF as well as the blend. The kinetics measured with mechanical and electronic delays are spliced together to give gap-free resolution from 1 ps to 1 ms. The BCP2 cast from CBZ has a clearly higher population (>40% of initial excitations) of charges that decays very little between 100 ps and 1 μs, providing an extended time window for charge pairs to separate in the device. The $\sim 25\%$ peak EQE measured for the corresponding BCP2-CBZ device is clear evidence that most of the interfacial charge pairs are effectively separated and extracted from the device.

Nevertheless, with a half-life of $t_{1/2} = 1.5\,\mathrm{ps}$, there is still considerable kinetic redundancy in the rate of charge generation for BCP2-CF block copolymer films when comparing with the exciton lifetime ($t_{1/2} \approx 100\,\mathrm{ps}$). Larger domains could still enable efficient charge generation while providing the morphology for more efficient charge separation and collection. The higher power conversion efficiencies observed for the blend of homopolymers support this conclusion. A diblock copolymer with a higher molecular weight might achieve this more effectively. Indeed, the almost 10-fold improvement in external quantum efficiency by doubling the molecular weight from BCP1 to BCP2 for the same block ratio is consistent with a coarser morphology.[10]

The results obtained from above steady state and time-resolved TA spectroscopy

as well as the device properties help to give an estimation about the thin film morphology. Fig. 11.7 shows a schematic with possible thin film morphologies. From the TA data we infer domain sizes well-below, around, and well-above the exciton diffusion length for BCP1 CBZ, BCP2 CBZ and the homopolymer blend, respectively. Scanning electron microscopy (SEM) of these films was carried out to correlate the excitation kinetics with the polymer morphology. The block copolymer films indeed suggest that morphologies of different coarsenesses are present (left two pictures). Even though the resolution of the two SEM images does provide quantitative information of the polymer domain size, it is obvious that BCP1 CBZ (left picture) exhibits a more finely dispersed morphology than BCP2 CBZ (middle picture). The blend film clearly displays large macroscopic domains, confirming the conclusion drawn from TA spectroscopy.

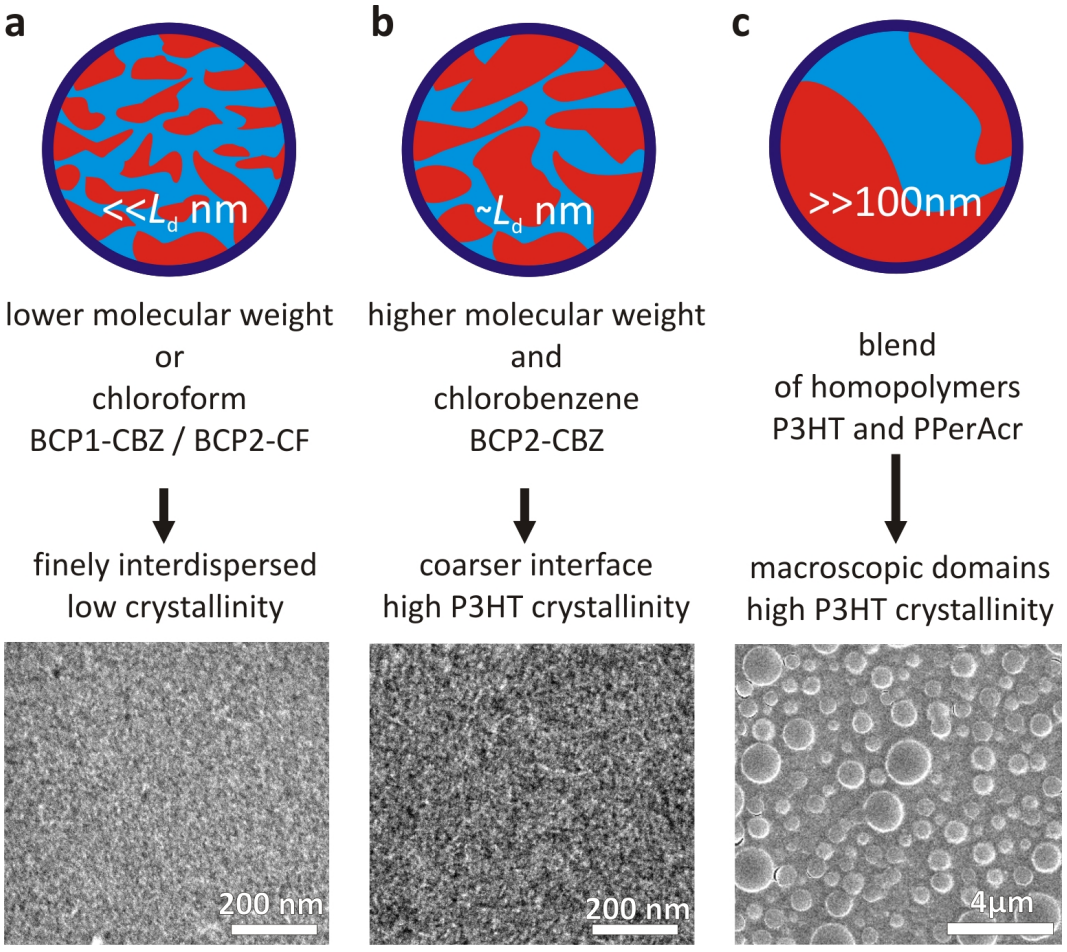

Figure 11.7: Schematics of attributed morphologies achieved by processing block copolymers from different conditions and corresponding scanning electron microscopy images. a) and b) depicts the block copolymers. The morphology is too small to be properly resolved by SEM. The domain size is deduced from spectroscopic data, estimating a finely interdispersed morphology much smaller than the exciton diffusion length LD (a) and in the order of the exciton diffusion length (b). The blend demixes on a macroscopic lengthscale (c).

Conclusion

In conclusion we investigated the kinetics of charge generation and dynamics in donor-acceptor block copolymer systems of P3HT-*b*-PPerAcr. Since the block copolymer phase separation is induced by the crystallization of the blocks, the use of different solvents and molecular weights, allowed to generate different domain sizes i.e. interfacial coarseness and different degrees of P3HT crystallinity. The measured charge generation timescales are less than $t_{1/2} = 1.5\,\text{ps}$ and there is considerable kinetic redundancy in the rate of charge generation for all block copolymer films when comparing with the exciton lifetime ($t_{1/2} \sim 100\,\text{ps}$). Such rapid charge generation implies that donor-acceptor interfaces are effectively distributed on lengthscales of just a few nanometers - significantly shorter than the $\sim 15\,\text{nm}$ lengthscale of bulk phase separation estimated by X-ray scattering (see suppl. information Fig. 11.8).[34] The incongruent lengthscales in thin films suggest that donor and acceptor blocks do not completely phase separate to achieve the predicted morphology. Molecularly rough interfaces and disrupted crystallinity impedes the field-induced separation of geminate charge pairs, resulting in the substantial charge recombination seen in TA measurements and PV response curves. The finely donor-acceptor inter-dispersion is also confirmed by the strongly quenched photoluminescence. Interfacial P3HT crystallinity is important for an efficient charge separation as the charge carrier mobility and the domain size are correlated as well. Low boiling point solvents like chlorobenzene and sufficiently large molecular weight of the P3HT block (here $M_n = 17.0\,\frac{\text{kg}}{\text{mol}}$) offer an enhanced P3HT crystallinity. Thus BCP2-CBZ results in high external quantum efficiencies which is strongly correlated with high populations of long-lived charges occupying crystalline regions from which they can be more easily extracted. Energy transfer between the composites can be excluded and long-lived charge pairs that are stable up to $1\,\mu\text{s}$ enable an efficient charge separation. However, the charge percolation and therefore its morphology still leave room for improvement. In a largely phase separated blend, for example, the fillfactor is higher by 20% and the open circuit voltage is increased by 0.18 V, although less than half the amount of charges are generated compared to BCP2. Slowing the rate of film formation via the use of high boiling-point solvents is an effective way of enhancing the interfacial crystallinity and improving charge mobilities. High EQEs are strongly correlated with high populations of long-lived charges occupying crystalline regions from which they can be easily extracted under the influence of an electric field. Our results suggest that diblock copolymers with a higher molecular weight, particularly for the P3HT block should result in morphologies that produce even more efficient OPV devices. The higher fill factors, open-circuit voltages, and PCEs observed for the blend of homopolymers supports this conclusion. The use of BCPs as blend compatibilisers[48] offers a promising alternative strategy that could provide larger phases and well-defined crystalline interfaces without the need for further synthetic investments in high molecular weight block copolymers.

Experimental

Sample preparation and characterization

The synthesis of the block copolymers and of PPerAcr has been described elsewhere.[49] The P3HT homopolymer was purchased from *Rieke*. Polymer thin films were spin-coated, either from a 0.6 wt% chloroform solution at 2000 rpm or from a 15 $\frac{\text{mg}}{\text{ml}}$ chlorobenzene solution at 900 rpm, respectively. In order to enhance the film formation in chlorobenzene films, 10 vol% of toluene was added.

Electron microscopy was carried out using a LEO Carl Zeiss STM scanning electron microscope. Photovoltaic devices were prepared on pre-structured and pre-cleaned ITO substrates, that were coated with a layer of PEDOT:PSS (*CDT ink*) and annealed. After spin-coating the active layer, an approximately 60 nm thick aluminum electrode was evaporated on top. All manufacturing steps from solution preparation to device fabrication were carried out in a nitrogen glove box. The devices were encapsulated before they were measured. The photocurrents were measured using a Keithley 237 source-measure-unit. The external quantum efficiency spectra (EQE) were obtained by illuminating the devices with a tungsten lamp (80 W) and a single-grating monochromator. The $J-V$ characteristics were recorded under simulated sunlight using a Lot Oriel solar simulator with AM 1.5 at 100 $\frac{\text{mW}}{\text{cm}^2}$.

Spectroscopy

The samples for spectroscopic measurements were prepared on quartz glass substrates. UV-Vis measurements were carried out with a Hewlett-Packard 8453 diode array spectrometer and the fluorescence spectra with a Cary Eclipse Fluorimeter. The photoluminescence quantum efficiencies (PLQE) were determined as described previously. The measurements were carried out using an Ar-Laser at ∼490 nm for exciting the sample within a nitrogen-purged integrating sphere. The emission was detected with a diode array spectrometer via an optical fibre.

The setup for TA spectroscopy has been described in detail elsewhere.[43,50] Briefly, a 1-kHz train of 60 fs pulses (800 J/pulse, $\lambda_0 = 800$ nm) is split to generate pump and probe pulses using a TOPAS optical parametric and a home-built broadband non-collinear optical parametric amplifier (NOPA),[51] respectively. The probe beam is delayed relative to the excitation beam via a computer-controlled Newport mechanical delay stage and focused to overlap nearly collinearly with the excitation beam in the sample. A portion of the probe beam does not overlap with the pump beam and is used as reference to normalise shot-to-shot fluctuations. The spectra of probe and reference beams are recorded for each shot with two 256 pixel photodiode arrays coupled to an imaging spectrograph. The pump beam is chopped at 500 Hz such that the transmission of alternate probe pulses can be compared to obtain the differential transmission as a result of excitation. Differential transmission spectra are obtained by doing so for each pixel, and temporal dynamics are compiled by collecting spectra for a range of relative probe delay times and repeating sweeps at least 10 times. After correcting for group velocity dispersion, the instrument limited time resolution is ∼ 120 fs, as judged by the signal rise time. In the case of TA measurements on timescales beyond nanoseconds, a Q-switched Nd:YVO_4 laser with 500 ps pulses was used as the excitation source

and synchronised with the Ti:Sapphire laser via an electronic delay generator. Samples were contained in a vacuum chamber ($\sim 10^{-5}$ mbar) during TA measurements.

Acknowledgement

JMH and RHF wish to acknowledge a grant from the U.K. Engineering and Physical Sciences Research Council (EPSRC). We acknowledge the financial support from the European network "PolyFilm" under RTN-6 and the German Research Council (DFG) projects SFB 481 and SPP1355. SH thanks Universität Bayern e.V. for the financial support in the form of a scholarship of the Bayerische Graduiertenförderung and the Elitenetzwerk Bayern (ENB) for their support.

Supplementary information

Block copolymer bulk structure

The bulk behaviour of BCP2 has been investigated in detail elsewhere.[33,34] The structural data as analysed by combined small and wide angle X-ray scattering is given in Fig. 11.8a. The block copolymer phase separation is indicted by the scattering vector at $q = 0.2\,\mathrm{nm}^{-1}$ relating to a lamellar morphology (see inset) with domain sizes of $\sim 15\,\mathrm{nm}$. Besides the phase separation each of the domains exhibits a distinct crystalline structure. The perylene bisimide moieties form face to face π-stacks with an intermolecular spacing of $c = 0.36\,\mathrm{nm}$. These stacks align into a 2-d oblique lattice. The P3HT domains instead form a lamellar crystalline structure. The lamellar phase separation also can be seen by scanning electron microscopy of a bulk sample that has been extensively annealed by solvent vapour (Fig. 11.8b). These structures correspond rather to bulk equilibrium structures and differ from thin film morphologies. The X-ray measurements were carried out at the ESRF in Grenoble, beamline ID02.

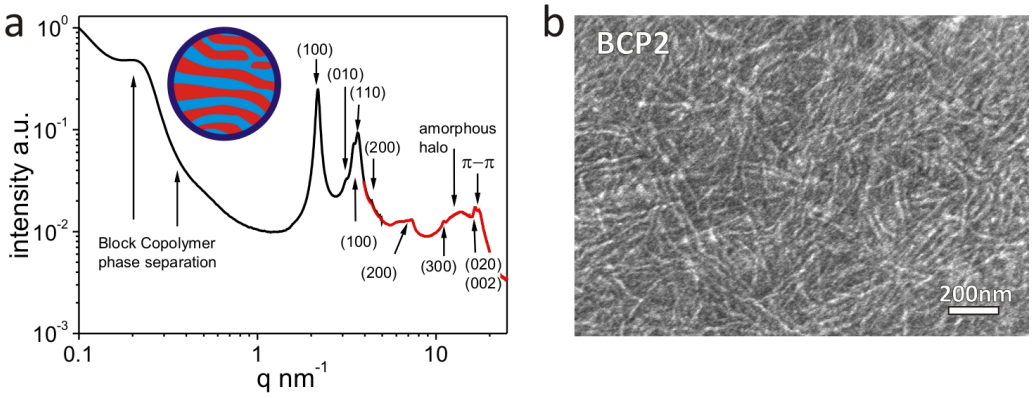

Figure 11.8: Bulk morphology of BCP2 analysed by means of combined SAXS (black) and WAXS (red) diffraction exhibits different hierarchical structures. The block copolymer phase separation is indicted by the scattering vector at $q = 0.2\,\mathrm{nm}^{-1}$ relating to a lamella morphology with a domain size of $\sim 15\,\mathrm{nm}$. The upper numbers index the monoclinic lattice of perylene bisimide stacks ($a = 3.086\,\mathrm{nm}$, $b = 2.196\,\mathrm{nm}$ and $\gamma = 81.2°$), whereby the perylene bisimide moieties form face to face π-stacks with an intermolecular spacing of $c = 0.36\,\mathrm{nm}$. The P3HT forms a lamellar crystalline structure as indexed by the lower numbers. c) SEM image of a 24 h solvent vapour annealed bulk sample of BCP2. Only extensive annealing results in a detectable phase separation. The inset shows a SEM image of a spincoated blend resolving large domains in its surface topology.

Space charge limited current analysis of diodes

The analysis of the space charge limitted currents (SCLC) used following expression:[38,52]

$$J = A(V - V_0)^2 e^{g(V-V_0)^{0.5}}, \tag{11.1}$$

$$A = \frac{9}{8}\epsilon\epsilon_0\mu_0\frac{1}{d^3}, \tag{11.2}$$

$$g = 0.891\gamma\frac{1}{\sqrt{d}}. \tag{11.3}$$

μ_0 describes the effective mobility, the parameter γ takes a field dependent mobility into account and d describes the thickness of the sample. V_0 is an offset to the voltage which includes the built-in voltage. The film thickness for chlorobenzene coated films were $d \approx 120\,\text{nm}$ and those from chloroform $d \approx 130\,\text{nm}$. The dielectric constant ϵ is estimated with $4\,\frac{\text{F}}{\text{cm}}$.[52] Fig. 11.9 shows the diode characteristics and the corresponding fit parameters are listed in Tab. 11.3.

Table 11.3: Space charge limited current (SCLC) fit parameters.

Device	A $[\frac{\text{mA}}{\text{V}^2\text{cm}^2}]$	V_0 [V]	g $[\text{V}^{-0.5}]$
BCP 1 CBZ	12.3406	0.8877	0.9021
BCP 2 CF	8.2731	0.3343	0.6199
BCP 2 CBZ	0.0300	0.5500	2.9679
Blend CBZ	$1.5 \cdot 10^{-4}$	0.3386	2.2319

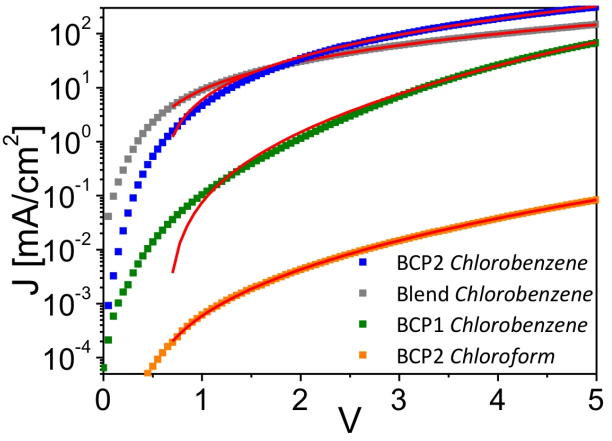

Figure 11.9: $J - V$ characteristics of hole only diodes with a gold top-electrode instead of an aluminum electrode. The red lines represent fits according to equation 11.1.

Absorption spectroscopy

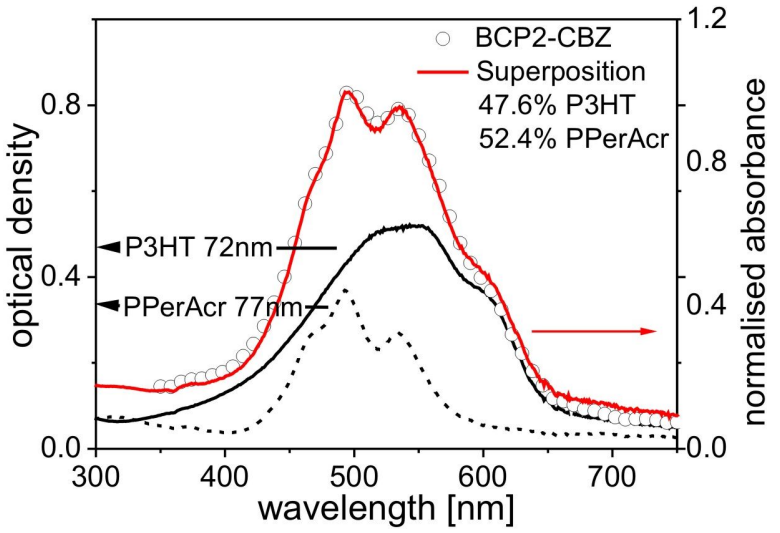

Figure 11.10: The BCP2-CBZ (open symbols) spectrum is fitted by a linear combination (red) of the two homopolymer spectra (black) with a ratio of 47.6% P3HT and 52.4%-PPerAcr which corresponds to a superposition of a weight ratio of 45%-P3HT and 55%-PPerAcr within the margin of error.

Bibliography

[1] G.A. Buxton and N. Clarke, *Predicting structure and property relations in polymeric photovoltaic devices*, Physical Review B **74**, 085207 (2006).

[2] F.S. Bates and G.H. Fredrickson, *Block copolymer thermodynamics: theory and experiment*, Annu. Rev. Phys. Chem. **41**, 525 (1990).

[3] I.W. Hamley, *The physics of block copolymers* (Oxford University Press, Oxford, 1998).

[4] H. Hoppe and N.S. Sariciftci, *Organic solar cells: An overview*, J. Mater. Res. **19**, 1924 (2004).

[5] K.M. Coakley and M.D. McGehee, *Conjugated polymer photovoltaic cells*, J. Chem. Mater. **16**, 4533 (2004).

[6] H. Spanggard and F.C. Krebs, *A brief history of the development of organic and polymeric photovoltaics*, Sol. energy Mater. Sol. Cells **83**, 125 (2004).

[7] C. Groves, R.A. Marsh, and N.C. Greenham, *Monte Carlo modeling of geminate recombination in polymer-polymer photovoltaic devices*, J. Chem Phys. **129**, 114903 (2008).

[8] S. Lindner, S. Hüttner, A. Chiche, M. Thelakkat, and G. Krausch, *Charge separation at self-assembled nanostructured bulk interfaces in block copolmers*, Angew. Chem. Int. Ed. **45**, 3364 (2006).

[9] M. Sommer, S. Lindner, and M. Thelakkat, *Microphase-separated donor-acceptor diblock copolymers: influence of HOMO energy levels and morphology on polymer solar cells*, Adv. Func. Mater. **17**, 1493 (2007).

[10] M. Sommer, S. Hüttner, U. Steiner, and M. Thelakkat, *Influence of molecular weight on the solar cell performance of double-crystalline donor-acceptor block copolymers*, Appl. Phys. Lett. **95**, 183308 (2009).

[11] S. Rajaram, P.B. Armstrong, B.J. Kim, and J.M.J. Fréchet, *Effect of addition of a diblock copolymer on blend morphology and performance of poly(3-hexylthiophene):perylene diimide solar cells*, Chem. Mater. **21**, 1775 (2009).

[12] Q. Zhang, A. Cirpan, T.P. Russel, and T. Emrick, *Donor-acceptor poly(thiophene-block-perylene diimide) copolymers: synthesis and solar cell fabrication*, Macromolecules **42**, 1079 (2009).

[13] Mariano Campoy-Quiles, Toby Ferenczi, Tiziano Agostinelli, Pablo G. Etchegoin, Youngkyoo Kim, Thomas D. Anthopoulos, Paul N. Stavrinou, Donal D. C. Bradley, and Jenny Nelson, *Morphology evolution via self-organization and lateral and vertical diffusion in polymer: fullerene solar cell blends*, Nat. Mater. **7**, 158 (2008).

[14] Youngkyoo Kim, Stelios A. Choulis, Jenny Nelson, Donal D. C. Bradley, Steffan Cook, and James R. Durrant, *Device annealing effect in organic solar cells with blends of regioregular poly(3-hexylthiophene) and soluble fullerene*, Appl. Phys. Lett. **86**, 063502 (2005).

[15] W. Ma, C. Yang, X. Gong, K. Lee, and A.J. Heeger, *Thermally stable, efficient polymer solar cells with nanoscale control o fthe interpenetrating network morphology*, Adv. Func. Mater. **15**, 1617 (2005).

[16] J.-F. Chang, B. Sun, D. W. Breiby, M. M. Nielsen, T. I. Sölling, M. Giles, I. McCulloch, and H. Sirringhaus, *Enhanced mobility of poly(3-hexylthiophene) transistors by spin-coating from high-boiling-point solvents*, Chem. Mater. **16**, 4772 (2004).

[17] R. Joseph Kline, Michael D. McGehee, Ekaterina N. Kadnikova, Jinsong Liu, Jean M. J. Fréchet, , and Michael F. Toney, *Dependence of regioregular poly(3-hexylthiophene) film morphology and field-effect mobility on molecular weight*, Macromol. **38**, 3312 (2005).

[18] R. J. Chesterfield, J. C. McKeen, C. R. Newman, P. C. Ewbank, D. A. daSilva Filho, J.-L. Brédas, L. L. Miller, K. R. Mann, and C. D. Frisbie, *Organic thin film transistors based on n-alkyl perylene diimides: charge transport kinetics as a function of gate voltage and temperature*, Phys. Chem. B **108**, 19281 (2004).

[19] S. Tatemichi, M. Ichikawa, T. Koyama, and Y. Taniguchi, *High mobility n-type thin-film tranisotrs based on N,N'-ditridecyl perylene diimide with thermal treatments*, Appl. Phys. Let. **89**, 112108 (2006).

[20] S. Hüttner, M. Sommer, and M. Thelakkat, *n-type organic field effect transistors from perylene bisimide block copolymers and homopolymers*, Appl. Phys. Lett. **92**, 093302 (2008).

[21] J. J. Dittmer, E. A. Marseglia, and R. H. Friend, *Electron trapping in dye/polymer blend photovoltaic cells*, Advanced Materials **12**, 1270 (2000).

[22] P.E. Keivanidis, I.A. Howard, and R.H. Friend, *Intermolecular interactions of perylene diimides in photovoltaic blends of fluorene copolymers: disorder effects on photophysical properties, film morphology and device efficiency*, Adv. Func. Mater. **18**, 3189Ű3202 (2008).

[23] S. Foster, C.E. Finlayson, P.E. Keivanidis, Y.-S. Huang, I. Hwang, R.H. Friend, M.B.J. Otten, L.-P. Lu, E. Schwartz, R.J.M. Nolte, and A.E. Rowan, *Improved performance of perylene-based photovoltaic cells using polyisocyanopeptide arrays*, Macromol. (2009).

[24] H.-Y. Chen, J. Hou, S. Zhang, Y. Liang, G. Yang, Y.Yang, L. Yu, Y. Wu, and G. Li, *Polymer solar cells with enhanced open-circuit voltage and efficiency*, Nat. Photon. **3**, 649 (2009).

[25] Bradley D. Olsen and Rachel A. Segalman, *Self-assembly of rod-coil block copolymers*, Mater. Sci. and Eng. **62**, 37 (2008).

[26] S. A. Jenekhe, *Polymer semiconductors: A fast mover with a bright spark*, Nat. Mater. **7**, 354 (2004).

[27] Y.-S. Huang, S. Westenhoff, I. Avilov, P. Sreearunotha, J.M. Hodgkiss, C. Deleener, R.H. Friend, and D. Beljonne, *Electronic structures of interfacial states formed at polymeric semiconductor heterojunctions*, Nat. Mater. **7**, 483 (2008).

[28] S. Hugger, R. Thomann, T. Heinzel, and T. Thurn-Albrecht, *Semicrystalline morphology in thin films of poly(3-hexylthiophene)*, Colloid. Polym. Sci. **282**, 932 (2004).

[29] J. Clark, C. Silva, R.H. Friend, and F.C. Spano, *Role of intermolecular coupling in the photophysics of disordered organic semiconductors: aggregate emission in regioregular polythiophene*, Phys. Rev. Let. **98**, 206406 (2007).

[30] Z. Wu, A. Petzold, T. Henze, T. Thurn-Albrecht, R.H. Lohwasser, M. Sommer, and M. Thelakkat, *Temperature and molecular weight dependent hierarchical equilibrium structures in semiconducting poly(3-hexylthiophene)*, Macromolecules **43**, 4646 (2010).

[31] P.J. Brown, D.S. Thomas, A. Köhler, J.S. Wilson, J.-S. Kim, C.M. Ramsdale, H. Sirringhaus, and R.H. Friend, *Effect of interchain interactions on the absorption and emission of poly(3-hexylthiophene)*, Phys. Rev. B **67**, 064203 (2003).

[32] M. Hoffmann, K. Schmidt, T. Fritz, T. Hasche, V.M. Agranovich, and K. Leo, *The lowest energy Frenkel and charge-transfer excitons in quasi-one-dimensional structures: application to MePTCDI and PTCDA crystals*, Chem. Phys. **258**, 73 (2000).

[33] S. Hüttner, M. Sommer, P. Kohn J. Hodgkiss, T. Thurn-Albrecht, U. Steiner, and M. Thelakkat, *Tunable charge transport in supramolecular assembled crystalline block copolymers*, submitted (2010).

[34] Peter Kohn, Michael Sommer, Sven Hüttner, Mukundan Thelakkat, and Thomas Thurn-Albrecht, *Crystallization induced phase separation in poly(3-hexyl thiophene)-block-poly(perylene bisimide acrylate) donor-acceptor block copolymer*, in preparation .

[35] Steffan Cook, Akihiro Furube, and Ryuzi Katoh, *Analysis of the excited states of regioregular polythiophene P3HT*, Energy Environ. Sci. **1**, 294 (2008).

[36] A.R. Campbell, J.M. Hodgkiss, S. Westenhoff, I.A. Howard, R.A. Marsh, C.R. McNeill, R.H. Friend, and N.C. Greenham, *Low-temperature control of nanoscale morphology for high performance polymer photovoltaics*, Nanolett. **8**, 3942 (2008).

[37] R.N. Marks, J.J.M. Halls, D.D.C. Bradley, R.H. Friend, and A.B. Holmes, *The photovoltaic response in poly(phenylene vinylene) thin-film devices*, J. Phys. Condens. Mater. **6**, 1379 (1994).

[38] P. N Murgatroyd, *Theory of space-charge-limited current enhanced by Frenkel effect*, J. Phys. D **3**, 151 (1970).

[39] U. Zhokhavets, T. Erb, H. Hoppe, G. Gobsch, and N.S. Sariciftci, *Effect of annealing of poly(3-hexylthiophene)/fullerene bulk heterojunction composites on structural and optical properties*, Thin Solid Films **496**, 679 (2006).

[40] Tomoaki Yago, Yoshiaki Tamaki, Akihiro Furube, and Ryuzi Katoh, *Self-trapping limited exciton diffusion in a monomeric perylene crystal as revealed by femtosecond transient absorption microscopy*, Phys. Chem. Chem. Phys. **10**, 4435 (2008).

[41] I.A. Howard, F. Laquai, P.E. Keivanidis, R.H. Friend, and N. Greenham, J. Phys. Chem. C. **113**, 21225 (2009).

[42] R. A. Marsh, C. R. McNeill, A. Abrusci, A. R. Campbell, and R. H. Friend, *A unified description of current-voltage characteristics in organic and hybrid photovoltaics under low light intensity*, Nanoletters **8**, 1393 (2008).

[43] J.M. Hodgkiss, G. Tu, S. Albert-Seifried, W.T.S. Huck, and R.H. Friend, *Ion-induced formation of charge-transfer states in conjugated polyelectrolytes*, J. Am. Chem. Soc. **131**, 8913 (2009).

[44] T. A. Ford, I. Avilov, D. Beljonne, and N. C. Greenham, *Enhanced triplet exciton generation in polyfluorene blends*, Phys. Rev. B **71**, 125212 (2005).

[45] H. Ohkita, S. Cook, Y. Astuti, W. Duffy, M. Heeney, S. Tierney, I. McCulloch, D.D.C. Bradley, and J.R. Durrant, *Radical ion pair mediated triplet formation in polymer-fullerene blend film*, Chem. Commun. **37**, 3939 (2006).

[46] K. Sakurai, H. Tachibana, N. Shiga, C. Terakura, M. Matsumato, and Y. Tokura, *Experimental determination of excitonic structure in polythiophene*, Phys. Rev. B **56**, 9552 (1997).

[47] A. Köhler and D. Blejonne, *The singlet-triplet exchange energy in conjugated polymers*, Adv. Funct. Mat. **14**, 11 (2004).

[48] Anthony J. Ryan, *Polymer science: Designer polymer blends*, Nature Mater. **1**, 8 (2002).

[49] M. Sommer, A. S. Lang, and M. Thelakkat, *Crystalline-crystalline donor-acceptor block copolymers*, Angew. Chem. Int. Ed. **47**, 7901 (2008).

[50] S. Westenhoff, I.A. Howard, and R.H. Friend, *Probing the morphology and energy landscape of blends of conjugated polymers with sub-10 nm resolution*, Phys. Rev. Lett. **101**, 016102 (2008).

[51] F. Laquai, A.K. Mishra, K.Müllen, and R.H. Friend, *Amplified spontaneous emission of poly(ladder-type phenylene)s - The influence of photophysical properties on ASE thresholds*, Adv. Funct. Mater. **18**, 3265 (2008).

[52] Helen Clubb, Ph.D. thesis, University of Cambridge, 2009.

Chapter 12

Annex: Block Copolymers as Compatibilisers for Binary Blends

Introduction

The demixing of polymer blends leads to macroscopic domains forming separated domains in a matrix or a co-continuous morphology, depending on the demixing process (see Chap. 3.3). Concerning the preparation of thin films by solvents (e.g. spincoating), the coarsening of phase separation is stopped as soon as the solvent is withdrawn, leaving a morphology that is kinetically trapped on its way towards the thermodynamic equilibrium. Therefore, the control on the kinetics of the solvent evaporation kinetics offers certain possibilities to adjust the blend morphology. By the use of solvents with different boiling points or the combination of co-solvents the evaporation kinetics can be controlled, allowing to modify the time for the blend phase separation. Whereas binary polymer blends typically phase separate on a micron scale,[1] the phase separation in block copolymers is restricted resulting in nanometer sized domains.[2] The actual domain size of block copolymers depends on the volume each block occupies. The domains size in amorphous block copolymers is in the order of the radius of gyration that scales with $\sqrt{N}$, where N is the number of monomer units. For stiff, rod-like polymers the domain size scales linearly.[3] Interactions leading to crystallisation of one or both blocks complicates the microphase separation and influences the domain sizes.[4]

The optimum domain size in bulk heterojunction solar cells is determined by a trade-off between the short exciton diffusion length but also the fact, that charge separation and charge percolation is more efficient in large domains.[5–7] The previous chapter showed that P3HT-*b*-PPerAcr (BCP2) provides large external quantum efficiencies.[8] The rather small number of monomers $N < 30$ limits the achievable domain sizes, but the ultra fast charge generation suggest even smaller domains below the exciton diffusion length. These results suggest domain sizes $\ll 5\,\mathrm{nm}$[9,10] originating from an incomplete micro-phase separation process after spincoating. The domains seem to be much smaller as the exciton diffusion limit. The low fill factor is a further indication for a non-optimal morphology.

Block copolymers can also be used to compatibilise polymer blends,[11] adjusting the domain size by lowering the interfacial tension between the two polymers, thereby slowing-down domain coarsening. This concept, using short donor-acceptor block copolymers has been applied lately to bulk heterojunction solar cells by Frechet et. al.[12,13]

Experimental

In the following we used ternary blends of P3HT and PPerAcr in a 1:1 ratio mixed with different amounts of block copolymer P3HT-*b*-PPerAcr. The block copolymer had an overall molecular weight of $M_n = 29.5\,\frac{\text{kg}}{\text{mol}}$ and a P3HT:PPerAcr ratio of 45%:55%. The devices were prepared and measured according to the procedures described in the previous chapter. The intensity of the white light illuminations was varied in a wide range in order to extract the characteristic OPV parameters as a function of intensity. Scanning force microscopy (Digital Instruments Dimension) was employed to study the surface topography.

Results and Discussion

Fig. 12.1 shows the photoluminescence quantum efficiency PLQE, the external quantum efficiency EQE and the extracted solar cell parameters such as the open circuit voltage V_{OC}, the short circuit current J_{SC}, the fill factor FF and power conversion efficiency η, measured under 1.5AM simulated sunlight at $100\,\frac{\text{mW}}{\text{cm}^2}$. Limitations in the material supply impeded large scale experiments, but the trends are clear. By increasing amount of copolymer concentration, the PLQE drops to less than 1% in agreement with the

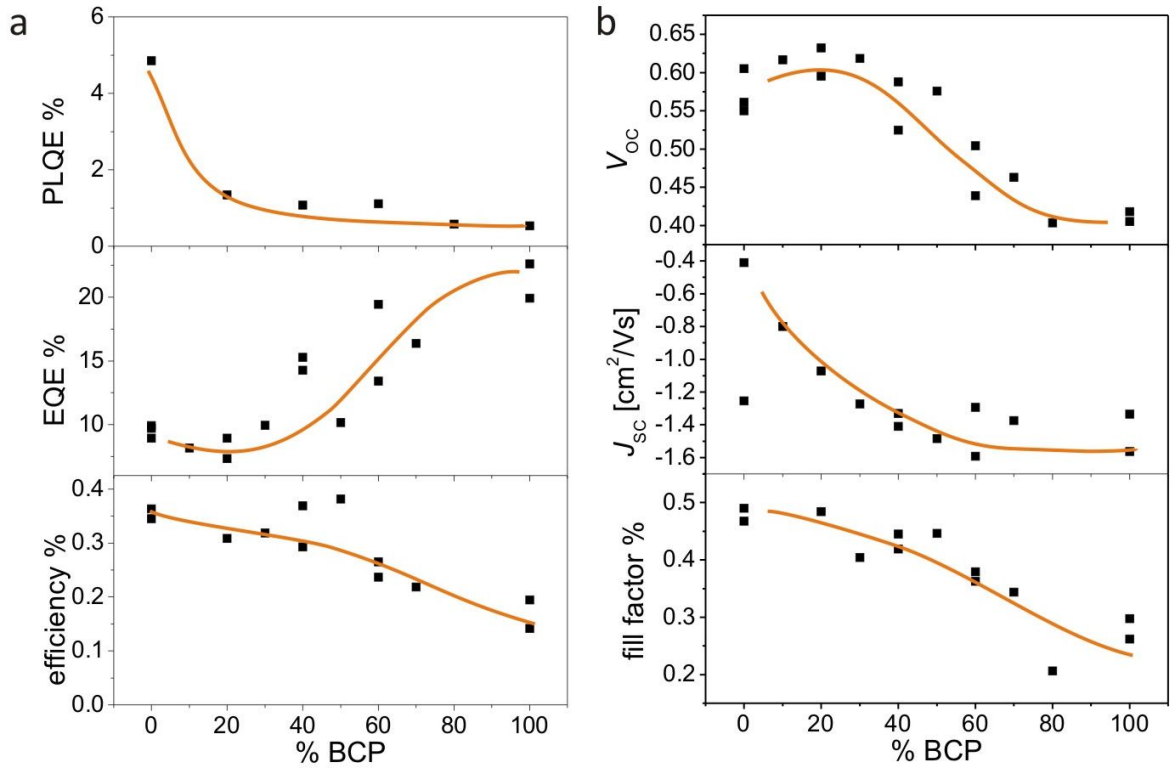

Figure 12.1: Device parameters of ternary blend block copolymer mixtures. The orange line is a guide to the eye. The external quantum efficiency and the short circuit current increase, whereby all other parameters tend to decrease. (The variations in the measurements result form the limited number of devices caused by a limited amount of available material.)

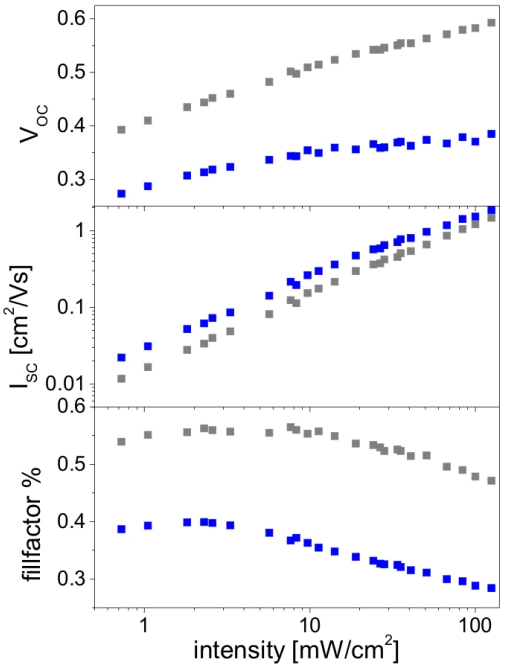

Figure 12.2: Light intensity dependent characterization of a blend (grey symbols) and block copolymer (blue symbols) device. The linear behaviour of the short circuit current at lower light intensities is consistent with geminate recombination as the main recombination process. The fill factor in the blend decreases only slightly by 8% but by 30% in the block copolymer device function at higher light intensities.

results of the previous chapter and the EQE increases consistently from 10% to 25%, leading to an increase of the short circuit current. Interestingly the open circuit voltage is steadily reduced with a higher load of the block copolymer and drops from $\sim 0.58\,\mathrm{V}$ to $\sim 0.4\,\mathrm{V}$ almost by $0.2\,\mathrm{V}$. The fill factor also drops from 50% in the blend to 30% in the neat block copolymer. As a consequence, the overall efficiency continuously decreases with a increasing the block copolymer content.

Intensity dependent measurements give information about the charge carrier formation and recombination processes i.e. the charges that can be extracted from the devices. In Fig. 12.2 the evolution of the V_{OC}, J_{SC} and the fill factor are depicted. At lower light intensity, where space-charge effects can be excluded, the J_{SC} is linear to the intensity which is often indicated as a signature for geminate recombination as the dominant loss mechanism. The open circuit voltage scales logarithmical with the light intensity.[14] The offset increases with copolymer load to almost $0.2\,\mathrm{V}$ and increases with a higher load of the block copolymer. This reduced open circuit voltage can originate from various mechanisms. One possible reason is a preferential alignment of the PPerAcr block of one at the electrode interfaces. Preferential surface wetting of one block copolymer block is well known.[15]

Similar observations were made in a variety of other heterojunction systems and point out geminate recombination of electrons and holes at the interface is the

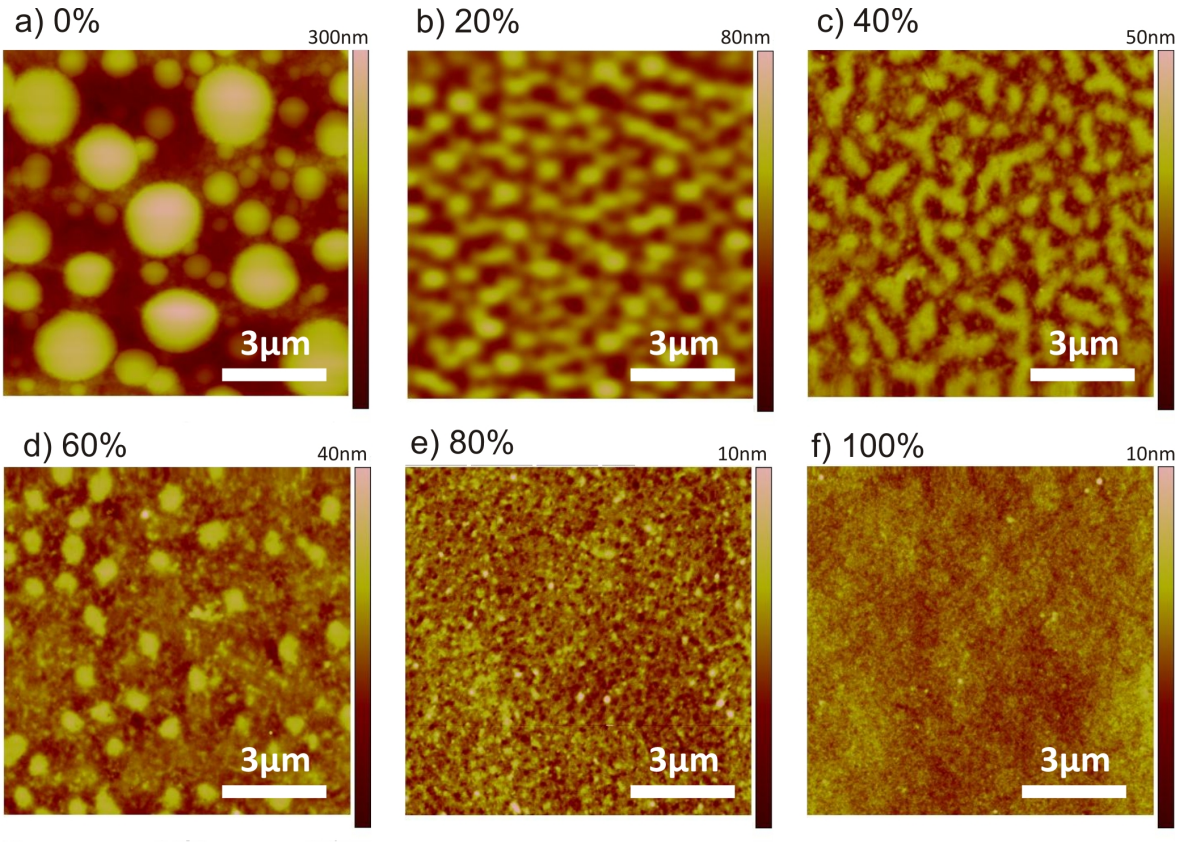

Figure 12.3: Scanning force microscopy scans of the topology of a ternary blend films. The surface becomes increasingly smoother with a higher load of P3HT-*b*-PPerAcr added to the blend.

main recombination process.[16] This may change reasonably at higher forward biases e.g. at the maximum power point which cannot easily be predicted. The fill factor shows a different behaviour. A 30% decrease of the fill factor can be observed in the block copolymer devices, while it only decreases by 8% in the blend with higher light intensity. One parameter influencing the fill factor is the lack of percolation paths and a non optimised phase morphology.

Fig. 12.3 shows the surface topology of ternary blends. Assuming a correlation between the the surface topology i.e. roughness and phase separation inside the film, the addition of block copolymer decreases the observed domain sizes as expected. Of course, the AFM images only reflect the surface topology. A direct information on the phase separation within the film stays hidden. Nonetheless a clear trend with increasing block copolymer content is visible: the coarseness decreases, which suggest decreasing macro-phases from the blend to the block copolymer with increasing block copolymer content.

Outlook

As an outlook, binary blends that are compatibilised with a block copolymer i.e. a surfactant can help to optimise the donor-acceptor interface. Domain size, interfacial crystallinity and the local mobility affect the charge separation.[17] So far, the combination of high charge generation of P3HT-*b*-PPerAcr block copolymers with the good fill factor of the polymer blend remains elusive. More studies, resolving the morphology evolution inside the film are necessary and might help to explain the decreased open circuit voltage and ultimately leading to an improved device efficiency. Alternative approaches may use binary blends of a homopolymer and a block copolymer in order to enhance one domain size specifically. Together with a use of asymmetric block copolymers this could help to identify the bottlenecks of the current approaches.

Bibliography

[1] J. M. G. Cowie, *Polymers - chemistry and physics of modern materials* (Blackie Acad. & Professional, London, 1994).

[2] I.W. Hamley, *The physics of block copolymers* (Oxford University Press, Oxford, 1998).

[3] Bradley D. Olsen and Rachel A. Segalman, *Self-assembly of rod-coil block copolymers*, Mater. Sci. and Eng. **62**, 37 (2008).

[4] I.W. Hamley, J.P.A. Fairclough, A. Ryan, F.S. Bates, and E. Towns-Andrews, *Crystallization of nanoscale-confined diblock copolymer chains*, Polymer **37**, 4425 (1996).

[5] H. Hoppe and N.S. Sariciftci, *Organic solar cells: An overview*, J. Mater. Res. **19**, 1924 (2004).

[6] S.R. Forrest, *The limits to organic photovoltaic cell efficiency*, MRS Bulletin **30**, 28 (2005).

[7] C. Groves, R.A. Marsh, and N.C. Greenham, *Monte Carlo modeling of geminate recombination in polymer-polymer photovoltaic devices*, J. Chem Phys. **129**, 114903 (2008).

[8] M. Sommer, S. Hüttner, U. Steiner, and M. Thelakkat, *Influence of molecular weight on the solar cell performance of double-crystalline donor-acceptor block copolymers*, Appl. Phys. Lett. **95**, 183308 (2009).

[9] S. Westenhoff, I.A. Howard, and R.H. Friend, *Probing the morphology and energy landscape of blends of conjugated polymers with sub-10 nm resolution*, Phys. Rev. Lett. **101**, 016102 (2008).

[10] A.R. Campbell, J.M. Hodgkiss, S. Westenhoff, I.A. Howard, R.A. Marsh, C.R. McNeill, R.H. Friend, and N.C. Greenham, *Low-temperature control of nanoscale morphology for high performance polymer photovoltaics*, Nanolett. **8**, 3942 (2008).

[11] Anthony J. Ryan, *Polymer science: Designer polymer blends*, Nature Mater. **1**, 8 (2002).

[12] K. Sivula, Z. T. Ball, N. Watanabe, and J. M. J. Frechet, *Amphiphilic diblock copolymer compatibilizers and their effect on the morphology and performance of polythiophene:fullerene solar cells*, Adv. Mater. **18**, 206 (2006).

[13] S. Rajaram, P.B. Armstrong, B.J. Kim, and J.M.J. Fréchet, *Effect of addition of a diblock copolymer on blend morphology and performance of poly(3-hexylthiophene):perylene diimide solar cells*, Chem. Mater. **21**, 1775 (2009).

[14] L.J.A. Koster, V.D. Mihailetchi, R. Ramaker, and P.W.M. Blom, *Light intensity dependence of open-circuit voltage of polymer:fullerene solar cells*, Appl. Phys. Lett. **86**, 123509 (2005).

[15] S. Y. Heriot and R. A. L. Jones, *An interfacial instability in a transient wetting layer leads to lateral phase separation in thin spin-cast polymer-blend films*, Nat. Mater. **4**, 782 (2005).

[16] R. A. Marsh, C. R. McNeill, A. Abrusci, A. R. Campbell, and R. H. Friend, *A unified description of current-voltage characteristics in organic and hybrid photovoltaics under low light intensity*, Nanoletters **8**, 1393 (2008).

[17] Christopher R. McNeill and Neil C. Greenham, *Conjugated-polymer blends for optoelectronics*, Adv. Mater. **21**, 3840 (2009).

List of Publications

Donor-acceptor block copolymers for photovoltaic applications – M. Sommer, S. Huettner and M. Thelakkat, J. Mater. Chem. 20, 10788-10797 (2010)

Donor-acceptor block copolymers with nanoscale morphology for photovoltaic – M. Sommer, S. Hüttner and M. Thelakkat, Advances in Polymer Science 228, Complex Macromolecular Systems II, 123-153 (2010)

Formation of nanopatterned polymer blends in photovoltaic devices – X. He, F. Gao, G. Tu, D. Hasko, S. Hüttner, U. Steiner, N.C. Greenham, R.H. Friend and W.T. S. Huck, Nanoletters 10, 1302-1307 (2010)

Dye-Sensitized Solar Cell Based on a Three-Dimensional Photonic Crystal – S. Guldin, S. Hüttner, M. Kolle, M.E. Welland, P. Müller-Buschbaum, R.H. Friend, U. Steiner, and N. Tétreault, Nanoletters 10, 2303-2309 (2010)

Control of solid-state dye-sensitized solar performance by block copolymer directed TiO_2 synthesis – P. Docampo, S. Guldin, M. Stefik, P. Tiwana, C. Orilall, S. Hüttner, U. Wiesner, U. Steiner and H.J. Snaith, Adv. Func. Mater. 20, 1787-1796 (2010)

Organic field effect transistors from triarylamine side-chain polymers – S. Hüttner, M. Sommer, Ullrich Steiner, M. Thelakkat, Appl. Phys. Lett. 96, 073503 (2010)

Monolithic route to efficient dye-sensitized solar cells employing diblock copolymers for mesoporous TiO_2 – M. Nedelcu, S. Guldin, M.C. Orilall, J. Lee, S. Hüttner, E.J.W. Crossland, S.C. Warren, C. Ducati, P.R. Laity, D. Eder, U. Wiesner, U. Steiner and H.J. Snaith, J. Chem. Mater. 20, 1261-1268 (2010)

Determination of charge carrier mobility of hole transporting polytriarylamine-based diodes – E.M. Barea, G. Garcia-Belmonte, M. Sommer, S. Hüttner, H.J. Bolink and M. Thelakkat, Thin Solid Films 518, 3351-3354 (2010)

Controlled solvent vapour annealing for polymer electronics – S. Hüttner, M. Sommer, A. Chiche, G. Krausch, U. Steiner and M. Thelakkat, Soft Matter 5, 4206-4211 (2009)

Influence of molecular weight on the solar cell performance of double-crystalline donor-acceptor block copolymers. – M. Sommer, S. Hüttner, U. Steiner, and M. Thelakkat,. Appl. Phys. Lett. 95, 183308 (2009)

Charge separation and recombination in self-organizing nanostructured donor-acceptor block-copolymer films – S. King, M. Sommer, S. Huettner, M. Thelakkat, S. Haque.J. Mater. Chem. 19, 5436-5441 (2009)

Block-copolymer directed synthesis of mesoporous TiO_2 for dye-sensitized solar cells – M. Nedelcu, J. Lee, E. J. W. Crossland , S. C. Warren, M. C. Orilall, S. Guldin, S. Hüttner, C. Ducati, D. Eder, U. Wiesner, U. Steiner, H.J. Snaith, Soft Matter 5, 134-139 (2009)

n-type organic field effect transistors from perylene bisimide block copolymers and homopolymers – S. Hüttner, M. Sommer, M. Thelakkat, Appl. Phys. Lett. 92, 093302 (2008)

Novel Electron-Conducting Block-Copolymers: Morphological, Optical and Electronic Properties – M. Sommer, S. Hüttner, S. Wunder, M. Thelakkat, Adv. Mater. 20, 2523-2527 (2008)

Charge separation at self-Assembled nanostructured bulk interface in block copolymers – S. Lindner, S. Hüttner, A. Chiche, M. Thelakkat, G. Krausch, Angewandte Chemie Int. Ed. 45, 3364-3368 (2006)

Submitted Manuscripts and Manuscripts in Preparation

Tunable charge transport using supramolecular self-assembly of nanostructured crystalline block copolymers – S. Hüttner, M. Sommer, J. Hodgkiss, P. Kohn, T. Thurn-Albrecht, R.H. Friend, U. Steiner, M. Thelakkat, submitted

Photophysics of double-crystalline donor-acceptor block copolymers from P3HT and perylene bisimide –S. Hüttner, J. Hodgkiss, M. Sommer, R.H. Friend, U. Steiner, M. Thelakkat – in preparation

Intermolecular interactions in perylene bisimide polymer architectures with increasing complexity – S. Hüttner, M. Sommer, J. Hodgkiss, P. Keivanidis, U. Steiner, M. Thelakkat – in preparation

Danksagung

Spätestens an dieser Stelle merkt man wie schnell die letzten Jahre vergangen sind und es nun an der Zeit ist, sich, soweit es überhaupt möglich ist, bei allen Personen zu bedanken, die mich auf dem Weg zur Doktorarbeit begleitet haben. Besonderer Dank gilt hier Prof. Mukundan Thelakkat und Prof. Ullrich Steiner, an deren Arbeitsgruppen ich diese Arbeit durchführen konnte. Großer Dank gebührt hier Michael Sommer - ohne ihn hätte es keine Materialen für diese Arbeit gegeben. Vielen Dank für die tolle, problemlose und effektive Zusammenarbeit, die vielen Diskussionen, gemeinsamen Versuche, das Korrekturlesen und die hohe Motivation.

Zunächst angefangen in der Physikalischen Chemie II bei Prof. Georg Krausch - an dieser Stelle ein Gruß nach Mainz - ging es dann nach einem guten Jahr nach Cambridge und der weiteren Projektfortsetzung stand nichts im Wege. Ich bin immer noch begeistert davon, wie einfach, schnell und unkompliziert das Ullrich Steiner und Mukundan Thelakkat das so organisiert haben. Die Eingewöhnung in die Gruppe stellte überhaupt kein Problem dar, nicht zuletzt durch die Kollegen und Freunde, die ich in der Thin Films and Interfaces Group fand – Danke. Dabei enstanden auch das ein oder andere Projekt. An dieser Stelle danke an Stefan Guldin für die Arbeit an den farbstoffsensitivisierten Solarzellen. Vielen Dank an Justin Hodgkiss für die Zusammenarbeit zur zeitaufgelösten Spektroskopie und der vielen detailierten Diskussionen. Genauso danke ich Panos Panagiotis und der restlichen Optoelectronics Group einschließlich Prof. Richard Friend für ihre Unterstützung. Maik Scherer danke ich für die Hilfe mit Latex und Nataliya Yufa fürs English proof-reading. Danke auch an Arnaud Chiche für seine Unterstützung zu Beginn der Arbeit sowie Mathias Kolle für seine Hilfe u.a. am Synchrotron. Hierfür gebührt großer Dank Peter Kohn, unserem Röntgenstrukturspezialisten, sowie Heiko Schoberth ein weiteres Mitglied des Grenoble Teams. Er hatte auch immer noch einen Platz in seinem Büro für mich frei, wenn ich mal nach Bayreuth kam. An dieser Stelle auch noch mal ein Dank an all die Freunde und Kollegen aus der PCII und der MCI – es hat immer Spaß gemacht Euch zu besuchen!

Zuletzt möchte ich mich noch mal bei meinem Bruder und vor allem bei meinen Eltern bedanken, die mich jederzeit zu 100% unterstützt haben.

Danke!

Erklärung

Die vorliegende Arbeit wurde selbständig von mir verfasst. Ich habe keine anderen als die angegebenen Hilfsmittel verwendet. Ferner habe ich nicht versucht, woanders eine Doktorarbeit einzureichen.

Bayreuth, Januar 2010

Sven Hüttner